Molecular Rheology of Complex Fluids

Huang, Qian; Rasmussen, Henrik Koblitz

Publication date:
2013

Document Version
Publisher's PDF, also known as Version of record

Molecular Rheology of Complex Fluids

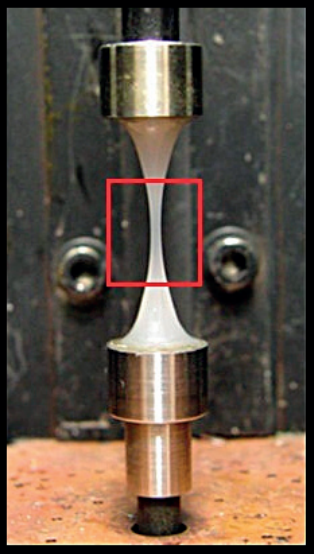

Qian Huang
Ph.D. Thesis
January 2013

DTU Chemical Engineering
Department of Chemical and Biochemical Engineering

Molecular Rheology of Complex Fluids

Qian Huang

Ph.D. Thesis

January 2013

DTU Chemical Engineering
Department of Chemical and Biochemical Engineering

Address: The Danish Polymer Centre
Department of Chemical and Biochemical Engineering
Technical University of Denmark
Building 227
DK-2800 Kgs. Lyngby
Denmark
Phone: +45 4525 6801
Web: www.dpc.kt.dtu.dk

Print: J&R Frydenberg A/S
København
June 2013

ISBN: 978-87-92481-99-3

Preface

This thesis presents the results of my Ph.D project carried out at the Danish Polymer Centre (DPC), Department of Chemical and Biochemical Engineering, Technical University of Denmark (DTU). The work was performed during the period from February 2010 to January 2013, under the supervision of Professor Ole Hassager, Associate Professor Anne Ladegaard Skov at DTU Chemical Engineering, and Associate Professor Henrik Koblitz Rasmussen at DTU Mechanical Engineering. This Ph.D project was funded under the Marie Curie Initial Training Network DYNACOP (DYNamics of Architecturally COmplex Polymers) in the European Union Seventh Framework (Grant Agreement No.: 214627).

I would like to express my sincere gratitude to my three supervisors for their full support throughout this project. I would like to thank my main supervisor Prof. Ole Hassager for his guidance, support and encouragement during these three years. It was extremely fortunate for me to have a supervisor that helped me in every aspect of scientific work, including reading and correcting my first article manuscript patiently nine times before publication. I really enjoyed discussing experimental results with him, and never forget the beautiful moonlight shining on the sea in Bornholm during our group trip. I would like to thank my supervisor Prof. Henrik K. Rasmussen for his help and support especially on the experimental work. I remember that on the first day of this project he said to me "If you meet any problems, you can find me. I am always here." And he was. I would also like to thank my supervisor Prof. Anne L. Skov for the fruitful and inspiring discussions.

I am grateful to all the people at the Danish Polymer Centre. I would like to thank Dr. José M. Román Marín for all his help on solving my problems in both experiments and simulations, and also for his patient listening and explanation regarding my weird questions. I would like to thank Dr. Nicolas J. Alvarez for his help and useful suggestions

on both my experiments and manuscripts. I would like to thank Dr. Irakli Javakhishvili for answering all my questions regarding size exclusion chromatography and sample preparation. I would like to thank Kim Chi Szabo for running SEC and DSC for my samples. I would also like to thank Vibeke H. Christiansen for helping me apply for visas, fill in travel claims, and find accommodations. Without her organization skill I could not have concentrated on my research work.

Also, I would like to thank the people from the workshop for the technical support on the FSR. I thank Ivan H. Pedersen, Henning V. Koldbech and Lars Møller for fixing the FSR when I damaged it, which happened several times. I also thank Henning V. Koldbech for designing and making the amazing mold and the quenching device for me, which improved my experiments a great deal.

Special thanks go to my DYNACOP colleagues. I thank Lawrence Hawke for his detailed explanation of the pom–pom model. I thank Serena Agostini for her useful suggestions about sample preparation. I thank Maxim Shivokhin for introducing the theories about star polymers when I was on my exchange visit at Université catholique de Louvain. I thank Helen Lentzakis for sharing the practical experience of extensional rheology measurements. I thank all the DYNACOP colleagues for the inspiring discussions and wonderful collaboration. We had a fantastic time during the DYNACOP project.

I would also like to thank Dr. David M. Hoyle from University of Durham, Olga Mednova and Prof. Kristoffer Almdal from DTU Nanotech, and all the other authors for the pleasant collaboration of our joint papers.

Finally, I wish to thank my parents for their love, support and encouragement.

Kgs.Lyngby, January 2013

Qian Huang

Abstract

The processing of polymer materials is highly governed by its rheology, and influences the properties of the final product. For example, a recurring problem is instability in extrusion that leads to imperfect plastic parts. The ability to predict and control the rheological behavior of polymer fluids as a function of molecular chemistry has attracted a long history of collaboration between industry and academia.

In industrial polymer processes, there is usually a combination of both shear and extensional flows. In some processing operations such as blow molding and fiber spinning, extensional flow is the dominant type of deformation. The polymer molecules experience a significant amount of chain orientation and stretching during these processes. Shear rheology measured by conventional shear rheometers is good at describing chain orientation, whereas extensional rheology gives a good way of inducing chain stretching. Accurate and reliable stress–strain measurements of extensional flow play a crucial role in the understanding of non–linear rheological properties of polymers. However, the non–linear extensional rheology has not been extensively studied.

It is known that the rheology of polymer melts is highly sensitive to molecular architecture, but the precise connection between architecture and non–linear rheology is still not fully understood. For example, linear polymer melts have the simplest architecture, but the possible existence of a qualitative difference on extensional steady–state viscosity between melts and solutions is still an open question. Branched polymer melts have more complex molecular structures. A stress maximum during the start–up of uniaxial extensional flow was reported in 1979 for a low–density polyethylene (LDPE) melt. Subsequently observations of a steady stress following a stress maximum were reported for two LDPE melts. However the rheological significance of the stress maximum as well as the existence of steady flow conditions following the maximum is still a matter of some debate.

This thesis focuses on the experimental study of extensional rheology of linear and branched polymer melts. We report the stress–strain measurements in extensional flows using a unique Filament Stretching Rheometer (FSR) in controlled strain rate mode and controlled stress mode. Extensional flow is difficult to measure reliably in laboratory circumstances. In this thesis we first present an updated control scheme that allows us to control the kinematics of polymer melts in an FSR, which is the foundation of our experimental work. Next we investigate four categories of polymer melts from the simplest system to the most complicated system, including 1) the narrow molar mass distribution (NMMD) linear polystyrene melts and solutions; 2) the bidisperse and polydisperse linear polystyrene melts; 3) the NMMD branched polystyrene melts; and 4) the polydisperse branched polyethylene melts. The experimental results are also compared with some developing theoretical models. Finally, to ensure the experimental data is accurate, the measurements from the FSR are compared with the data from some other extensional rheometers as well.

Resumé

Molekylær Reologi af Komplekse Væsker

Polymerbaserede produkter fremstilles ved forarbejdning af polymere materialer i smeltet tilstand. Kvaliteten af det færdige produkt afhænger stærkt af polymerens mekaniske egenskaber i smeltet tilstand, dvs. af polymere smelters reologiske egenskaber. Sammenhængen mellem polymere smelters molekylære arkitektur og deres reologiske egenskaber har derfor i lang tid været emnet for samarbejder mellem industri og universiteter.

I industrielle forarbejdningsprocesser er der sædvanligvis en kombination af forskydningsfelter og forlængelsesfelter. I nogle processer, som blæsestøbning og fiberdannelse er forlængelse en dominerende deformationstype. Kædemolekylerne oplever en betragtelig grad af orientering og stræk. Forskydningsreologi som udføres i kommercielt tilgængelige reometre er god til at beskrive orientering af kæderne, men forlængelsesreologi er meget bedre til at beskrive strækning af molekylerne. Nøjagtige og troværdige målinger af forlængelsesreologi er af afgørende betydning for at forstå og afdække polymerers ikke-lineære egenskaber i forlængelse, herunder at beskrive kædemolekylernes stræk. Men der er desværre en mangel på nøjagtige og troværdige målinger af polymerers egenskaber i forlængelse.

Sammenhængen mellem molekylær arkitektur er ved at være godt beskrevet for små deformationer hvor der er en lineær sammenhæng mellem deformation og spænding. Her drejer det sig primært om at bestemme et antal tidskonstanter i det såkaldte relaksationsmodul. Men for store deformationer hvor polymererne har en ikke-lineær sammenhæng mellem deformation og spænding er situationen stadig langt fra forstået. Selv for hvad der burde være det simplet tænkelige molekyle, nemlig et lineært polystyren molekyle er det stadig et uafklaret spørgsmål om der er en kvalitativ forskel mellem

forlængelsesviskositen for monodisperse smelter og monodisperse opløsninger. Forgrenede molekyler må formodes at have en endnu mere kompleks reologisk opførsel. Således har målinger i start-up af forlængelse med konstant hastighed af low-desnity polyethylen (LDPE) udvist et maksimum i udviklingen spændingen tilbage i 1979. Men den molekylære betydning af maksimet såvel som eksistensen af en konstant stømningstilstand efter maksimet er stadig et uafklaret spørgsmål.

Fokus i denne afhandling er på det eksperimentelle studium af forlængelsesreologi af lineære og forgrenede molekyler. Jeg rapporterer reologiske målinger opnået på et "Filament Stræk Reometer" (FSR), som opererer i såvel kontrolleret deformation som kontrolleret spændings modus. Afhandlingen begynder med en præsentation af en ny kontrolalgoritme til reometeret. Dernæst beskrives målinger for fire kategorier af systemer fra de simpleste til de mest komplekse: 1) Systemer med lineære molekyler med snæver molvægtsfordeling (NMMD), 2) Bidisperse og polydisperse systemer af lineære molekyler, 3) NMMD forgrenede polymerer og endelig 4) polydisperse forgrenede polymerer. Eksperimenterne sammenlignes med teoretiske forudsigelser hvor det giver mening. Endelig sammenlignes data også med målinger fra andre forlængelsesreometre.

Contents

Chapter 1

Introduction

1.1 Background of Polymer Dynamics and Rheology

Polymer fluids exhibit complex dynamics and rheology, which affect the processing and properties of the final products. For example, a recurring problem is instability in extrusion that leads to imperfect plastic parts. The ability to predict and control the rheological behavior of polymer fluids as a function of molecular chemistry has attracted a long history of collaboration between industry and academia.

Different models based on different theories have been proposed to describe the dynamics of polymeric fluids from dilute solutions to melts. One important example is the Rouse model [Rouse (1953)]. It is the simplest version of the bead–spring model which assumes the polymer chain is represented by a series of beads connected by springs. The Rouse model originally deals with the dynamics of polymer chains in dilute solutions. This model neglects the hydrodynamic interactions and therefore does not provide the correct relaxation time for the conformation change of the chains. For example, in the Rouse model, the longest relaxation time is proportional to M^2, where M is the molecular weight of a polymer chain. But in experiments the observed exponent for a polymer chain in a theta solvent is 1.5 rather than 2. Although the Rouse model does not predict the chain dynamics accurately in dilute solutions, it has been found to describe very well the viscoelastic behavior of unentangled solutions at high concentrations as well as unentangled melts, where the hydrodynamic interactions are

shielded. Therefore it is still an important model. The Rouse relaxation time is also widely used in the investigation of concentrated polymer solutions and melts.

However, the Rouse model only describes the chain dynamics in a region of molecular weight where the polymer chains are not long enough to form entanglements. When the polymer chains become longer and entangled with each other, the polymeric fluid becomes more complex. The first important model that deals with the dynamics of concentrated polymer solutions and melts above the entanglement molecular weight is the well–known tube model. In the tube model, a linear flexible polymer chain, called a test chain, is surrounded and entangled with many neighboring chains. The entanglements form a tube–like region which confines the movement of the test chain. The test chain can only move back–and–forth along the tube like a snake. This movement is called reptation. The concept of the tube model and the reptation theory was originally introduced by de Gennes (1979) in 1971. In the late 1970s a molecular rheological constitutive equation based on the reptation theory has been developed by Doi and Edwards (1986) for a concentrated polymer system.

The original Doi–Edwards (DE) model was subsequently further developed by incorporating additional molecular mechanisms, e.g. the contour length fluctuations (CLF) [Doi (1981)] and the constraint release (CR), in the theoretical framework. The DE model with these modifications quantitatively explains different aspects of the linear viscoelastic properties of linear flexible polymers, including the famous 3.4 power law in the prediction of the zero shear rate viscosity. The DE model has also been extended to predict the nonlinear viscoelastic properties by introducing the mechanisms of chain stretch [Marrucci and Grizzuti (1988)] and convective constraint release (CCR) [Marrucci and Ianniruberto (1996)]. Besides the linear polymer chains, constitutive equations based on the DE model, e.g. the pom–pom model [McLeish and Larson (1998)], are also developed for branched polymers which have more complex structures.

The combination of the above corrections and modifications has refined the original tube model and the reptation theory, which gives a better understanding of the dynamics of the concentrated polymer system. However, following the development of experimental techniques, more rheological observations which can not be explained by the tube model have come out. For example, recent experiments by Bach *et al.* (2003a) showed that the extensional steady–state viscosity of entangled polystyrene melts decreased monotonically with increasing the strain rate, while other experiments [Bhattacharjee *et al.* (2002)] on entangled polystyrene solutions showed that the viscosity initially decreased and then followed by increase. The tube model that includes the mechanisms of chain stretch and CCR reasonably described the above behavior of polymer solutions. But it could not capture the monotonic thinning of polymer melts. While new theoretical investigations are needed, more rheological experiments, especially in the nonlinear viscoelastic region, are important for the validation of the developing theoretical models. This is also one of the main purpose of this Ph.D thesis.

1.2 Extensional Flow and Extensional Rheometers

1.2.1 Description of Extensional Flow

In industrial polymer processes, there is usually a combination of both shear and extensional flows. In some processing operations such as blow molding and fiber spinning, extensional flow is the dominant type of deformation. The polymer molecules experience a significant amount of chain orientation and stretching during these processes. Shear rheology measured by conventional shear rheometers is good at describing chain orientation, whereas extensional rheology gives a good way of inducing chain stretching. However, the non–linear extensional rheology has not been extensively studied.

The velocity fields of simple extensional flows are generalized as [Bird *et al.* (1987)]

$$\begin{aligned} v_x &= -\frac{1}{2}\dot{\epsilon}\,(1+b)\,x \\ v_y &= -\frac{1}{2}\dot{\epsilon}\,(1-b)\,y \\ v_z &= +\dot{\epsilon} z \end{aligned} \tag{1.1}$$

where $\dot{\epsilon}$ is the elongation rate and $0 \leq b \leq 1$. Some typical extensional flows are obtained for particular choices of the parameter b, such as the uniaxial elongational flow ($b = 0, \dot{\epsilon} > 0$), the biaxial elongational flow ($b = 0, \dot{\epsilon} < 0$) and the planar elongational flow ($b = 1$). The general form of the total stress tensor for extensional flow is expressed as

$$\boldsymbol{\pi} = p\boldsymbol{\delta} + \boldsymbol{\tau} = \begin{pmatrix} p+\tau_{xx} & 0 & 0 \\ 0 & p+\tau_{yy} & 0 \\ 0 & 0 & p+\tau_{zz} \end{pmatrix} \tag{1.2}$$

where p is the pressure and $\boldsymbol{\delta}$ is the unit tensor. The most frequently reported extensional flow in experiments is the uniaxial elongational flow. As illustrated in Figure 1.1, in a uniaxial elongational flow, a cuboid of material with initial length L_0 at time $t = 0$ is stretched to the length L at time t in the z direction. The Hencky strain ϵ is defined as

$$\epsilon = \ln \lambda = \ln \left(L(t)/L_0\right), \tag{1.3}$$

where λ is the stretch ratio. For an incompressible material the Hencky strain can also be calculated from the deformations either in the x direction or in the y direction as

$$\epsilon = -2\ln\left(a(t)/a_0\right). \tag{1.4}$$

The elongation rate is defined as $\dot{\epsilon} = d\epsilon/dt$. From Eq.1.3 it can be seen that for a constant elongation rate we have

$$L(t) = L_0 e^{\epsilon} = L_0 e^{\dot{\epsilon}\Delta t}. \tag{1.5}$$

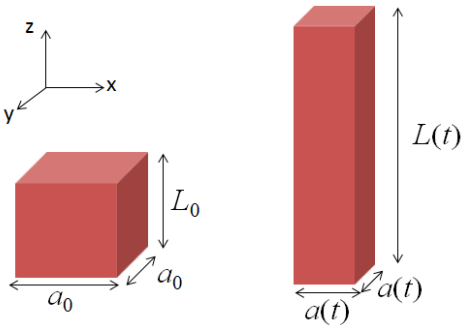

Figure 1.1: Illustration of uniaxial extension

Accurate and reliable stress–strain measurements of extensional flows play a crucial role in the understanding of nonlinear rheological properties of polymers. Constitutive models are also challenged to capture the stress–strain response in a more extreme situation with the large deformations in extensional flow. However, compared to shear flow, extensional flow is much more difficult to produce and measure reliably in laboratory circumstances. This is because firstly, the interactions of the test polymer fluid with any solid interface would introduce a shear component, which gives problems to generate a pure extensional flow. Secondly, in shear flow, the neighboring fluid elements are separated linearly in time under a constant shear rate; while in extensional flow, the neighboring fluid elements are separated exponentially in time under a constant elongation rate, which can be seen from either Eq.1.1 or Eq.1.5. This distinguish feature requires the extensional rheometers have the capability to produce much larger deformations to the material in a short time than shear rheometers under some controlled manner (e.g. constant strain rate).

1.2.2 Development of Extensional Rheometers

During the last decades, different types of extensional rheometers have been developed. Some typical and important examples include the Rheometrics Melt Extensiometer (RME) [Meissner (1972); Meissner and Hostettler (1994)], the Münstedt Tensile Rheometer (MTR) [Münstedt (1979)], the Filament Stretching Rheometer (FSR) [McKinley and Sridhar (2002)], and the Sentmanat Extensional Rheometer (SER) [Sentmanat (2004)].

The Rheometrics Melt Extensiometer (RME)

In 1960s the conventional way of measuring the extensional stress of polymer melts was using the clamping systems, which was similar as in the tensile testing of metals. However, these measurements were limited to small deformations, due to the difficulty of achieving the requirement that the speed of the movable clamp has to increase exponentially. In the early 1970s, this problem was solved by Meissner (1972) who introduced the 'rotational clamps' technique. With the subsequent modifications [e.g. Laun and Münstedt (1978); Raible *et al.* (1979)] of the Meissner type rheometer, the polymer melt samples could be stretched under constant strain rate up to a Hencky strain of $\epsilon = 7$ where ϵ is defined in Eq.1.3. With the capability of achieving such large deformation, the possible existence of the stress overshoot in extensional flows of branched polymers was observed for the first time in a low–density polyethylene (LDPE) melt [Raible *et al.* (1979)]. The Meissner type rheometer was further improved by replacing the rotational clamps to conveyor belts [Meissner and Hostettler (1994)]. This design was commercialized by Rheometric Scientific as the Rheometrics Melt Extensiometer (RME) which was one of the most common rheometers to measure the extensional stress of polymer melts.

The Münstedt Tensile Rheometer (MTR)

In 1970s another type of extensional rheometer based on the improvement of conventional clamping systems was introduced by Münstedt (1979). The Münstedt Tensile Rheometer (MTR) was able to do extensional measurements under either constant strain rates or constant tensile stresses on a small amount of materials. Recoil and relaxation experiments could also be performed on the MTR. But the Hencky strain that the MTR could reach was below 4, which was not as large as the modified version of the Meissner type rheometer that appeared in the same period.

The Filament Stretching Rheometer (FSR)

Another way to probe the extensional stress is using the filament stretching rheometers. The filament stretching rheometers were initially designed for measuring the extensional viscosity of polymer solutions. Due to their low viscosity property, polymer

solutions used to be measured on some other rheometers such as opposing jets and spin–line rheometers. However these rheometers generate a flow which contains a shear component, and therefore is very difficult to measure the extensional viscosity accurately. In a filament stretching rheometer, a test sample is usually placed in between of a top plate and bottom plate. Although there is still a shear component in the flow near the two plates, the center part of the filament during stretching is considered to be pure extensional flow.

An early filament stretching device was introduced by Matta and Tytus (1990). In their work, the FSR worked as a constant force (by gravity) mode rather than a constant strain rate mode. This design was soon improved by Sridhar *et al.* (1991) as the velocity of the moving plate could be controlled. However, during a filament stretching, while the length of the filament increases exponentially in time, the mid–diameter does not decrease exponentially as the ideal case, due to the nonslip boundary at the two ends of the filament. Therefore the true strain rate at the center part of the filament is not constant. In the further work by Tirtaatmadja and Sridhar (1993), they monitored the mid–diameter change of the filament during stretching, and then adjusted the separation rate of the two end plates, so that the true strain rate based on the mid–diameter of the filament could be kept constant. This trial–and–error procedure is known as the 'open loop control', and it normally requires several iterative experiments to find the desired separation rate of the end plates. Anna *et al.* (1999) suggested using a PID controller to control the end plates separation from the online monitoring of the mid–diameter of the filament. This is known as the 'closed loop control'. However Anna *et al.* (1999) did not successfully implemented the closed loop control in a filament stretching device. The filament stretching devices designed for polymer solutions normally work at room temperature. In 2003, an FSR was firstly designed for measuring polymer melts at high temperatures by Bach *et al.* (2003b). Subsequently the authors also implement the closed loop control and successfully measured two monodisperse polystyrenes [Bach *et al.* (2003a)] for the first time on the FSR. Since then the FSR is capable to probe the extensional rheology of polymer melts such as polystyrene and LDPE base on a small amount of samples. Bach *et al.* (2003b) did not report the details of their close loop control scheme. Recently the control scheme based on Bach *et al.* (2003b) has been updated and published by Román Marín *et al.* (2013).

The Sentmanat Extensional Rheometer (SER)

The Sentmanat Extensional Rheometer (SER) is a universal testing platform introduced by Sentmanat (2004). It incorporates dual wind–up drums to stretch polymer melts and elastomers under uniform extensional deformation. Although the SER was originally designed as an extensional rheometer, this platform can be easily accommodated onto a number of conventional rotational rheometers. The versatility and simple manipulation quickly made SER become one of the most popular extensional rheometers. In recent years a lot of extensional experiments have been performed by using an SER. Similar platform was soon designed by TA Instruments as Extensional Viscosity Fixture (EVF).

However, both SER and EVF can only reach a maxium Hencky strain of around 3.5.

All the above extensional rheometers directly measure the force (or torque) during stretching. Some other interesting rheometers, e.g. the Cross Slot Extensional Rheometer (CSER) [Hassell *et al.* (2009)], measure the stress through birefringence patterns and stress optical coefficient. Measurements from SER, FSR and CSER are compared with each other in Chapter 10 of this thesis.

1.3 The Filament Stretching Rheometer at DTU

The extensional rheometer used in this Ph.D project is a filament stretching rheometer, which is designed by Bach *et al.* (2003b), and located at the Technical University of Denmark (DTU). This FSR is equipped with an oven to allow measurements from 15 °C to 200 °C. The test sample is usually placed in between of two cylindrical steel plates. The bottom plate is stationary and the top plate stretches the sample vertically. Nitrogen is used during the experiments to avoid sample degradation. The FSR usually works in a controlled strain rate mode. The online control scheme is based on Bach *et al.* (2003a) and updated by Román Marín *et al.* (2013). In 2012, the first adaptation of the FSR to operate in a controlled stress mode is also implemented by Alvarez *et al.* (2012). The control schemes for controlled strain rate mode and controlled stress mode can be found in Chapter 2 and 9, respectively.

The types of experiments that the FSR can do include the uniaxial extension, the stress relaxation and the reversed flow. Large amplitude oscillatory extension (LAOE) [Bejenariu *et al.* (2010)] and planar extension [Jensen *et al.* (2010)] are also reported for polymer networks by using the FSR, but not for polymer melts and also not included in this thesis. By injecting cooled nitrogen into the oven through a special device, the FSR is also able to quench a stretched filament in a short time within 5 seconds. The quenched filament can be used for further investigation such as neutron scattering.

1.3.1 Uniaxial extension

Like other extensional rheometers, the most frequently reported measurements using the FSR are the transient stress in a startup of uniaxial extension. A thorough review of filament stretching rheometry has been written by McKinley and Sridhar (2002). As for the FSR at DTU, the force $F(t)$ during extension is measured by a load cell which is connected to the bottom plate, and the diameter $2R(t)$ at the mid–filament plane is measured by a laser micrometer. The Hencky strain is calculated from the observation

of $R(t)$ as

$$\epsilon(t) = -2\ln\left(R(t)/R_0\right), \tag{1.6}$$

where R_0 is the initial radius of the sample before stretching. The strain rate is defined as $\dot{\epsilon} = d\epsilon/dt$. It can be seen from Eq.1.6 that for a constant strain rate $\dot{\epsilon}_0$, the mid–diameter $2R(t)$ of the sample deceases exponentially as $R(t) = R_0 \exp\left(-0.5\dot{\epsilon}_0 t\right)$. With the assumption of symmetric as well as axis–symmetric mid–filament plane, the mean value of the stress difference over the plane are calculated from the observations of $R(t)$ and $F(t)$ as [Szabo (1997)]

$$\langle\sigma_{zz} - \sigma_{rr}\rangle = \frac{F(t) - m_f g/2}{\pi R(t)^2}, \tag{1.7}$$

where m_f is the weight of the filament and g is the gravitational acceleration. Eq.1.7 has ignored the inertial and surface tension effects. The complete force balance can be found in Szabo (1997). At small strains during the startup, part of the stress difference comes from the radial variation due to the shear components in the deformation field, especially at small aspect ratios $\Lambda_0 = L_0/R_0$ where L_0 is the initial length of the sample. This effect may be compensated by a correction factor where the corrected mean value of the stress difference is defined as [Rasmussen *et al.* (2010)]

$$\langle\sigma_{zz} - \sigma_{rr}\rangle_{corr} = \langle\sigma_{zz} - \sigma_{rr}\rangle\left(1 + \frac{\exp\left(-5\epsilon/3 - \Lambda_0^3\right)}{3\Lambda_0^2}\right)^{-1} \tag{1.8}$$

This relation ensures less than 3% deviation from the correct initial stress. For large strains the correction vanishes and the radial variation of the stress in the symmetry plane becomes negligible [Kolte *et al.* (1997)]. The extensional stress growth coefficient is defined as $\bar{\eta}^+ = \langle\sigma_{zz} - \sigma_{rr}\rangle_{corr}/\dot{\epsilon}$.

In the previous work at DTU, the polymer melts that have been investigated under uniaxial extension of the FSR include four monodisperse linear polystyrene melts [Bach *et al.* (2003a); Nielsen *et al.* (2006a)], three bidisperse linear polystyrene melts [Nielsen *et al.* (2006a)], a polydisperse linear polystyrene melt [Rasmussen *et al.* (2007)], two well–defined branched polystyrene melts [Nielsen *et al.* (2006b)], and four commercial polyethylene melts [Bach *et al.* (2003b); Rasmussen *et al.* (2005)].

1.3.2 Stress relaxation

In a stress relaxation measurement, the startup of the flow is a uniaxial extension as described in Section 1.3.1. During the stress relaxation phase starting at an arbitrarily given Hencky strain of ϵ_0, the stretching is stopped, giving $\dot{\epsilon} = 0$.

Measurements of stress relaxation following uniaxial extension is difficult to do due to the necking instability [Wang *et al.* (2007)]. Recently new technique to measure stress relaxation has been reported for a monodisperse polystryrene melt of molecular weight 145kg/mol by using the FSR at DTU [Nielsen *et al.* (2008)]. With the aid of the closed loop controller, the filament diameter in the mid–plane is controlled accurately and therefore the Hencky strain can be controlled even during the necking phase [Wang *et al.* (2007); Lyhne *et al.* (2009)]. Subsequently the well–defined pom–pom polystyrene which has been measured in uniaxial extension by Nielsen *et al.* (2006b) was further measured in stress relaxation by Rasmussen *et al.* (2009) using the FSR. Yu *et al.* (2011a) also measured the commercial polystyrene and LDPE melts in stress relaxation, but the purpose was to evaluate the pseudotime principle for nonisothermal polymer flows. Except the work in this Ph.D thesis, the above measurements are all the previous work at DTU on stress relaxation, and apparently the data are very limited.

1.3.3 Reversed flow

In a reversed flow measurement, the startup of the flow is also a uniaxial extension as described in Section 1.3.1. During the startup we define $\dot{\epsilon}_0^+ = \dot{\epsilon}$. When the sample is stretched to an arbitrarily given Hencky strain of ϵ_0, the flow is reversed and in the reversed flow phase we define $\dot{\epsilon}_0^- = -\dot{\epsilon}$, where $\dot{\epsilon}_0^+$ and $\dot{\epsilon}_0^-$ stay positive, constant and equal. At some time t_R the stress changes sign from positive to negative (tension to compression). The strain recovery is defined as $\epsilon_R = \epsilon_0 - \epsilon(t_R)$ [Nielsen and Rasmussen (2008)]. If the flow is continued for $t > t_R$, the filament will buckle at some time.

Measurements of reversed flow have been reported by using other extensional rheometers [e.g. Meissner (1972); Wagner and Stephenson (1979)] in the form of free recovery. In such type of measurements the stress equals zero in the reversed flow phase. Therefore it is a controlled stress experiment as opposed to the controlled strain experiment. The technique to measure reversed biaxial flow in a controlled strain mode has been reported by Nielsen and Rasmussen (2008) using the FSR at DTU with the aid of the closed loop controller. The test polymer melt was the monodisperse polystryrene with the molecular weight of 145kg/mole. Besides this polystyrene melt, in the previous work at DTU the only polymer that has been measured under reversed flow is a linear polyisoprene melt with a molecular weight of 483kg/mole.

1.3.4 Filament quenching

In a uniaxial extension, when a polymer melt is stretched to some desired Hencky strain, the liquid bridge can be quenched by a series of cooled nitrogen jets. In this way the temperature of the test sample is lowered below its melting point or glass transition point in a few seconds whereby the molecular configurations are frozen. The quenched filament can be used for further investigation such as the small angle neutron scattering (SANS) experiments. Such experiment has been reported by Hassager *et al.* (2012). This is the only published work using the filament quenched on the FSR at DTU.

During filament quenching, the cooled nitrogen is injected to the oven through a specially designed quenching device as shown in Figure 1.2. This device consists of three tiny tubes in front of the filament bridge and another three tubes in the back. These six tubes are hold by an arm which can move with the laser micrometer during stretching and thus always let the tubes surround the center part of the stretched filament. In the work of Hassager *et al.* (2012), the arm was made of stainless steel which caused a problem of lowering the oven temperature even before quenching. In Figure 1.2, the arm has been replaced by a new one made of plastic material. In this Ph.D project, it was planned to make SANS experiments for the polystyrene melts shown in Figure 1.2. However, due to the unexpected delay of the SANS experiments, this part is not included in the thesis.

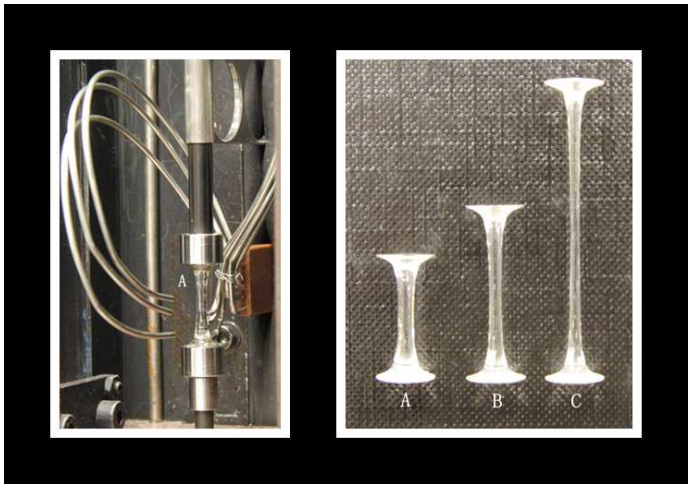

Figure 1.2: Left: quecching device in the FSR. Right: queched polystyrene filaments of different Henchy strains. A: $\epsilon = 1$; B: $\epsilon = 1.5$; C: $\epsilon = 2$.

1.4 Thesis Outline

This Ph.D project is part of the DYNACOP (DYNamics of Architecturally COmplex Polymers) project which is funded under the Initial Training Network of Marie Curie Programme in the European Union Seventh Framework. The DYNACOP project involves eight universities, two research centres and two industrial companies across Europe. The scientific objective of DYNACOP is to obtain a fundamental understanding of the flow behaviour and the dynamics of topologically complex macromolecular fluids and their roles in processing. As part of DYNACOP, this Ph.D project focuses on the extensional rheology of complex fluids. The aim of this Ph.D project is to link molecularly based model calculations across different length scales in the context of accurate experimental data.

As shown in Figure 1.3, four categories of polymer melts have been investigated throughout the thesis from the simplest system to the most complicated system. The experimental work is carried out primarily on the rheological characterization using the unique filament stretching rheometer which has been described in Section 1.3. Most of the measurements are performed under the controlled strain rate mode. The control scheme to maintain a constant strain rate in the FSR for polymer melts is described in Chapter 2.

	Linear	Branched
Nearly Monodisperse	Polystyrene Melts & Solutions	Star & H Shaped Polystyrene Melts
Polydisperse	Bidisperse & Commercial Polystyrene Melts	LDPE & HDPE

Figure 1.3: Types of polymer materials that have been measured and reported in this thesis

Chapter 3 and 4 deal with the polymer melts in category 1, which is the simplest case. The previous work by Bhattacharjee *et al.* (2002) and Bach *et al.* (2003a) showed that there is a difference in extensional steady–state viscosity between entangled polymer melts and solutions; but the molecular dynamics is unknown. Chapter 3 investigates the possible influence from the entanglement molecular weight. In Chapter 3, two monodisperse polystyrene melts of molecular weight 285 and 545kg/mole, as well as their solutions, are measured on the FSR. The results indicate that the possible reason which causes the difference between polymer melts and solutions could be the different

finite extensibility of the polymer chains. Chapter 4 investigates the possible influence from the monomeric friction. In chapter 4, the polymer solutions diluted from the 545kg/mole polystyrene melt with the same concentration but with different solvents are compared in both shear and extensional flows. The results indicate that the possible reason which causes the difference between polymer melts and solutions could also be the stretch/orientation–induced reduction of monomeric friction.

Chapter 5 and 6 deal with the polymer melts in category 2. Chapter 5 starts from the uniaxial extension of bidisperse linear polymer melts, which is the simplest case of polydisperse systems. Two well–entangled polystyrene blends made from the monodisperse 285 and 545kg/mol polystyrene melts are measured on the FSR. The results of the steady–state viscosity of these two blends seem to follow the simple mixing rules. In Chapter 6, a polydisperse linear polystyrene melt is measured on the FSR in different types of experiments including uniaxial extension, stress relaxation and reversed flow. The extensional steady–state viscosity vs strain rate of the polydisperse melt is found to scale as $\bar{\eta}_{\text{steady}} \sim \dot{\epsilon}^{-0.25}$, in which the exponent is in between of the monodisperse polystyrene melts and the solutions that have been measured in Chapter 3.

Chapter 7 deals with the polymer melts in category 3. Well–defined branched polymers are considered as model polymers to get insight of the complex physics. Therefore the polymer melts in category 3 are especially important for the validation of the developing theoretical models. Chapter 7 starts from the star polystyrene melts, which is the simplest case of branched polymer melts. One symmetric and two asymmetric star polystyrene melts which contain the same backbone of molecular weight 180kg/mole, are compared in shear rheology with a linear polystyrene melt which also has the molecular weight of 180kg/mole. One of the two asymmetric star melts is further measured in extensional flows. An H–shaped polystyrene melt is also measured in extensional flows in this chapter. However, due to the limited amount of materials and the difficulties in handling the experiments, the data of the extensional measurements are very limited.

Chapter 8, 9 and 10 deal with the polymer melts in category 4. This category is the most complicated one, but many commercially used polymers such as LDPE belong to this category. In Chapter 8, the two LDPE melts which showed a stress overshoot in uniaxial extension as reported by Rasmussen *et al.* (2005), are further investigated in stress relaxation and reversed flow. The observations indicate that after the overshoot the branched LDPE melts are less elastic and behave similarly to linear polymers. In Chapter 9, the first adaptation of the FSR to operate in controlled stress mode is presented. One of the LDPE melts that have been measured under constant strain rate by Rasmussen *et al.* (2005), is measured under constant stress in this chapter. The experimental findings support the existence of a stress maximum in fast stretching of branched polymer melts. The ultimate steady extensional flow state is shown to be independent of prehistory, be it constant strain rate or constant stress. In Chapter 10, three polyethylene melts are measured and compared on different types of extensional

rhometers including SER, FSR and CSER. The results from the three rheometers are shown to be consistent with each other.

Finally, in Appendix A, the factors that influence the accuracy of the FSR measurements are discussed. Some previous measurements from the FSR are compared with the results made in this thesis. Chapter 2, 8, 9 and 10 are based on the published (or submitted) journal articles. Related joint author statements are included in Appendix B.

Chapter 2

A Control Scheme for Filament Stretching Rheometers with Application to Polymer Melts

2.1 Introduction

Experimental realization of well–defined extensional flows in polymeric fluids has been a very difficult task. The pursuit of reliable data has led to the development of various testing platforms. As mentioned in Chapter 1, for uniaxial characterization of polymer melts, the most commonly used rheometers include the Münsted tensile rheometer (MTR) [Münstedt (1979)], the Meissner elongational rheometer (commercialized as RME) [Meissner and Hostettler (1994)], the filament stretching rheometer (FSR) [Sridhar *et al.* (1991)] and more recently the Sentmanat extensional rheometer (SER) [Sentmanat (2004)].

The MTR, RME and SER, often referred to as integral methods, are designed to impose an overall uniform deformation on the sample, each with a different mechanism. Given an initial sample geometry, the integral methods apply a uniform deformation using a prescribed mechanical motion that relates to a known strain, which is independent of the rheology of the material. Imaging techniques are necessary in order to validate the uniaxial flow. In most cases, undesired deviations from uniaxial deformation are attenuated or suppressed by changing the initial geometry of the sample [Schulze *et*

al. (2001); Yu *et al.* (2010, 2011b)]. Measurements on polymer melts using integral techniques have been reported by different research groups [Münstedt *et al.* (1998); Wagner *et al.* (2000); Aho *et al.* (2010)].

Filament stretching rheometers attracted attention in the 1990s because of interest in uniaxial extensional properties of dilute polymer solutions [McKinley and Sridhar (2002)]. Inspired by the original design of Cogswell (1968) and the work of Matta and Tytus (1990), Sridhar *et al.* (1991) developed a filament stretching device where the relative plate motion is prescribed. Subsequent filament stretching devices followed the same conceptual design [McKinley and Sridhar (2002)], including the one used in this work [Bach (2003)].

In the FSR, the extensional properties of a fluid are probed by placing a cylindrical sample between two parallel plates. The plates are pulled apart and the force is measured by a load cell connected to one of the plates. Due to no slip occurring at the plates, a uniform deformation along the axis of extension cannot be achieved. This effect is particularly important during the start–up of the flow and gives rise to non–uniform radial and axial stress distributions. However, the experimental works of Spiegelberg *et al.* (1996) and the numerical investigations by Kolte *et al.* (1997) showed that ideal uniaxial flow is achieved when a constant rate of strain is prescribed at the axial mid–plane of the filament. Unfortunately, predicting a plate motion that achieves constant rate of strain at the mid–plane involves a complete knowledge of the constitutive behavior of the fluid. Thus, uniaxial extension data can be obtained by a trial–and–error procedure [Orr and Sridhar (2011)], which is tedious, sometimes not convergent and may not be feasible when the amount of sample is limited, or by implementing an active control system that prescribes the plate motion based on the continuous monitoring of the mid-filament diameter. The first and (to our knowledge) only control scheme presented in the literature to date is by Anna *et al.* (1999). In their work the authors employed a PID controller as a feedback mechanism. The control scheme of Anna *et al.* (1999) aimed at probing the extensional rheological properties of Boger fluids for a range of strain rates from 1 to 5 s^{-1}.

The first measurements on polymer melts in a FSR were presented by Bach *et al.* (2003b). The melts were two types of commercial low–density polyethylene. No active control was used in those tests and the prescribed plate motion was obtained by iterative trial–and–error for each of the rates of strain. Following these experiments, a successful implementation of an active control scheme permitted the characterization of narrow molecular weight distribution polystyrene [Bach *et al.* (2003a)] within a strain rate interval of 0.0003–0.3 s^{-1} with deviations in the diameter below 2% with respect to the targeted profile. While the control algorithm was not explicitly reported, it has been utilized subsequently in measurements of steady state viscosity of low–density polyethylene (LDPE) [Rasmussen *et al.* (2005)], stress relaxation after cessation of uniaxial flow [Nielsen *et al.* (2008)], and reverse flow experiments [Nielsen and Rasmussen (2008); Rasmussen *et al.* (2007)]. In addition, the method could be easily

applied to soft polymeric networks [Bejenariu *et al.* (2010)]. In a separate development, Bischoff White *et al.* (2012) presented elongational data of polypropylene melts obtained by feedback control with deviations as high as 10% in diameter for a strain rate of 1 s^{-1}.

In this work we present the details of a control scheme that allows us to control the kinematics of polymer melts in a filament stretching rheometer. It is based upon the work of Bach (2003) and consists of a combination of feed–back and feed–forward control. This control scheme does not prevent cohesive failure in a material. The performance of the control loop working in a controlled strain rate mode is demonstrated on a commercial grade low–density polyethylene. This control scheme is extended to a controlled stress mode for creep measurements in Chapter 9.

2.2 Uniaxial Extension

Standard flows are divided into shear and shearfree flows [Bird *et al.* (1987)]. Uniaxial extension falls under the category of shearfree flows. Similarly as mentioned in Section 1.2.1 of Chapter 1, the relative motion between particles of a fluid undergoing homogeneous uniaxial extension is described in cylindrical coordinates by the following velocity field assuming incompressibility

$$v_r(t) = -\frac{1}{2}\dot{\epsilon}(t)r \tag{2.1a}$$

$$v_z(t) = \dot{\epsilon}(t)z, \tag{2.1b}$$

where $\dot{\epsilon}(t)$ is the instantaneous rate of extension. Re–formulating Eqs.2.1a and 2.1b in terms of the evolution of a fluid particle position gives

$$r(t) = r(t')\exp\left(-\frac{1}{2}\epsilon(t',t)\right) \tag{2.2a}$$

$$z(t) = z(t')\exp\left(\epsilon(t',t)\right), \tag{2.2b}$$

where $\epsilon(t,t')$ is the strain experienced by a fluid element from time t' to t and is given by

$$\epsilon(t',t) = \int_{t'}^{t} \dot{\epsilon}(t'')\mathrm{d}t''. \tag{2.3}$$

For polymer melts subject to a deformation, the stress calculated at an arbitrary time t is a function of the whole deformation history. The implicit logarithmic definition of the strain in Eqs.2.1a and 2.1b results in a consistent way of describing the strain path experienced by a fluid element and is referred to as the Hencky strain. For flows at a constant rate of extension ($\dot{\epsilon}$), the Hencky strain is given by

$$\epsilon(t', t) = \dot{\epsilon} \cdot (t - t'). \tag{2.4}$$

Due to the lack of uniformity of the flow along the axis of extension inherent to FSRs, a definition of the strain based on the diameter at the mid–plane of the filament, ϵ, and a strain definition based on the relative plate position, ϵ_z, are not the same and are defined as

$$\epsilon = -2 \ln\left(\frac{D(t)}{D_0}\right) \tag{2.5a}$$

$$\epsilon_z = \ln\left(\frac{L(t)}{L_0}\right), \tag{2.5b}$$

where L_0 and D_0 are the initial length and diameter of the filament and $L(t)$ and $D(t)$ are the length and the diameter of the filament at time t. In control language, ϵ is the controlled variable and ϵ_z is the actuated variable.

2.3 Filament Stretching Rheometer and Constant Rate of Strain Extension

The first uniaxial constant extension rate experiments using a FSR were reported by Tirtaatmadja and Sridhar (1993) for dilute polymer solutions. The methodology consisted of determining the time–dependent velocity function that led to the desired exponential decrease in the mid–filament diameter using a trial–and–error approach. However, the methodology was cumbersome and susceptible to errors in the strain rate. Orr and Sridhar (2011) proposed a more consistent approach to obtain uniaxial data. A sample was stretched by moving the plates apart at a constant rate of strain, $\dot{\epsilon}_z$, while the mid–plane diameter was monitored. The resulting diameter profile was fitted to an arbitrary function and inverted so that the following relationship was obtained

$$\frac{L(t)}{L_0} = g\left(\frac{D_0}{D(t)}\right). \tag{2.6}$$

Thus Eq. 2.6 would provide the plate trajectory that renders the desired diameter evolution provided the function g does not depend on the strain rate. Discrepancies in the diameter are eliminated by iterative tests. For the Boger fluids investigated by Orr and Sridhar (2011) and the strain rate interval employed (2–4 s^{-1}), Eq.2.6 manifested a low sensitivity to changes in the strain rate and therefore was referred to as a *kinematic master curve*. Overall, the approach may be understood as an open loop control scheme, i.e. an experimental recipe constructed from an iterative procedure. The kinematic curve given by Eq.2.6 is fundamentally different for dilute solutions and melts [Bach *et al.* (2003b)]. In addition, melts are very sensitive to changes in the strain rate and consequently applying the method of Orr and Sridhar (2011) becomes a laborious process [Bach *et al.* (2003b)]. Another major limitation to this method is the requirement of Eq.2.6 to be monotonic, which we will show in the next sections does not hold for all polymer melts. Therefore, this method is not readily applied to polymer melts.

The first attempt to obtain systematic measurements in a FSR using a closed loop control scheme was done by Anna *et al.* (1999). A real time feed–back control loop was implemented to impose uniaxial extension in the mid–filament plane. A digital PID controller was used to calculate the position of the plates based on the continuous sampling of the mid–filament plane carried out by a digital laser micrometer. The controller computed a *desired* diameter (D_{cmd}) at a time step $i + 1$ using the following position algorithm

$$D_{cmd}(i+1) = D_{ideal}(i+1) + K_p \delta D(i) + K_i \Delta t \sum_{k=0}^{i} \delta D(k) + \frac{K_d}{\Delta t} \left[\delta D(i) - \delta D(i-1)\right], \quad (2.7)$$

where Δt is the actuation time step and the contributions from proportional, integral and derivative terms are tuned by varying K_p, K_i and K_d respectively. The error in the diameter is represented by $\delta D = D_{ideal} - D_{meas}$. In this scheme, the *desired* diameter must be converted into a distance between plates using a kinematic relationship such as Eq. 2.6. Using a 1–dimensional filament slender theory, Anna *et al.* (1999) proposed the following local kinematic relationship

$$L_p(i+1) = L_p(i) \left[\frac{D_{meas}(i)}{D_{cmd}(i+1)} \right]^{p(i)} \quad (2.8)$$

where the evolution of $p(i)$ must be determined for different materials, rates of extension, and Hencky strains. This scheme has three parameters and one parametric function. The latter is related to the fluid while the other three are the controller gains which are highly correlated and difficult to determine for this operation. Furthermore,

the algorithm includes the derivative part of the PID controller which makes the algorithm very sensitive to noise. The control scheme proved unstable producing large oscillations in the force measurements. According to the authors, small fluctuations about the set point diameter were propagated and amplified in the plate motion.

2.4 Control Scheme For Polymer Melts

While most standard control theory focuses on processes where the goal is to reach or preserve a stationary set point, the uniaxial stretching of a filament requires a continuous update of the set point. In the scheme proposed here, the motion of the plates is commanded by a control scheme that combines feed–forward and feed–back actions. The feed–back contribution is a digital PI controller. The feed–forward part is introduced to account for the change in the set point with time. By definition the feed–forward contribution must contain information about the kinematics of the mid–filament diameter. Since the feed–forward action provides a prediction for the needed actuation, we have chosen to exclude the derivative term in the feed–back loop. Omitting the derivative term provides a smoother controller scheme since it is well known that derivative action is sensitive to measurement noise. Unlike in the case of Anna *et al.* (1999), we have chosen to cast the control scheme in terms of Hencky strain. Thus, the plate motion at time step $i + 1$ is determined by the following equation

$$\epsilon_z(i+1) = \epsilon_z(i) + \Delta\epsilon_z^{ff}(i) + K_p\left[\delta\epsilon(i) - \delta\epsilon(i-1)\right] + K_i\Delta t\left[\delta\epsilon(i)\right], \tag{2.9}$$

where ϵ and ϵ_z are the Hencky strain definitions given in Eq.2.5, $\Delta\epsilon_z^{ff}$ is the feed–forward contribution, and the error $\delta\epsilon$ is calculated as follows

$$\delta\epsilon(i) = \epsilon_{ideal}(i) - \epsilon_{meas}(i) = 2\ln\left(\frac{D_{meas}(i)}{D_{ideal}(i)}\right). \tag{2.10}$$

The feed forward increment in eq.(2.9) is calculated as follows

$$\epsilon_z^{ff}(i) = f(\epsilon(i+1)) - f(\epsilon(i)) \tag{2.11}$$

where $f(\epsilon)$ is a guess for the relationship of Eq.2.6 recast in terms of strain. Apart from the inclusion of the feed–forward term, this scheme has two important differences with respect to Eq.2.7. First, the implementation in Eq.2.7 corresponds to a position algorithm whereas Eq.2.9 is a velocity algorithm. A velocity algorithm is simpler to

apply and uses the current error during an experiment, not the full sum of all control errors. Second, the incremental algorithm is cast in terms of strain, rather than plate separation and diameter, providing a more linear dependency between controlled and actuated variables. Since we rely on linear control theory, this ensures a more stable and satisfactory performance of the controller. Controlling the strain also allows for a plausible model for the feed-back term. Overall, this algorithm eliminates the need for an uncertain relation between diameter and plate separation and instead moves the uncertainty to the PI controller and its tuning.

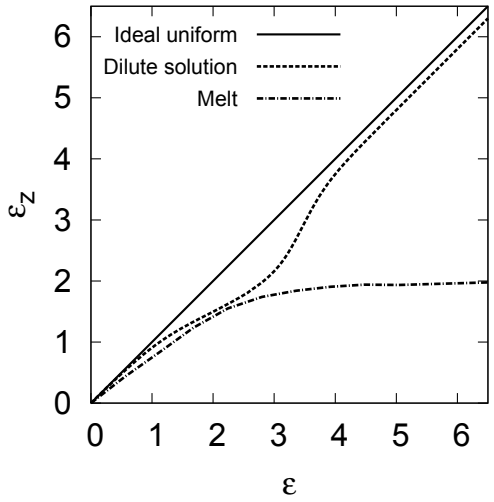

Figure 2.1: Examples of axial strain evolutions causing constant rate of strain deformation in the mid–filament for a dilute solution and a melt.

The feed–forward term in Eq.2.11 demands the selection of a function that describes the kinematics. A typical relationship between ϵ_z and ϵ for two types of fluids is shown in Figure 2.1. A simple function with two parameters that captures the slope (α) at small strains and the plateau region at high strains (d) shown in Figure 2.1 for a polymer melt is given by

$$\epsilon_z^{ff} = f(\epsilon) = \frac{\alpha\epsilon d}{\alpha\epsilon + d}. \tag{2.12}$$

In all experiments, Eq.2.12 is used, where $\alpha = 1$ and $d = 2.5$. The response of this function is evaluated by conducting an experiment for a constant strain rate of 0.03 s^{-1} with no feed–back action. The results are shown in Figure 2.2. The solid line in Figure 2.2 represents the ideal path. When no feed–back action is applied, a slow

non–exponential decrease of the effective diameter is observed. For comparison, we also plot the evolution of the diameter corresponding to an exponential plate separation in time, $\dot{\epsilon}_z = 0.03\ s^{-1}$. In this case, the effective diameter decreases much faster than targeted and the filament eventually fails. The disparity in Figure 2.2 between Eq.2.12 and the actual kinematic curve is to be corrected by the feed–back action.

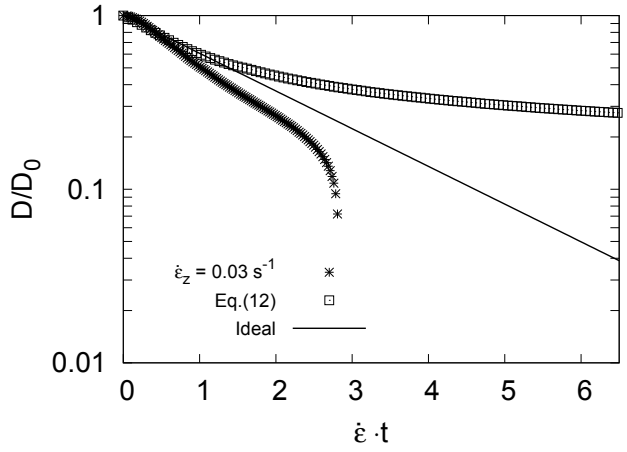

Figure 2.2: Effect of the feed–forward term in the evolution diameter of LDPE3020D in the absence of feed–back control. The targeted effective diameter decays exponentially at $\dot{\epsilon} = 0.03\ s^{-1}$. The evolutions of the mid–filament diameter for a plate motion profile following Eq.2.12, with $\alpha = 1$ and $d = 2.5$ (⊡), and following an exponential separation in time $\dot{\epsilon}_z = 0.03\ s^{-1}$ are presented.

Typically, tuning a feed–back controller requires or implicitly assumes a model describing the dynamical behavior of the process [Seborg *et al.* (2004)]. Unfortunately due to the unknown kinematics, we do not possess this information a priori. Furthermore, the vast majority of tuning techniques are developed for continuous processes with a fixed set point. Recall that in our case the set point is changing with time. Due to the moving set point a fast response is beneficial. The actuation time of our system is $\Delta t = 4$ ms, which corresponds to the fastest actuation our current setup can support.

The scheme proposed is both simple and robust towards measurement noise in the apparatus. The model needed for the feed–forward part is qualitatively well–founded for the fluids under consideration here and only contains two parameters. Likewise, the feed–back term is dependent on two parameters which determine how aggressively the control will attempt to reduce the error observed in Figure 2.2. The tuning of these parameters most likely depends on both the fluid and the operation of the apparatus.

2.5 Apparatus

The vertical FSR used here was first constructed and adapted to melts by Bach *et al.* (2003a,b). A detailed description of the oven design and the mechanical motion may be found in the work of Bach *et al.* (2003b). In this section, a brief description of the parts involved in the measurement and control is given.

The apparatus consists of a stationary bottom plate and a mobile upper plate. The bottom plate is mounted onto a tension/compression Futek lrf400 load cell with a capacity of 4.5 N and a 0.05% error rated on the maximum capacity for non–linearity and hysteresis. The output signal is amplified to $\pm 10\,V$ and collected by the data acquisition system. The weight cell is located outside the thermostated environment. The translation of the upper plate is achieved by a step motor (Stebon FDT603) with a step drive (Parker OEM650). The rotational motion of the motor is converted into translational motion by a reinforced belt system. A second belt system holding the laser micrometer is positioned in the mid–plane separation between upper and bottom plates and translated at half of the speed of the upper plate so that it follows the mid-filament diameter during the extension. The linear motion of the plates is determined by the rotation of the motor, which is monitored by an encoder. The diameter of the mid-filament is measured in real-time by a Keyence LS7500 digital micrometer. The accuracy in diameter is approximately $\pm 10\,\mu m$. The laser micrometer has a lower limit of 0.3 mm. Using our apparatus with an initial sample diameter of 9 mm, the maximum attainable Hencky strain is ~ 6.8.

The control of the step motor and the sampling are performed by a cRIO–9022 purchased from National Instruments. The controller commands the motion of the step motor through an interface module NI-9512 and carries out the data acquisition using a 16–bit $\pm 10\,V$ analog to digital converter NI–9205. The related programming is done in Labview.

2.6 Materials and Sample Preparation

The control scheme is tested and validated using Lupolen 3020D, a commercial grade low–density polyethylene supplied by BASF. The samples were prepared by hot pressing the polymer into cylindrical pellets of 9 mm diameter and 2.5 mm height at 140°C for 10 minutes and then allowed to slowly cool. The same batch was previously characterized in a FSR by Rasmussen *et al.* (2005) and more recently by Huang *et al.* (2012). The force measurements shown here are consistent with those obtained in both works. All experiments presented here were performed at 130°C. The samples were loaded on the bottom plate of the rheometer and brought into contact with upper plate after it

reached 130°C. Stresses induced in the sample by this operation are monitored by the weight cell and the sample is always allowed to completely relax before initiating the experiment.

2.7 Results and discussion

The PI controller was tuned by systematically varying the gains in a series of experiments conducted $\dot{\epsilon}$ =0.03 s^{-1}. Using stand–alone proportional and integral actions and a combination of both, we evaluate the performance of the control scheme. In these experiments, we use Eq.2.12 for the feed–forward kinematic expression. After tuning the controller, we investigate the effects of the feed–forward term on the control of the kinematics as well as the performance of the controller at higher strain rates.

The proportional controller acts linearly on the current error and is regulated by the gain K_p. Figure 2.3 shows the evolution of the mid–filament diameter for experiments using only the proportional controller for four values of K_p. By gradually varying the gain from 0 to 5 we show the performance of the stand–alone proportional controller in achieving a satisfactory effective diameter. It is clear from Figure 2.3 that low values of the gain ($K_p < 1$) do not drive the diameter to the set point. When the gain is increased, $K_p \geq 1$, the plate motion becomes oscillatory and unstable. This behavior is more clearly seen in Figure 2.4 where the deviation from the targeted diameter is plotted as fractional error for the four different gains.

The integral term is built on the cumulative error of the process and is often used to eliminate the residual offset inherent to the proportional action. Figure 2.5 shows the evolution of the diameter for different values of the integral gain and $K_p = 0$. Unlike in the proportional control scheme, the diameter is always driven to the set point. Fig.2.6 offers a more comprehensive picture of the performance of this controller. Small values of the integral gain ($K_i < 1$ s^{-1}) result in a slow response and deviations up to 10%. Intermediate values of the integral gain ($1 \leq K_i \leq 2$ s^{-1}) accomplish a very satisfactory control of the effective diameter in terms of accuracy, with a maximum deviation below 1%, and stability during the entire accessible window of strain in this apparatus. When the integral gain is increased ($K_i = 10$ s^{-1}), the controller produces continuous oscillations around the set point from the start-up of the experiment until it becomes unstable at Hencky strain values near 4. These oscillations also affect severely the quality of the force measurements. The upturn observed in Figures 2.6(a)–(d) at $\dot{\epsilon} \cdot t \approx 0$ is due to slack in the belts when the motor initiates.

The resulting kinematic curve for LDPE3020D at $\dot{\epsilon} = 0.03 s^{-1}$ is shown in Figure 2.7(a). The kinematic curve is plotted along with Eq.2.12 and the plate motion for an ideal uniform deformation of the filament. The difference between Eq.2.12 and the kinematic

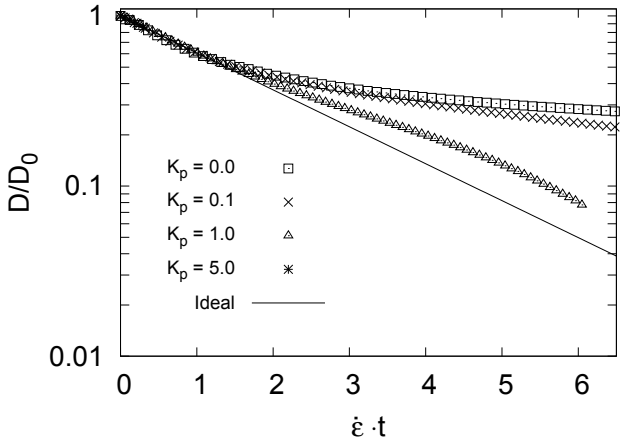

Figure 2.3: Effect of the proportional gain on the diameter control of the LDPE samples. Only proportional control is employed (K_i =0 s^{-1}) . The imposed strain rate ($\dot{\epsilon}$) is 0.03 s^{-1}. The kinematic curve used in the feed-forward term is given by Eq.2.12.

curve measured demonstrates the fundamental role of the feed–back control on achieving the desired kinematics. It is important to note that there exists a maximum in the measured kinematic curve in Figure 2.7(a). This maximum is usually associated with the existence of an instability and leads to a failure in the sample in integral techniques. Without the feed–back term, the control of the filament for $\epsilon > 4$ is not possible. The uncorrected stress growth coefficient Rasmussen *et al.* (2010) across the mid–plane diameter is presented in Figure 2.7(b) and is calculated as

$$\eta^{+} = \frac{F(t)}{(\pi/4)D(t)^2\dot{\epsilon}}, \tag{2.13}$$

where $F(t)$ is the force increment respect to $\dot{\epsilon} \cdot t = 0$ measured at the bottom end plate during the experiment. In order to obtain a correct measurement, the LDPE sample must be allowed to completely relax before initiating the experiment. A wavelet treatment for noise reduction Huang *et al.* (2012) was applied to the force measurements.

Figure 2.8 shows the combined effect of proportional and integral actions for a fixed K_i and a varying K_p. It is clear from Figure 2.8(a)–(d) that there is no significant change in the error when $K_p \neq 0$. In fact, the inclusion of a large proportional gain, $K_p = 1.0$, reduces the achievable Hencky strain due to the onset of oscillations in the plate motion. Compared to the rate of deformation, the actuation and sampling are so fast that high frequency components of the analog signal noise are captured,

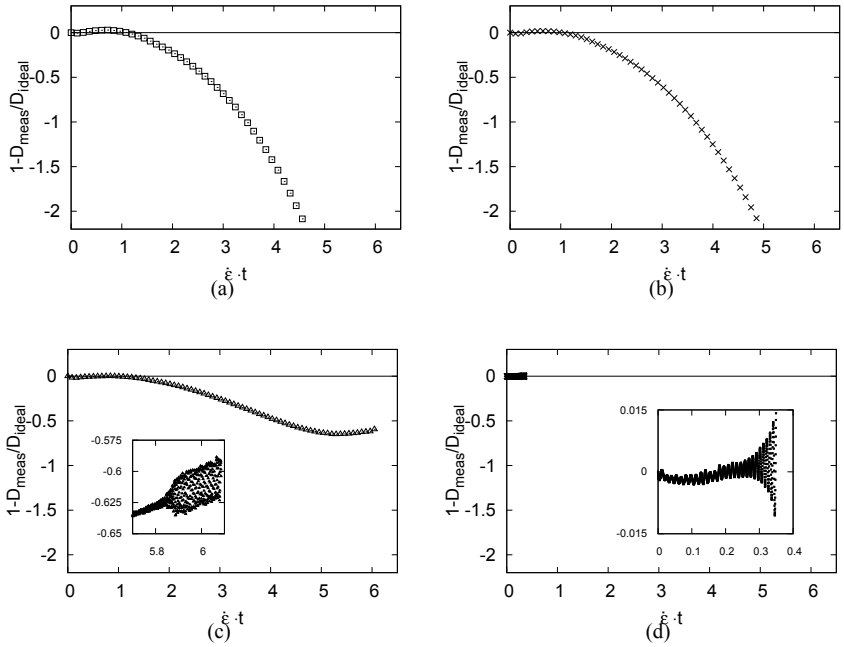

Figure 2.4: Fractional error of the controlled diameter for the experiments shown in Figure 2.3. (a) $K_p = 0.0$, (b) $K_p = 0.1$, (c) $K_p = 1.0$, (d) $K_p = 5.0$.

undermining the performance of the controller. Based on our configuration and the results presented here, the stand–alone integral controller provides the most satisfactory combination of accuracy and stability in the measurements. For this reason we adopt this configuration even though the detuning of the proportional action is not customary in linear control theory.

To investigate the influence of the feed–forward term on the integral controller, we fix $K_i = 2.0\ \mathrm{s}^{-1}$ (cf. Figure 2.6(c)) and the parameters in Eq.2.12 are modified so that two limiting cases are considered. In the first case the feed–forward contribution is omitted by setting $\alpha = 0$ and in the second case a constant rate of axial strain is prescribed to the plates by selecting $d >> \alpha\epsilon$ and $\alpha = 1$. The fractional error for the new feed-forward expressions is shown in Figure 2.9. Both experiments produce satisfactory diameter profiles with deviations below 1%. Omitting the feed–forward term provides no approximation to the kinematic curve during the start–up and induces a small offset error that is not eliminated until the kinematic curve reaches a plateau. Conversely, setting $f(\epsilon) = \epsilon$ leads to a better approximation during the start–up but gives rise to a small constant offset error as the plateau is attained, which eventually leads to the onset of oscillations in the plate motion. Both experiments shown in Figure 2.9 produced similar stresses measurements while the control remained stable. Thus, a

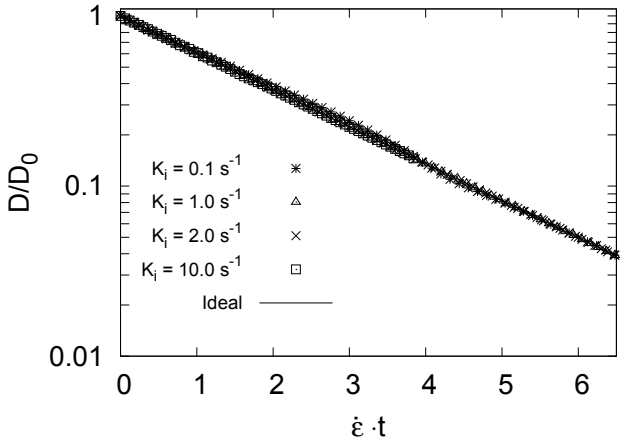

Figure 2.5: Effect of the integral gain on the diameter control of the LDPE samples. The controller is strictly integral (K_p= 0). The imposed strain rate is ($\dot{\epsilon}$) 0.03 s^{-1}. The kinematic curve used in the feed-forward term is given by Eq.2.12.

poor choice of a feed–forward term does not have a dramatic impact on the accuracy of the controlled diameter but may induce an instability if the predicted trend in the feed-forward term opposes the one of the actual kinematics of the material.

Since there is a connection between actuation time and controllable rate of strain, we examine the performance of the control algorithm at higher strain rates, i.e. $\dot{\epsilon}$ =0.1 s^{-1} using the optimal control parameters determined for 0.03 s^{-1}. Figure 2.10 shows the fractional error for $\dot{\epsilon}$ =0.1 s^{-1} and the resulting stress. In Figure 2.10(a), the fractional error at low and moderate strains increases but the overall accuracy of the diameter remains below 2% and the control is stable. In order to achieve as good a performance as in $\dot{\epsilon}$ = 0.03 s^{-1}, a faster actuation or a more aggressive integral action is needed. Since our system does not support faster actuations than 4 ms, the integral gain was re-scaled by a factor of ≈ 3.3 corresponding to the increase in rate of deformation. The resulting fractional error is shown in Figure 2.11(a). For $\dot{\epsilon} \cdot t < 3.5$, the fractional error is reduced compared to fig.2.10 and is comparable to the error shown in Figure 2.6(c). For $\dot{\epsilon} \cdot t > 3.5$, the feed–back regulation is too aggressive provoking unstable oscillations in the plate motion.

These test suggest that as the filament thins it exhibits more sensitivity to the control action and therefore a modulation of the integral gain is required. We illustrate this approach by using a simple continuous sigmoid function to generate a smooth transition

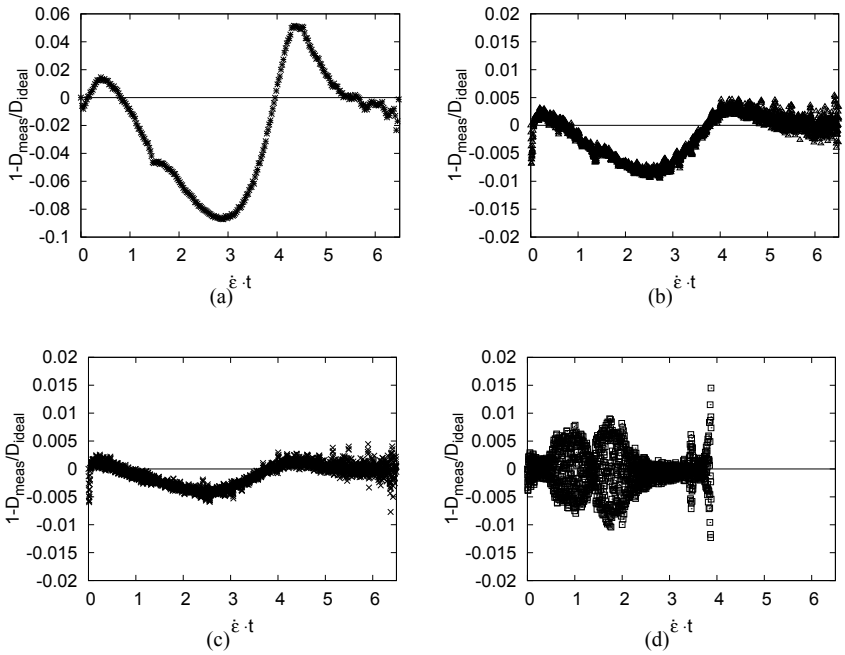

Figure 2.6: Fractional error of the controlled diameter for the experiments shown in Figure 2.5. (a) $K_i = 0.1$ s^{-1}, (b) $K_i = 1.0$ s^{-1}, (c) $K_i = 2.0$ s^{-1}, (d) $K_i = 10.0$ s^{-1}. Note that the scale in case (a) is different from the rest of the experiments.

in the gain from 6.6 to 2 s^{-1} as a function of the Hencky strain

$$\frac{K_i(\dot{\epsilon}_{exp})}{K_i(\dot{\epsilon}_{ref})} = 1 + \left[\frac{\dot{\epsilon}_{exp}}{\dot{\epsilon}_{ref}} - 1\right] \frac{arccot(\epsilon - \epsilon_0)}{\pi}, \tag{2.14}$$

where $\dot{\epsilon}_{ref}$ is any strain rate that provides an accurate and stable control of the effective diameter, $\dot{\epsilon}_{exp}$ is the applied strain rate, and ϵ_0 sets the strain interval over which the transition occurs. The selection of the parameter ϵ_0 in Eq.2.14 is based on the information provided in Figure 2.11(a), namely the Hencky strain where the oscillations begin. The results using Eq.2.14 are presented in Figure 2.12. The overall accuracy is maintained with respect to that shown in Figure 2.11(a) and the stability is preserved during the experiment. This simple approach allows for melts to be probed at higher deformation rates without losing accuracy or duration of the stability.

Finally, we illustrate the dependency of the kinematics on the rate of deformation by showing the kinematic curve obtained at $\dot{\epsilon} = 0.1$ s^{-1} in Figure 2.12(c) so that the reader can evaluate the difference with Figure 2.7(a).

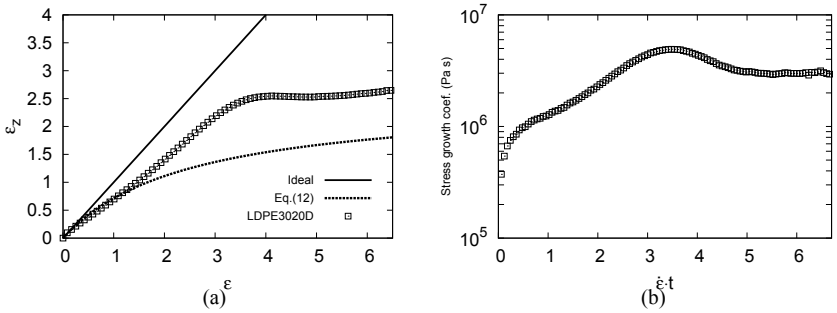

Figure 2.7: Kinematic curve (a) and uncorrected stress growth coefficient (b) corresponding to the experiment shown in Figure 2.6(c).

2.8 Conclusions

We have presented a robust algorithm for controlling the kinematics of a filament stretching rheometer using a combination of pure integral feed–back and a simple feed–forward control. The feed–back scheme is cast as a velocity algorithm and uses ϵ and ϵ_z as the controlled and actuated variables, respectively. A pure integral controller provides the most satisfactory performance maintaining the maximum deviation in the controlled diameter below 2% without inducing oscillations. At high Hencky strains, aggressive control actions result in loss of stability and consequently a modulation of the integral gain may be required as the rate of strain is increased. The implementation of feed–forward is not mandatory for success, but when well represented will reduce the error and eliminate oscillations in the plate motion. This control scheme is extended to a controlled stress mode for creep measurements in Chapter 9.

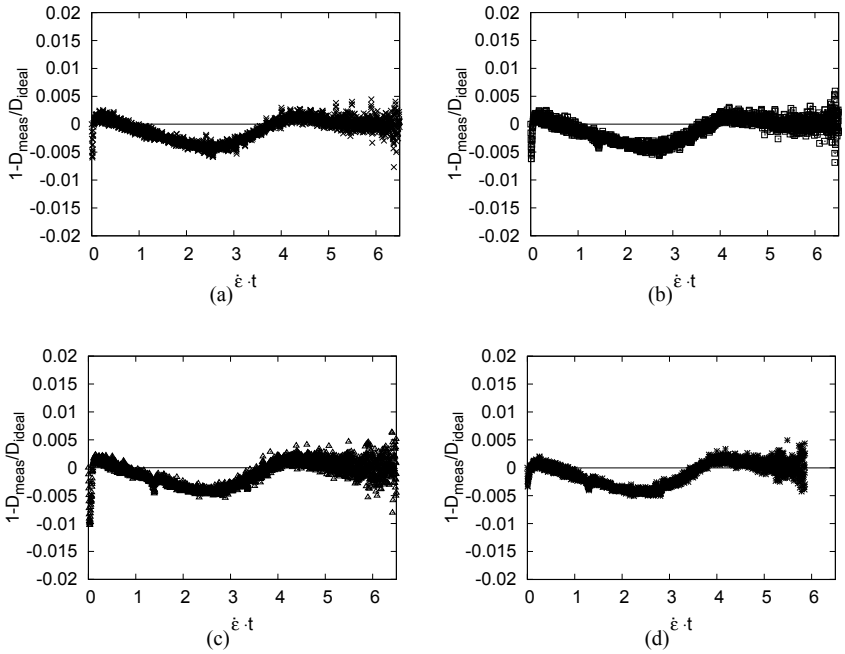

Figure 2.8: Fractional error of the controlled diameter for experiments using proportional and integral control. The proportional gain is varied while the integral gain is kept constant at $K_i = 2.0s^{-1}$. (a) $K_p = 0.0$, (b) $K_p = 0.1$, (c) $K_p = 0.3$, (d) $K_p = 1.0$.

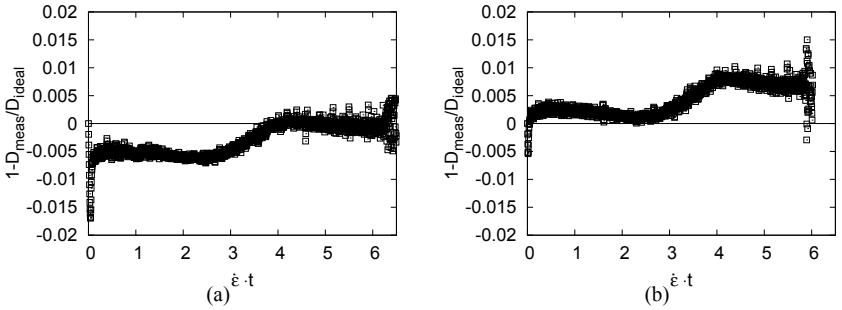

Figure 2.9: Fractional error for two different kinematic functions: (a) $f(\epsilon) = 0$, (b) $f(\epsilon) = \epsilon$. The experiments were carried out at 0.03 s^{-1} using pure integral control ($K_i = 2.0\ s^{-1}$).

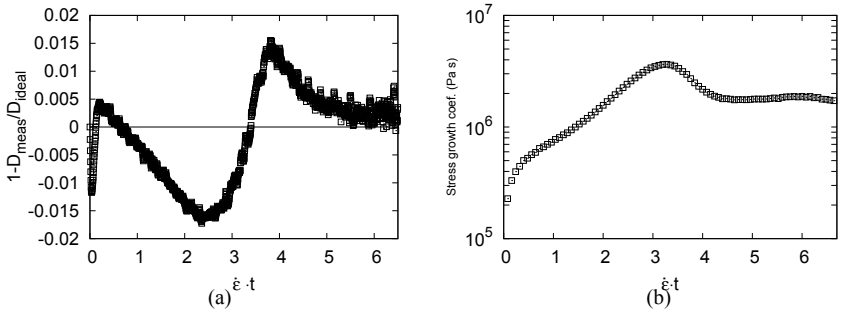

Figure 2.10: LDPE3020D tested at $\dot{\epsilon} = 0.1s^{-1}$. The controller settings are identical to those used in Figure 2.6(c). (a) fractional error, (b) uncorrected stress growth coefficient.

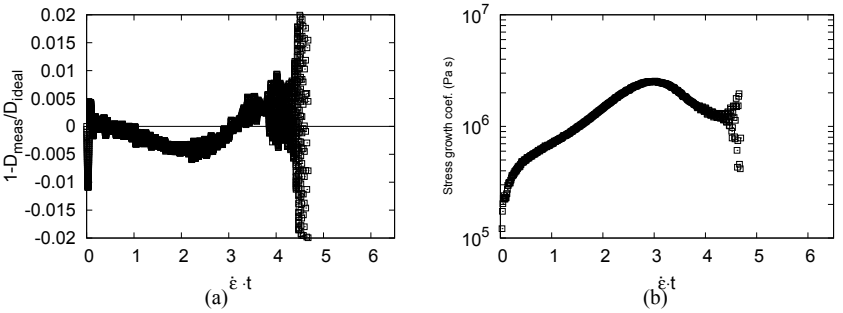

Figure 2.11: LDPE3020D tested at $\dot{\epsilon} = 0.1s^{-1}$. The controller settings are $K_p = 0$ and K_i=6.6 s^{-1}. (a) fractional error, (b) uncorrected stress growth coefficient.

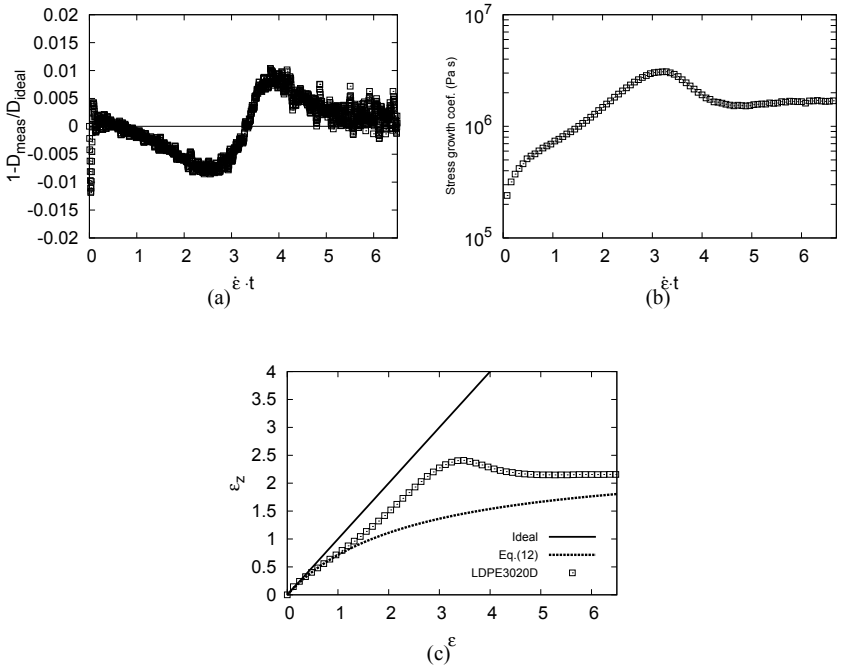

Figure 2.12: LDPE3020D tested at $\dot{\epsilon}$ =0.1 s^{-1}. The controller settings are $K_p = 0$ and K_i modulated between 6.6 and 2.0 s^{-1} using Eq.2.14 with $\epsilon_0 = 2.2$. (a) fractional error, (b) uncorrected stress growth coefficient, (c) kinematic curve.

Chapter 3

Are Entangled Polymer Melts Different from Solutions: Role of Entanglement Molecular Weight

3.1 Introduction

The possible existence of a qualitative difference on extensional steady state viscosity between polymer solutions and melts is still an open question. Experiments on entangled polystyrene solutions [Bhattacharjee *et al.* (2002)] showed that the extensional steady state viscosity initially decreased with increasing the strain rate; but when the strain rate became higher than the order of inverse Rouse time, it started to increase. In contrast, experiments on entangled polystyrene melts [Bach *et al.* (2003a); Luap *et al.* (2005)] showed that the extensional steady state viscosity decreased monotonically even at the strain rate higher than the inverse Rouse time with similar number of entanglements per chain. Such contradiction also exists in model predictions. The tube model [Bhattacharjee *et al.* (2002)] that includes the mechanisms of chain stretch and convective constraint release was capable of describing the behavior of the polystyrene solutions. However, it could not capture the monotonic thinning behavior of polystyrene melts. The interchain pressure model [Wagner *et al.* (2005)] captured the monotonic thinning of polystyrene melts. However, it did not specify the difference between melts and solutions.

When an entangled polymer melt is diluted in some solvent, one obvious change is that the number of entanglements per chain Z decreases and the entanglement molecular weight M_e increases. Since M_e directly relates to the tube diameter in the tube model [Doi and Edwards (1986)], the increase of M_e results in the dilation of the tube. In the previous work, the dynamic tube dilation (DTD) mechanism, which is intimately related to the double reptation mechanism, has been investigated both theoretically and experimentally for polymer blends consisted of long and short chains. For example, Watanabe *et al.* (2004) tested the molecular picture of DTD for viscoelastic and dielectric data of two binary blends of linear *cis*–polyisoprenes. This data was subsequently reanalyzed by Ruymbeke *et al.* (2012) to determine the value of the dilution exponent. Wagner (2011) also evaluated the effect of DTD on chain stretch in nonlinear rheology of polymer melts. In his work a modified molecular stress function model was proposed and it well predicted the extensional steady–state viscosity of three polystyrene blends measured by Nielsen *et al.* (2006a). Recently Read *et al.* (2012) proposed a full–chain constitutive model which with some success captured the linear and nonlinear rheology of the bimodal blends when compared with the experimental data of six series of polyisoprene blends as well as two series of polystyrene blends. This model included all the frequently used contributions for reptation, constraint release, contour length fluctuation and stretch relaxation into a physical picture of thin and fat tubes. A thin tube representing entanglements with both long and short chains and a fat tube representing entanglements with other long chains only. It can be easily imagined that if the short chains in a binary blend are short enough and not entangled with each other, the thin tube disappears and the blend is equivalent to a polymer solution. However, in all of the reported binary blends above, the short chains are entangled with each other and can not be directly related to the case of polymer solutions. Auhl *et al.* (2009) studied some bimodal blends of linear polyisoprene melts in which the short chains are not entangled. However they only reported the measurements of such blends in shear rheology. The short chains in the blends that they reported in extensional rheology are still highly entangled. Moreover, none of their extensional experiments reached the steady–state region. And the weight fraction of the long chains in their bimodal blends was limited to the semi–dilute region where the hydrodynamic interaction may still be present.

Besides the influence of tube dilation, another effect of increasing M_e is the increase of finite chain extensibility. Due to the maximum stretch ratio $\lambda_{\max} = \sqrt{N_e}$, where N_e is the number of Kuhn steps per entanglement, the solutions which have larger values of M_e can be stretched to larger ratios than their relative melts. However, none of the above models took account of this effect. Yaoita *et al.* (2011) put the finite extensibility in the primitive chain network simulation, but it could still not capture the monotonic thinning of polymer melts.

The purpose of the present work is to make well–defined experiments to directly evaluate the influence of M_e and N_e on the rheological behavior of entangled polymer melts and solutions. We carefully synthesized two nearly monodisperse polystyrenes

with molar masses of 285 and 545 kg/mole, respectively. We then prepared three binary blends from either of the two polystyrenes and a 2 kg/mole styrene oligomer. The chains of the oligomer are far below the entanglement molecular weight (M_e = 13.3kg/mol for polystyrene) and therefore the three blends are equivalent to solutions. The main reason that we choose a styrene oligomer as the solvent is because a polystyrene and a styrene oligomer have the same solubility parameters, and the interaction parameter χ for the system is thus minimized. The two melts and the three solutions are then measured in both shear and extensional flows. We will show the difference between the melts and solutions in nonlinear rheology which is directly related to their different M_e. We have also tried to use dibutyl phthalate (DBP), which is a commonly used good solvent for polystyrenes, to make the solutions. However, extensional measurements for these samples were failed.

3.2 Experimental Details

3.2.1 Synthesis and chromatography

The two polystyrenes PS-290k and PS-550k with narrow molecular weight distributions have been synthesized by living anionic polymerization according to the standard procedure [Ndoni *et al.* (1995)][1]. Sec-butyllithium was employed as the initiator, and the reaction was carried out for 3 hours at 30 °C. Size exclusion chromatography (SEC) was employed for samples characterization. The SEC system consists of a SIL-10AD injector (Shimadzu), a triple Viscotek detector and two PLgel Mixed C and Mixed D columns. Stabilized tetrahydrofuran (THF) was used as the eluent and the flow rates have been adjusted according to Irganox signals accurately. Glass transition temperature T_g was measured by the differential scanning calorimetry (DSC). The styrene oligomer OS-2k was bought from Sigma–Aldrich. Table 3.1 summarizes the weight average molecular weight M_w, the polydispersity index PDI and the T_g of the synthesized polystyrenes as well as the oligomer.

Table 3.1: The molecular weight and the glass transition temperature of the polystyrenes and the styrene oligomer

Sample Name	M_w[g/mol]	PDI	T_g[°C]
PS-550k	545000	1.12	106.5
PS-290k	285000	1.09	107.5
OS-2k	1920	1.08	60.5

[1] Synthesis and size exclusion chromatography for PS-290k and PS-550k were carried out by Olga Mednova at Department of Micro– and Nanotechnology, Technical Unicersity of Denmark

3.2.2 Preparation of solutions

The polystyrene solutions were made from either PS-290k or PS-550k diluted in OS-2k. The solutions were prepared by dissolving both the polystyrene and the oligomer in THF and stirring at room temperature overnight. When the components were well dissolved and mixed, the THF solution was cautiously put into methanol drop by drop and the blends were recovered by precipitation. Finally the blends were dried under vacuum at 50 °C for a week. Considering that the methanol may partly dissolve OS-2k during precipitation at room temperature, the concentrations of all the polystyrene solutions were determined by the peak areas of the bimodal curve in SEC. For each polystyrene solution, two randomly picked parts were checked in SEC in order to make sure the concentration is homogenous.

The entanglement molecular weight $M_{e,s}$ of the polystyrene solutions is calculated as [Bhattacharjee *et al.* (2002)]

$$M_{e,s} = M_{e,m}\phi^{-1}, \tag{3.1}$$

where $M_{e,m}$ is the entanglement molecular weight of the polystyrene melt and ϕ is the weight fraction of the polystyrene in the solution. Eq.3.1 is only valid for $c > 0.1\text{g/cm}^3$, where $c = \rho\phi$ and ρ is the density of the melt. The density of the polystyrene melts at 130 °C is $\rho = 1.008\text{g/cm}^3$ according to Mark (2006). The lowest concentration of the polystyrene solutions in this work is 44%. Therefore Eq.3.1 can be used for all the solutions here. We take $M_{e,m} = 13.3\text{kg/mol}$ for polystyrene melts as reported by Bach *et al.* (2003a). The number of entanglements per chain is calculated as $Z = M/M_e$, where M is the molecular weight of the polystyrene. The weight fraction ϕ, the glass transition temperature T_g, the entanglement molecular weight M_e and the number of entanglements per chain Z of the prepared solutions as well as of the two melts are listed in Table 3.2.

Table 3.2: The properties of the polystyrene melts and solutions

Sample Name	Components	ϕ[wt%]	T_g[°C]	Z	M_e[g/mol]
PS-550k	550k	100% 550k	106.5	41.0	13300
PS-290k	290k	100% 290k	107.5	21.4	13300
Solution-1	290k+2k	72%(±1%) 290k	94.0	15.4	18472
Solution-2	290k+2k	44%(±1%) 290k	85.0	9.4	30227
Solution-3	550k+2k	58%(±1%) 550k	91.0	23.8	22931

3.2.3 Mechanical spectroscopy

The linear viscoelastic (LVE) properties of the polystyrene melts and solutions were obtained from small amplitude oscillatory shear flow measurements. An 8mm plate–plate geometry was used on an ARES–G2 rheometer from TA instruments. The measurements for the two melts were performed at 130, 150 and 170 °C under nitrogen. Using the data, the temperature shift factor a_T was fitted to the WLF equation

$$\log_{10} a_T = \frac{-c_1^0 (T - T_0)}{c_2^0 + (T - T_0)}, \tag{3.2}$$

where $c_1^0 = 8.99$, $c_2^0 = 81.53$K, $T_0 = 130\,°C$, and T is temperature in °C. The measurements for the polystyrene solutions were performed at temperatures between 110 and 170 °C. The shift factor a_T for the solutions was not fitted to a single WLF equation but listed in Table 3.3 due to their different T_g. For each polystyrene sample, the data were shifted to a single master curve at 130 °C using the time–temperature superposition procedure.

Table 3.3: The temperature shift factor a_T for the polystyrene solutions

Sample Name	110 to 130 °C	120 to 130 °C	150 to 130 °C	170 to 130 °C
Solution-1	180.06	9.56	0.039	–
Solution-2	56.03	–	–	–
Solution-3	–	7.57	0.051	0.0058

3.2.4 Extensional stress measurements

The extensional stress of the polystyrene samples was measured by a filament stretching rheometer (FSR) equipped with an oven to allow measurements from room temperature to about 200 °C [Bach *et al.* (2003b)]. Before the elongational measurements, all the polystyrene samples were molded into cylindrical test specimens using a special mould with a fixed radius $R_0 = 2.7$mm. The mould was connected to a vacuum pump. The initial length L_0 of the cylindrical test specimens was controlled by weighing a proper amount of the samples before putting them into the mould. The L_0 of each cylindrical test specimen was varied between 1.3mm and 1.6mm, giving an aspect ratio $\Lambda_0 = L_0/R_0$ between 0.48 and 0.59. The polystyrene melts were pressed at approximately 150 °C and annealed at this temperature for 15min under vacuum to ensure that the polymer chains were completely relaxed. The polystyrene solutions were pressed at approximately 130 °C and annealed for 15min under vacuum as well. The samples

were checked by SEC again after the extensional stress measurements to ensure that there was no degradation or concentration change.

All the polystyrene samples were pre–stretched to a radius R_p ranging from 1.5mm to 2mm at either 160 °C (for the melts) or 140 °C (for the solutions) prior to the elongational experiments. After pre–stretching, the temperature was decreased to 130 °C for the extensional stress measurements of the melts. As for the solutions the temperature was decreased to either 110 °C or 120 °C according to their different T_g. Nitrogen was used in the whole procedure.

During the elongation, the force $F(t)$ is measured by a load cell and the diameter $2R(t)$ at the mid-filament plane is measured by a laser micrometer. At small deformation in the startup of the elongational flow, part of the stress difference comes from the radial variation due to the shear components in the deformation field. This effect may be compensated by a correction factor as described in Rasmussen *et al.* (2010). The Hencky strain and the mean value of the stress difference over the mid–filament plane are then calculated as

$$\epsilon(t) = -2\ln\left(R(t)/R_0\right) \tag{3.3}$$

and

$$\langle\sigma_{zz} - \sigma_{rr}\rangle = \frac{F(t) + m_f g/2}{\pi R(t)^2} \cdot \frac{1}{1 + \left(R(t)/R_0\right)^{10/3} \cdot \exp\left(-\Lambda_0^3\right)/\left(3\Lambda_0^2\right)}. \tag{3.4}$$

The strain rate is defined as $\dot{\epsilon} = d\epsilon/dt$. To approach a constant strain rate, the diameter at the mid–filament plane is required to decrease exponentially during stretching. A recently updated control scheme [Román Marín *et al.* (2013)] is employed in the FSR to ensure the accurate constant strain rate. The extensional stress growth coefficient is defined as $\bar{\eta}^+ = \langle\sigma_{zz} - \sigma_{rr}\rangle/\dot{\epsilon}$.

3.3 Results

3.3.1 Linear viscoelasticity

Figure 3.1 presents the LVE data fitted with the continuous Baumgaertel-Schausberger-Winter (BSW) relaxation spectrum [Baumgaertel *et al.* (1990)] of the two polystyrene

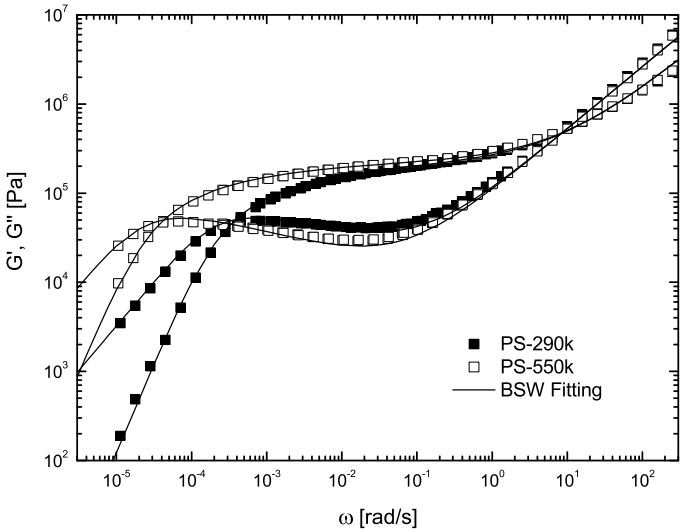

Figure 3.1: LVE data fitted with the BSW spectrum for PS-550k and PS-290k at 130 °C.

melts PS-290k and PS-550k. The LVE data and BSW fittings for the polystyrene solutions are shown in Figure 3.2. The relaxation modulus $G(t)$ is found from the continuous spectrum $H(\tau)$, given by

$$G(t) = \int_0^\infty \frac{H(\tau)}{\tau} \exp\left(-t/\tau\right) \mathrm{d}\tau, \tag{3.5}$$

$$H(\tau) = n_e G_N^0 \left[\left(\frac{\tau}{\tau_{\max}} \right)^{n_e} + \left(\frac{\tau}{\tau_c} \right)^{-n_g} \right] h\left(1 - \tau/\tau_{\max}\right), \tag{3.6}$$

where $h(x)$ is the Heaviside step function, n_e is the absolute value of the slope of the $[\log\omega\,,\log G'']$ curve at intermediate frequencies ω, n_g is the slope of $[\log\omega\,,\log G'']$ for $\omega \to \infty$, τ_c is the crossover relaxation time, and G_N^0 is the plateau modulus.

For the nearly monodisperse polystyrene melts and solutions, the values of n_e and n_g are fixed to 0.23 and 0.70, respectively [Jackson and Winter (1995)]. The value of G_N^0 for the melts is also treated as a fixed parameter. At 130 °C we use $G_N^0 = 250$kPa found by Bach *et al.* (2003a). The adjustable parameters τ_c and $\tau_{\max}$ for the melts are found

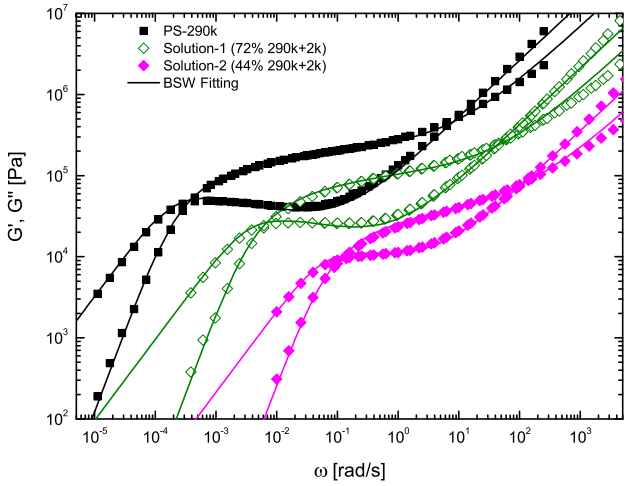

(a) LVE for PS-290k, Solution-1 and Solution-2

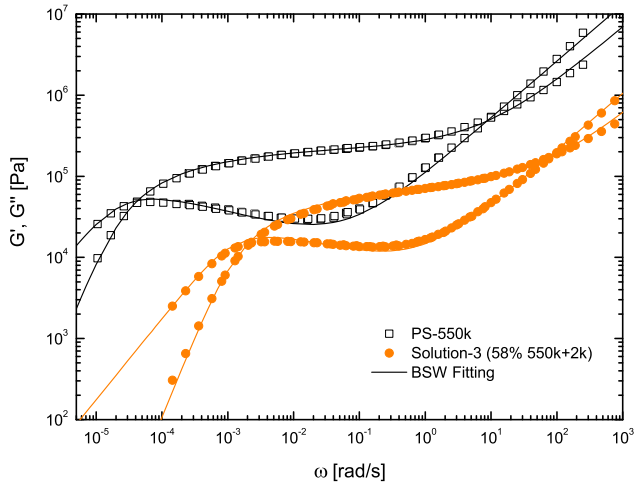

(b) LVE for PS-550k and Solution-3

Figure 3.2: LVE data fitted with the BSW spectrum for the polystyrene solutions at 130 °C.

by the least–squares fitting to the LVE data. Since the plateau modulus G_N^0 is defined as

$$G_N^0 \equiv \alpha \frac{cRT}{M_e}, \tag{3.7}$$

combined with Eq.3.1 we get

$$G_{N,s}^0 = \phi^2 G_{N,m}^0. \tag{3.8}$$

In Eq.3.7, α is a constant with a value of either 1 according to Ferry (1980) or 4/5 according to the Doi–Edwards (DE) model without the independent alignment assumption (IAA) [Doi and Edwards (1986)]. But this difference does not affect Eq.3.8 since we fix $\left(G_N^0\right)_{\text{melt}} = 250\text{kPa}$. Therefore for the solutions the remaining adjustable parameters are also τ_c and $\tau_{\max}$. They are again found by the least–squares fitting to the LVE data. The parameters of the BSW spectrum for all the polystyrene samples at 130 °C are given in Table 3.4. The zero shear rate viscosity is calculated as

$$\eta_0 = \int_0^\infty G(s)\mathrm{d}s = n_e G_N^0 \tau_{\max}\left(\frac{1}{1+n_e} + \frac{1}{1-n_g}\left(\frac{\tau_c}{\tau_{\max}}\right)^{n_g}\right), \tag{3.9}$$

which is also listed in Table 3.4.

Table 3.4: Material properties obtained from the BSW spectrum at 130 °C

Sample Name	n_e	n_g	G_N^0[Pa]	τ_c[s]	$\tau_{\max}$[s]	η_0[Pa · s]
PS-550k	0.23	0.7	250000	0.4	61540	$2.8796{\cdot}10^9$
PS-290k	0.23	0.7	250000	0.4	6890	$3.2352{\cdot}10^8$
Solution-1	0.23	0.7	129600	0.075	391.4	$9.5824{\cdot}10^6$
Solution-2	0.23	0.7	48400	0.024	22.83	$2.1359{\cdot}10^5$
Solution-3	0.23	0.7	84100	0.051	1113	$1.7569{\cdot}10^7$

Besides the parameters in Table 3.4, we would also like to estimate a time scale for stretch relaxation of the chains from the LVE data. Such a time scale is often taken to be represented by the longest stretch relaxation time τ_1 of the Rouse model. It should be noted that here the Rouse time τ_1 is a factor of 2 smaller than the value of the Rouse rotational relaxation time τ_R as described in Larson *et al.* (2003). The τ_1 can be

evaluated from the coefficient a with [Osaki *et al.* (2000); Osaki *et al.* (2001)]

$$\tau_1 = \left(\frac{aM}{1.111cRT}\right)^2, \tag{3.10}$$

where M is the molecular weight of the polymer in kg/mol, $c = \rho\phi$ is the concentration in kg/m^3, R is the gas constant with the value 8.314J/(mol · K), T is the temperature in K, and a is obtained from G' in the power law range $G'(\omega) = a\omega^{1/2}$. Alternatively, the τ_1 can be also evaluated from the zero shear rate viscosity η_0 with [Menezes and Graessley (1982)]

$$\tau_1 = \frac{6M\eta_0}{\pi^2 cRT}\left(\frac{M_c}{M}\right)^{2.4} \tag{3.11}$$

when $M > M_c$. Here M_c is the critical molecular weight with the value 35kg/mol for polystyrene melts [Ferry (1980); Luap *et al.* (2005)]. As for the polystyrene solutions, the value of M_c can be assumed to be proportional to the entanglement molecular weight M_e [Fetters *et al.* (1999); Osaki *et al.* (2001)].

The evaluated Rouse time τ_1 for polystyrene melts and solutions from both Eq.3.10 and Eq.3.11 are summarized in Table 3.5. The Rouse rotational relaxation time τ_R^{LM} evaluated from the linear theory [Likhtman and McLeish (2002)] are also listed in Table 3.5 for comparison. These three methods give a good agreement with each other. For further use, the average Rouse time τ_R of these three methods is selected. The equilibration time τ_e for one entanglement is defined as $\tau_e = \tau_R/Z^2$, which could be compared to the BSW parameter τ_c in Table 3.4. The values of $Z^2\tau_c$, which should be close to τ_R, are also listed in Table 3.5.

Table 3.5: Evaluated time scales for the polystyrene melts and solutions at 130 °C

Sample Name	$2\tau_1$[s], Eq.3.10	$2\tau_1$[s], Eq.3.11	τ_R^{LM}[s]	τ_R[s]	$Z^2\tau_c$[s]
PS-550k	850.2	776.8	779	802	672.4
PS-290k	232.5	216.3	216	222	183.2
Solution-1	20.6	19.6	19.0	19.7	17.8
Solution-2	2.28	2.33	2.40	2.34	2.12
Solution-3	33.2	30.2	31.2	31.5	28.9

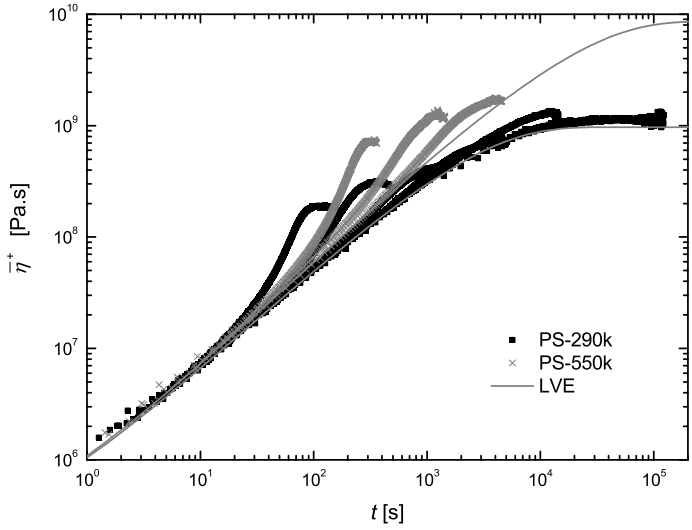

Figure 3.3: The measured extensional stress growth coefficient as a function of the time for PS-290k and PS-550k at 130 °C. Strain rate for PS-290k (from left to right): $0.03, 0.01, 0.003, 0.001, 0.0003, 0.00003\text{s}^{-1}$; Strain rate for PS-550k (from left to right): $0.01, 0.003, 0.001\text{s}^{-1}$.

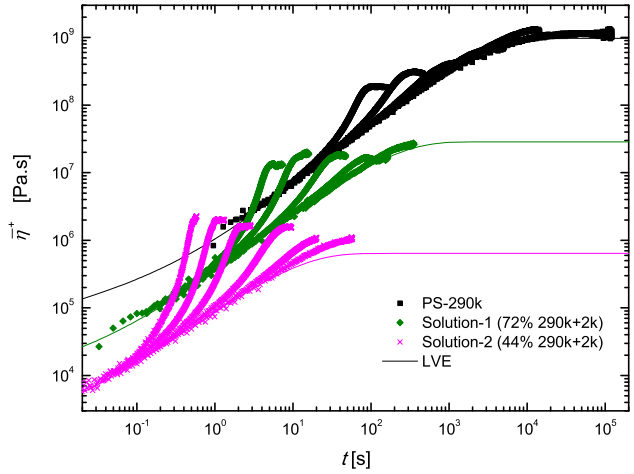

(a) Strain rate for Solution-1 (from left to right): $0.57, 0.29, 0.096, 0.029, 0.0096\text{s}^{-1}$; Strain rate for Solution-2 (from left to right): $5.6, 3.36, 1.68, 0.56, 0.168, 0.056\text{s}^{-1}$.

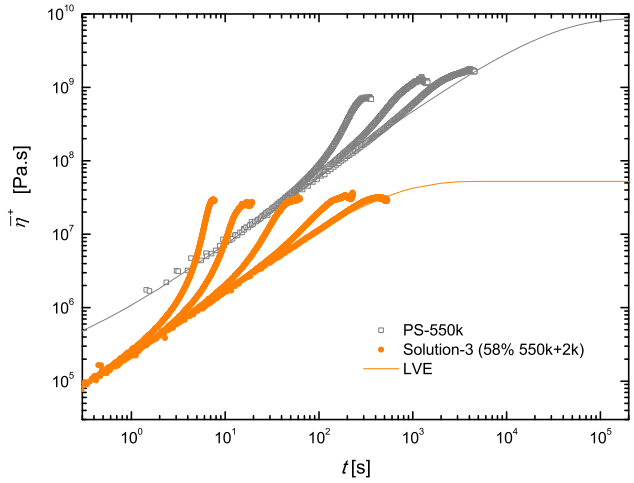

(b) Strain rate for Solution-3 (from left to right): $0.45, 0.23, 0.076, 0.023, 0.0076\text{s}^{-1}$.

Figure 3.4: The measured extensional stress growth coefficient as a function of the time for the polystyrene solutions at 130 °C

3.3.2 Startup and steady–state elongational flow

Figure 3.3 shows the measured extensional stress growth coefficient $\bar{\eta}^{+}$ as a function of the time at 130 °C for the polystyrene melts. The solid lines in the figure are predictions from the LVE parameters listed in Table 3.4. The lowest strain rate for PS-290k was measured at 170 °C and shifted to 130 °C with the shift factor in Eq.3.2. Similar plots for the polystyrene solutions at 130 °C are shown in Figure 3.4. Solution-1 and Solution-3 were originally measured at 120 °C, while Solution-2 was originally measured at 110 °C. In Figure 3.4 the data are shifted to 130 °C with the shift factors listed in Table 3.3. It seems that the strain hardening effect is more pronounced in the solutions especially at low concentrations compared with the melts.

The extensional steady–state viscosity $\bar{\eta}_{\text{steady}}$ is plotted as a function of the strain rate in Figure 3.5 for all the polystyrene samples at 130 °C. The $\bar{\eta}_{\text{steady}}$ shows a monotonic thinning for the two melts PS-290k and PS-550k, which is in agreement with Bach *et al.* (2003a). But the three solutions show obvious different behaviors compared with the melts. The $\bar{\eta}_{\text{steady}}$ of Solution-1 seems to have three regions. It initially decreases with increasing strain rate in the first region. It then goes to a plateau region while the strain rate keeps increasing. Finally it decreases again with even faster strain rate in the third region. Solution-2 and Solution-3 only have the plateau region which may due to the limited strain rates. The $\bar{\eta}_{\text{steady}}$ of Solution-2 even shows a slight increase with increasing strain rate.

3.4 Discussion

3.4.1 Influence of entanglement molecular weight

For the well–entangled polystyrene melts, the entanglement molecular weight M_e is identical. Changing molecular weight only changes the number of entanglements Z. The influence of Z is well known. For example, in shear flow the zero shear rate viscosity for the melts scales as $\bar{\eta}_0 \sim Z^{3.4}$. In extensional flow, the steady–state viscosity also scales with Z^2 for large extension rate of polystyrene melts as discussed in Bach *et al.* (2003a) and Nielsen *et al.* (2006a).

However, when a polystyrene melt is diluted, the entanglement molecular weight increases according to Eq.3.1. This change causes increase of the tube diamter in the tube model [Doi and Edwards (1986)]. To evaluate the effect of the tube dilation, it would be interesting to compare the behavior of the molecules in shear and extensional flows in the opposite way: With the same number of entanglements Z but different M_e. In Figure 3.6(a), Solution-3 which has $Z = 23.8$ is compared with the melt PS-290k

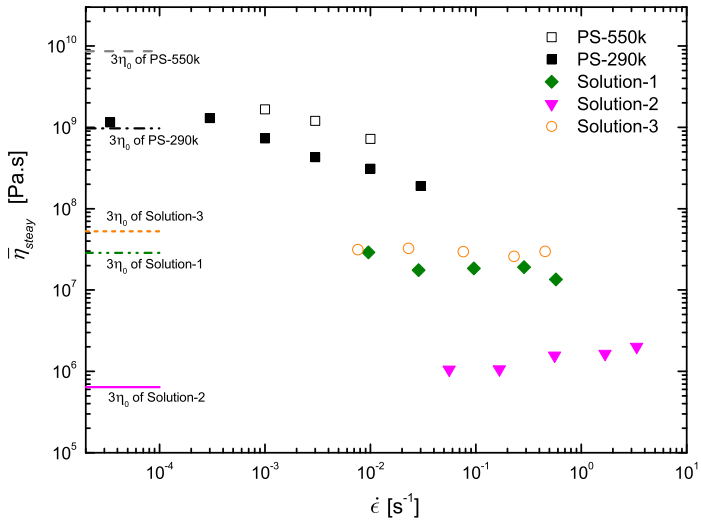

Figure 3.5: The extensional steady–state viscosity as a function of the strain rate for all the polystyrene samples at 130 °C.

which has $Z = 21.4$ in the oscillatory shear flow. Since the glass transition temperatures T_g of the solution and the melt are quite different, they are compared under non–dimensional parameters with $\tilde{\omega} = \omega\tau_c$, $\tilde{G}' = G'/G_N^0$, and $\tilde{G}'' = G''/G_N^0$, where τ_c and G_N^0 can be found in Table 3.4. In this way, the crossover point at the high frequency part of Solution-3 in Figure 3.2(b), and the similar point of PS-290k in Figure 3.1, are shifted to overlap each other in Figure 3.6(a). Figure 3.6(b) compares Solution-1 which has $Z = 15.4$ with the melt PS-200k which has $Z = 15.0$ in the same way as Figure 3.6(a). The shear data and the BSW parameters of PS-200k are taken from Bach *et al.* (2003a). It can be seen that with the same value of Z, the G' and G'' data of the melts and solutions can be superimposed with each other. Since Solution-3 has a slightly larger number of entanglements than the melt PS-290k, their G', G'' curves do not completely overlap in the low frequency part.

The behavior of Solution-3 and PS-290k in extensional flow is compared in Figure 3.7(a), also under non–dimensional parameters which scale the same way as in Figure 3.6(a). Similar comparison for Solution-1 and PS-200k is presented in Figure 3.7(b). The extensional data of PS-200k is again taken from Bach *et al.* (2003a). The thin lines in Figures 3.7(a) and 3.7(b) are the LVE predictions. Deviations from the thin lines are signatures of non–linear strain hardening. It is apparent that the solutions and melts show similar linear behavior also in extension, but very different non–linear strain hardening behavior, as already mentioned in Section 3.3.2. In Figure 3.6, the influence of M_e is actually erased by normalizing the data with G_N^0. However it seems that the influence of M_e can not be erased in the extensional flow by doing the same way.

In Figure 3.8 we compare the non–dimensional steady–state viscosity of the melts and solutions from Figure 3.7, but normalized by the time scale of τ_R. It is equivalent to normalizing the data by τ_c, since $\tau_R \approx Z^2\tau_c$ and the values of Z for the solutions are close to the values for the relative melts in this figure. The Weissenberg number is defined as $Wi_R = \dot{\epsilon}\tau_R$. It can be seen from both Figure 3.8(a) and 3.8(b) that at $Wi_R > 1$ where the polymer chains are stretched, the non–dimensional steady–state viscosity of the solutions are higher than the melts. This observation indicates that with the higher values of M_e, the polymer chains could be stretched further. It can also be directly seen from Figure 3.7(a) that the non–dimensional stress growth coefficient in the startup of the flow is almost the same for Solution-3 and PS-290k, due to their same Weissenberg number as shown in Figure 3.8(a). However, with the lower value of M_e, the extensibility of PS-290k seems rather limited and the flow turns to a steady state much earlier than Solution-3.

The higher steady–state viscosity seen in the solutions at $Wi_R > 1$ may be due to their higher maximum stretch ratios. The maximum stretch ratio is defined as $\lambda_{\max} = \sqrt{N_e}$, where N_e is the number of Kuhn steps per entanglement. The values of N_e for some typical polymer melts, such as polyethylene (PE), isotactic polypropylene (*i*-PP) and polyisoprene (PI), can be found in Fetters *et al.* (1996). Their maximum stretch ratios

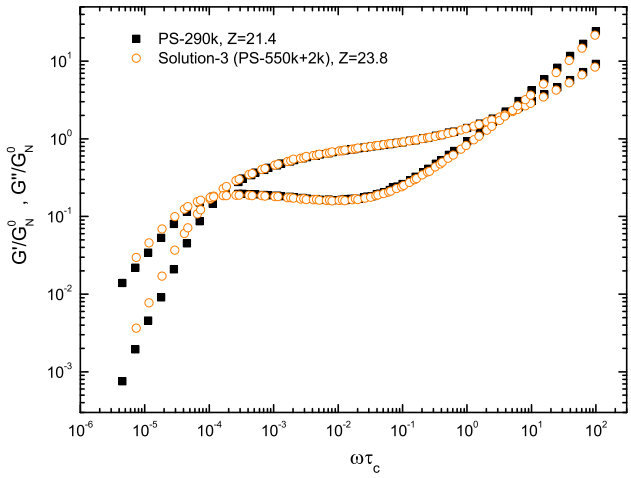

(a) Comparison of LVE for Solution-3 and PS-290k

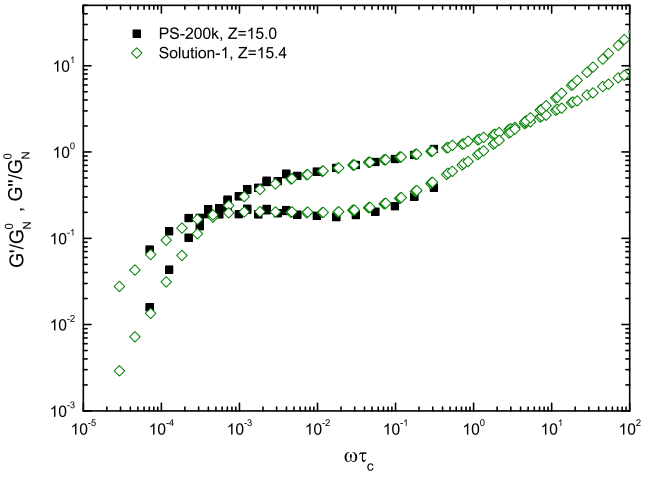

(b) Comparison of LVE for Solution-1 and PS-200k

Figure 3.6: Comparison of the polystyrene melts and solutions under non–dimensional parameters in small amplitude oscillatory shear flow.

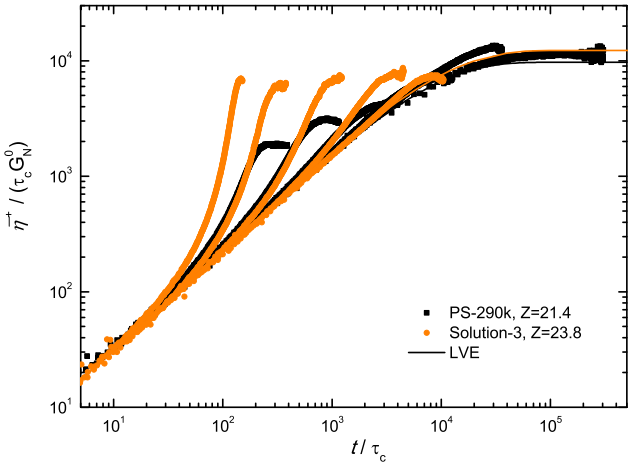

(a) Comparison of transient extensional flow for Solution-3 and PS-290k

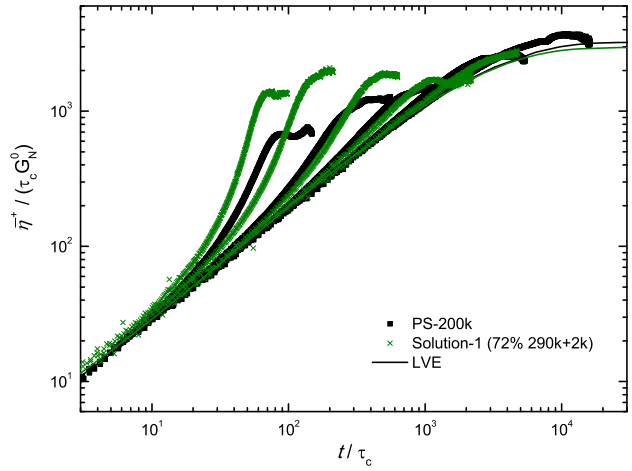

(b) Comparison of transient extensional flow for Solution-1 and PS-200k

Figure 3.7: Comparison of the polystyrene melts and solutions under non–dimensional parameters in the startup of extensional flow.

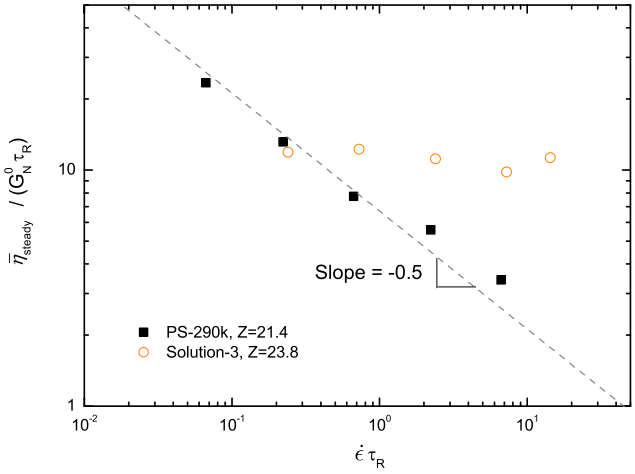

(a) Comparison of steady extensional flow for Solution-3 and PS-290k

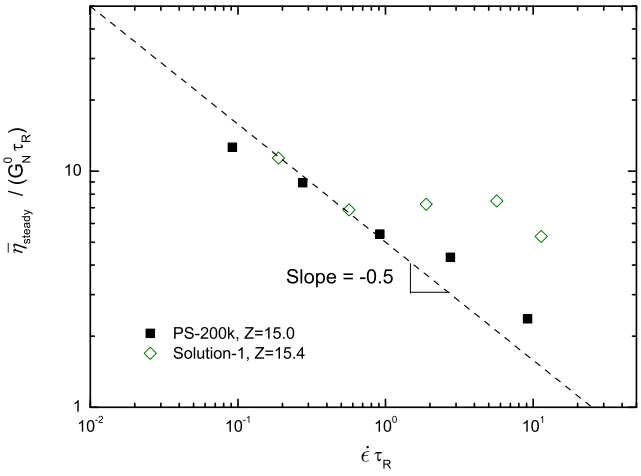

(b) Comparison of steady extensional flow for Solution-1 and PS-200k

Figure 3.8: Comparison of the polystyrene melts and solutions under non–dimensional parameters in the steady–state extensional flow.

$\lambda_{\max}$ are listed in Table 3.6. The value of N_e for atactic polystyrene (a-PS) can not be directly found in Fetters *et al.* (1996), but can be calculated from

$$Ne = a^2/b^2,$$
$$b = \frac{\left\langle R^2\right\rangle_0}{R_{\max}} = \frac{\left\langle R^2\right\rangle_0}{M}\frac{M}{R_{\max}} = \frac{\left\langle R^2\right\rangle_0}{M}\frac{nm_b}{nl\cos(\theta/2)} = \frac{\left\langle R^2\right\rangle_0}{M}\frac{m_b}{l\cos(\theta/2)}, \tag{3.12}$$

where a is the tube diameter, b is the Kuhn length, $\left\langle R^2\right\rangle_0$ is the mean square end-to-end distance of the polymer chain, $R_{\max}$ is the fully extended size of the chain, M is the molecular weight of the chain, m_b is the average molecular weight per backbone bond, l is the backbone bond length, and θ is the backbone bond angle. According to Fetters *et al.* (1996), for a-PS at 413K, $a = 85.2$Å, $\left\langle R^2\right\rangle_0/M = 0.437$Å^2, $l = 1.5$Å, $\cos(\theta/2) = 0.83$, and $m_b = 52$. Inserting the values into Eq.3.12, we get $N_e = 21.8$, which is in agreement with Fang *et al.* (2000). If the molar mass of a Kuhn–segment is M_0, it is easy to get $M_e = N_e M_0$. The values of M_0 for polystyrene melts and solutions are supposed to be the same. Therefore according to Eq.3.1, the values of N_e for polystyrene solutions are calculated as $N_{e,s} = N_{e,m}\phi^{-1} = 21.8\phi^{-1}$, which are also listed in Table 3.6. Assuming that $\lambda_{\max}$ is the relevant parameter for the non–linear behavior, Solution-2 should behave similarly to PI melts and Solution-3 should behave similarly to i-PP melts. Previous experiments on PE melts [Rasmussen *et al.* (2005)] have shown that the steady–state viscosity also decreases monotonically as a function of strain rate. It may be due to the value of $\lambda_{\max}$ of PE melts is even lower than that of a-PS melts.

Table 3.6: The maximum stretch ratio $\lambda_{\max}$ for polymer melts and solutions

Sample Name	T[K]	ϕ	N_e	$\lambda_{\max}$
PE	413	100%	6.89	2.6
i-PP	463	100%	36.5	6.0
PI	298	100%	46.5	6.8
a-PS	413	100%	21.8	4.7
Solution-1	413	72%	30.3	5.5
Solution-2	413	44%	49.5	7.0
Solution-3	413	58%	37.6	6.1

3.4.2 Constitutive modeling

It has been shown by Wagner *et al.* (2005) that the behavior of polystyrene melts in extensional flow could be captured by the molecular stress function (MSF) theory [Wagner and Schaeffer (1993)] incorporating with the interchain pressure concept [Marrucci

and Ianniruberto (2004)]. In this section the MSF model is compared with the experimental data of the polystyrene solutions. The stress tensor of the general MSF model is given by the integral[Wagner and Schaeffer (1993)]

$$\sigma(t) = \int_{-\infty}^{t} M(t-t') f^2(t,t') \mathbf{S}_{\mathrm{DE}}^{\mathrm{IAA}} \mathrm{d}t'. \tag{3.13}$$

In Eq.3.13, $M(s) = -\mathrm{d}G(s)/\mathrm{d}s$ is the memory function defined in terms of the relaxation modulus in Eq.3.5. $f(t,t')$ is the tube segment stretch defined as

$$f(t,t') = a_0/a(t,t'), \tag{3.14}$$

where $a(t,t')$ and a_0 are the tube diameters during stretching and in equilibrium respectively; $\mathbf{S}_{\mathrm{DE}}^{\mathrm{IAA}}$ is the DE strain tensor with IAA [Doi and Edwards (1986)] given by

$$\mathbf{S}_{\mathrm{DE}}^{\mathrm{IAA}}(t,t') = 5\left\langle \frac{\mathbf{E}\cdot\mathbf{u}\ \mathbf{E}\cdot\mathbf{u}}{|\mathbf{E}\cdot\mathbf{u}|^2} \right\rangle = 5\mathbf{S}(t,t'), \tag{3.15}$$

where $\mathbf{u}$ is the unit vector and $\mathbf{E}$ is the relative deformation gradient tensor. The bracket in Eq.3.15 denotes an average over an isotropic distribution and the analytical formulas can be found in Urakawa *et al.* (1995). There are different expressions for the molecular stress function $f(t,t')$ in Eq.3.13. For example, if the affine chain deformation is assumed to be balanced by the linear spring force, f is given by the MSF–Rouse model as[Wagner *et al.* (2005)]

$$\frac{\partial}{\partial t} f = f(\boldsymbol{\kappa} : \mathbf{S}) - \frac{f-1}{\tau_R} \tag{3.16}$$

with the initial condition $f(t',t') = 1$. $\boldsymbol{\kappa}$ is the transpose of the velocity gradient ($\kappa_{ij} = \partial v_i/\partial x_j$). Eq.3.16 does not take account of the finite extensibility. It results in a diverging steady–state elongational viscosity when $Wi_R \to 1$. Wagner *et al.* (2005) put the interchain pressure concept [Marrucci and Ianniruberto (2004)] into the MSF model which limits the chain stretch, and the molecular stress function f is given by

$$\frac{\partial}{\partial t} f = f\left[(\boldsymbol{\kappa} : \mathbf{S}) - \frac{f\left(f^3-1\right)}{\tau_a}\right], \tag{3.17}$$

with the initial condition $f(t',t') = 1$. τ_a is the tube diameter relaxation time. Eq.3.17 predicts a monotonic thinning of the steady–state viscosity with increasing strain rate, which can obviously not describe the plateau region shown in the polystyrene solutions here. Recently Wagner (2011) proposed that chain stretch is balanced by two restoring tensions with 1/3 contribution from Eq.3.16 and 2/3 contribution from Eq.3.17. For the long chain component in a diluted system, the evolution equation f_L is given by

$$\frac{\partial}{\partial t} f_L = f_L \left(\boldsymbol{\kappa} : \mathbf{S}\right) - \frac{1}{3}\frac{f_L - 1}{\tau_{R,L}} - \frac{2}{3}\phi^2 \frac{f_L^2\left(f_L^3 - 1\right)}{3\tau_{R,L}}. \tag{3.18}$$

In the limit of large Weissenberg number $\dot{\epsilon}\tau_{R,L}$, the steady value of f_L in Eq.3.18 can be got from

$$\dot{\epsilon}\tau_{R,L} = \frac{1}{3}\frac{f_{L,steady} - 1}{f_{L,steady}} + \frac{2}{9}\phi^2 f_{L,steady}\left(f_{L,steady}^3 - 1\right). \tag{3.19}$$

As shown in Figure 3.9(a), $f_{L,steady}^2/(\dot{\epsilon}\tau_{R,L})$ decreases monotonically with increasing $\dot{\epsilon}\tau_{R,L}$. Therefore Eq.3.18 can not predict the plateau region of the steady–state viscosity shown in the polystyrene solutions either.

Alternatively, Eq.3.16 can be modified by introducing a nonlinear spring coefficient $c(f)$ as [Rolón–Garrido *et al.* (2006)]

$$\frac{\partial}{\partial t} f = f\left(\boldsymbol{\kappa} : \mathbf{S}\right) - \frac{c(f)f - 1}{\tau_R}, \tag{3.20}$$

where

$$c(f) = \frac{\left(3 - f^2/\lambda_{\max}^2\right)\left(1 - 1/\lambda_{\max}^2\right)}{\left(3 - 1/\lambda_{\max}^2\right)\left(1 - f^2/\lambda_{\max}^2\right)}. \tag{3.21}$$

In Eq.3.21, $\lambda_{\max}$ is the maximum chain stretch ratio defined as $\lambda_{\max} = \sqrt{N_e}$, where N_e is the number of Kuhn steps per entanglement. Combined with Eq.3.1, it can be seen that $\lambda_{\max}^2 \sim \phi^{-1}$. For polystyrene melts we use $\lambda_{\max} = 4.7$ [Fang *et al.* (2000)]. From Eq.3.20 and Eq.3.21 it can be derived that in the limit of large Weissenberg number

$\dot{\epsilon}\tau_R$, the steady value of f follows

$$\dot{\epsilon}\tau_R = \frac{\left(1 - 1/\lambda_{\max}^2\right)\left(3 - f_{steady}^2/\lambda_{\max}^2\right)}{\left(3 - 1/\lambda_{\max}^2\right)\left(1 - f_{steady}^2/\lambda_{\max}^2\right)} - \frac{1}{f_{steady}}. \tag{3.22}$$

Plotting $f_{steady}^2/(\dot{\epsilon}\tau_R)$ as a function of $\dot{\epsilon}\tau_R$ in Figure 3.9(b), it shows three regions rather than monotonic decreasing. Therefore Eq.3.20 has a chance to describe the extensional behaviors of the polystyrene solutions. Figure 3.10 compares the simulation results from the modified MSF–Rouse model using Eq.3.20 with the experimental data. This parameter–free model reasonably describes the startup of the flow for the polystyrene solutions. It also captures the trend of the steady–state extensional viscosity for the solutions. But for the higher concentration solutions such as Solution-1, the model overestimate the steady–state viscosity at intermediate Weissenberg number; and for the lower concentration solutions such as Solution-2, the model underestimate the steady–state viscosity at high Weissenberg number. This model can not describe the monotonic thinning of the steady–state extensional viscosity for the melts.

3.5 Conclusions

The two nearly monodisperse polystyrene melts PS-290k and PS-550k, and the three polystyrene solutions made from either PS-290k or PS-550k diluted in OS-2k, have been measured in the uniaxial extensional flow using the FSR. The entanglement molecular weight (M_e) scales inversely with the polymer volume fraction in the concentrated domain investigated. It is possible to scale the time constant and the plateau modulus such that polystyrene melts and concentrated polystyrene solutions with the same number of entanglements per chain (Z) have identical LVE properties both in shear and extension. Polystyrene melts and solutions with the same Z differ, however in the non–linear extensional properties. Strain hardening increases with the number of Kuhn steps per entanglement (N_e). Assuming that the maximum stretch ratio ($\lambda_{\max} = \sqrt{N_e}$) is the relevant parameter for the non–linear behavior, Solution-2 ($\lambda_{\max} = 7.0$) should behave similarly to PI melts ($\lambda_{\max} = 6.8$) and Solution-3 ($\lambda_{\max} = 6.1$) should behave similarly to *i*-PP melts ($\lambda_{\max} = 6.0$). Further experiments on PI and *i*-PP melts will be interesting. A parameter–free MSF–Rouse model incorporated with the finite extensibility can qualitatively describe the behavior of the polystyrene solutions in extensional flow at $Wi_R > 1$. But this model can however not predict the flow behavior of the polystyrene melts. Experiments of stress relaxation following the uniaxial extension will be desired to investigate the different stretch–relaxation mechanism for the melts and solutions. Further investigation on the influence of the solvents will be also required.

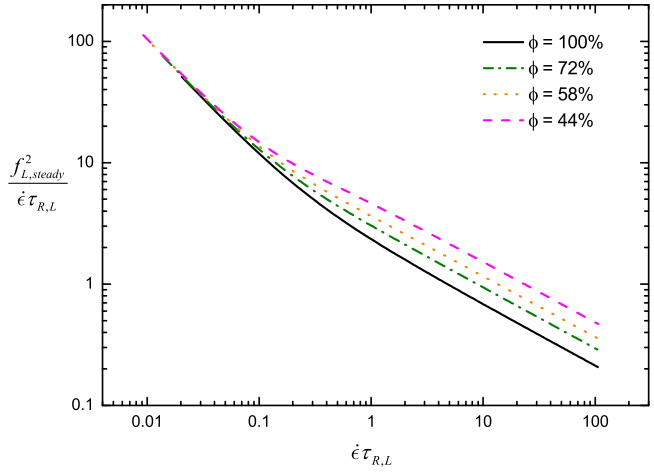

(a) Test of the molecular stress function f from Eq.3.18

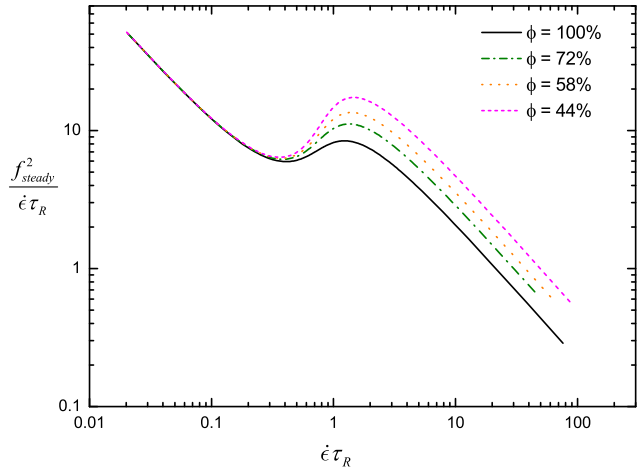

(b) Test of the molecular stress function f from Eq.3.20

Figure 3.9: The steady value of the molecular stress function f as a function of the Weissenberg number.

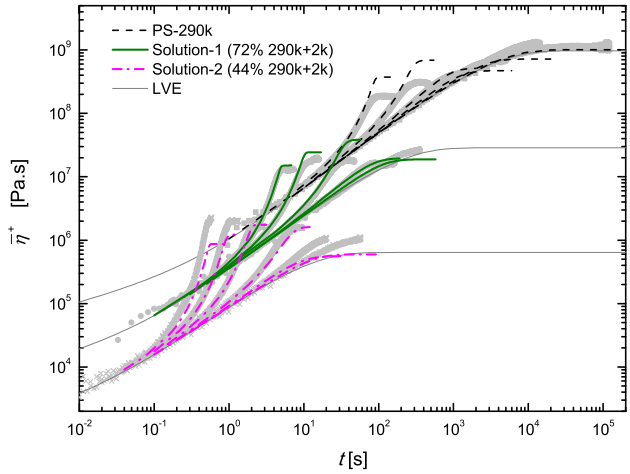

(a) Simulation results for PS-290k, Solution-1 and Solution-2

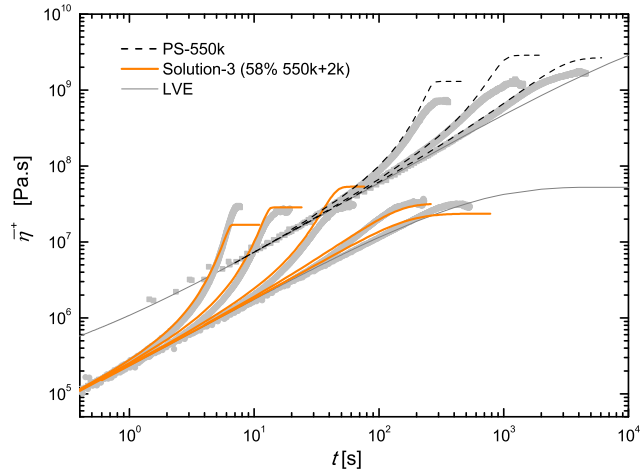

(b) Simulation results for PS-550k and Solution-3

Figure 3.10: Simulation results of the MSF–Rouse model combined with the finite extensibility for the polystyrene melts and solutions at 130 °C.

Chapter 4

Are Entangled Polymer Melts Different from Solutions: Role of Monomeric Friction

4.1 Introduction

The molecular dynamics behind the viscoelastic behavior of polymer melts in extensional flow is still not fully understood. This is so even for the monodisperse linear melts which is the simplest case. For example, as mentioned in Chapter 3, monodisperse linear polystyrene melts show monotonic thinning in extensional steady state viscosity vs elongational rate [Bach *et al.* (2003a); Luap *et al.* (2005)], while monodisperse linear polystyrene solutions show thinning followed by thickening [Bhattacharjee *et al.* (2002)]. The monotonic thinning behavior of polystyrene melts can not be described by the tube model [Doi and Edwards (1986)] combined with the frequently used contributions for chain stretch [Marrucci and Grizzuti (1988)] and convective constraint release [Marrucci and Ianniruberto (1996)].

In Chapter 3 we have reported that the entangled polystyrene melts and solutions, which behave similarly in linear viscoelasticity, show very different rheological behavior in extensional flow. The polystyrene solutions are more strain hardening than the melts. One possible reason is that the entanglement molecular weight M_e in polystyrene solutions is higher than the value in polystyrene melts. And due to the maximum stretch

ratio $\lambda_{\max} = \sqrt{N_e}$, where N_e is the number of Kuhn steps per entanglement, the solutions which have larger values of M_e can be stretched to larger ratios than their relative melts, resulting in larger values of extensional steady state viscosity. However, in Chapter 3, we did not take the possible influence from solvents into account. The solvent we used in Chapter 3 is a styrene oligomer OS-2k with a molar mass 2 kg/mole. The OS-2k contains about 3 Kuhn–segments per chain [Fang *et al.* (2000)], and is therefore an anisotropic medium. Ianniruberto *et al.* (2012) proposed that an anisotropic medium could cause a stretch/orientation–induced reduction of the monomeric (Kuhn–segment's) friction. Recently Yaoita *et al.* (2012) analyzed the stress relaxation data of entangled polymer melts [Nielsen *et al.* (2008)] and solutions [Bhattacharjee *et al.* (2003)] both following uniaxial extension. From those data they evaluated the magnitude of the stretch/orientation–induced reduction of monomeric friction and used it in their simulation. The simulated results satisfactorily described the monotonic thinning of extensional steady state viscosity for the polymer melts and the thinning followed by thickening seen for the solutions. However, their work was based on very limited experimental data in which the melts and solutions can not be compared directly.

The purpose of the present work is to make well–defined experiments to directly evaluate the influence of monomeric (Kuhn–segment's) friction on the rheological behaviors of entangled polymer melts and solutions. We diluted a polystyrene melt of 545 kg/mole to the same concentration with different solvents. The solvents that we used include two styrene oligomers with molar masses of 1 kg/mole and 4 kg/mole, corresponding to less than 2 Kuhn–segments and about 7 Kuhn–segments [Fang *et al.* (2000)] per chain, respectively. We will show the difference between these solutions in nonlinear rheology which is directly related to the monomeric friction from the solvents with different Kuhn–segments. The results are also compared with a solution diluted in a 2 kg/mole styrene oligomer which has been reported in Chapter 3.

4.2 Experimental Details

4.2.1 Preparation of solutions

The polystyrene solutions were made from the polystyrene PS-550k diluted in two different styrene oligomers. The PS-550k, which is from the same batch as in Chapter 3, has a molar mass $M_w = 545\text{kg/mol}$ and a polydispersity index $PDI = 1.12$. The styrene oligomers OS-4k and OS-1k were both bought from Sigma–Aldrich. Their properties, as well as the property of the 2 kg/mole styrene oligomer OS-2k from Chapter 3, are summarized in Table 4.1.

The Solution-4k which contains PS-550k diluted in OS-4k was prepared by dissolving

Table 4.1: The properties of the styrene oligomers. The molecular weight of one Kuhn–segment for polystyrene melts is around 590 g/mole according to [Fang *et al.* (2000)].

Sample Name	M_w[g/mol]	*PDI*	Number of Kuhn–segments
OS-4k	4290	1.04	7.3
OS-1k	972	1.12	1.6
OS-2k	1920	1.08	3.3

both components in tetrahydrofuran (THF), and the blend was recovered by precipitation in methanol. The procedure is the same as described in Chapter 3. While in Chapter 3 the OS-2k was observed partly dissolved in methanol, it seemed that the OS-4k was not dissolved in methanol at all, and the concentration of the Solution-4k was well controlled. However, the molecular weight of OS-1k is lower than OS-2k, and it is more difficult to handle during precipitation. Therefore the Solution-1k which contains PS-550k diluted in OS-1k was prepared by dissolving both components in benzene, and the blend was recovered by freeze–drying[1]. The concentrations of both polystyrene solutions were checked in size exclusion chromatography (SEC). As described in Chapter 3, the entanglement molecular weight $M_{e,s}$ of the polystyrene solutions is calculated as $M_{e,s} = M_{e,m}\phi^{-1}$, where $M_{e,m}$ is the entanglement molecular weight of the polystyrene melt and ϕ is the weight fraction of the polystyrene in the solution. We take $M_{e,m} = 13.3$kg/mol for polystyrene melts as reported by Bach *et al.* (2003a). The number of entanglements per chain is calculated as $Z = M/M_e$, where M is the molecular weight of the polystyrene. The properties of Solution-4k and Solution-1k are listed in Table 4.2. The properties of the polystyrene melt PS-290k and the polystyrene solution Solution-2k, both reported in Chapter 3, are also listed in Table 4.2 for comparison.

Table 4.2: The properties of the polystyrene solutions

Sample Name	Components	ϕ (550k) [wt%]	M_e [g/mol]	Z	notes
Solution-4k	550k+4k	52.5%(±1%)	25333	21.5	
Solution-1k	550k+1k	52.0%(±1%)	25577	21.3	
Solution-2k	550k+2k	58.0%(±1%)	22931	23.8	from Chapter 3 (Solution-3)
PS-290k	290k	100% 290k	13300	21.4	from Chapter 3

[1] Solution-1k was prepared by Yumi Matsumiya at Institute for Chemical Research, Kyoto University

4.2.2 Measurements of linear and nonlinear rheology

The linear viscoelastic (LVE) properties of the polystyrene solutions were obtained from small amplitude oscillatory shear flow measurements. An 8mm plate–plate geometry was used on an ARES–G2 rheometer from TA instruments. The measurements for Solution-4k were performed at 130, 150 and 170 °C under nitrogen, while the measurements for Solution-1k were performed at 90, 110 and 130 °C under nitrogen. For each polystyrene solution the data were shifted to a single master curve at 130 °C using the time–temperature superposition (TTS) procedure. The shift factors a_T for the solutions are listed in Table 4.3

Table 4.3: The temperature shift factor a_T for the polystyrene solutions

Sample Name	90 to 130 °C	110 to 130 °C	150 to 130 °C	170 to 130 °C
Solution-4k	–	–	0.035	0.0031
Solution-1k	372.74	11.03	–	–

The nonlinear viscoelastic properties of the polystyrene solutions were obtained from stress–strain measurements in uniaxial extensional flows. The measurements were performed using a filament stretching rheometer (FSR) equipped with an oven to allow measurements from room temperature to about 200 °C [Bach *et al.* (2003b)]. Before the elongational measurements, all the polystyrene samples were molded into cylindrical test specimens under vacuum with a fixed radius $R_0 = 2.7$mm. The initial length L_0 of the cylindrical test specimens was varied between 1.3mm and 1.6mm, giving an aspect ratio $\Lambda_0 = L_0/R_0$ between 0.48 and 0.59. The samples made of Solution-4k were pressed at approximately 150 °C and annealed at this temperature for 15min under vacuum to ensure that the polymer chains were completely relaxed. The samples made of Solution-1k were pressed at approximately 110 °C and annealed for 15min under vacuum as well. All the polystyrene samples were pre–stretched to a radius R_p ranging from 1.5mm to 2.5mm at either 160 °C (for Solution-4k) or 120 °C (for Solution-1k) prior to the elongational experiments. After pre–stretching, the temperature was decreased to either 130 °C (for Solution-4k) or 90 °C (for Solution-1k) for the extensional stress measurements. Nitrogen was used in the whole procedure. The Hencky strain ϵ and the mean value of the stress difference $\langle \sigma_{zz} - \sigma_{rr} \rangle$ over the mid–filament plane is calculated by Eq.3.3 and 3.4, respectively. The strain rate is defined as $\dot{\epsilon} = d\epsilon/dt$. The FSR works in a controlled strain rate mode here. The extensional stress growth coefficient is defined as $\overline{\eta}^{+} = \langle \sigma_{zz} - \sigma_{rr} \rangle / \dot{\epsilon}$.

4.3 Results

4.3.1 Linear viscoelasticity

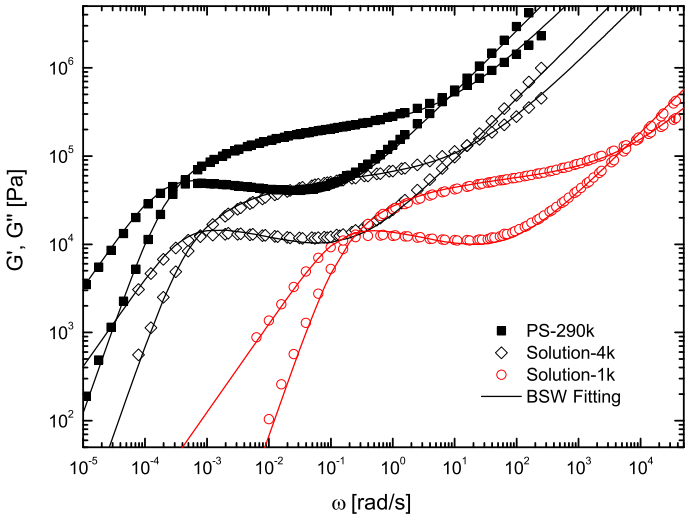

Figure 4.1: LVE data fitted with the BSW spectrum (solid lines) for Solution-4k and Solution-1k at 130 °C. The data for PS-290k at 130 °C is from Chapter 3

Figure 4.1 presents the LVE data fitted with the continuous Baumgaertel-Schausberger-Winter (BSW) relaxation spectrum [Baumgaertel *et al.* (1990)] of the two polystyrene solutions Solution-4k and Solution-1k. The LVE data of the polystyrene melt PS-290k from Chapter 3 is also presented in the figure for comparison. Table 4.4 lists the properties obtained from the BSW parameters for the two solutions. In the table, n_e is the absolute value of the slope of the $[\log\omega\ ,\ \log G'']$ curve at intermediate frequencies ω, and n_g is the slope of $[\log\omega\ ,\ \log G'']$ for $\omega \to \infty$. The values of n_e and n_g are fixed to 0.23 and 0.70 respectively [Jackson and Winter (1995)] for the nearly monodisperse polystyrene solutions. G_N^0 is the plateau modulus. As described in Chapter 3, the values of $G_{N,s}^0$ for the solutions are predicted to be

$$G_{N,s}^0 = \phi^2 G_{N,m}^0. \tag{4.1}$$

For polystyrene melts we use $G^0_{N,m}$ = 250kPa at 130 °C [Bach *et al.* (2003a)]. Since Solution-4k and Solution-1k have almost the same concentration, their plateau modulus are supposed to be the same according to Eq.4.1. It can be seen from Figure 4.1 that the G' G'' curves of Solution-1k only have a horizontal shift compared with the curves of Solution-4k; the vertical shift is not observed, confirming the same plateau modulus of the two solutions. The parameter τ_c which is the crossover relaxation time, and the parameter $\tau_{\max}$ which is the maximum relaxation time, are fitting parameters in the BSW spectrum. They are found by the least–squares fitting to the LVE data, where the relaxation modulus $G(t)$ is given by

$$G(t) = \int_0^\infty \frac{H(\tau)}{\tau} \exp\left(-t/\tau\right) \mathrm{d}\tau, \tag{4.2}$$

$$H(\tau) = n_e G_N^0 \left[\left(\frac{\tau}{\tau_{\max}}\right)^{n_e} + \left(\frac{\tau}{\tau_c}\right)^{-n_g}\right] h\left(1 - \tau/\tau_{\max}\right). \tag{4.3}$$

In Eq. 4.3 $h(x)$ is the Heaviside step function. The zero shear rate viscosity is calculated as

$$\eta_0 = \int_0^\infty G(s)\mathrm{d}s = n_e G_N^0 \tau_{\max}\left(\frac{1}{1+n_e} + \frac{1}{1-n_g}\left(\frac{\tau_c}{\tau_{\max}}\right)^{n_g}\right), \tag{4.4}$$

and the Rouse relaxation time is estimated as $\tau_R = Z^2\tau_c$, which are also listed in Table 4.4. The Rouse relaxation time estimated from different methods for polystyrene solutions have been compared in Chapter 3.

Table 4.4: Material properties obtained from the BSW spectrum at 130 °C

Sample Name	n_e	n_g	G^0_N[Pa]	τ_c[s]	$\tau_{\max}$[s]	η_0[Pa · s]	τ_R[s]
Solution-4k	0.23	0.7	68900	0.2	3176	$4.1111{\cdot}10^7$	92.5
Solution-1k	0.23	0.7	67600	0.00057	9.853	$1.2510{\cdot}10^5$	0.26

4.3.2 Startup and steady–state elongational flow

Figure 4.2 shows the measured extensional stress growth coefficient $\bar{\eta}^+$ as a function of the time at 130 °C for Solution-4k and Solution-1k. The solid lines in the figure are predictions from the LVE parameters listed in Table 4.1. The extensional data of PS-290k from Chapter 3 is also presented in the figure for comparison. The measurements

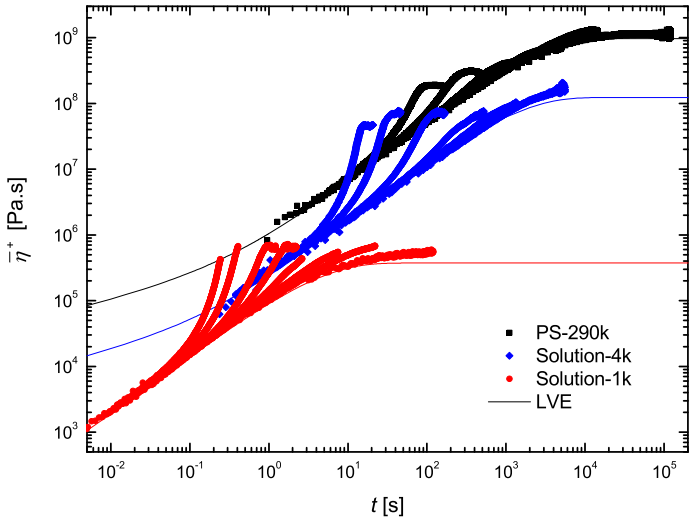

Figure 4.2: The measured extensional stress growth coefficient as a function of the time for Solution-4k and Solution-1k at 130 °C. Strain rate for Solution-4k (from left to right): $0.2, 0.1, 0.03, 0.01, 0.003, 0.0001\text{s}^{-1}$; Strain rate for Solution-1k (from left to right): $11.2, 7.45, 3.73, 2.24, 1.12, 0.373, 0.112, 0.0112\text{s}^{-1}$. The data for PS-290k is from Chapter 3

of Solution-1k were originally made at 90 °C (except the lowest rate) and shifted to 130 °C with the shift factor listed in Table 4.3. In order to check the shift factors in the nonlinear region, the samples were also measured at 95 °C and 110 °C for one strain rate respectively, and the shift factors are in agreement with the ones found in the LVE measurements. The lowest rate for Solution-1k in Figure 4.2 was originally measured at 130 °C, and the measurements of Solution-4k were all performed at 130 °C. As reported in Chapter 3, it can be seen in Figure 4.2 that both polystyrene solutions are more strain hardening that the melt. It seems that Solution-1k is even more strain hardening than Solution-4k although they have the same concentration.

Figure 4.3 presents the measurements of Solution-4k and Solution-1k from Figure 4.2 in the form of extensional stress vs Hencky strain. All the samples of Solution-4k were stretched above Hencky strain 4 and reached the steady state. However, for Solution-1k only two rates reached the steady state. The samples stretched at the lowest four strain rates only reached a Hencky strain up to 3, since the filaments were observed losing symmetry at higher Hencky strains. The samples for the highest two strain rates broke during stretching. They broke at the exact same stress, which might be an indication that the maximum stretch ratio is reached.

Figure 4.4 plots the extensional steady–state viscosity as a function of strain rate for Solution-4k and Solution-1k at 130 °C. The data for PS-290k and Solution-2k(Solution-3 in Chapter 3) taken from Chapter 3 are also presented for comparison. As observed for another polystyrene solution in Chapter 3(Solution-1), the steady–state viscosity of Solution-4k also shows three regions. It initially decreases with increasing strain rate in the first region. It then goes to a plateau region while the strain rate keeps increasing. Finally it decreases again with even faster strain rate in the third region. Solution-1k only has the plateau region due to the very limited data of steady–state viscosity.

4.4 Discussion

As shown in Table 4.2, Solution-4k and Solution-1k have the same number of entanglements per chain Z and the same entanglement molecular weight M_e. The only difference between the two solutions is the solvent. As shown in Figure 4.1, the G' G'' curves of Solution-1k have a horizontal shift compared with the curves of Solution-4k, which is due to their different glass transition temperatures and probably the different friction coefficients. As discussed in Chapter 3, the horizontal and vertical shifts of the LVE data can be corrected under non–dimensional parameters as $\tilde{\omega} = \omega\tau_c$, $\tilde{G}' = G'/G_N^0$, and $\tilde{G}'' = G''/G_N^0$, where τ_c and G_N^0 can be found in Table 4.4. In this way, the solutions are compared under the same crossover relaxation time scale. The LVE data of Solution-4k and Solution-1k from Figure 4.1 are plotted under such non–dimensional parameters in Figure 4.5. Since the Rouse relaxation time $\tau_R = Z^2\tau_c$ and the two solutions have

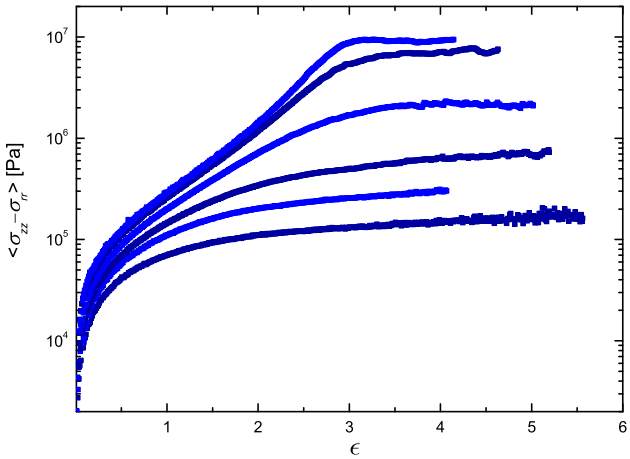

(a) Strain rate for Solution-4k (from top to bottom): 0.2, 0.1, 0.03, 0.01, 0.003, 0.0001s^{-1}.

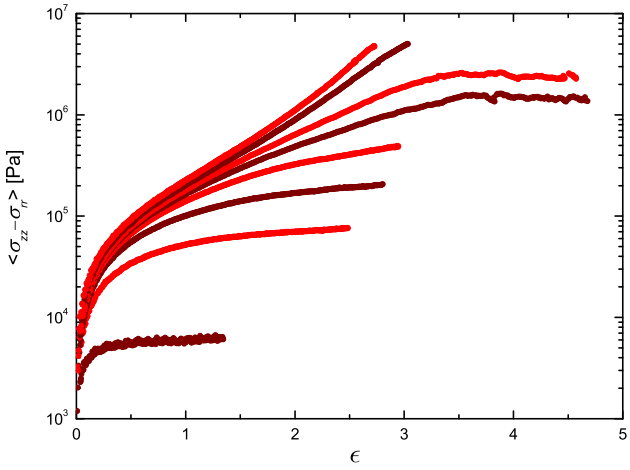

(b) Strain rate for Solution-1k (from top to bottom): 11.2, 7.45, 3.73, 2.24, 1.12, 0.373, 0.112, 0.0112s^{-1}.

Figure 4.3: The measured extensional stress as a function of Hencky strain for (a)Solution-4k and (b)Solution-1k at 130 °C.

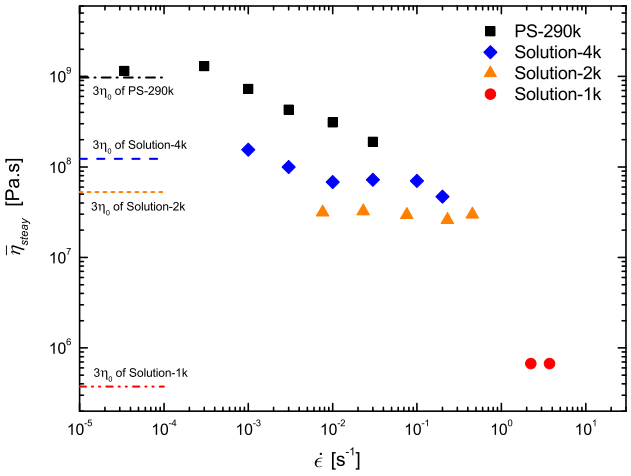

Figure 4.4: The extensional steady–state viscosity as a function of the strain rate for all the polystyrene samples at 130 °C.

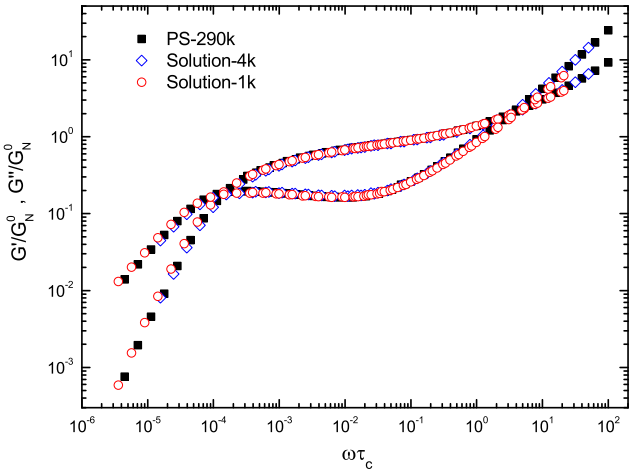

Figure 4.5: Comparison of Solution-4k, Solution-1k and PS-290k under non–dimensional parameters in the oscillatory shear flow.

the same values of Z, they are also compared under the same Rouse time scale in this figure. The polystyrene melt PS-290k which has the same Z with the two solutions is also plotted in Figure 4.5 for comparison. The $\tilde{G}'$ $\tilde{G}''$ curves of the three samples are completely superimposed with each other, which is in agreement with the observations in Figure 3.6 from Chapter 3.

Figure 4.6 compares the polystyrene solutions of different solvents in extensional flow, also under non–dimensional parameters which are normalized in the same way as in Figure 4.5. Figure 4.6(a) compares Solution-4k with Solution-2k. The data of Solution-2k are taken from Chapter 3 (Solution-3). Solution-2k has similar values of both Z and M_e with Solution-4k, but its solvent OS-2k only has $1/2$ Kuhn–segments per chain as the solvent OS-4k. However, it seems that the difference between the two solvents has little influence in nonlinear rheology, since Solution-2k behaves similarly as Solution-4k in extensional flow as shown in Figure 4.6(a). Figure 4.6(b) compares Solution-4k with Solution-1k. Solution-1k has exactly the same values of both Z and M_e with Solution-4k, but its solvent OS-1k only has $1/4$ Kuhn–segments as OS-4k. While Solution-2k shows little difference from Solution-4k in Figure 4.6(a), Solution-1k is observed to be much more strain hardening than Solution-4k in Figure 4.6(b). This observation indicates that the solvent OS-1k gives higher friction than both OS-2k and OS-4k in the solutions. Furthermore, Figure 4.6 also shows that all the solutions are more strain hardening than the melt PS-290k that has the same LVE prediction, which is in agreement with the observations in Figure 3.7 from Chapter 3.

Figure 4.7 compares the non–dimensional steady–state viscosity of all the three solutions and the melt, but normalized by the time scale of τ_R. It is equivalent to normalizing the data by τ_c, since we define $\tau_R = Z^2\tau_c$ and the values of Z for all the samples here are almost the same. The Weissenberg number is defined as $Wi_R = \dot{\epsilon}\tau_R$. All the polystyrene samples in this figure have the same number of entanglements Z. The three solutions also have the same entanglement molecular weight M_e which is larger than the M_e of the melt. It can be seen that when $Wi_R > 1$, the steady–state viscosity of all the three solutions goes to a plateau region, while the viscosity of the melt still decreases. The levels of the steady–state viscosity in the plateau region for Solution-4k and Solution-2k are close to each other, while Solution-1k has a much higher steady–state viscosity level. The reason could be that the solvents of both OS-4k and OS-2k have more than two Kuhn–segments, and are therefore anisotropic media; but the solvent OS-1k only has around one Kuhn–segment, and is therefore an isotropic medium which is close to a 'real' solvent. As proposed by Ianniruberto *et al.* (2012), an anisotropic medium can cause a stretch/orientation–induced reduction of the monomeric (Kuhn–segment's) friction. Therefore Solution-1k should have higher friction in extensional flow than both Solution-4k and Solution-1k, resulting in more strain hardening and consequently the higher steady–state viscosity level. Furthermore, the polystyrene melt PS-290k is also an anisotropic medium itself. The friction in PS-290k could be close to the friction in either Solution-4k or Solution-2k. For this reason, the difference in steady–state viscosity at $Wi_R > 1$ between PS-290k and either Solution-4k

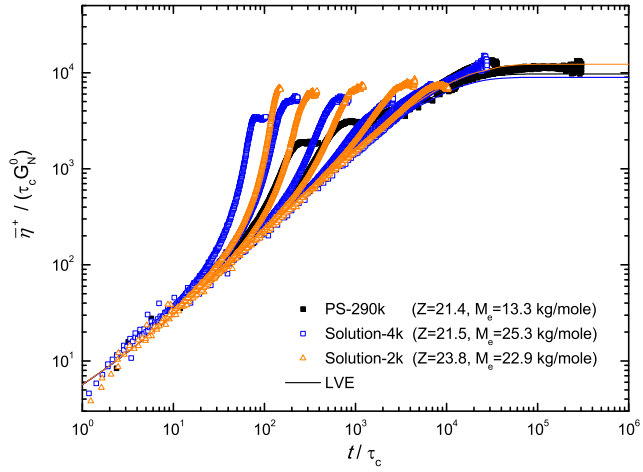

(a) Comparison of transient extensional flow for Solution-2k, Solution-4k and PS-290k

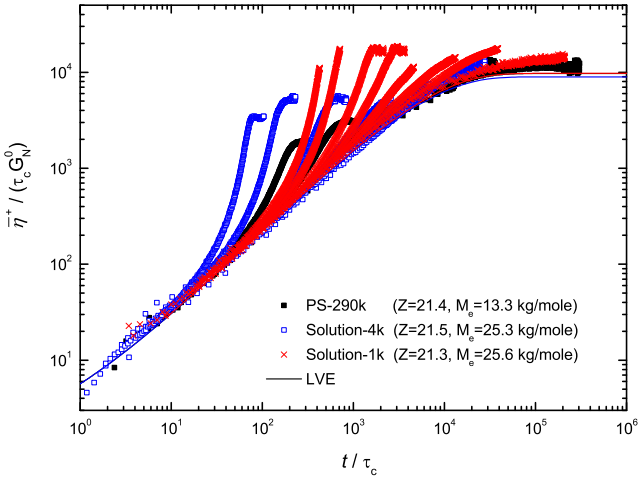

(b) Comparison of transient extensional flow for Solution-1k, Solution-4k and PS-290k

Figure 4.6: Comparison of the polystyrene solutions under non–dimensional parameters in the startup of extensional flow.

or Solution-2k should be mainly because of the M_e, as discussed in Chapter 3. The difference between polystyrene melts and 'real' polystyrene solutions should be because of the influences from both M_e and monomeric friction.

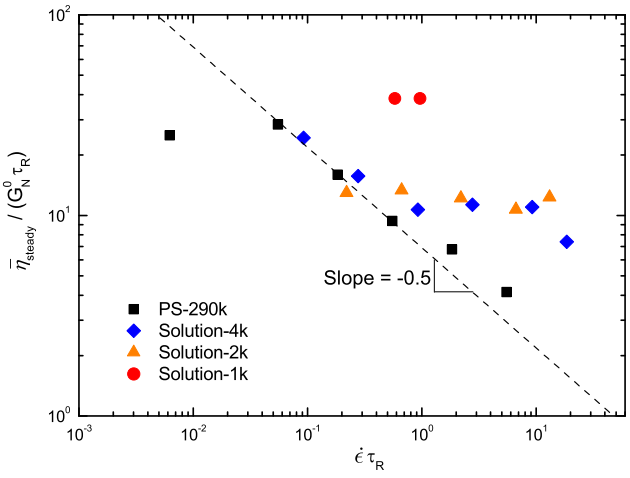

Figure 4.7: Comparison of all the polystyrene solutions and the melt under non–dimensional parameters in the steady–state extensional flow.

4.5 Conclusions

The polystyrene solutions Solution-4k, Solution-2k (taken from Solution-3 in Chapter 3) and Solution-1k are compared in shear and extensional flows. The three solutions have the same number of entanglements per chain Z and the same entanglement molecular weight M_e. Their solvents OS-4k, OS-2k and OS-1k are all styrene oligomers, but with different molar masses of 4 kg/mole, 2 kg/mole and 1 kg/mole respectively. Both OS-4k and OS-2k have more than two Kuhn–segments per chain, and are therefore potentially anisotropic media. OS-1k only has around one Kuhn–segment per chain, and is therefore an isotropic medium. All the solutions perform identically in the LVE limit when compared under the same Rouse time scale with non–dimensional parameters. Solution-4k and Solution-2k also behave similarly in extensional flows, while Solution-1k shows much more strain hardening than the other two solutions, when compared under the same Rouse time scale as well. This observation directly shows that the solvents influence the nonlinear viscoelastic behaviors of polymer solutions. It indicates that

anisotropic media such as OS-4k and OS-2k can cause a stretch/orientation–induced reduction of the monomeric (Kuhn–segment's) friction as proposed by Ianniruberto *et al.* (2012), resulting in lower extensional steady–state viscosity. More measurements for polystyrene solutions which contain the solvents with less than one Kuhn–segment per chain, as well as 'real' solvents other than styrene oligomers could be interesting. Stress relaxation measurements following uniaxial extension will be need for further investigations of the stretch/orientation–induced reduction of the monomeric friction.

Chapter 5

Extensional Rheology of Well–Entangled Bidisperse Linear Melts

5.1 Introduction

Elongational steady–state viscosity $\bar{\eta}_{\text{steady}}$ of well–entangled monodisperse linear melts has found to be a monotone decreasing function of the strain rate as reported by Bach *et al.* (2003a). This observation is also confirmed in the measurements of the two polystyrene melts PS-290k and PS-550k in Chapter 3. In the above experiments, the $\bar{\eta}_{\text{steady}}$ does not exceed $3\eta_0$ for any strain rate, where η_0 is the zero shear rate viscosity. However, when the molecular weight of a polystyrene melt decreases to less than around 10 entanglements per chain, the steady elongational viscosity vs elongational rate goes through a maximum, as observed by Nielsen *et al.* (2006a) for the two polystyrene melts PS-50k and PS-100k. Nielsen *et al.* (2006a) also reported that for the bimodal blends which contain a high molecular weight polystyrene PS-390k and either of of the low molecular weight polystyrene PS-50k or PS-100k, a maximum in the steady elongational viscosity vs elongational rate was observed as well. And this maximum increases as the concentration of the high molecular weight chains decreases.

As discussed in Chapter 3, the polystyrene solutions with lower concentrations of the long chains show more strain hardening, due to the higher entanglement molecular

weight M_e of the long chains. The higher values of M_e result in tube dilations in the tube model [Doi and Edwards (1986)]. It is possible that the low molecular weight polystyrenes such as PS-50k and PS-100k also behave partly like a solvent in the bimodal blends. Wagner (2011) has taken the effect of dynamic tube dilation into the interchain pressure model [Wagner *et al.* (2005)] and the simulation results well predicted the Elongational steady–state viscosity of the bimodal blends measured by Nielsen *et al.* (2006a).

The purpose of the present study is to investigate the extensional rheology of bidisperse linear melts without the effect of tube dilation. In this chapter, the components in the bimodal blends are the polystyrene melts PS-290k and PS-550k which have been measured in Chapter 3. Both PS-290k and PS-550k melts are well–entangled, and their elongational steady–state viscosity decreases monotonically with increasing strain rate. Therefore the bidisperse blends made from PS-290k and PS-550k are supposed to avoid the influence caused by the entanglement molecular weight which has been discussed in Chapter 3. The monomeric friction in the bidisperse blends are supposed to be close to the friction in the pure melts. Therefore the influence from friction change caused by isotropic solvents, which has been discussed in Chapter 4, is also supposed to be avoided. We will show that the well–entangled bidisperse blends behave similarly as the monodisperse melts in the steady–state elongational viscosity vs elongational rate.

5.2 Preparation of Blends

The two bidisperse polystyrene blends were made from the PS-290k and PS-550k polystyrenes with different weight ratios. Blend-1 contains 10% weight fraction of PS-550k and Blend-2 contains 50% weight fraction of PS-550k. The PS-290k and PS-550k polystyrenes used in this study are both from the same batches as in Chapter 3. The blends were prepared by dissolving the two components in tetrahydrofuran (THF) and stirring at room temperature overnight. When the polystyrenes were well dissolved and mixed, the THF solution was cautiously put into methanol drop by drop and the blends were recovered by precipitation. Finally the blends were dried under vacuum at 70 °C for 3 days.

5.3 Linear Viscoelastic Properties

The linear viscoelastic (LVE) properties of the two polystyrene blends were obtained from small amplitude oscillatory shear flow measurements. An 8mm plate–plate geometry was used on an ARES–G2 rheometer from TA instruments. The measurements

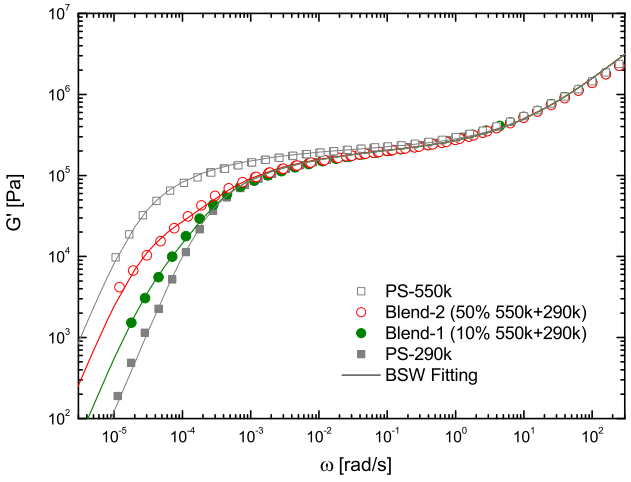

(a) G' data fitted with the BSW spectrum

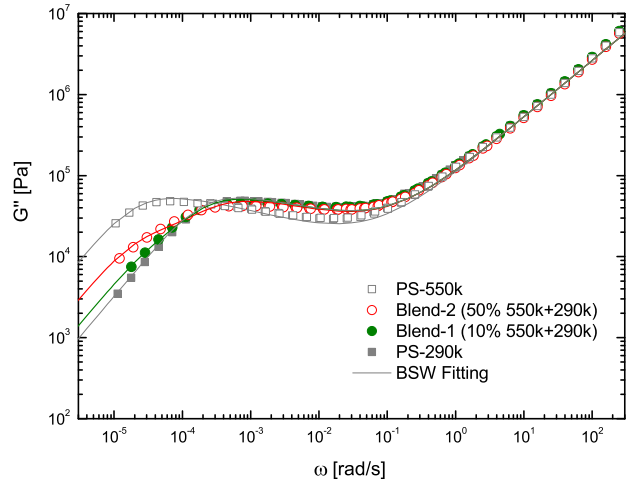

(b) G'' data fitted with the BSW spectrum

Figure 5.1: LVE data fitted with the two–mode BSW spectrum for the polystyrene blends at 130 °C. The data for PS-290k and PS-550k are from Chapter3.

were performed at 130, 150 and 170 °C. All the data were shifted to a single master curve at 130 °C using the time–temperature superposition procedure. The time–temperature shift factors were found to agree with the fitted WLF equation in Chapter 3 for the monodisperse polystyrene melts:

$$\log_{10} a_T = \frac{-c_1^0 (T - T_0)}{c_2^0 + (T - T_0)}, \tag{5.1}$$

where $c_1^0 = 8.99$, $c_2^0 = 81.53$K, $T_0 = 130\,^\circ$C, and T is temperature in °C. Figure 5.1 presents the LVE data fitted with the continuous Baumgaertel-Schausberger-Winter (BSW) relaxation spectrum [Baumgaertel *et al.* (1990)] of the two blends. The LVE data and the BSW fitting for the two melts PS-290k and PS-550k from Chapter 3 are also presented in Figure 5.1 for comparison. The relaxation modulus for the bidisperse blends is treated as the summation of two individual spectra $G(t) = G_1(t) + G_2(t)$. The individual spectrum is given by

$$G_i(t) = \int_0^\infty \frac{H_i(\tau)}{\tau} \exp(-t/\tau)\, \mathrm{d}\tau, \;\; i = 1, 2 \tag{5.2}$$

$$H_i(\tau) = n_e G_{N,i}^0 \left[\left(\frac{\tau}{\tau_{\max,i}} \right)^{n_e} + \left(\frac{\tau}{\tau_c} \right)^{-n_g} \right] h(1 - \tau/\tau_{\max,i}), \tag{5.3}$$

where $h(x)$ is the Heaviside step function, n_e is the slope of the $[\log\omega\,,\, \log G']$ curve at intermediate frequencies ω, n_g is the slope of $[\log\omega\,,\, \log G'']$ for $\omega \to \infty$, τ_c is the crossover relaxation time, and G_N^0 is the plateau modulus. The individual contributions to the modulus is constrained in a way that $G_N^0 = G_{N,1}^0 + G_{N,2}^0$ is constant [Nielsen *et al.* (2006a)]. Similarly as the polystyrene melts, the values of n_e and n_g for the blends are fixed to 0.23 and 0.70, respectively; the values of τ_c and G_N^0 at 130 °C are fixed to $\tau_c = 0.4$s and $G_N^0 = 250$kPa respectively. The adjustable parameters $\tau_{\max,i}$ are found by the least–squares fitting to the LVE data. The parameters of the BSW spectrum for the two blends at 130 °C are listed in Table 5.1. The characteristic relaxation time is defined as

$$\tau_{a,i} = \frac{\int_0^\infty G_i(s) s \mathrm{d}s}{\int_0^\infty G_i(s) \mathrm{d}s} \approx \tau_{\max,i} \left(\frac{1 + n_e}{2 + n_e} \right), \tag{5.4}$$

and the zero shear rate viscosity is calculated as

$$\bar{\eta}_{0,i} = \int_0^\infty G_i(s)\mathrm{d}s = n_e G^0_{N,i}\tau_{\max,i}\left(\frac{1}{1+n_e} + \frac{1}{1-n_g}\left(\frac{\tau_{\max,i}}{\tau_c}\right)^{-n_g}\right), \tag{5.5}$$

which are also listed in Table 5.1.

Table 5.1: Material properties obtained from the BSW spectrum at 130 °C

Sample Name	Components [wt%]	n_e	n_g	G^0_N [Pa]	τ_c [s]	$\tau_{\max}$ [s]	τ_a [s]	$\bar{\eta}_0$ [Pa · s]
Blend-1	10% PS-550k	0.23	0.7	31700	0.4	39726	21912	2.2579E8
	90% PS-290k	0.23	0.7	218300	0.4	5648	3115.3	2.3173E8
Blend-2	50% PS-550k	0.23	0.7	73700	0.4	61260	33789	8.4505E8
	50% PS-290k	0.23	0.7	176300	0.4	4037	2226.7	1.3395E8

5.4 Startup and Steady-State Elongational Flow

The uniaxial elongational stress of the polystyrene blends was measured by a filament stretching rheometer (FSR)[Bach *et al.* (2003b)]. Before the elongational measurements, the blends were molded into cylindrical test specimens under vacuum at approximately 150 °C, and annealed at this temperature for 15min. The initial radius of the cylindrical test specimens was $R_0 = 2.7$mm. The initial length L_0 was varied between 1.3mm and 1.6mm, giving an aspect ratio $\Lambda_0 = L_0/R_0$ between 0.48 and 0.59. All the samples were pre–stretched to a radius R_p ranging from 1.5mm to 2mm at 155 °C prior to the experiments. After pre–stretching, the temperature was decreased to 130 °C for the elongational stress measurements. Nitrogen was used in the whole procedure. The samples after the elongational stress measurements were checked by size exclusion chromatography (SEC) and compared with the fresh samples to ensure no degradation.

During the elongation, the force $F(t)$ is measured by a load cell and the diameter $2R(t)$ at the mid–filament plane is measured by a laser micrometer. The Hencky strain ϵ and the mean value of the stress difference $\langle\sigma_{zz} - \sigma_{rr}\rangle$ over the mid–filament plane are calculated by Eq.3.3 and Eq.3.4, respectively. The strain rate is defined as $\dot{\epsilon} = d\epsilon/dt$, and the extensional stress growth coefficient is defined as $\bar{\eta}^+ = \langle\sigma_{zz} - \sigma_{rr}\rangle / \dot{\epsilon}$.

Figure 5.2 shows the measured extensional stress growth coefficient $\bar{\eta}^+$ as a function of the time at 130 °C for the two polystyrene blends. The solid lines in the figure are predictions from the LVE parameters listed in Table 5.1. The extensional data and LVE

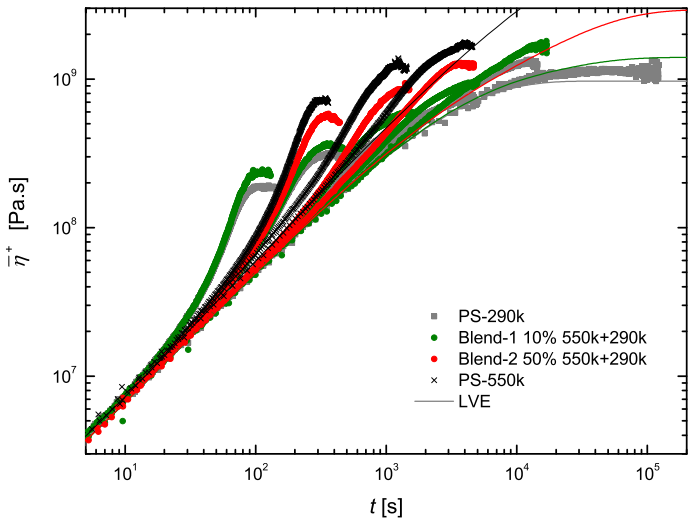

Figure 5.2: The measured extensional stress growth coefficient as a function of the time for the polystyrene blends at 130 °C. Strain rate for Blend-1 (from left to right): $0.03, 0.01, 0.003, 0.001, 0.0003\text{s}^{-1}$; Strain rate for Blend-2 (from left to right): $0.01, 0.003, 0.001\text{s}^{-1}$. The data for PS-290k and PS-550k are from Chapter3.

predictions for PS-290k and PS-550k taken from Chapter 3 are also presented in the figure for comparison. Similarly as the oscillatory shear data shown in Figure 5.1, the extensional data of the two blends in Figure 5.2 just locate in between of the two melts PS-290k and PS-550k.

The extensional steady–state viscosity $\bar{\eta}_{\text{steady}}$ is plotted as a function of the strain rate in Figure 5.3 for the two blends as well as the two melts at 130 °C. At strain rates larger than $\tau_{a,i}^{-1}$ of both components, the $\bar{\eta}_{\text{steady}}$ for the two blends shows a same trend as the melts. This is not surprising because the entanglement molecular weight M_e of the blends here is supposed to be the same as the melts. Therefore the influence of M_e on the steady–state viscosity, which has been shown in Chapter 3, is not supposed to be seen here. As described in Chapter 3, the Rouse rotational relaxation time τ_R for PS-290k and PS-550k at 130 °C is 222s and 802s respectively. For the well–entangled blends here, we assume $\tau_{R,\text{blends}} = \phi_{\text{PS-290k}}\tau_{R,\text{PS-290k}} + \phi_{\text{PS-550k}}\tau_{R,\text{PS-550k}}$, where ϕ is the weight fraction of the component. Figure 5.4 plots the non–dimensional steady–state viscosity as a function of the Weissenberg number for the blends and melts. The Weissenberg number is defined as $Wi_R = \dot{\epsilon}\tau_R$. All the data superimposed to a 'master curve' in Figure 5.4, indicating the assumption of the Rouse time for the blends is reasonable. The slope of the 'master curve' is approximately -0.43, which is in agreement with the slope -0.42 ± 0.03 founded by Nielsen *et al.* (2006a) for the melts.

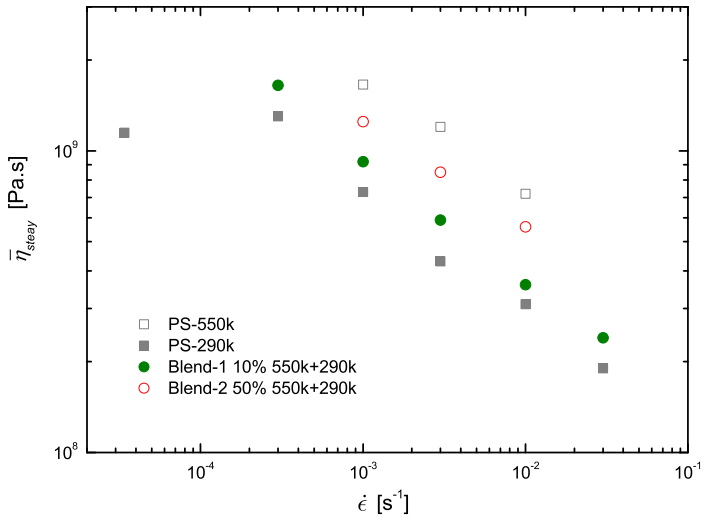

Figure 5.3: The extensional steady–state viscosity as a function of the strain rate for the polystyrene blends at 130 °C. The data for PS-290k and PS-550k are from Chapter3.

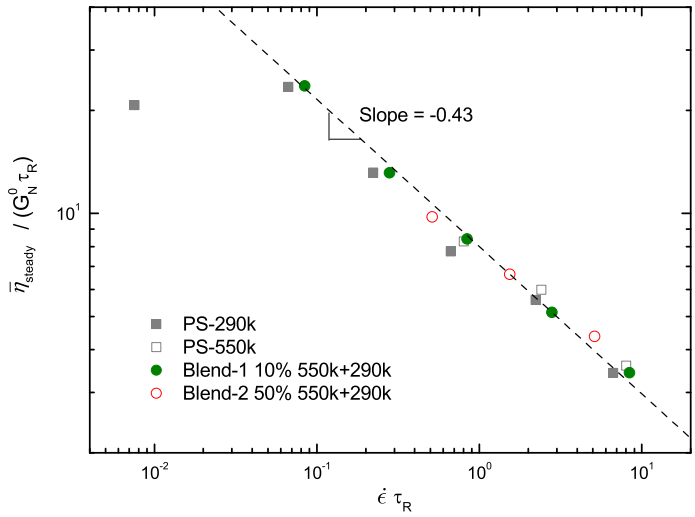

Figure 5.4: Comparison of the polystyrene blends and melts under non–dimensional parameters in the steady–state extensional flow. The data for PS-290k and PS-550k are from Chapter3.

5.5 Constitutive Modeling

It has been shown by Wagner *et al.* (2005) that the extensional steady–state viscosity of the well–entangled polystyrene melts could be captured by the interchain pressure (ICP) model. The ICP concept was originally proposed by Marrucci and Ianniruberto (2004). The stress tensor of the ICP model is given by Eq.3.13 and Eq.3.17 in Chapter 3. Figure 5.5 compares the simulation results of the ICP model with the extensional data for PS-290k and PS-550k. The tube diameter relaxation time τ_a is fitted as 2000s for PS-290k and 7200s for PS-550k at 130C. The model reasonably captures the extensional steady–state viscosity of the two melts.

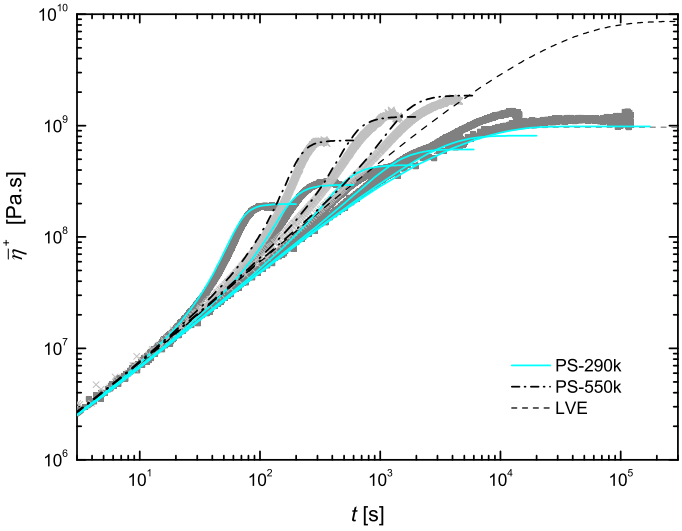

Figure 5.5: Comparison of the ICP model prediction with the extensional data for PS-290k and PS-550k at 130 °C.

Since the extensional steady–state viscosity of both Blend-1 and Blend-2 has the same trend as the melts, it would be interesting to check if the ICP model can also describe the behavior of the well–entangled blends. For the bidisperse blends we use a two–mode version of the ICP model in the form

$$\boldsymbol{\sigma}(t) = \sum_{i=1}^{2} \int_{-\infty}^{t} \frac{\partial G_i(t-t')}{\partial t'} f_i^2(t,t') \mathbf{S}_{\mathrm{DE}}^{\mathrm{IAA}} \mathrm{d}t', \tag{5.6}$$

where $G_i(t-t')$ is the relaxation modulus defined in Eq.5.2, $\mathbf{S}_{\mathrm{DE}}^{\mathrm{IAA}}$ is the Doi–Edwards strain tensor with the independent alignment assumption [Doi and Edwards (1986)] defined in Eq.3.15, and $f_i(t,t')$ is the molecular stress function given by

$$\frac{\partial}{\partial t} f_i = f_i \left[(\boldsymbol{\kappa} : \mathbf{S}) - \frac{f_i \left(f_i^3 - 1 \right)}{\tau_{a,i}} \right] \tag{5.7}$$

with the initial condition $f_i(t',t') = 1$. Figure 5.6 shows the simulation results of the two–mode ICP model with $\tau_{a,1} = 2000s$ and $\tau_{a,2} = 7200s$ for Blend-1 and Blend-2. The model well described Blend-1 which only contains 10% of PS-550k. The model also well described the startup of the flows for Blend-2, but underestimate the steady–state viscosity, indicating the tube diameter relaxation time $\tau_{a,i}$ for the long chain part could be enhanced. In Figure 5.6, a stress calculated from a simple mixing rule as $\sigma_{\mathrm{blend}}(t) = \phi_{\mathrm{PS-290k}}\sigma_{\mathrm{PS-290k}}(t) + \phi_{\mathrm{PS-550k}}\sigma_{\mathrm{PS-550k}}(t)$ is also plotted for comparison. It can be seen that for Blend-1, there is little difference between the calculation of the two–mode ICP model and the ICP model using simple mixing rule. However, for Blend-2, the latter calculation does not describe the startup of the flows as well as the two–mode ICP model, but it captures the steady–state viscosity much better.

5.6 Conclusions

The two bidisperse polystyrene blends made from PS-290k and PS-550k, with weight fraction 10% and 50% of the high molecular component respectively, have been measured in the uniaxial extensional flow. At strain rate higher than $\tau_{a,i}^{-1}$ of both components, the extensional steady–state viscosity of the well–entangled blends shows the same trend as the nearly monodisperse melts. The viscosity decreased monotonically with increasing the strain rate, and scales as $\bar{\eta}_{\mathrm{steady}} \sim \dot{\epsilon}^{-4.3}$. The influences from entanglement molecular weight and monomeric friction coefficient which have been shown in Chapter 3 and 4, are not shown in the well–entangled blends when compared with the monodisperse melts. The Rouse time and the level of the extensional steady–state viscosity of the two blends seem to follow the simple mixing rule. A two–mode interchain pressure model well captures the startup of the flow, but underestimate the level of the steady–state viscosity for the blend with higher weight fraction of the long chain part.

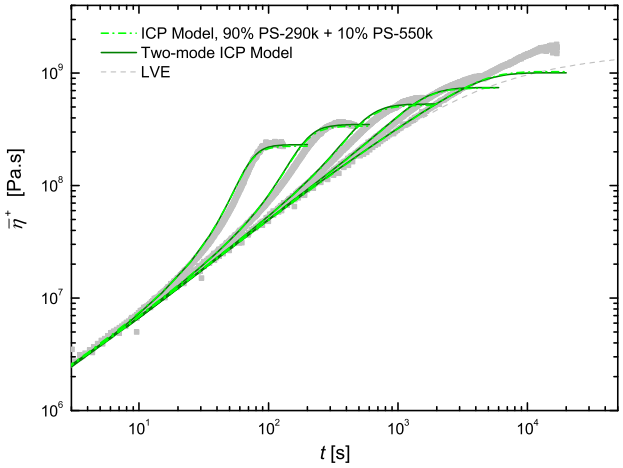

(a) ICP model prediction for Blend-1

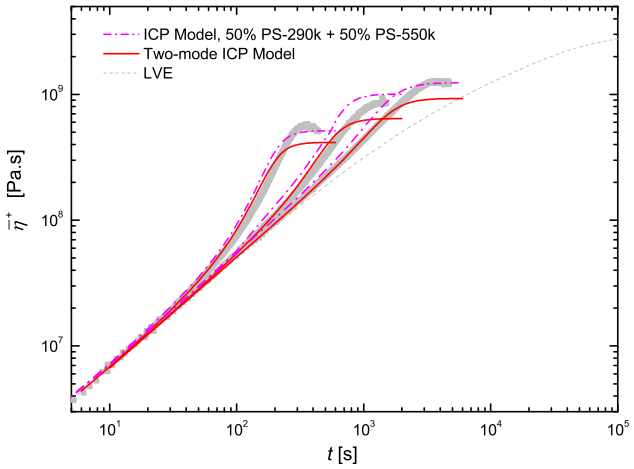

(b) ICP model prediction for Blend-2

Figure 5.6: Comparison of the ICP model prediction with the extensional data for the polystyrene blends at 130 °C.

Chapter 6

Extensional Rheology of Polydisperse Linear Melts

6.1 Introduction

In Chapter 3 and 4 we have investigated the linear polystyrene systems which contain entangled long chains diluted in unentangled short chains. The extensional steady–state viscosity of such system shows a plateau region at Weissenberg number bigger than 1. In Chapter 5 we have investigated the linear polystyrene systems which only contain well–entangled long chains. The extensional steady–state viscosity of such system shows a monotone decreasing function of the strain rate even at Weissenberg number bigger than 1. In the present chapter, we investigate a linear polystyrene system which contains all the above components, including entangled long chains with different molecular weight and unentangled short chains. Such a system is simply a polydisperse linear polystyrene melt. The melt is measured in uniaxial extensional flows in this chapter. We will show the trend of the extensional steady–state viscosity is different from the systems in Chapter 3–5. Stress relaxation and reversed biaxial flows both following the uniaxial extension of this melt are also performed in this chapter.

6.2 Material

The material used in this work is a commercial linear polystyrene provided by Aldrich (CAS 0993-53-6). The polystyrene has been previously characterized in differential scanning calorimetry (DSC) and size exclusion chromatography (SEC) by Rasmussen *et al.* (2007), and the properties are listed in Table 6.1. Rasmussen *et al.* (2007) also measured the polystyrene in both shear and extensional flows. They used a three–mode Baumgaertel-Schausberger-Winter (BSW) relaxation spectrum [Baumgaertel *et al.* (1990)] to describe the linear viscoelastic (LVE) properties. Here we fit their LVE data with the Maxwell model

$$G(s) = \sum_i \frac{g_i}{\tau_i} e^{-(s)/\tau_i}, \tag{6.1}$$

where the relaxation spectrum g_i and τ_i are also listed in Table 6.1. Figure 6.1 presents the LVE data with the Maxwell fitting. The original LVE data from Rasmussen *et al.* (2007) was given at 150 °C. Here we have shifted it to 120 °C using the time–temperature superposition procedure. The time–temperature shift factor was found by the WLF equation

$$\log_{10} a_T = \frac{-c_1^0 (T - T_0)}{c_2^0 + (T - T_0)}, \tag{6.2}$$

where $c_1^0 = 8.86$, $c_2^0 = 101.6$K, and $T_0 = 136.5$ °C according to Rasmussen *et al.* (2007). The average relaxation time τ_0 in Table 6.1 is defined as

$$\tau_0 = \frac{\sum_i g_i \tau_i^2}{\sum_i g_i \tau_i}. \tag{6.3}$$

6.3 Startup of Uniaxial Extension

The transient extensional stress growth coefficient in the startup of the uniaxial extensional flow has been measured by Rasmussen *et al.* (2007), but with very limited strain rates. Here we present measurements with more strain rates at 120 °C. The polystyrene was supplied in pellets. Before the measurements it was hot pressed into cylindrical test samples at 160 °C, with radius $R_0 = 4.5$mm and length $L_0 = 2.0$mm, giving an aspect ratio $\Lambda_0 = L_0/R_0 = 0.444$. The cylindrical test samples were then stretched by a

Table 6.1: Properties of the linear polystyrene melt CAS 0993-53-6 [Rasmussen *et al.* (2007)]. The linear viscoelastic spectrum is fitted to the data from Rasmussen *et al.* (2007)

Polymer melt	Linear polystyrene	
Product	CAS 0993-53-6	
M_w[kg/mol]	230	
M_n[kg/mol]	60	
M_w/M_n	3.7	
T_g[°C]	99	
	τ_i[s]	g_i[Pa]
	0.0184128	8273280
	0.0933335	220217
	0.473101	305447
	2.39812	113201
	12.1559	66602.2
Relaxation spectrum	61.6175	43915.6
at 120 °C	312.335	39156.3
	1583.20	29441.2
	8025.16	17645.3
	40679.0	6625.04
	206199	1101.86
	1045210	110.796
τ_0[s] at 120 °C	220380	

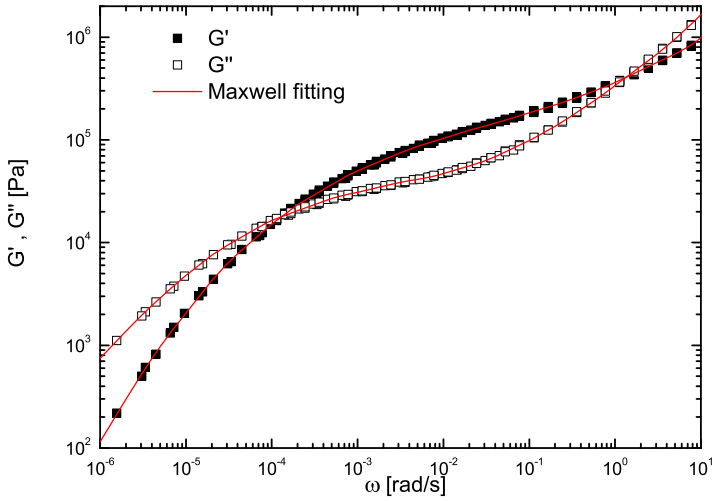

Figure 6.1: LVE data [Rasmussen *et al.* (2007)] fitted with the Maxwell spectrum for polystyrene CAS 0993-53-6 at 120 °C.

filament stretching rheometer (FSR) [Bach *et al.* (2003b)]. During the elongation, the force $F(t)$ was measured by a load cell and the diameter $2R(t)$ at the mid–filament plane was measured by a laser micrometer. All the test samples were pre–stretched to a radius R_p ranging from 1.5mm to 2.5mm at 170 °C prior to the experiments. Here the main purpose of pre–stretching is to avoid the force exceeding the working range of the load cell. After pre–stretching, the temperature was decreased to 120 °C for the elongational measurements. Nitrogen was used during the whole procedure to avoid sample degradation. The Hencky strain ϵ and the mean value of the stress difference $\langle\sigma_{zz} - \sigma_{rr}\rangle$ over the mid–filament plane are calculated by Eq.3.3 and Eq.3.4, respectively. The strain rate is defined as $\dot{\epsilon} = d\epsilon/dt$, and the extensional stress growth coefficient in the startup of the flow is defined as $\bar{\eta}^{+} = \langle\sigma_{zz} - \sigma_{rr}\rangle/\dot{\epsilon}$. During the startup of the uniaxial extension, the strain rate is kept as a constant $\dot{\epsilon}_0$ with the aid of an online control scheme [Román Marín *et al.* (2013)].

Figure 6.2(a) presents the extensional stress growth coefficient as a function of the time for the polystyrene at 120 °C. The measurement at $\dot{\epsilon}_0 = 0.0003\text{s}^{-1}$ was also repeated at 140 °C and shifted back to 120 °C. The shift factor was found to be in agreement with Eq.6.2. The measurements at $\dot{\epsilon}_0 < 0.0003\text{s}^{-1}$ in the figure were all originally measured at either 140 °C or 150 °C and shifted back to 120 °C. Figure 6.2(b) plots the corresponding stress–strain curves for each strain rate from Figure 6.2(a). All the measurements at $\dot{\epsilon}_0 \leq 0.01\text{s}^{-1}$ reached the steady stress. At $\dot{\epsilon}_0 > 0.01\text{s}^{-1}$, the test samples broke during the stretching and thus the steady stress was not approached. The samples broke at almost the same stress level, as also observed for Solution-1k in Chapter 4.

Figure 6.3 shows the steady–state viscosity as a function of the strain rate for the polystyrene at 120 °C. For the strain rates where the test samples broke during the elongation, the maximum values of the stress growth coefficient $\sigma_{\max}/\dot{\epsilon}_0$ are plotted. As mentioned in Chapter 3–5, for the well–entangled polystyrene melts and blends where the entanglement molecular weight is approximately 13300g/mol, the steady–state viscosity decreases with increasing the strain rate as $\bar{\eta}_{\text{steady}} \sim \dot{\epsilon}^{-0.5}$. However, for the polystyrene solutions which is diluted in an unentangled styrene oligomer, where the entanglement molecular weight of the polystyrene is bigger than 13300g/mol, the steady–state viscosity shows a plateau region with increasing the strain rate as $\bar{\eta}_{\text{steady}} \sim \dot{\epsilon}^{0}$. The investigated polydisperse polystyrene here contains both well–entangled and unentangled molecules. The figure of the molecular weight distribution can be found in Rasmussen *et al.* (2007). Therefore it is not surprising that in Figure 6.3 the steady–state viscosity decreases as $\bar{\eta}_{\text{steady}} \sim \dot{\epsilon}^{-0.25}$, which is in between of a well–entangled polystyrene melts and a polystyrene solution. At strain rates higher than 0.01s^{-1}, the samples broke during the elongation and the maximum value of the stress growth coefficient scales as $\sigma_{\max}/\dot{\epsilon}_0 \sim \dot{\epsilon}^{-1}$, which may be an indication that the maximum stretch ratio is achieved.

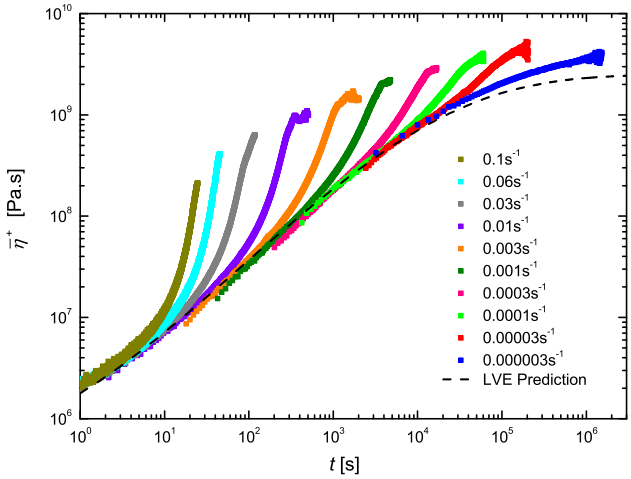

(a) The extensional stress growth coefficient as a function of the time.

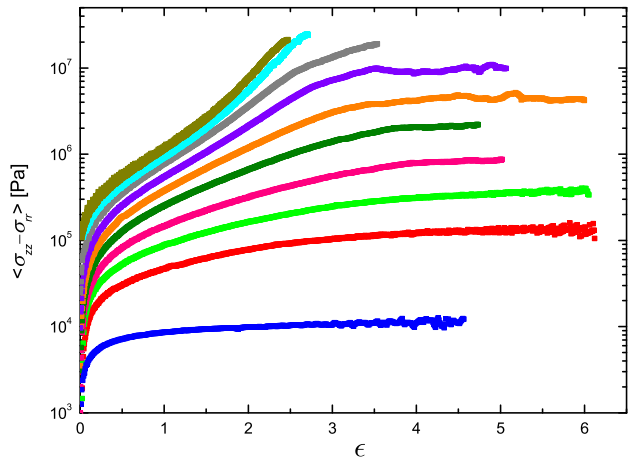

(b) The extensional stress as a function of the Hencky strain. (From bottom to top) $\dot{\epsilon}_0$ = 0.000003, 0.00003, 0.0001, 0.0003, 0.001, 0.003, 0.01, 0.03, 0.06, 0.1s^{-1}

Figure 6.2: Measurements of the startup of uniaxial extension at different strain rates for the polystyrene CAS 0993-53-6 at 120 °C.

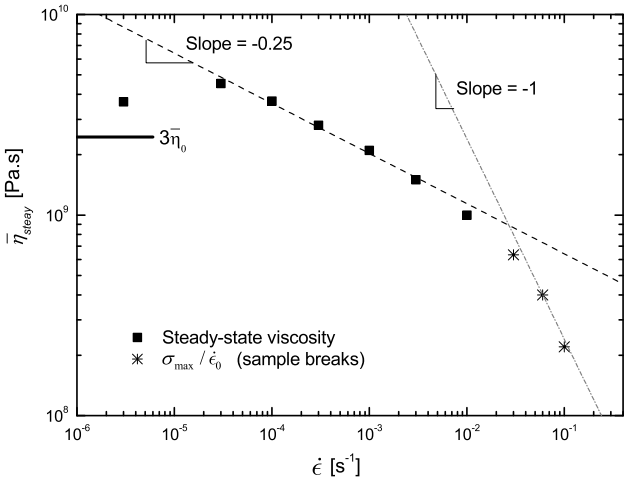

Figure 6.3: The extensional steady–state viscosity as a function of the strain rate for the polystyrene CAS 0993-53-6 at 120 °C. For the strain rates where the test samples broke during the elongation, the maximum values of the stress growth coefficient are plotted.

6.4 Stress Relaxation

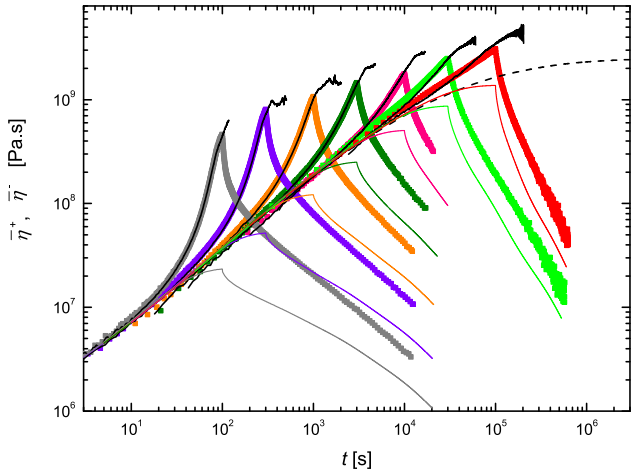

Figure 6.4: Measurements of stress relaxation following the uniaxial extension at different strain rates for the polystyrene CAS 0993-53-6 at 120 °C. (From right to left) $\dot{\epsilon}_0 = 0.00003, 0.0001, 0.0003, 0.001, 0.003, 0.01, 0.03\text{s}^{-1}$. The solid lines in the figure are Doi–Edwards predictions with IAA.

The startup of the stress relaxation experiments was uniaxial extension at different strain rate $\dot{\epsilon}_0$ as described in Section 6.3. For each strain rate the flow was stopped at Hencky strain $\epsilon_0 = 3$, and the stress during the relaxation phase was measured. The mid–filament radius during the stress relaxation was kept constant by the active control loop, giving $\dot{\epsilon} = 0$. The extensional stress decay coefficient is defined as $\bar{\eta}^- = \langle \sigma_{zz} - \sigma_{rr} \rangle / \dot{\epsilon}_0$, where $\dot{\epsilon}_0$ is the strain rate in the start–up of the flow.

Figure 6.4 shows the measured stress growth and decay coefficients as a function of the time at 120 °C. The measurements for the lowest two strain rates were originally performed at 140 °C and shifted to 120 °C, with the shift factor calculated from Eq.6.2. The solid lines in the figure are the predictions from the original reptation based model introduced by Doi and Edwards (1979). The stress tensor in the Doi–Edwards (DE) model is expressed as

$$\boldsymbol{\sigma}(t) = \int_{-\infty}^{t} \frac{\partial G(t-t')}{\partial t'} \mathbf{S}_{\mathrm{DE}}(t,t')\mathrm{d}t', \tag{6.4}$$

where $G(t-t')$ is defined in Eq.6.1 and $\mathbf{S}_{\mathrm{DE}}$ is the relative strain. The rigorous form and the independent alignment approximation (IAA) of $\mathbf{S}_{\mathrm{DE}}$ are given by Eq.6.5 and Eq.6.6, respectively.

$$\mathbf{S}_{\mathrm{DE}}^{\mathrm{Rigorous}}(t,t') = \frac{15}{4}\frac{1}{\langle|\mathbf{E}\cdot\mathbf{u}|\rangle}\left\langle\frac{\mathbf{E}\cdot\mathbf{u}\;\mathbf{E}\cdot\mathbf{u}}{|\mathbf{E}\cdot\mathbf{u}|}\right\rangle, \tag{6.5}$$

$$\mathbf{S}_{\mathrm{DE}}^{\mathrm{IAA}}(t,t') = 5\left\langle\frac{\mathbf{E}\cdot\mathbf{u}\;\mathbf{E}\cdot\mathbf{u}}{|\mathbf{E}\cdot\mathbf{u}|^2}\right\rangle = 5\mathbf{S}(t,t'). \tag{6.6}$$

In both equations, $\mathbf{u}$ is the unit vector and $\mathbf{E}$ the relative deformation gradient tensor. The bracket denotes an average over an isotropic distribution and the analytical formulas can be found in Urakawa *et al.* (1995). The solid lines in Figure 6.4 are the DE predictions with the IAA. As reported by Nielsen *et al.* (2008), the elongational stress for the nearly monodisperse polystyrene decays nearly toward a DE based stress at large times. However, it seems that the measured stress for the polydisperse polystyrene in the relaxation phase remains considerably larger than the DE prediction in Figure 6.4. This slower relaxation process may be the consequence of the higher monomeric friction coefficient caused by the short chains as discussed in Chapter 4.

6.5 Reversed Flow

The reversed flow experiments was also performed following uniaxial extension at different strain rate $\dot{\epsilon}_0$ as described in Section 6.3. During the startup of uniaxial stretching we define $\dot{\epsilon}_0^+ = \dot{\epsilon}$ and in the reversed flow phase we define $\dot{\epsilon}_0^- = -\dot{\epsilon}$, where $\dot{\epsilon}_0^+$ and $\dot{\epsilon}_0^-$ stay positive, constant and equal. Figure 6.5(a) shows the measured transient stress as a function of Hencky strain in the startup and reversed flow at different strain rate. All the measurements were performed at 120 °C. For each strain rate the flow was reversed at Hencky strain $\epsilon_0 = 3$. At some time t_R in the reversed flow phase, the stress changes sign from positive to negative (tension to compression). The strain recovery is defined as $\epsilon_R = \epsilon_0 - \epsilon(t_R)$ [Nielsen and Rasmussen (2008)]. Figure 6.5(b) shows the strain recovery as a function of strain rate for all the measurements from Figure 6.5(a). It can be seen that the recovered strain ϵ_R increases monotonically with increasing the strain rate $\dot{\epsilon}_0$. When the strain rate is high enough, the polystyrene melt behaves like a network, and the recovered strain will not depend on the strain rate, resulting in the tendency to the steady state region at high rate in Figure 6.5(b). The dashed and solid lines in Figure 6.5(b) are predictions from the DE model with and without the IAA respectively, as described in Section 6.4. Here we plot both results with and without the IAA, because the IAA may lead to significant deviations from the rigorous model

in reversed flows [Doi (1980)]. As reported in Nielsen and Rasmussen (2008), the DE model overestimates the recovered strain for the nearly monodisperse polystyrene. Here the DE model overestimates the recovered strain for the polydisperse polystyrene as well.

Figure 6.6(a) shows the measured transient stress as a function of Hencky strain for the fixed strain rate $\dot{\epsilon}_0^+ = \dot{\epsilon}_0^- = 0.003\text{s}^{-1}$. The flow was reversed at different Hencky strains ϵ_0 ranged from 1 to 4. Figure 6.6(b) plots the recovered strain ϵ_R as a function of the imposed strain ϵ_0 for all the measurements from Figure 6.6(a). With the fixed strain rate, the strain recovery also increases monotonically with increasing the imposed Hencky strain. The recovered strain reaches a constant value when the imposed Hencky strain is large enough, indicating the startup of the flow reaches the steady state at the given Hencky strain before reversing.

6.6 Conclusions

The polydisperse linear polystyrene melt, with a weight average molecular weight 230 kg/mole and a polydispersity index 3.7, has been measured in unaxial extensional flows. The extensional steady–state viscosity of the melt is found to decrease as $\bar{\eta}_{\text{steady}} \sim \dot{\epsilon}^{-0.25}$, in which the exponent is in between of well–entangled polystyrene melts ($\bar{\eta}_{\text{steady}} \sim \dot{\epsilon}^{-0.5}$) and polystyrene solutions ($\bar{\eta}_{\text{steady}} \sim \dot{\epsilon}^{0}$). Stress relaxation and reversed biaxial flows both following the uniaxial extension of the melt have also been measured. In the stress relaxation phase, the polydisperse melt is observed to relax slower than the monodisperse melt. In the reversed flow measurements, the melt is found to behave like a network at high rates where the strain recovery saturates.

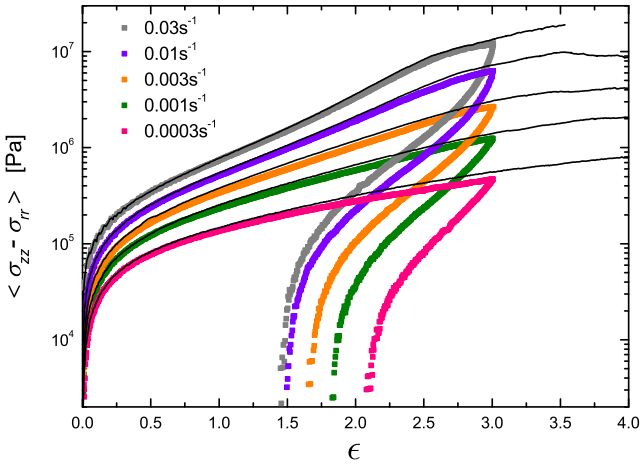

(a) The measured stress as a function of the Hencky strain at different strain rates. The solid lines in the figure are the uniaxial extensional data from Figure 6.2(b)

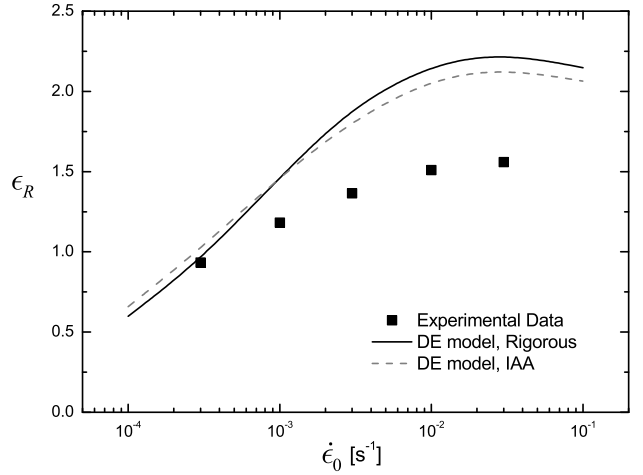

(b) The recovered strain as a function of the stain rate. The dashed and solid lines in the figure are Doi–Edwards predictions with and without IAA, respectively.

Figure 6.5: Measurements of reversed flows following the uniaxial extension at different strain rates for the polystyrene CAS 0993-53-6 at 120 °C.

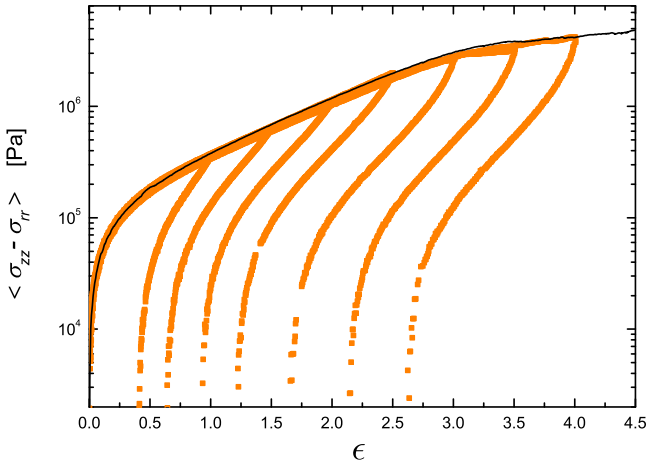

(a) The measured stress as a function of the Hencky strain at different imposed Hencky strains. The solid lines in the figure are the uniaxial extensional data from Figure 6.2(b)

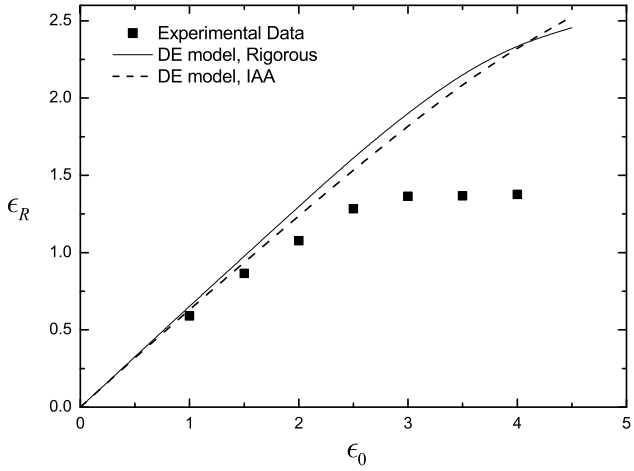

(b) The recovered strain as a function of the imposed Hencky strain. The dashed and solid lines in the figure are Doi–Edwards predictions with and without IAA, respectively.

Figure 6.6: Measurements of reversed flows following the uniaxial extension at different imposed Hencky strains with the fixed strain rate $\dot{\epsilon}_0^+ = \dot{\epsilon}_0^- = 0.003\text{s}^{-1}$ for the polystyrene CAS 0993-53-6 at 120 °C.

Chapter 7

Elongational Steady–State Viscosity of Well–Defined Star and H–shaped Polymer Melts

7.1 Introduction

From Chapter 3 to Chapter 6 we have investigated the viscoelastic behavior of linear polystyrene melts in extensional flows. From Chapter 7 we measure the extensional rheology of branched polymer melts. Branched polymers are more complex than linear polymers, not only because of their molecular structures but also because of their rheological behavior. The ability to predict and control the rheological behavior of polymer fluids as a function of molecular chemistry has attracted a long history of collaboration between industry and academia. It is known that the rheology of polymer melts is highly sensitive to branching, but the precise connection between branching architecture and non–linear rheology is still not fully understood.

Branched polymers have different molecular structures such as star, H, comb and dendritic shapes. The simplest case of branched polymers is a star–shaped polymer. A star–shaped polymer has only one branch point per molecule and therefore always has a free end for each arm, which allows the branch to retract quickly under flow. This feature has a significant difference from the molecules which contain multiple branch points on a same chain, because the molecular strands that lie between two branch

points have no free ends and hence retract slower. The simplest architecture that has a molecular strand with no free end is one with just two branch points. It can be an H–shaped polymer that has a backbone in between of the two branch points and two arms on each branch point. It can also be a pom–pom polymer [McLeish and Larson (1998)] if there are more than two arms on each of the two branch points.

Measurements on monodisperse branched polymers of well–defined molecular structures are especially important for the validation of the developing theoretical models. In the previous works, star [e.g. Milner and McLeish (1997), Frischknecht *et al.* (2002), Lee *et al.* (2005)] and H–shaped [e.g. McLeish *et al.* (1999), Shie *et al.* (2003)] polymer melts have been well studied both experimentally and theoretically in shear rheology. But few experiments have been done in extensional flows. Nielsen *et al.* (2006b) measured an asymmetric star and a pom–pom polymer in the startup of extensional flows in which the steady–state viscosity could be determined. These data are the only published data of elongational steady–state viscosity for branched polymers of known architecture. Recently Ianniruberto and Marrucci (2013) analyzed the data measured by Nielsen *et al.* (2006b) and reported that branched polystyrene melts behave like linear melts in the steady state of fast elongational flows. However, this conclusion is based on very limited experimental data.

In the present chapter, we measure an asymmetric star polystyrene Star-20k and an H–shaped polystyrene H2A1 in the startup and steady state of elongational flows. We compare the elongational steady–state viscosity of the two branched polymer melts with the viscosity of the linear melts that we investigated in the previous chapters. We also check if the branched melts behave similarly as the linear melts in the steady state of fast elongational flows as reported by Ianniruberto and Marrucci (2013). The asymmetric star polymer Star-20k is also compared with some other star and linear melts in shear rheology.

7.2 The Asymmetric Star Polystyrene

7.2.1 Molecular structure

A series of three–arm star polystyrenes was synthesized in which two of the arms had the same molecular weight of 90 kg/mole and the third arm varied in molecular weight from 0 (i.e., a linear polymer) to 90 kg/mole (i.e., a symmetric star)[1]. All the samples were synthesized using living anionic polymerization. Size exclusion chromatography (SEC) was employed for samples characterization. Table 7.1 summarizes the number average molecular weight M_n, the polydispersity index *PDI* and the glass transition

[1] Synthesis and size exclusion chromatography were carried out by Serena Agostini at Durham University.

temperature T_g of all the samples. The glass transition temperature was measured using the differential scanning calorimetry (DSC).

Table 7.1: The molecular weight of the star polystyrenes

Sample Name	Long Arm M_n[g/mol]	*PDI*	Short Arm M_n[g/mol]	*PDI*	Whole M_n[g/mol]	*PDI*	T_g[°C]
PS-180k	–	–	–	–	182500	1.02	107.5
Star-10k	90000	1.03	10000	1.05	193300	1.02	108.0
Star-20k	90000	1.03	19600	1.05	202000	1.03	108.0
Star-90k	90000	1.03	–	–	279700	1.03	105.0

7.2.2 Linear viscoelasticity

The linear viscoelastic (LVE) properties of all the polystyrene samples in Table 7.1 were obtained from small amplitude oscillatory shear flow measurements. An 8mm plate–plate geometry was used on an ARES–G2 rheometer from TA instruments. The measurements were performed at 130, 150 and 160 °C. For each sample the data were shifted to a single master curve at 130 °C using the time–temperature superposition procedure. The time–temperature shift factors for PS-180k, Star-10k and Star-20k were found to agree with the fitted WLF equation in Chapter 3 for the monodisperse polystyrene melts:

$$\log_{10} a_T = \frac{-c_1^0 (T - T_0)}{c_2^0 + (T - T_0)}, \tag{7.1}$$

where $c_1^0 = 8.99$, $c_2^0 = 81.53$K, $T_0 = 130\,°$C, and T is temperature in °C. Figure 7.1 presents the LVE data of all the samples. The data from PS-180k, Star-10k and Star-20k overlap in the high–frequency Rouse regime. The original data for Star-90k has a horizontal shift compared with the other samples. In the figure the G' G'' curves for Star-90k have been horizontally shifted with a factor of 0.5, so that the crossover point at the high frequency part overlaps the other three samples. It can be seen that the terminal time increases with increasing the length of the third arm of the stars. The linear polymer PS-180k has the shortest terminal time and the symmetric star polymer Star-90k has the longest terminal time.

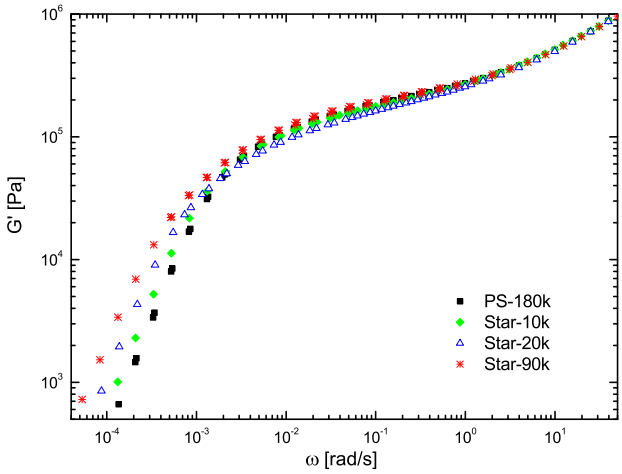

(a) G' curves for PS-180k, Star-10k, Star-20k and Star-90k. The plot for Star-90k has been horizontally shifted with a factor of 0.5 from the original data

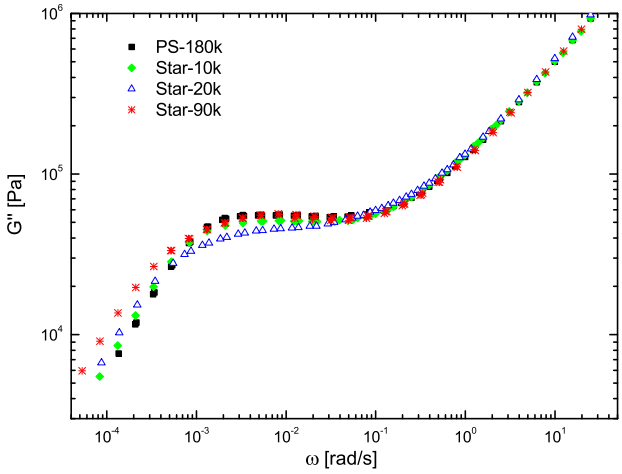

(b) G'' curves for PS-180k, Star-10k, Star-20k and Star-90k. The plot for Star-90k has been horizontally shifted with a factor of 0.5 from the original data

Figure 7.1: LVE data for PS-180k, Star-10k, Star-20k and Star-90k at 130 °C.

7.2.3 Nonlinear viscoelasticity

The nonlinear viscoelastic properties were obtained from stress–strain measurements in uniaxial extensional flows, using the filament stretching rheometer (FSR) which has been described in the previous chapters. Here we only report the data for Star-20k. The sample was molded into cylindrical test specimens under vacuum at approximately 140 °C, with a fixed radius $R_0 = 2.7$mm. The initial length L_0 of the cylindrical test specimens was varied between 1.3mm and 1.6mm, giving an aspect ratio $\Lambda_0 = L_0/R_0$ between 0.48 and 0.59. All the test specimens were pre–stretched to a radius R_p ranged from 1.5mm to 2.3mm at 150 °C prior to the elongational experiments. After pre–stretching, the temperature was decreased to 130 °C for the extensional stress measurements. Nitrogen was used in the whole procedure. The samples were checked by SEC again after the extensional stress measurements to ensure that there was no degradation.

Figure 7.2 presents the measured extensional stress growth coefficient $\bar{\eta}^+$ as a function of the time at 130 °C for Star-20k. The extensional stress growth coefficient is defined as $\bar{\eta}^+ = \langle \sigma_{zz} - \sigma_{rr} \rangle / \dot{\epsilon}$, and the strain rate is defined as $\dot{\epsilon} = d\epsilon/dt$. The Hencky strain ϵ and the mean value of the stress difference $\langle \sigma_{zz} - \sigma_{rr} \rangle$ over the mid–filament plane are calculated by Eq.3.3 and Eq.3.4, respectively. The dashed line in the figure is the LVE prediction calculated by

$$\bar{\eta}^+ = 3 \sum\nolimits_i g_i \tau_i \left(1 - e^{-t/\tau_i}\right), \tag{7.2}$$

where g_i and τ_i are obtained by fitting the LVE data of Star-20k in Figure 7.1 with the Maxwell model described in Section 6.2. All the measurements in Figure 7.2 reached the steady state, and Figure 7.3 plots the elongational steady–state viscosity as a function of strain rate for Star-20k also at 130 °C. It can be seen that the steady–state viscosity decreases approximately as $\bar{\eta}_{\text{steady}} \sim \dot{\epsilon}^{-0.26}$, which is similar as the tube dilation effect seen for the polydisperse linear melt in Chapter 6.

7.3 The H–Shaped Polystyrene

7.3.1 Molecular structure

The H–shaped polystyrene H2A1 is from the same batch that was synthesized by Roovers and Toporowski (1981). It contains a backbone between two branch points with the molecular weight $M_b = 44$kg/mol, and two arms on each branch point with the molecular weight $M_a = 46$kg/mol for each arm. The sample is checked in size

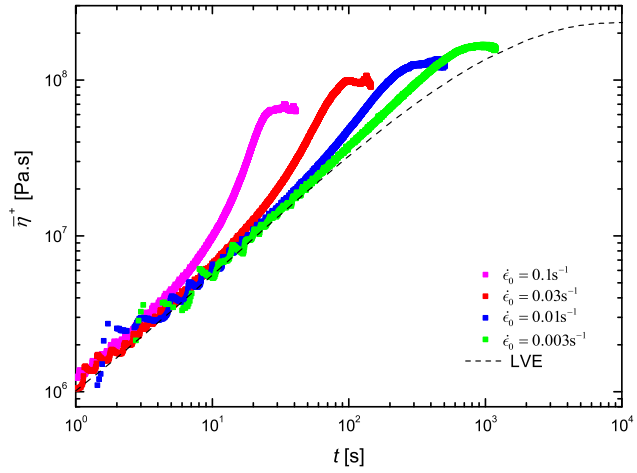

Figure 7.2: The measured extensional stress growth coefficient as a function of the time for Star-20k at 130 °C. The dashed line is the LVE prediction.

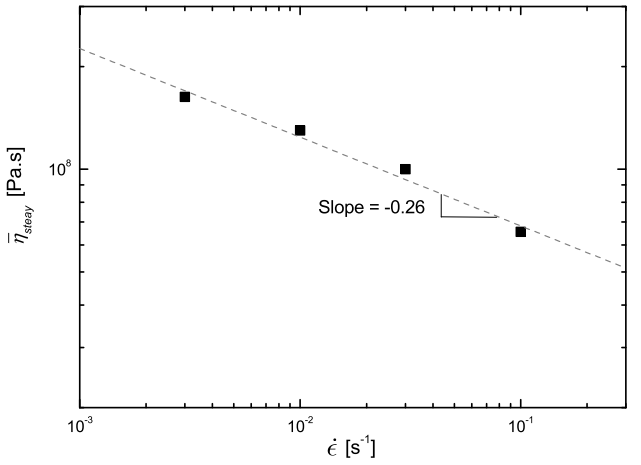

Figure 7.3: The extensional steady–state viscosity as a function of the strain rate for Star-20k at 130 °C.

exclusion chromatography (SEC) at DTU. The weight average molecular weight for the whole molecule is M_w = 235kg/mol with a polydispersity index PDI = 1.02, which is in agreement with the molecular weight reported by Roovers and Toporowski (1981). Detailed information about synthesis and chromatography can also be found in Roovers and Toporowski (1981).

7.3.2 Nonlinear viscoelasticity

The nonlinear viscoelastic property of H2A1 was obtained from stress–strain measurements in uniaxial extensional flows, using the same FSR and following the same procedures as described in Section 7.2.3. The only difference was that the samples were pre–stretched at higher temperature of 160 °C, due to the slower relaxation process of the H–shaped structure. Furthermore, because of the very limited amount (100mg) of the material, we had to reuse the stretched samples for several times. After the measurements, one of the stretched samples was checked in SEC again. However, it was observed that around 8% of the molecules lost arms. The influence from samples degradation on the accuracy of FSR measurements is discussed in Appendix A.

Figure 7.4 shows the measured extensional stress growth coefficient $\bar{\eta}^+$ as a function of the time at 130 °C for the H–shaped polystyrene H2A1. The dashed line in the figure is the LVE prediction calculated by Eq.7.2[2]. As mentioned in Chapter 5, the elongational steady–state viscosity $\bar{\eta}_{\text{steady}}$ of the monodisperse linear polystyrene melts does not exceed $3\eta_0$ for any strain rate, where η_0 is the zero shear rate viscosity. This observation is also seen for the asymmetric star polystyrene melt Star-20k in Figure 7.2. But for H2A1, it can be seen in Figure 7.4 that at the lowest four rates, $\bar{\eta}_{\text{steady}}$ exceeds $3\eta_0$, indicating that the H–shaped melts are more strain hardening than both the linear and star melts. Nielsen *et al.* (2006b) reported an stress overshoot in the transient extensional flow for a nearly monodisperse pom–pom polystyrene melt. However the overshoot is not observed for the H–shaped polystyrene melt here. Figure 7.5 presents the elongational steady–state viscosity as a function of the strain rate for H2A1. The steady–state viscosity decreases approximately as $\bar{\eta}_{\text{steady}} \sim \dot{\epsilon}^{-0.6}$, which is similar as the branched low–density polyethylene melts reported by Rasmussen *et al.* (2005).

7.4 Comparison of the Elongational Steady Stress

Ianniruberto and Marrucci (2013) reported that the behavior of asymmetric stars and pom–pom polymers in steady–state elongational flow is very close to that of linear

[2]The LVE property of H2A1 was measured by Helen Lentzakis at Foundation for Research and Technology Hellas in Greece. Helen Lentzakis also participated in the FSR measurements for H2A1 at DTU.

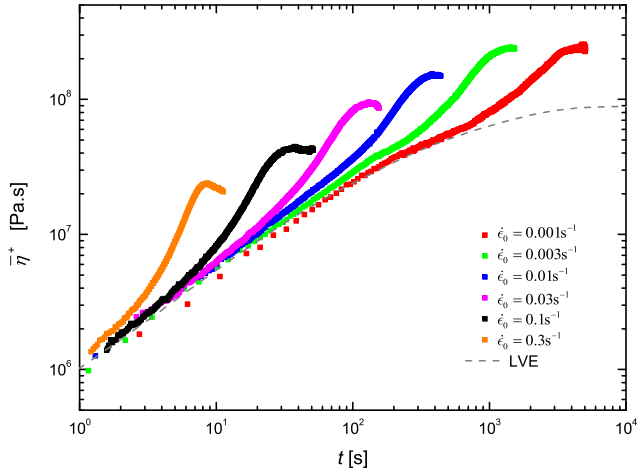

Figure 7.4: The measured extensional stress growth coefficient as a function of the time for H2A1 at 130 °C. The dashed line is the LVE prediction.

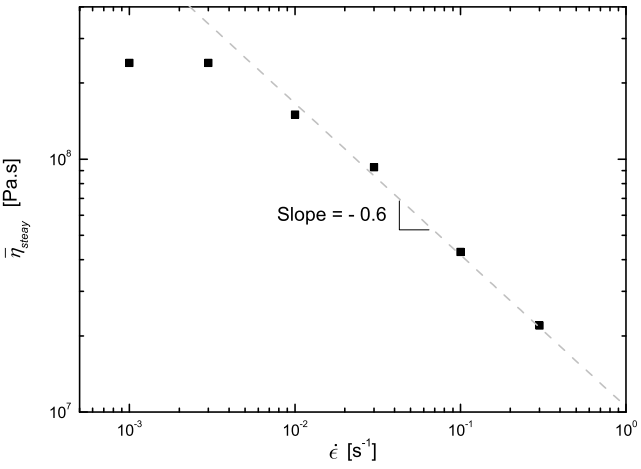

Figure 7.5: The extensional steady–state viscosity as a function of the strain rate for H2A1 at 130 °C.

polymers, especially for strain rates larger than the reciprocal Rouse time. However, this conclusion was based on very limited experimental data. Here we compare the elongational steady stress of the asymmetric star melt Star-20k and the H–shaped melt H2A1 with the linear melt PS-290k that we measured in Chapter 3.

Similarly as in Chapter 3, we define the Weissenberg number $Wi_R = \dot{\epsilon}\tau_R$, where τ_R is the Rouse rotational relaxation time. The τ_R for the linear melt PS-290k has been already estimated in Chapter 3 as 222s at 130 °C. For the asymmetric star melt Star-20k, since the short arm (20kg/mole) only contains one entanglement, the Rouse time should be dominated by the two long arms (90kg/mole for each arm). Therefore the Rouse time for Star-20k is estimated as equivalent to the linear chain with the molecular weight 180kg/mole. The Rouse time for the H–shaped melt H2A1 is calculated as [Ianniruberto and Marrucci (2013)]

$$\tau_R = \tau_{R,b}\left(\frac{\lambda}{q} + 4\lambda\frac{M_a}{M_b} + 4\frac{M_a^2}{M_b^2}\right), \tag{7.3}$$

where $\tau_{R,b}$ is the Rouse time of the linear backbone, q is the number of arms on each branch point ($q = 2$), λ is the backbone stretch ratio ($\lambda = 1.88$ according to Ianniruberto and Marrucci (2013)), M_a is the molecular weight of one arm, and M_b is the molecular weight of the backbone. The estimated Rouse times for PS-290k, Star-20k and H2A1 at 130 °C are listed in Table 7.2. Figure 7.6 compares the elongational steady stress as a function of the Weissenberg number for the linear and branched polystyrene melts. All the data superimpose to a 'master line' at Weissenberg number bigger than 1, showing the same behavior of the linear and branched melts in fast steady–state elongational flow. This result is in agreement with the observation reported by Ianniruberto and Marrucci (2013).

Table 7.2: Evaluated Rouse time for the linear and branched polystyrene melts at 130 °C

Sample Name	PS-290k	Star-20k	H2A1
τ_R[s]	222	88.6	69.7

7.5 Conclusions

Two well–defined branched polymer melts, Star-20k and H2A1, have been measured in uniaxial extensional flows. Star-20k is a three–arm star polystyrene in which two of the arms have the same molecular weight of 90 kg/mole and the third arm is 20 kg/mole.

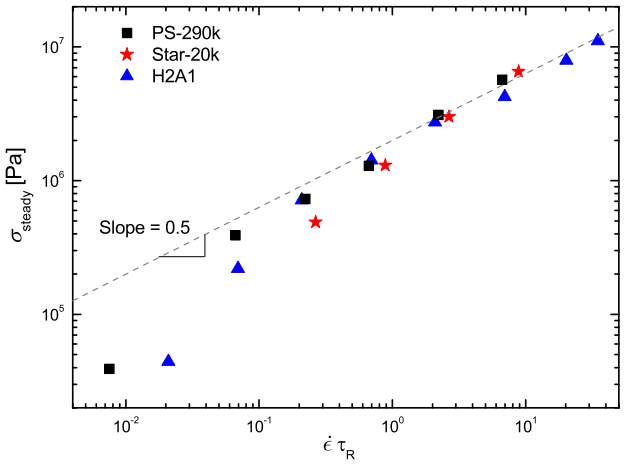

Figure 7.6: Comparison of the steady stress as a function of Weissenberg number between the linear and branched polystyrene melts.

In the measured range of strain rate, the elongational steady–state viscosity of Star-20k decreases approximately as $\overline{\eta}_{\text{steady}} \sim \dot{\epsilon}^{-0.26}$, which is similar as the polydisperse linear melt in Chapter 6. H2A1 is an H–shaped polystyrene that contains a backbone with the molecular weight M_b = 44kg/mol and two arms on each branch point with the molecular weight M_a = 46kg/mol for each arm. The elongational steady–state viscosity of H2A1 decreases approximately as $\overline{\eta}_{\text{steady}} \sim \dot{\epsilon}^{-0.6}$, which is similar as the low–density polyethylene melts reported by Rasmussen *et al.* (2005). The steady stress of the two branched polystyrenes has been compared with a linear polystyrene PS-290k (from Chapter 3) as a function of Weissenberg number. It shows that both Star-20k and H2A1 behave like PS-290k in fast extensional flows where the Weissenberg number is bigger than 1, which is in agreement with the observation reported by Ianniruberto and Marrucci (2013).

Chapter 8

Stress Relaxation and Reversed Flow of LDPE Melts Following Uniaxial Extension

8.1 Introduction

Extensional flow is the dominant type of deformation in many industrial polymer processes. However, it still presents challenges both experimentally and theoretically to capture and explain the stress–strain responses. Accurate and reliable stress–strain measurements of the extensional flow play a crucial role in the understanding of nonlinear rheological properties of polymers.During the last decades different types of extensional rheometers have been developed, such as the Rheometrics Melt Extensiometer (RME) [Meissner (1972); Meissner and Hostettler (1994)], the Münstedt Tensile Rheometer (MTR) [Münstedt (1979)], the Sentmanat Extensional Rheometer (SER) [Sentmanat (2004)] and the Filament Stretching Rheometer (FSR) [McKinley and Sridhar (2002)]. The most frequently reported measurements using these extensional rheometers are either the steady or the transient stress in start–up of uniaxial extension. Measurements of stress relaxation with the SER [Sentmanat *et al.* (2005)] are limited to low Hencky strains due to the necking instability [Wang *et al.* (2007)]. Measurements of reversed flow have been reported for low-density polyethylene (LDPE) melts [Meissner (1971); Wagner and Stephenson (1979)] in the form of free recovery. This is a controlled stress experiment as opposed to the controlled strain experiment to be

considered here. The recovered strains can therefore not be directly compared.

Recently new techniques to measure stress relaxation [Nielsen *et al.* (2008)] and reversed biaxial flow [Nielsen and Rasmussen (2008)] both following uniaxial extension, as well as large amplitude oscillatory extension (LAOE) [Bejenariu *et al.* (2010)], have been presented. These experiments were performed with an FSR modified for high-temperature measurements of polymer melts by Bach *et al.* (2003b). With the aid of a closed loop controller, the filament diameter in the mid–plane is controlled accurately and therefore the extension rate can be controlled even during the necking phase [Wang *et al.* (2007); Lyhne *et al.* (2009)]. Work regarding stress relaxation and reversed flow using the FSR has been done on both linear [Nielsen *et al.* (2008); Nielsen and Rasmussen (2008)] and branched [Rasmussen *et al.* (2009)] narrow molar mass distribution (NMMD) polymer melts, but not yet on polydisperse melts. Measurements of NMMD polymer melts of known structures are important for the understanding of nonlinear flow properties. However, many commercially available polymers, such as LDPE, are branched and highly polydisperse. A maximum in the transient elongational stress coefficient of LDPE was observed by Raible *et al.* (1979) and modeled by Wagner *et al.* (1979) for the first time. Recently Read *et al.* (2011) proposed a predictive scheme of the linear and nonlinear response for industrial polymers. They compared the nonlinear predictions with the measurements of uniaxial extension for three LDPE melts. However the experimental data was limited below a Hencky strain of 3.5.

FSR measurements on LDPE melts have previously been reported by Bach *et al.* (2003b) and Rasmussen *et al.* (2005). In the latter investigation one the samples was extended to a Hencky strain of 7 and a steady stress following the overshoot was reported. In order to investigate further the extensional dynamics of LDPE, especially the rheological behavior associated with the overshoot, we will present the measurements of stress relaxation and reversed biaxial flow both following the uniaxial extension on two commercial LDPEs.

8.2 Materials

Two types of commercial LDPEs, Lupolen 3020D and Lupolen 1840D provided by BASF, have been chosen for this study. The Lupolen 3020D and 1840D LDPE melts have been previously characterized in shear by Bastian (2001) and by Rasmussen *et al.* (2005), respectively. Rasmussen *et al.* (2005) also measured the extensional stress growth coefficient in uniaxial elongation for both melts. The LDPE samples we used in this study are both from the same batches as in Rasmussen *et al.* (2005), and the elongation measurements are in agreement with Rasmussen *et al.* (2005) as well.

The properties of the LDPE melts are listed in Table 8.1. The Lupolen 1840D has much

wider molar mass distribution. The molecular structure of the Lupolen 1840D, among other LDPE melts, has been discussed in Nordmaier *et al.* (1990a, 1990b). The linear viscoelastic spectrum for Lupolen 3020D from Bastian was originally given at 170 °C. In Table 8.1 we have shifted it to 130 °C with the time-temperature shift factor $a_T = 6.4$ obtained from Rasmussen *et al.* (2005). The average relaxation time τ_0 is defined as

$$\tau_0 = \frac{\sum_i g_i \tau_i^2}{\sum_i g_i \tau_i} \tag{8.1}$$

where g_i and τ_i are listed in Table 8.1. Both LDPEs were supplied in pellets and were hot pressed into cylindrical test samples at 130 °C, with radius $R_0 = 4.5$mm and length $L_0 = 2.5$mm, giving an aspect ratio $\Lambda_0 = L_0/R_0 = 0.556$.

Table 8.1: Properties of the Lupolen 3020D and Lupolen 1840D LDPE melts. Linear viscoelastic spectrum from Bastian (2001) for Lupolen 3020D (130 °C) and Rasmussen *et al.* (2005) for Lupolen 1840D (130 °C)

Polymer melt	LDPE		LDPE	
Product	Lupolen 3020D		Lupolen 1840D	
M_w[kg/mol]	300		490	
M_n[kg/mol]	37.5		16	
M_w/M_n	8		30.6	
T_m[°C]	114		110	
	τ_i[s]	g_i[Pa]	τ_i[s]	g_i[Pa]
	0.009421	140281.5	0.0115	129000
	0.061312	53547.1	0.107	43600
	0.319808	33532.91	0.56	24200
Relaxation spectrum	1.8272	20196.16	3.35	12700
at 130 °C	10.4064	9170.150	17.3	6200
	57.9328	3551.614	95.5	2900
	329.024	983.4258	823	831
	2097.92	101.618		
τ_0[s] at 130 °C	636.612		523.117	

8.3 Filament Stretching Rheometry

The experiments are performed with an FSR equipped with an oven to allow measurements from room temperature to about 200 °C [Bach *et al.* (2003b)]. Nitrogen is used during the elongation to avoid sample degradation. The force $F(t)$ is measured by a load cell and the diameter $2R(t)$ at the mid-filament plane is measured by a laser

micrometer. The Hencky strain and the mean value of the stress difference over the mid–filament plane [Szabo (1997)] are calculated from observations of $R(t)$ and $F(t)$ as

$$\epsilon(t) = -2\ln\left(R(t)/R_0\right) \tag{8.2}$$

and

$$\langle \sigma_{zz} - \sigma_{rr} \rangle = \frac{F(t) - m_f g/2}{\pi R(t)^2}, \tag{8.3}$$

where m_f is the weight of the filament and g the gravitational acceleration. At small strains during the startup, part of the stress difference comes from the radial variation due to the shear components in the deformation field, especially at small aspect ratios. This effect may be compensated by a correction factor where the corrected mean value of the stress difference is defined as [Rasmussen *et al.* (2010)]

$$\langle \sigma_{zz} - \sigma_{rr} \rangle_{corr} = \langle \sigma_{zz} - \sigma_{rr} \rangle \left(1 + \frac{\exp\left(-5\epsilon/3 - \Lambda_0^3\right)}{3\Lambda_0^2} \right)^{-1} \tag{8.4}$$

This relation ensures less than 3% deviation from the correct initial stress. For large strains the correction vanishes and the radial variation of the stress in the symmetry plane becomes negligible [Kolte *et al.* (1997)].

The strain rate is defined as $\dot{\epsilon} = d\epsilon/dt$. During the startup of uniaxial stretching we define $\dot{\epsilon}_0^+ = \dot{\epsilon}$ and in the reversed biaxial flow we define $\dot{\epsilon}_0^- = -\dot{\epsilon}$, where $\dot{\epsilon}_0^+$ and $\dot{\epsilon}_0^-$ stay positive, constant and equal. During the stress relaxation starting at an arbitrarily given Hencky strain of ϵ_0, the mid-filament radius is kept constant by the active control loop, giving $\dot{\epsilon} = 0$. The Weissenberg number is defined as $Wi = \dot{\epsilon}\tau_0$.

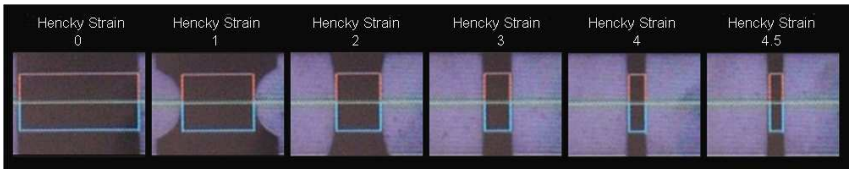

Figure 8.1: Contour of the Lupolen 3020D filament at different Hencky strain values during a uniaxial stretching at 130 °C with $\dot{\epsilon}_0^+ = 0.03\text{s}^{-1}$.

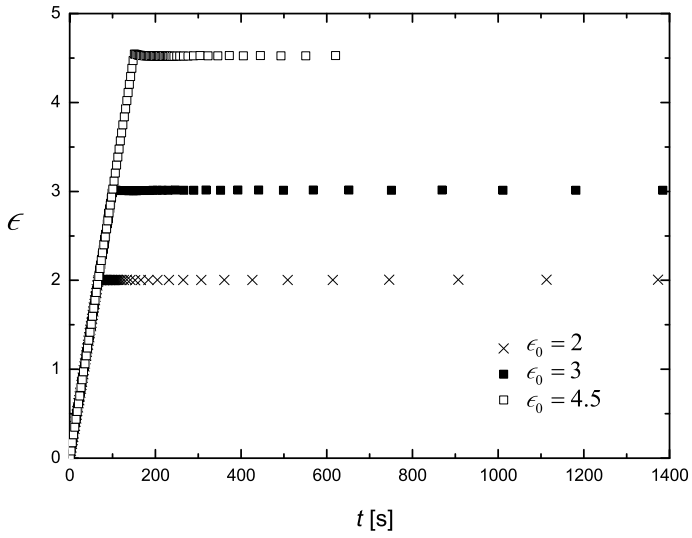

Figure 8.2: Hencky strain ϵ of the Lupolen 3020D samples measured by the FSR at 130 °C as a function of time t. The startup of the flow is uniaxial elongation with $\dot{\epsilon}_0^+ = 0.03\text{s}^{-1}$; the flow was stopped at $\epsilon_0 = 2, 3$ and 4.5 respectively.

The key feature of the FSR that allows us to control the strain rate is that the location of the thinnest part of the filament can be predicted. Provided a critical strain rate $\dot{\epsilon}_{sag} = \rho g L_0/\eta_0$ is exceeded [McKinley and Sridhar (2002)] the thinnest part of the filament is expected to occur in the mid-plane. Therefore the strain rate $\dot{\epsilon}_{sag}$ gives a lower limit for the rates at which the FSR control scheme will work. To ensure that the FSR is working correctly we therefore check that the test samples should stay symmetric across the mid-filament plane as well as axisymmetric during extension [Burghelea *et al.* (2011); Rasmussen and Hassager (2012)]. The following figures 8.1 to 8 illustrate the samples controlled by the FSR in the measurements of stress relaxation and reversed flow.

In Figure 8.1 the dark part shows the contour of the Lupolen 3020D filament from the laser monitor at different Hencky strain values during a uniaxial stretching. The flow was stopped at Hencky strain $\epsilon_0 = 4.5$ and followed by the stress relaxation. Figure 8.2 shows the corresponding Hencky strain as a function of time, including the other two measurements where the flow was stopped at $\epsilon_0 = 2$ and 3 respectively.

Figure 8.3 shows the quenched Lupolen 3020D filament when the flow was stopped at Hencky strain $\epsilon_0 = 4.5$ and relaxed for 100 seconds, while Figure 8.4 shows the quenched Lupolen 1840D filament when the flow was stopped at $\epsilon_0 = 5.0$ and relaxed for 100 seconds as well. We quenched the filaments by opening the oven and exposing the samples to the atmosphere. The quenching process took around 15 seconds. During this time there was no control by the closed loop, thus 0.05 – 0.08mm decreases of the mid-diameter of the quenched samples were observed. Figure 8.5 and Figure 8.6 show the corresponding contours scanned by the laser micrometer of the same filaments in Figure 8.3 and Figure 8.4, respectively. Figure 8.3 and 8.4 depict the front side of the filaments while Figure 8.5 and 8.6 show the left side of the filaments. In Figure 8.5 and 8.6, the position $Y = 0$ indicates where the mid-plane of the filament is located. The quenched sample in Figure 8.5 is almost perfectly symmetric across the mid–plane.

Figure 8.7 shows the contour of the Lupolen 1840D filament from the laser monitor at different Hencky strain values during a uniaxial stretching followed by a reversed biaxial flow. The flow was reversed at $\epsilon_0 = 4.5$. At some time t_R the stress changes sign from positive to negative (tension to compression). The strain recovery is defined as $\epsilon_R = \epsilon_0 - \epsilon(t_R)$ [Nielsen and Rasmussen (2008)]. If the flow is continued for $t > t_R$, the filament will buckle at some time as shown in Figure 8.7 (Hencky strain 3). Figure 8.8 shows the corresponding Hencky strain of Lupolen 1840D as a function of time, including the other five measurements where the flow was reversed at different Hencky strains ϵ_0 ranging from 2 to 4. The figure contains kinematic data for some unbuckled filaments under compression. However no force measurements are reported for filaments under compression.

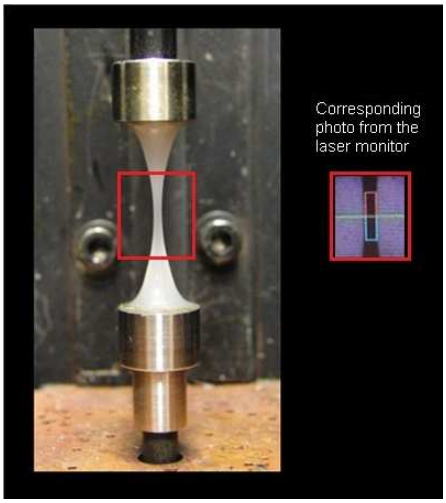

Figure 8.3: Quenched Lupolen 3020D filament. The flow was stopped at $\epsilon_0 = 4.5$ ($\dot{\epsilon}_0^+ = 0.03\text{s}^{-1}$) and relaxed for 100 seconds.

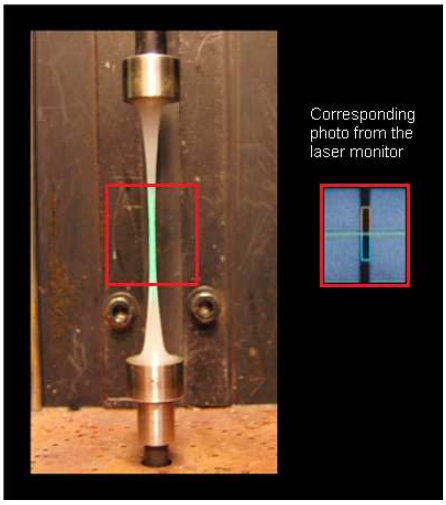

Figure 8.4: Quenched Lupolen 1840D filament. The flow was stopped at $\epsilon_0 = 5.0$ ($\dot{\epsilon}_0^+ = 0.01\text{s}^{-1}$) and relaxed for 100 seconds.

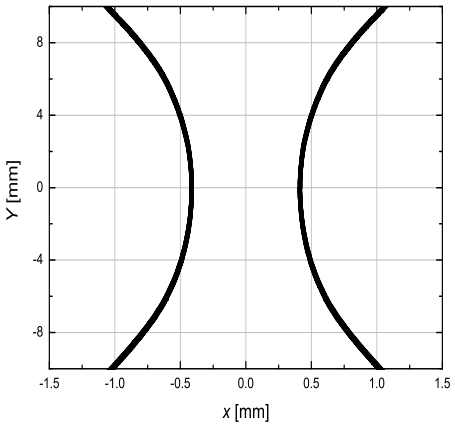

Figure 8.5: Contour scanned by the laser micrometer of the quenched Lupolen 3020D filament delimited by the red square in figure 8.3. The flow was stopped at $\epsilon_0 = 4.5$ ($\dot{\epsilon}_0^+ = 0.03\text{s}^{-1}$) and relaxed for 100 seconds.

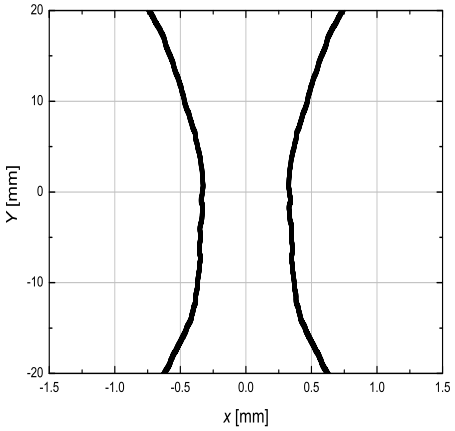

Figure 8.6: Contour scanned by the laser micrometer of the quenched Lupolen 1840D filament delimited by the red square in figure 8.4. The flow was stopped at $\epsilon_0 = 5.0$ ($\dot{\epsilon}_0^+ = 0.01\text{s}^{-1}$) and relaxed for 100 seconds.

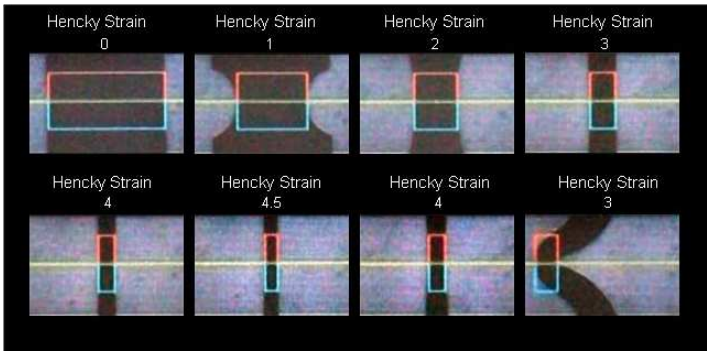

Figure 8.7: Contour of the Lupolen 1840D filament at different Hencky strain values during a uniaxial stretching with $\dot{\epsilon}_0^+ = 0.01\text{s}^{-1}$ followed by a reversed biaxial flow with $\dot{\epsilon}_0^- = 0.01\text{s}^{-1}$ at 130 °C. The flow was reversed at $\epsilon_0 = 4.5$.

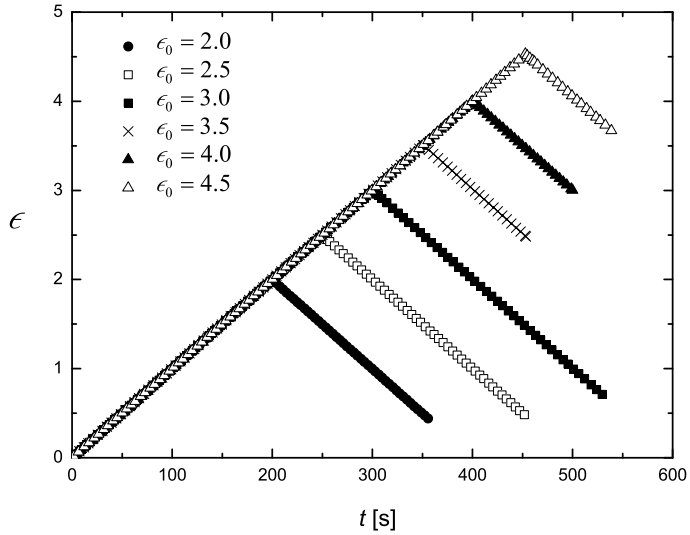

Figure 8.8: Hencky strain ϵ of Lupolen 1840D samples measured by FSR at 130 °C as a function of the time t. The startup of the flow was uniaxial elongation with $\dot{\epsilon}_0^+ = 0.01\text{s}^{-1}$. The flow was reversed at $\epsilon_0 = 2.0, 2.5, 3.0, 3.5, 4.0$ and 4.5 respectively with the identical strain rate $\dot{\epsilon}_0^- = 0.01\text{s}^{-1}$

8.4 Sress Relaxation

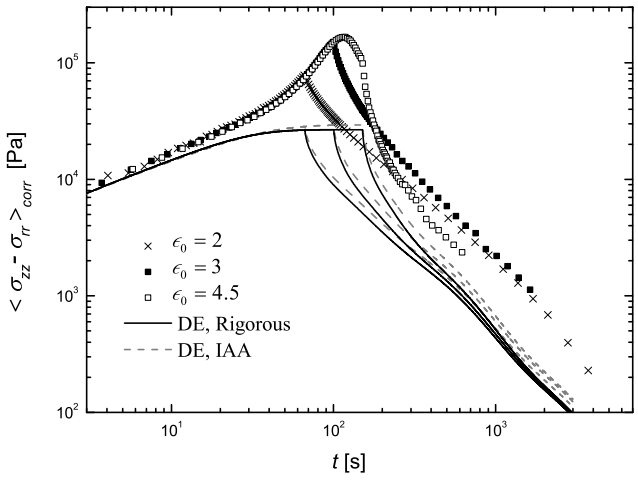

Figure 8.9: The corrected extensional stress of Lupolen 3020D as a function of time at 130 °C with $\dot{\epsilon}_0^+ = 0.03\text{s}^{-1}$ ($Wi = 19.1$). The flow was stopped at an extension of $\epsilon_0 = 2, 3$ and 4.5 respectively. The dashed and solid lines are the corresponding DE predictions with and without IAA, respectively.

The experiments of stress relaxation were performed at 130 °C following startup of uniaxial elongation. The flow was stopped at different Hencky strains before and after the overshoot and the stress was followed during the relaxation phase. Figure 8.9 and 8.10 show the experimental results of Lupolen 3020D and 1840D, respectively. In the figures each measurement was repeated twice and the plots present the de-noised data after wavelet processing [Mallat (2009)]. In order to obtain a manageable data set, we picked one data point from every ten points in the data set after wavelet processing. We also analyzed the data by taking the average value of every ten data points in the original data set, which gave a good agreement with the wavelet analysis. Figure 8.11 compares the raw data and the data after wavelet processing. The raw data shows the three measurements of Lupolen 1840D with $\dot{\epsilon}_0^+ = 0.01\text{s}^{-1}$ and $\epsilon_0 = 4.5$. This raw data is the most scattering case among all the measurements.

The lines in Figure 8.9 and 8.10 show the predicted results of the original reptation

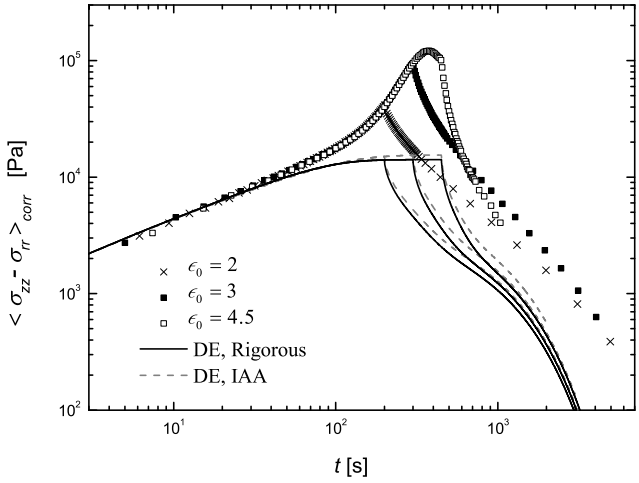

Figure 8.10: The corrected extensional stress of Lupolen 1840D as a function of time at 130 °C with $\dot{\epsilon}_0^+ = 0.01\text{s}^{-1}$ ($Wi = 5.2$). The flow was stopped at an extension of $\epsilon_0 = 2, 3$ and 4.5 respectively. The dashed and solid lines are the corresponding DE predictions with and without IAA, respectively.

based model introduced by Doi and Edwards (1979). The stress tensor is expressed as

$$\boldsymbol{\sigma}(t) = \int_{-\infty}^{t} M(t-t')\mathbf{S}_{\text{DE}}(t,t')\text{d}t', \tag{8.5}$$

where $M(t-t')$ is the memory function with

$$M(t-t') = \sum_i \frac{g_i}{\tau_i} e^{-(t-t')/\tau_i}. \tag{8.6}$$

Inherently in the original Doi–Edwards (DE) model is a specific form of the linear viscoelastic memory function $M(t-t')$ developed for monodisperse linear polymers. This form will clearly not fit the linear viscoelastic properties of the highly branched and polydisperse LDPE melts. Hence we use the memory function corresponding to the experimentally determined relaxation function with parameters g_i and τ_i in table 8.1. Thus when we refer to Eq.8.5 as the DE model this relates to the non-linear properties of the equation. $\mathbf{S}_{\text{DE}}$ is the relative strain. The rigorous form and the independent

alignment approximation (IAA) of $\mathbf{S}_{\mathrm{DE}}$ are given by Eq.8.7 and Eq.8.8, respectively.

$$\mathbf{S}_{\mathrm{DE}}^{\mathrm{Rigorous}}(t,t') = \frac{15}{4}\frac{1}{\langle|\mathbf{E}\cdot\mathbf{u}|\rangle}\left\langle\frac{\mathbf{E}\cdot\mathbf{u}\;\mathbf{E}\cdot\mathbf{u}}{|\mathbf{E}\cdot\mathbf{u}|}\right\rangle, \tag{8.7}$$

$$\mathbf{S}_{\mathrm{DE}}^{\mathrm{IAA}}(t,t') = 5\left\langle\frac{\mathbf{E}\cdot\mathbf{u}\;\mathbf{E}\cdot\mathbf{u}}{|\mathbf{E}\cdot\mathbf{u}|^2}\right\rangle = 5\mathbf{S}(t,t'). \tag{8.8}$$

In both equations, $\mathbf{u}$ is the unit vector and $\mathbf{E}$ the relative deformation gradient tensor. The bracket denotes an average over an isotropic distribution and the analytical formulas can be found in Urakawa *et al.* (1995) for uniaxial and biaxial deformations. K–BKZ representations [Bird *et al.* (1987)] that closely approximate the DE model with and without IAA for general deformations have been provided by Currie (1982) and Hassager and Hansen (2010), respectively. It appears from Figures 8.9 and 8.10 that the IAA closely approximates the rigorous model in this situation.

A significantly different flow behavior is observed in the stress relaxation performed before ($\epsilon_0 = 2$ and 3) and after the overshoot ($\epsilon_0 = 4.5$). The measured stress decays much faster after the overshoot for both melts. Similarly to linear NMMD polymer melts [Nielsen *et al.* (2008)], the elongational stress seems to decay nearly toward a DE based stress at large times after the overshoot has been passed. At smaller imposed strains, the stress of the branched LDPE melts (in Figure 8.9 and 8.10) remains considerably larger than the DE prediction. This is similar to the observations in Rasmussen *et al.* (2009) for a branched NMMD polystyrene melt.

We also analyzed the stress decay by fitting the data with a sum of exponentially decaying modes as

$$\frac{\sigma^-(t)}{\sigma^-(0)} = \sum\nolimits_i A_i \exp\left(-t/\tilde{\tau}_i\right), \tag{8.9}$$

where $\sigma^-(0)$ is the stress when the flow is stopped in Figure 8.9 and 8.10. Figure 8.12 shows the average relaxation time $\tilde{\tau}_0$ as a funtion of the imposed Hencky strain. Here the average relaxation time is defined as $\tilde{\tau}_0 = \sum_i A_i\tilde{\tau}_i / \sum_i A_i$. Both melts show that in extensional stress decay, the average relaxation time decreases with higher imposed Hencky strain. The average relaxation times τ_0 for small Hencky strain defined in Eq.8.1 have been included in the figure for reference.

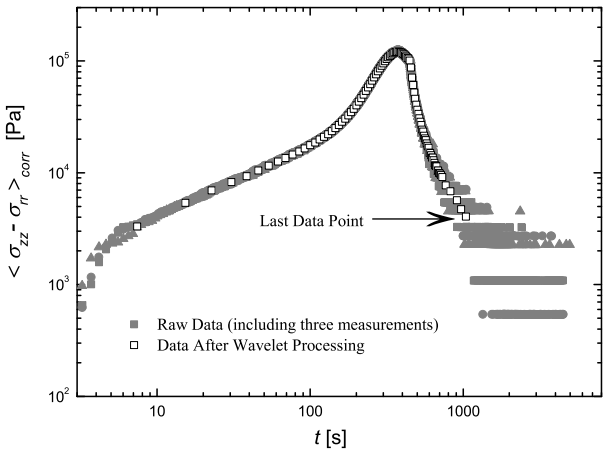

Figure 8.11: Comparison of the raw data and the data after wave processing for Lupolen 1840D ($\dot{\epsilon}_0^+ = \dot{\epsilon}_0^- = 0.01\text{s}^{-1}$, $\epsilon_0 = 4.5$) at 130 °C.

8.5 Reversed Flow

In Figure 8.13 and 8.14 we show the measured extensional stress as a function of Hencky strain for the reversed biaxial flow on Lupolen 3020D and Lupolen 1840D respectively at 130 °C. In the figures only the plots which are reversed at $\epsilon_0 \geq 4.5$ were duplicated and represent the de-noised data after the wavelet treatments. We did not repeat the measurements which were reversed at Hencky strain lower than 4.5. For these measurements we simply picked one data point from every ten points in the original experimental data set and thus the corresponding plots show the data without noise reduction. The solid lines in the figures show the rigorous DE predictions.

Different behavior in the reversed extensional flow has been observed, before and after the overshoot as well. Before the overshoot, the experimental observations depart increasingly from the DE predictions with increasing imposed maximal strain (ϵ_0). However, when the flow is reversed at even higher Hencky strain (after the overshoot), the deviations seem to reduce. In Figure 8.15 we show the measured strain recovery ϵ_R as a function of Hencky strain ϵ_0 for Lupolen 3020D and 1840D. It can be seen more clearly that before the overshoot the strain recovery increases, while after the overshoot it decreases, which indicates that the melt becomes less elastic.

In order to investigate further the strain recovery, we made more measurements for

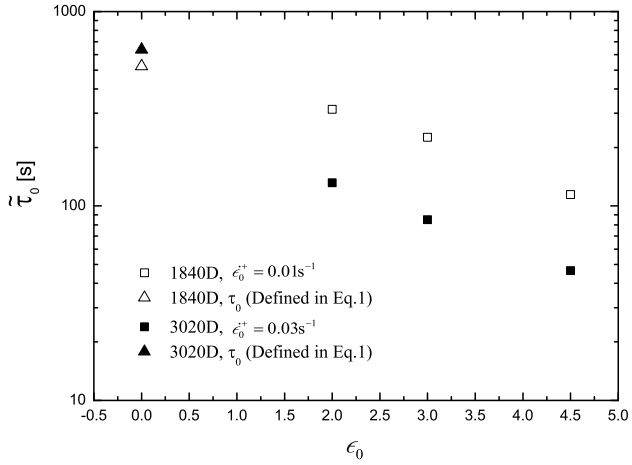

Figure 8.12: The average relaxation time in extensional stress decay of Lupolen 3020D and 1840D as a function of Hencky strain at 130 °C

Lupolen 3020D with different strain rates $\dot{\epsilon}_0^+$ in the startup and the corresponding $\dot{\epsilon}_0^- = \dot{\epsilon}_0^+$ in the reversed flow. Figure 8.16 shows the experimental results and the DE predictions. Before the overshoot, the strain recovery ϵ_R increases with higher Hencky strain ϵ_0 and higher strain rate $\dot{\epsilon}_0^+$, and all the values are higher than the DE predictions. This is likely to be the result of chain stretch not presented in the DE model. But after the overshoot, ϵ_R decreases with ϵ_0 and $\dot{\epsilon}_0^+$. This may indicate that there is less chain stretch after the maximum. The experimental data on $\dot{\epsilon}_0^+ = 0.03s^{-1}$ also shows that the strain recovery ϵ_R tends to reach a constant value for large strains. This observation, however, is based on limited data. Furthermore, here the rigorous DE predictions show observable differences from the DE with IAA. Indeed it is expected that the IAA will lead to significant deviations from the rigorous model in reversed flow [Doi (1980)].

8.6 Discussion

Both the measurements of stress relaxation and reversed flow indicate that the branched LDPE melts show a similarity to linear polymers after the overshoot, since the experimental data recovers to the DE predictions. However, the DE model can not predict the strain hardening effect of the highly branched LDPE melts. There is a significant deviation between the measured data and the predicted behavior in the start-up. It is

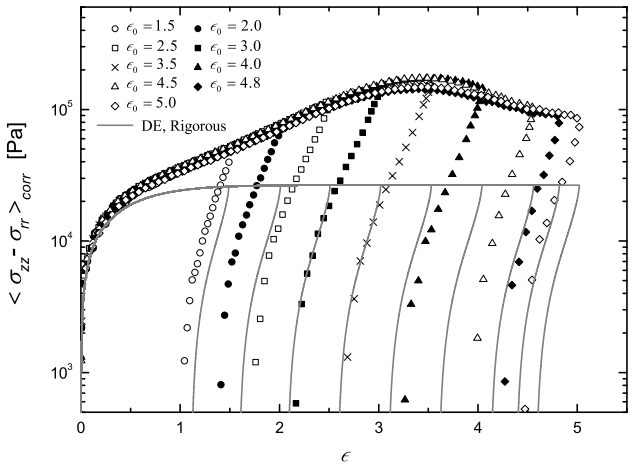

Figure 8.13: The corrected startup and reversed stress of Lupolen 3020D at 130 °C as a function of Hencky strain. The startup of the flow was uniaxial elongation with $\dot{\epsilon}_0^+ = 0.03\text{s}^{-1}$ ($Wi = 19.1$). The flow was reversed at $\epsilon_0 = 1.5, 2, 2.5, 3, 3.5, 4, 4.5, 4.8$ and 5.0 respectively with the identical strain rate $\dot{\epsilon}_0^- = 0.03\text{s}^{-1}$. The solid lines are the corresponding rigorous DE predictions.

necessary to take other effects than pure configurational stress into account.

While a clear understanding of the molecular phenomena involved in the stress overshoot does not seem available presently, we wish to compare the experimental observations of Lupolen 3020D with the predictions from two of the commonly used constitutive theories: The pom–pom model and the interchain pressure model. Since the Lupolen 3020D melt is highly polydisperse, we will use a multi mode version for each model.

The pom–pom model was originally proposed by McLeish and Larson (1998) with both an integral and a differential form. A multi mode version of the pom–pom model was proposed by Inkson *et al.* (1999) for various LDPE melts. Blackwell *et al.* (2000) improved the multi mode pom–pom fit by smoothing the sharp transitions of the model. Subsequently an extended pom–pom (XPP) model was proposed by Verbeeten *et al.* (2001) to overcome several drawbacks of the original pom–pom model, and more recently the XPP model was used by Oishi *et al.* (2011) to simulate viscoelastic free surface flows.

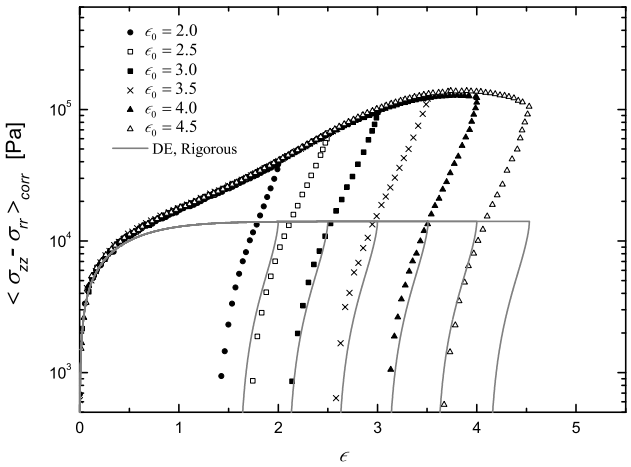

Figure 8.14: The corrected startup and reversed stress of Lupolen 1840D at 130 °C as a function of Hencky strain. The startup of the flow was uniaxial elongation with $\dot{\epsilon}_0^+ = 0.01\text{s}^{-1}$ ($Wi = 5.2$). The flow was reversed at $\epsilon_0 = 2, 2.5, 3, 3.5, 4$ and 4.5 respectively with the identical strain rate $\dot{\epsilon}_0^- = 0.01\text{s}^{-1}$. The solid lines are the corresponding rigorous DE predictions.

Since the pom–pom model has not been used to predict stress relaxation and reversed flow followng uniaxial extension, here we compare our experimental data with the multi mode version of the original pom–pom model. The stress tensor of the differential approximation of a multi mode pom–pom model is expressed as [Inkson *et al.* (1999)]

$$\boldsymbol{\sigma} = \sum_{i=1}^{n} \boldsymbol{\sigma}_i = \sum_{i=1}^{n} g_i \lambda_i^2 (t), \mathbf{S}_{\text{PP},i} (t) \tag{8.10}$$

where $\mathbf{S}_{\text{PP},i}$ represents the evolution of orientation and λ_i [Blackwell *et al.* (2000)] represents the evolution of backbone stretch for each mode i given by

$$\mathbf{S}_{\text{PP},i} = \frac{3\mathbf{A}_i}{\text{trace}\,(\mathbf{A}_i)}, \tag{8.11}$$

$$\frac{\partial}{\partial t}\mathbf{A}_i = \boldsymbol{\kappa} \cdot \mathbf{A}_i + \mathbf{A}_i \cdot \boldsymbol{\kappa}^T - \frac{1}{\tau_i}(\mathbf{A}_i - \mathbf{I}), \tag{8.12}$$

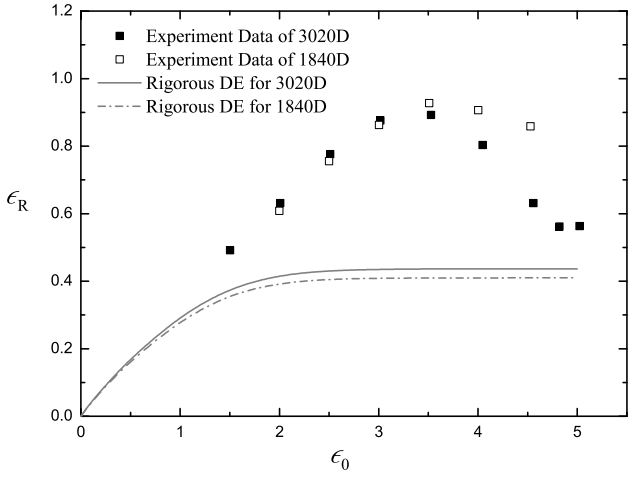

Figure 8.15: The strain recovery as a function of Hencky strain for Lupolen 3020D ($\dot{\epsilon}_0^+ = \dot{\epsilon}_0^- = 0.03\text{s}^{-1}$, $Wi = 19.1$) and 1840D ($\dot{\epsilon}_0^+ = \dot{\epsilon}_0^- = 0.01\text{s}^{-1}$, $Wi = 5.2$) at 130 °C. The lines are the rigorous DE predictions.

$$\frac{\partial}{\partial t}\lambda_i = \lambda_i\left(\boldsymbol{\kappa} : \mathbf{S}_{\text{PP},i}\right) - \frac{1}{\tau_{s,i}}\left(\lambda_i - 1\right)e^{\nu_i(\lambda_i - 1)} \tag{8.13}$$

with the initial conditions $\mathbf{A}_i(-\infty) = \mathbf{I}$ and $\lambda_i(-\infty) = 1$. $\boldsymbol{\kappa}$ is the transpose of the velocity gradient ($\kappa_{ij} = \partial v_i/\partial x_j$), $\tau_{s,i}$ is the relaxation time for stretch, $\nu_i = 2/(q_i - 1)$ [McLeish (2002)] and q_i is the number of arms on each branch point of the pom–pom polymer. There are four fitting parameters in the pom–pom equations for each mode i: g_i, τ_i, $\tau_{s,i}$ and q_i. The linear viscoelastic parameters g_i and τ_i are directly obtained from the relaxation spectrum in Table 8.1. The values of $\tau_{s,i}$ and q_i associated with the nonlinear properties are adjusted by "trial and error". In the reversed flow, when $\lambda_i < 1$, there is a modification for the parameter τ_i given by [Lee *et al.* (2001)]

$$\frac{1}{\tau_i^*} = \begin{cases} \dfrac{1}{\tau_i} & \text{for } 1 \le \lambda_i \le q_i \\ \dfrac{1}{\tau_i} + \dfrac{1}{\lambda_i}\dfrac{\partial \lambda_i}{\partial t} - \boldsymbol{\kappa} : \mathbf{S}_{\text{PP},i} & \text{for } \lambda_i < 1 \end{cases} \tag{8.14}$$

The interchain pressure concept was originally proposed by Marrucci and Ianniruberto

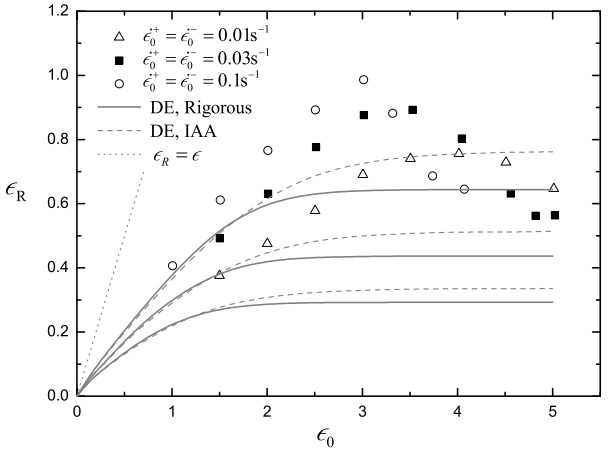

Figure 8.16: The strain recovery as a function of Hencky strain for Lupolen 3020D at 130 °C with different strain rates $\dot{\epsilon}_0^+ = \dot{\epsilon}_0^- = 0.01, 0.03, 0.1\text{s}^{-1}$ ($Wi = 6.4, 19.1, 63.7$). The dashed and solid lines are the corresponding DE predictions with and without IAA, respectively.

(2004). The stress tensor of the interchain pressure model developed initially for linear monodisperse melts [Wagner *et al.* (2005)] is given by the integral

$$\boldsymbol{\sigma}(t) = \int_{-\infty}^{t} M(t-t')f^2(t,t')5\mathbf{S}(t,t')\mathrm{d}t', \tag{8.15}$$

where f represents the evolution of the tension in a chain segment given by

$$\frac{\partial}{\partial t}f = f\left[(\boldsymbol{\kappa} : \mathbf{S}) - \frac{f\left(f^3-1\right)}{\tau_a}\right] \tag{8.16}$$

with the initial condition $f(t',t') = 1$. τ_a is the tube diameter relaxation time. For the highly polydisperse LDPE melt we use a multi mode version in the form

$$\boldsymbol{\sigma}(t) = \sum\nolimits_i \int_{-\infty}^{t} \frac{g_i}{\tau_i} e^{-(t-t')/\tau_i} f_i^2(t,t')5\mathbf{S}(t,t')\mathrm{d}t', \tag{8.17}$$

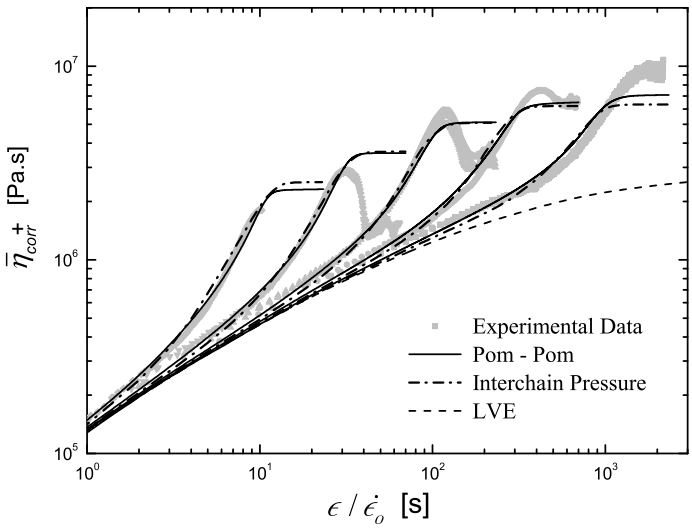

Figure 8.17: Comparison of the measured extensional stress growth coefficient $\bar{\eta}^+_{corr} = \langle \sigma_{zz} - \sigma_{rr} \rangle_{corr} / \dot{\epsilon}_0$ for Lupolen 3020D with the pom–pom model, the interchain pressure model and the linear viscoelastic (LVE) prediction, at strain rates (from right to left) $\dot{\epsilon}_0 = 0.003, 0.01, 0.03, 0.1, 0.3 \mathrm{s}^{-1}$ ($Wi = 1.9, 6.4, 19.1, 63.7, 191.0$) at 130 °C. The fitting parameters are listed in Table 8.2. The experimental data is obtained from Rasmussen *et al.* (2005).

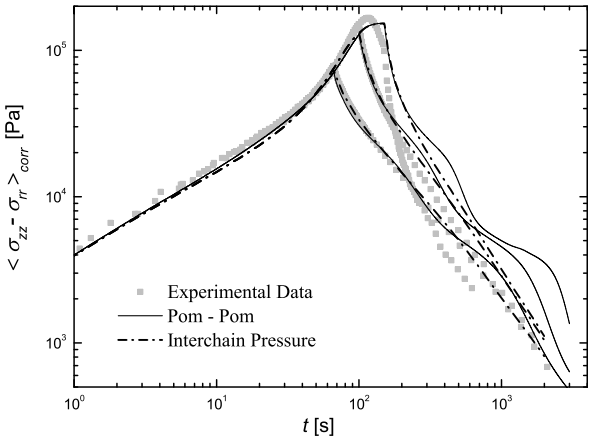

Figure 8.18: Comparison of the measured stress relaxation for Lupolen 3020D at 130 °C with the pom–pom model and the interchain pressure model, at strain rate $\dot{\epsilon}_0^+ = 0.03\text{s}^{-1}$ ($Wi = 19.1$) in the startup. The fitting parameters are listed in Table 8.2.

$$\frac{\partial}{\partial t} f_i = f_i \left[(\boldsymbol{\kappa} : \mathbf{S}) - \frac{f_i \left(f_i^3 - 1 \right)}{\tau_{a,i}} \right] \tag{8.18}$$

with three fitting parameters for each mode i: g_i, τ_i and $\tau_{a,i}$. The values of g_i and τ_i are the same with the ones in the pom–pom equations. The values of $\tau_{a,i}$ are again adjusted by "trial and error".

Table 8.2 shows the fitting parameters used in the multi mode pom–pom model and the multi mode interchain pressure model for Lupolen 3020D. Figure 8.17 compares the predicted extensional stress growth coefficient at different strain rates with the experimental data. Neither of the two models can predict the overshoot. But they both approximately fit the startup of the measurements before the overshoot at different strain rates. Wagner and Rolón-Garrido (2008) proposed a modified interchain pressure model which captures the overshoot for a pom–pom polystyrene. We did not consider this model here, because in stress relaxation ($\dot{\epsilon} = 0$) the tube diameter relaxation time τ_a in the modified model goes to infinity, and the interchain pressure effect vanishes in the evolution equation.

Figure 8.18 compares the predictions of stress relaxation of the two models with the

Table 8.2: Fitting parameters used in the multi mode pom–pom model and the multi mode interchain pressure model for the Lupolen 3020D melt at 130 °C

	Relaxation spectrum		Pom–pom		Interchain pressure
Mode i	τ_i [s]	g_i [Pa]	q_i	$\tau_{s,i}$ [s]	$\tau_{a,i}$ [s]
1	0.009421	140281.5	2	0.001713	50
2	0.061312	53547.1	2	0.011354	50
3	0.319808	33532.91	2	0.061502	50
4	1.8272	20196.16	2	0.358275	50
5	10.4064	9170.150	3	2.08128	50
6	57.9328	3551.614	4	12.8740	400
7	329.024	983.4258	6	131.610	10000
8	2097.92	101.618	6	2097.92	200000

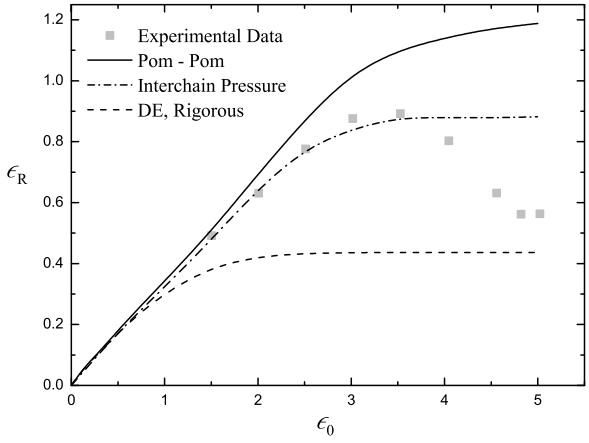

Figure 8.19: Comparison of the measured strain recovery for Lupolen 3020D with the pom–pom model, the interchain pressure model and the rigorous DE model at 130 °C at strain rate $\dot{\epsilon}_0^+ = \dot{\epsilon}_0^- = 0.03\text{s}^{-1}$ ($Wi = 19.1$). The fitting parameters are listed in Table 8.2.

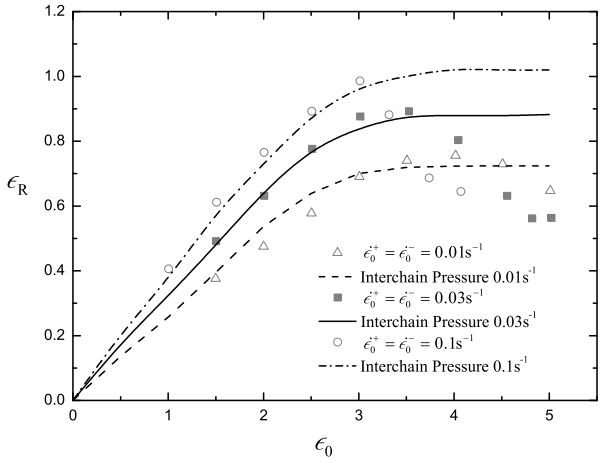

Figure 8.20: Comparison of the measured strain recovery with the multi mode interchain pressure prediction for Lupolen 3020D at 130 °C at different strain rates $\dot{\epsilon}_0^+ = \dot{\epsilon}_0^- = 0.01, 0.03, 0.1s^{-1}$ ($Wi = 6.4, 19.1, 63.7$). The fitting parameters are listed in table 8.2.

experimental results from Figure 8.9. Both models seem to describe the stress data in the relaxation phase when the relaxation is initiated at $\epsilon_0 = 2$ and 3, that is before the stress maximum is reached. However the models do not capture the rapid stress decay during the relaxation which is initiated after the stress maximum ($\epsilon_0 = 4.5$). In addition the pom–pom model exhibits an oscillatory behaviour not present in the data. This may due to the differential formulation that constitutes an approximation of the pom–pom integral constitutive equation.

In Figure 8.19 we compare our data for strain recovery ($\dot{\epsilon}_0^+ = \dot{\epsilon}_0^- = 0.03s^{-1}$, Figure 8.16) with predictions of the DE model, the pom–pom model and the interchain pressure model. None of the models capture the qualitative feature of a maximum in recoverable strain. The interchain pressure model gives a better prediction up to the recovery maximum corresponding in strain more or less to the strain for the stress maximum. The DE model interestingly gives the best prediction for the material stretched well beyond the stress maximum. While this may be fortuitous it may also be interpreted as evidence that the branching structure plays very little role in the dynamics after the stress maximum.

Finally as shown in Figure 8.20, the prediction of the strain recovery from the interchain pressure model can fit the data before the overshoot quantitatively for several

different strain rates in the startup. This is similar to the observations for the pom–pom polystyrene melt data [Rasmussen *et al.* (2009)].

8.7 Conclusions

We have measured stress relaxation and reversed biaxial flow, both following uniaxial extension, on Lupolen 3020D and Lupolen 1840D LDPE melts using an FSR. These branched polymers show stress overshoots followed by steady stress in uniaxial extension as previously reported by Rasmussen *et al.* (2005). After the overshoot the stress relaxation measurements show a remarkably faster decrease in the transient stress compared with the measurements before the overshoot. In reversed flow the strain recovery increases with the applied total Hencky strain until the strain at which the maximum in the stress is observed. After the overshoot the strain recovery decreases with total applied Hencky strain and it saturates at high strain values. Overall these measurements show that the melts become less elastic after the stress maximum.

Both the measurements of stress relaxation and reversed flow indicate that the branched LDPE melts behave similarly to linear polymers after the overshoot, since the experimental data recovers to the DE predictions. Both the multi mode pom–pom model and the multi mode interchain pressure model can quantitatively predict the start-up of the uniaxial elongation before the overshoot. Neither model is able to capture even qualitatively the stress relaxation or strain recovery of the material exhibited after the overshoot. Clearly the dynamics involved in the stress overshoot exhibited by branched polymers still needs new theoretical insight.

Chapter 9

Creep Measurements Confirm Steady Flow after Stress Maximum in Extension of Branched Polymer Melts

9.1 Introduction

Predicting the viscoelastic properties of branched polymer melts from their molecular architecture remains one of the great challenges in polymer physics [Read *et al.* (2011); Larson (2011); Hutchings *et al.* (2012)]. One outstanding problem is the lack of consensus of the evolution of stress in start–up of constant strain rate extensional flow. While one laboratory [Rasmussen *et al.* (2005)] has reported a maximum in stress followed by a steady value, other laboratories have legitimately questioned the maximum [Burghelea *et al.* (2011); Rasmussen and Hassager (2012); Burghelea *et al.* (2012)] and even challenged the existence of steady extensional flow [Wang *et al.* (2007); Lyhne *et al.* (2009)]. The molecular origin of a stress–maximum is unclear and state–of–the–art molecular models [Read *et al.* (2011); Larson (2011); Hutchings *et al.* (2012)] do not contain the qualitative feature of a maximum, thereby implicitly suggesting that the maximum may be an artifact.

We here report observations of extensional flow not with a constant strain rate, but

with a constant stress (creep). In addition to probing the transient behavior, the creep protocol also allows the measurement of the ultimate steady extensional viscosity. The uniqueness of the steady extensional viscosity independent of the start–up protocol is apparently not a settled matter as evidenced by the reporting of two viscosities at the same steady strain rate [Münstedt *et al.* (1998); Andrade and Maia (2011)]. The experiments will also be compared to the LVE predictions [Sips (1950)[1]] to illustrate the departure from linear material behavior.

A major challenge in extensional rheometry is that large deformations are needed to approach a steady flow state. Deformations are measured in units of Hencky strain defined as $\epsilon = \ln \lambda$ where $\lambda = L/L_0$ is the stretch ratio, L_0 being the initial length and L the final length of a given cylindrical slice. The strain rate, $\dot{\epsilon}$ is the time derivative of the Hencky strain. In the classical controlled deformation extensional experiment, a constant $\dot{\epsilon}$ is imposed and the stress is monitored as a function of time. Typically Hencky strains larger than four are required to establish a steady tensile stress. However in many extensional flow devices, sample inhomogeneity will prevent control of the kinematics at approximately the same Hencky strain, such that a steady flow cannot be observed.

9.2 The Control Scheme for Creep Measurements

9.2.1 The apparatus

The only extensional rheometer that can achieve absolute in situ control of the kinematics is the filament stretching rheometer (FSR)[McKinley and Sridhar (2002); Bach *et al.* (2003b)]. In an FSR, a cylindrical sample is placed between two parallel end plates and the extensional flow is induced by pulling these plates apart. The filament does not deform homogeneously along the axis of extension due to the no–slip occurring at the end–plates. However, it has been demonstrated that by locally controlling the deformation at the mid–filament diameter, the resulting measurements are equivalent to those obtained by imposing an overall homogeneous deformation [McKinley and Sridhar (2002)].

In samples with small initial aspect ratios, the no–slip boundary condition provokes significant deviations from ideal uniaxial deformation in the start–up of the flow. Some expressions for correcting the kinematics have been mathematically derived [McKinley and Sridhar (2002)] and successfully applied [Rasmussen *et al.* (2010)]. The non–homogeneous flow allows for two logarithmic strain definitions: an axial strain ϵ_z based

[1] Sips was able to use the LVE result to predict the creep response of a poly(isobutylene) sample that was stretched up to a total deformation of 6%.

on the plate separation L and a true local strain ϵ based on the mid–filament diameter D given by

$$\epsilon_z = \log\left(\frac{L}{L_0}\right) \tag{9.1}$$

$$\epsilon = -2\log\left(\frac{D}{D_0}\right), \tag{9.2}$$

respectively. The latter equation is often referred to as the Hencky strain. In the above equations L_0 and D_0 are the initial length and initial diameter of the sample.

The vertical filament stretching rheometer used in this work consists of a stationary bottom plate and a mobile upper plate. To perform a creep experiment, a simultaneous sampling of the tensile force and the mid–filament diameter is required. The force measurements are carried out by a load cell mounted on the bottom plate. The diameter of the mid–filament is measured in real–time by a digital micrometer. More details concerning the FSR can be found in Chapter 2.

9.2.2 The control scheme

Traditionally, an FSR is operated in controlled strain rate mode. In this work we have adapted the FSR to operate in controlled stress (creep) mode. While extensional creep testing has been performed with other devices[Meissner (1972); Münstedt *et al.* (1998); Stadlbauer *et al.* (2004); Andrade and Maia (2011)], this represents the first adaptation of an FSR–device to operate in controlled stress mode.

Creep measurements are possible using an active control system that prescribes the plate motion in the FSR based on the simultaneous sampling of the force exerted at the bottom plate and the radius of the mid–filament. The stress is defined as

$$\sigma(t) = \mathrm{CF}\frac{F(t)}{\pi R(t)^2}, \tag{9.3}$$

where the CF stands for the correction factor that decouples the extensional stress contribution from the shear contribution at small aspect ratios described previously in Rasmussen *et al.* (2010). The control scheme is an extension of the work that has been described in Chapter 2 and combines a feed–forward and a feed–back term. The feed–back term is a digital integral controller. The feed–forward term is incorporated to

enhance the initial stress adjustment. The scheme, cast as a velocity algorithm, determines the $i + 1$ plate position using

$$\epsilon_z(i+1) = \epsilon_z(i) + \epsilon_z^{ff}(i) + \epsilon_z^{fb}(i) = \epsilon_z(i) + \Delta f(i) + K_I \Delta t \left[\delta\sigma(i)\right], \tag{9.4}$$

where K_I is the integral gain, Δt the actuation time (set to 4 ms in all experiments) and $\Delta f(i)$ is the incremental contribution of the feed–forward term to the time step i. The error is calculated as

$$\delta\sigma(i) = \left[\sigma_0 - \mathrm{CF}\frac{F(i)}{\pi R(i)^2}\right]\frac{1}{\sigma_0}, \tag{9.5}$$

where σ_0 is the set point stress, $F(i)$ is the force exerted by the filament on the lower plate, and $R(i)$ is the mid–filament radius. The tuning of the integral gain was carried out by manual adjustment. It was observed that large values of the integral gain render the controller unstable, while significantly low values cause the set point to be reached very slowly. By using strictly the feed–back term, a stable control of the tensile stress applied to the filament was achieved and the time for the imposed stress to adjust to the set point was approximately 10s. The inclusion of the feed–forward term considerably reduced the response time to 1s. This is clearly seen in Figure 9.1 where the instantaneous imposed tensile stress is plotted as a function of time for the two control configurations. Despite the difference in start–up in Figure 9.1, the same steady state viscosity was obtained for both experiments. This signifies that for the range of stresses presented here the initial response time of the control scheme does not affect the resulting steady state viscosity.

There is a significant difference in the path that the plate motion undergoes for constant rate of extension and creep experiments. A subject of some controversy involving the existence of a maximum has been that the plate motion in the controlled deformation experiments might artificially induce the observed maximum in the stress [Burghelea *et al.* (2011)]. For example, for Hencky strain rates above $\dot{\epsilon}$ =0.03 s^{-1}, the control system reverses the plate motion in order to maintain a constant rate of deformation. This is best seen in Figure 9.2 where the plate position in terms of ϵ_z is plotted as a function of the center filament diameter represented by ϵ. The curves depict the displacement of the axial plates necessary to attain an arbitrary decrease in diameter for both a constant stress and a constant strain rate experiment. While the presence of a small maximum is clearly observed for the constant rate of extension experiment, a monotone increase of the plate separation is observed in the case of controlled stress.

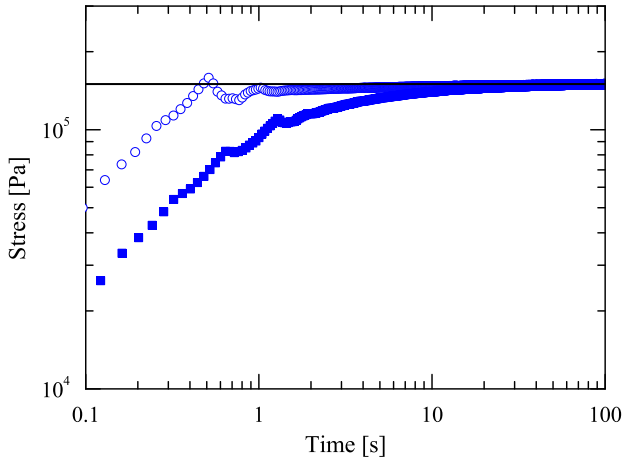

Figure 9.1: (solid squares) A constant stress experiment using only the feed–back action. (open circles) A constant stress experiment using both the feed–back and the feed–forward actions.

9.3 Material and Sample Preparation

The long–chain–branched polymer melt used in this work is the low–density polyethylene (LDPE) Lupolen 3020D, which is from the same batch of the LDPE used in Chapter 2 and 8. Samples for the shear measurements were prepared by hot–pressing the LDPE as supplied into a cylindrical mold with a 25mm diameter and a 1mm height at 140 °C for 10 minutes. Samples for the FSR measurements were prepared by hot–pressing the LDPE as supplied into a cylindrical mold with a 9mm diameter and a 2.5mm height at 140°C for 10 minutes. The mold was then released from the press and allowed to cool down slowly.

FSR samples were loaded onto the rheometer bottom plate. Isothermal conditions at the preset temperature, i.e. 130°C, were attained by a control system regulating the heaters surrounding the thermostat environment. Once the polymer was melted, the upper plate was brought into contact with the sample. Before initiating an experiment, complete relaxation of the sample was ensured by annealing the sample for a sufficient amount of time. The shear measurements were performed using an ARES–G2 rheometer from TA instruments with a 25mm parallel plate attachment.

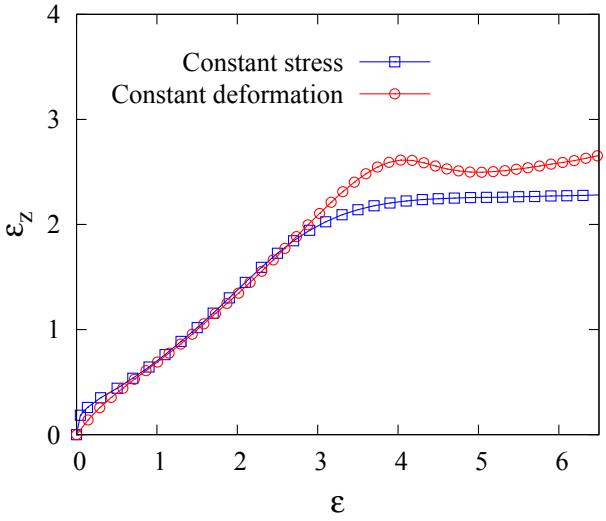

Figure 9.2: The axial strain as a function of the Hencky strain for a controlled stress ($\sigma_0 = 40$ kPa) and a controlled deformation ($\dot{\epsilon} = 0.03$ s^{-1}) experiment.

9.4 Linear Viscoelasticity

In the classical linearized theory of elasticity, the stress in a deformed material is proportional to the magnitude of deformation. The corresponding generalization to materials with relaxation is the theory of linear viscoelasticity (LVE). A frequently used LVE model is the multi–mode Maxwell model[Bird *et al.* (1987)] whereby the shear stress σ is a superposition of individual modes so that $\sigma = \sum \sigma_i$. The individual modes are given by

$$\sigma_i + \tau_i \frac{\mathrm{d}\sigma_i}{\mathrm{d}t} = g_i \tau_i \dot{\gamma}, \qquad i = 1, 2 \cdots n. \tag{9.6}$$

where $\dot{\gamma}(t)$ is the shear rate. The moduli g_i and relaxation times τ_i form a set of $2n$ material parameters that completely characterize the LVE properties. Numerical values for the model melt Lupolen 3020D [Wagner and Rolón-Garrido (2012)] are reproduced in Table 9.1. In creep a total stress σ_0 is imposed at time $t = 0$ such that Eq.9.6 is

augmented by the constraint,

$$\sum_{i=1}^{n} \sigma_i(t) = \sigma_0. \tag{9.7}$$

The total shear deformation $\gamma(t) = \int_0^t \dot{\gamma}(t')\mathrm{d}t'$ is monitored as a function of time. The creep compliance $J(t) = \gamma(t)/\sigma_0$ is then given by

$$J(t) = J_0 + \frac{t}{\eta_0} + \sum_{k=1}^{n-1} j_k \left(1 - \exp(-t/\lambda_k)\right). \tag{9.8}$$

The parameters in the compliance expression are the instantaneous compliance $J_0 = 1/\sum g_i$, the zero shear–rate viscosity $\eta_0 = \sum g_i \tau_i$, the $(n-1)$ retardation times λ_k and the $(n-1)$ compliance coefficients j_k. The initial conditions for Eq.9.6 become

$$\sigma_i(0) = \frac{g_i}{G_0}\sigma_0 \tag{9.9}$$

where $G_0 = \sum g_i$. Eqs.9.6, 9.7 and 9.9 are conveniently solved by Laplace transformation. The solution for $Y(s) = \int_0^\infty \dot{\gamma}(t)\exp(-st)\mathrm{d}t$ becomes

$$Y(s) = \frac{\sigma_0}{G_0} \frac{\sum_i \frac{g_i}{1+s\tau_i}}{s\sum_i \frac{g_i\tau_i}{1+s\tau_i}} \tag{9.10}$$

The inverse transformation is performed by standard methods to yield the expression in Eq.9.8. The retardation times are given as $\lambda_k = -1/s_k$ where the s_k are the zeros of

$$S(s) = \sum_i \frac{g_i\tau_i}{1+s\tau_i}. \tag{9.11}$$

The compliance coefficients are given after some simplification as

$$j_k = \frac{\lambda_k^2}{\sum_i \frac{g_i\tau_i^2}{(1+s_k\tau_i)^2}} \tag{9.12}$$

The same result was obtained by Sips (1950) but by a different procedure.

Numerical values of (λ_k, j_k) are also given in Table 9.1. The retardation times are located in the intervals between the n relaxation times so that $\lambda_i \in [\tau_i; \tau_{i+1}]$, $i = 1, 2 \cdots n-1$.. In particular that the longest retardation time λ_7 is less than half the value of the longest relaxation time τ_8 such that the transition to steady flow is faster in creep than in prescribed deformation. Hence if the interest is only in the steady flow, creep is the more effective path to reach that state [Münstedt *et al.* (1998)]. The extensional compliance $\bar{J}(t) = \epsilon(t)/\sigma_0$ by definition is a factor of three smaller than the shear compliance $J(t)$.

Table 9.1: Parameters for LDPE Lupolen 3020D melt (130 °C)

i	g_i[Pa]	τ_i[s]	j_i[Pa^{-1}]	λ_i[s]
1	$2.245\ 10^5$	$3.954\ 10^{-3}$	$2.310\ 10^{-6}$	$8.292\ 10^{-3}$
2	$7.120\ 10^4$	$2.965\ 10^{-2}$	$2.932\ 10^{-6}$	$4.888\ 10^{-2}$
3	$4.515\ 10^4$	$1.393\ 10^{-1}$	$5.215\ 10^{-6}$	$2.405\ 10^{-1}$
4	$2.789\ 10^4$	$6.377\ 10^{-1}$	$9.893\ 10^{-6}$	$1.178\ 10^{0}$
5	$1.628\ 10^4$	$2.893\ 10^{0}$	$2.059\ 10^{-5}$	$5.930\ 10^{0}$
6	$8.541\ 10^3$	$1.322\ 10^{1}$	$5.180\ 10^{-5}$	$3.222\ 10^{1}$
7	$4.039\ 10^3$	$6.880\ 10^{1}$	$4.599\ 10^{-4}$	$4.331\ 10^{2}$
8	$7.132\ 10^2$	$1.066\ 10^{3}$		

9.5 Creep Measurements

All the creep measurements were performed at 130 °C. Figure 9.3 shows the imposed stress as a function of time. The extensional compliance $\bar{J}(t)$ measured in the FSR is compared with the LVE prediction from Eq.9.8 in Figure 9.4. Departure from the full line is a manifestation of the non–linear mechanical properties of the melt. A good agreement with LVE is obtained for an imposed stress σ_0 up to 1000 Pa, but for larger imposed stresses, the melt is less compliant than that predicted by LVE. This is indeed to be expected as it corresponds to extensional strain hardening observed in controlled deformation experiments [Rasmussen *et al.* (2005)]. In Figure 9.4(b), we compare the extensional compliance measured in the FSR with the shear compliance measured in an ARES–G2. Also in shear, we observe a deviation from the LVE at stresses above 1000 Pa, but the material becomes more compliant than predicted from LVE. This behavior corresponds to the shear thinning typically encountered in start–up of steady shear flow. The deviation at times less than 10s may be due to limitations in the dynamic control of the shear rheometer.

In creep, the ultimate steady extensional flow is characterized by a constant slope of

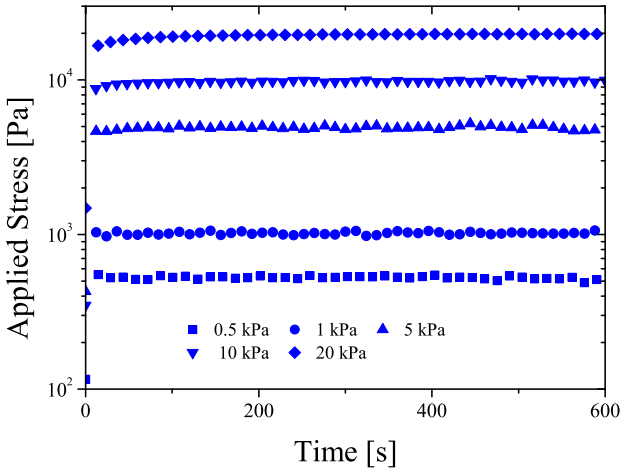

Figure 9.3: Stress in the filament mid–plane measured as function of time for five predefined stress levels.

the compliance or equivalently a constant value of $\dot{\epsilon}$ such as in the case for $\sigma_0 = 40$kPa in Figure 9.5. At stresses above approximately 80kPa, we observe an inflexion point in the compliance corresponding to a minimum in the slope before a steady flow is established. The phenomenon is illustrated in Figure 9.5 for $\sigma_0 = 150$kPa with a minimum occurring at approximately $\epsilon = 3$. The minimum in Figure 9.5 corresponds closely to the maximum in stress observed in controlled deformation experiments previously reported in Rasmussen *et al.* (2005). This is illustrated further in Figure 9.6, where the ratio of $\sigma/\dot{\epsilon}$ is plotted as a function of Hencky strain for the two extensional rheometry protocols: Constant strain rate ($\dot{\epsilon}$ constant and $\sigma = \sigma(t)$) and constant stress ($\sigma = \sigma_0$ and $\dot{\epsilon} = \dot{\epsilon}(t)$). While there is no a priori reason to expect the two ratios to be the same, the similarity between the paths, could indicate that the molecular mechanism behind the stress maximum is also behind the inflexion point in the compliance [2].

Another important observation from Figure 9.6 is that both protocols eventually approach constant values of $\sigma/\dot{\epsilon}$ lasting approximately 1–2 Hencky strain units before the measurements are terminated due to insufficient resolution. The steady flow state after the maximum can only be reached with an active control on the FSR. The steady ratios are identified as the extensional viscosity at the given stretch rates [3].

[2] It should be noted that the top plate trajectories undergo two very different paths, see Figure 9.2.

[3] Note that the steady viscosity is not dependent on the rate at which the control scheme reaches the set–point, see Figure 9.1.

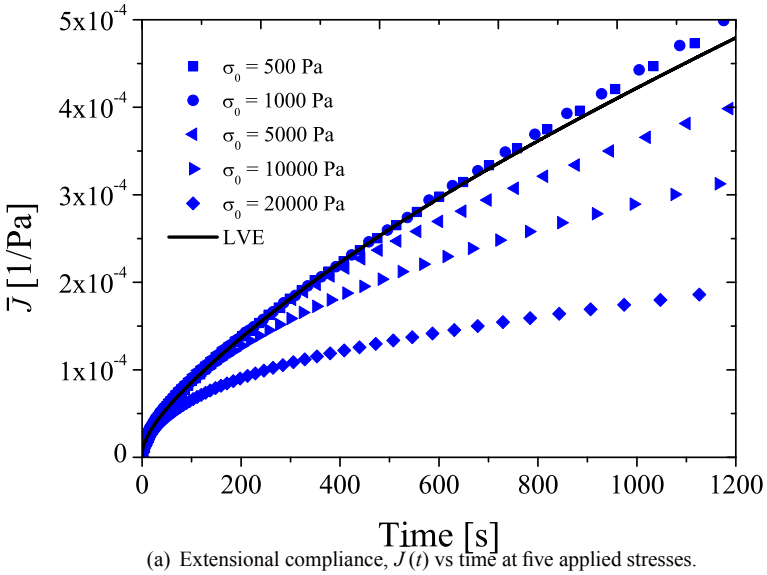

(a) Extensional compliance, $J(t)$ vs time at five applied stresses.

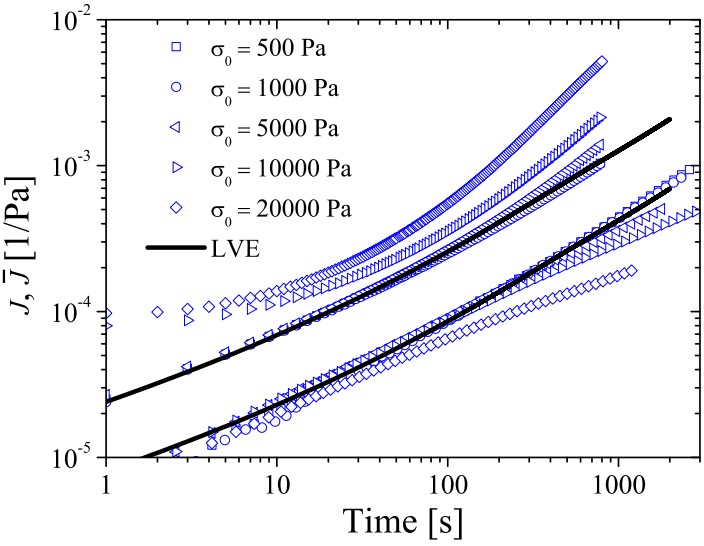

(b) Comparison of shear compliance (top curves) and extensional compliance vs time for five applied stresses (log–log scales).

Figure 9.4: Comparison of the extensional compliance with the LVE prediction (the solid lines) from Eq.9.8.

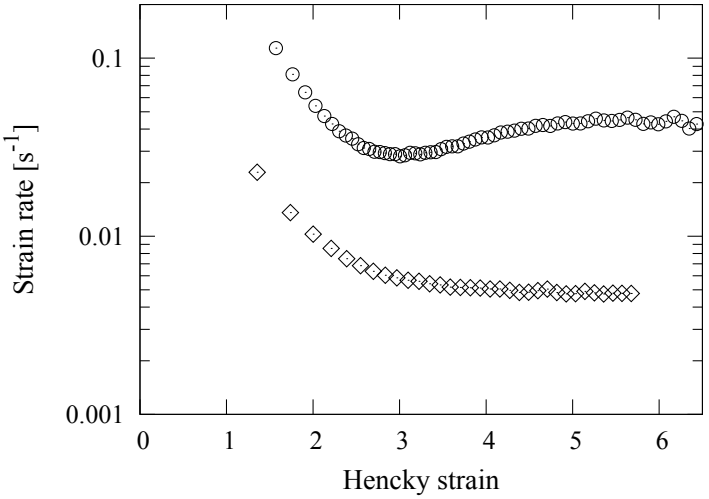

Figure 9.5: Hencky strain rate as a function of Hencky strain for constant applied σ_0 = 40kPa (bottom) and σ_0 = 150kPa (top). For σ_0 larger than approximately 80kPa the strain rate goes through a minimum before reaching a steady state value.

In Figure 9.7, we compare our measurements of steady extensional viscosity obtained in creep with values obtained in controlled strain rate [Rasmussen *et al.* (2005)]. Within experimental accuracy the two protocols give the same extensional viscosity. The extensional viscosity exhibits a maximum and an ultimate power–law behavior with the viscosity scaling approximately as $\dot{\epsilon}^{-0.5}$ over almost two decades in $\dot{\epsilon}$.

9.6 Conclusions

The experimental findings support the existence of a stress maximum in fast stretching of branched polymer melts, in contrast to state-of-the-art models that exhibit a monotonic increase in stress in controlled deformation experiments[Read *et al.* (2011); Larson (2011); Hutchings *et al.* (2012)]. The stress scaling at steady state after the maximum suggests that the maximum marks a transition to a flow state in which branched polymers behave as linear polymers. Indeed the current scenario for relaxation in branched melts in the LVE regime considers a hierarchy of relaxation (from outside to inside) and an effective conversion of a branched chain into a linear chain. If we assume the same scenario in the non–linear regime, the $\dot{\epsilon}^{-0.5}$ decrease of the viscosity might correspond to the same power law behavior found for linear melts [Bach *et al.* (2003a)].

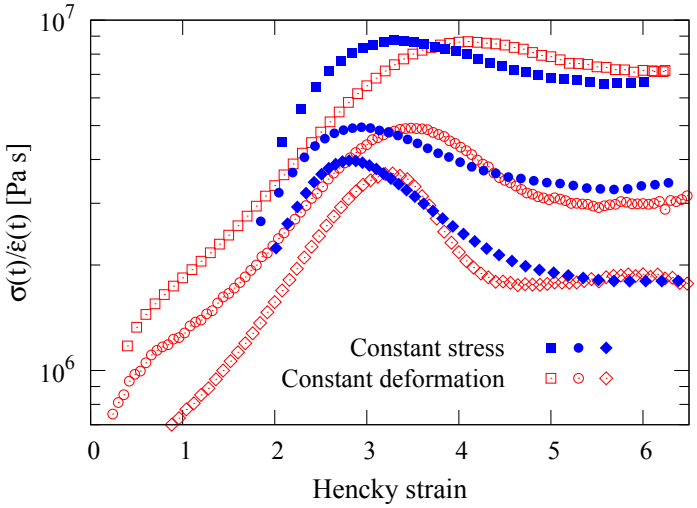

Figure 9.6: $\sigma/\dot{\epsilon}$ as a function of Hencky strain ϵ for constant stress (closed symbols) and constant strain rate (open symbols) experiments. The constant stress experiments correspond to □ 80kPa, ○ 100kPa, and ◇ 200kPa. The constant strain rate experiments correspond to □ $0.01s^{-1}$, ○ $0.03s^{-1}$, and ◇ $0.1s^{-1}$.

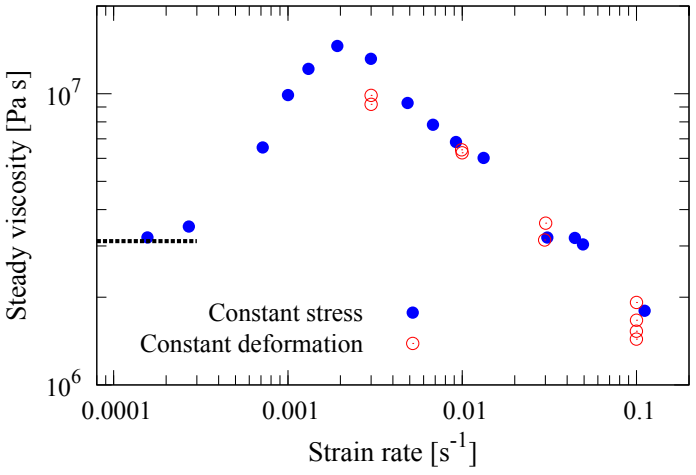

Figure 9.7: Steady viscosity as a function of Hencky strain rate $\dot{\epsilon}$ for constant stress (closed symbols) and constant strain rate (open symbols) experiments [Rasmussen *et al.* (2005)]. The dashed line represents 3 times the zero shear–rate viscosity determined from the LVE.

Chapter 10

Transient Overshoot Extensional Rheology of Long–Chain Branched Polyethylenes: Experimental Comparisons between Different Rheometers

10.1 Introduction

The true steady–state value for the extensional stress growth is still an open topic in the field of polymer melts. Constitutive modeling is often compared with shear and extensional flows to fit various parameters of the model. Extensional flow is much stronger than shear flow as it orientates and stretches chains more severely. Not having steady–state values for the extensional stress makes understanding and modeling molecular rheology in extensional flow challenging.

A maximum in the transient extensional stress has been reported for low–density polyethylene (LDPE) melts by Raible *et al.* (1979), but a steady–state stress after the maximum was not observed. Recently Rasmussen *et al.* (2005) used a filament stretching rheometer with active feedback to measure the elongational viscosity of two LDPEs at strains beyond the onset of localized necking of the sample. However, even with

active feedback a true steady–state flow condition is impossible to establish in filament stretching flows [see, for instance, McKinley and Sridhar (2002)] since an unlimited deformation is required and the sample cross–sections become very small. Despite this, the observation of an effective steady–state stress at high strains following a stress maximum was reported for two LDPE melts (Lupolen3020D and Lupolen1840D). In subsequent work, a similar high–strain steady-state stress plateau following a stress maximum has been reported for a model branched (Pompom) polystyrene of known architecture [Nielsen *et al.* (2006b)].

However, whether the transient overshoot in extensional flows is a real material property or an experimental artifact, as well as the true steady state values for the extensional stress growth, are still open questions [see, for instance, Burghelea *et al.* (2011)]. In this chapter, we compare extensional stress measurements on a set of Long–Chain Branched (LCB) polymer melts using three different extensional rheometers: The Sentmanat extensional rheometer (SER) [Sentmanat (2004)], the actively controlled filament stretching rheometer (FSR) [Bach *et al.* (2003b)], and the cross–slot extensional rheometer (CSER) [Auhl *et al.* (2011)]. The latter two are capable achieving steady–state flows although in different strain–rate regimes. We will show that the extensional stress at large strains is in good agreement, suggesting that it is possible to define an effective steady–state extensional stress for these materials.

10.2 Materials

Three different branched polyethylene melts were studied: A highly branched LDPE Dow150R and two moderately branched high–density polyethylenes (HDPE) HDB4 and HDB6 (see Table 10.1). These materials have been used in a number of previous rheological studies. The linear rheology of HDB4 and HDB6 has been reported by Das *et al.* (2006) and that of Dow150R by Hassell *et al.* (2008). The shear and uniaxial extension rheology were measured at the same temperature as the subsequent FSR and CSER experiments [Auhl *et al.* (2011)]. Shear flow experiments were conducted with an ARES rheometer (Advanced Rheometric Expansion System, Rheometric Scientific) in order to obtain both the linear rheological and nonlinear shear flow behavior. The nonlinear flow behavior in uniaxial elongation was measured using the uniaxial stretching device SER attached to the ARES rheometer. Specimen dimensions (compression molded to 1mm thick and 10mm wide samples) at test temperature were corrected to consider thermal expansion by using the room–temperature density and the thermal expansion coefficient of the samples. All of the rheological experiments were carried out under a nitrogen atmosphere. Further rheological tests to assess the thermal stability of the samples were conducted to ensure that the molar mass distribution and the molecular structure did not change during experiments. Thermal stability of at least 10^4s was found for all materials.

Table 10.1: Material properties of polyethylenes studied.

Sample	Code	M_w[kg/mol]	M_w/M_n	T[°C]	η_0[kPa · s]
LDPE1	Dow150R	242	11	160	368
HDPE1	HDB4	96	2.1	155	200
HDPE2	HDB6	68	2.2	155	50

10.3 Extensional Rheometry

10.3.1 Filament stretching rheometry

Extensional measurements using the SER rheometer are limited to cases where the sample remains homogeneous. In order to explore higher strains as the deformation becomes inhomogeneous, we require an experiment in which the material whose stress is being measured experiences a kinematically steady extensional flow. These measurements are performed with an FSR equipped with an oven to allow measurements up to about 200 °C [Bach *et al.* (2003b)]. The key feature of this rheometer is that it uses active feedback through the measurement of the mid–plane diameter to control the strain rate at the mid–plane of the filament, which provided that a critical strain rate $\dot{\epsilon}_{sag} = \rho g L_0/\eta_0$ is exceeded [McKinley and Sridhar (2002)] in the thinnest part of the filament. Therefore, on–line measurements of the midplane diameter serve the dual purpose of recording the actual strain and strain–rate at the mid–filament plane and providing input for the feedback control on the plate motion to achieve desired kinematics. Specifically, the Hencky strain and the mean value of the stress difference over the mid–filament plane [Szabo (1997)] are calculated from observations of the diameter $D(t)$ and the force on the bottom plate $F(t)$ as

$$\epsilon(t) = -2\ln\left(D(t)/D_0\right) \tag{10.1}$$

and

$$\langle \sigma_{zz} - \sigma_{rr} \rangle = \frac{F(t) - m_f g/2}{\pi R(t)^2}, \tag{10.2}$$

where the angular brackets denote an average over the symmetry plane, $R(t) = D(t)/2$ is the radius of the filament, g the gravitational acceleration, and m_f the weight of the polymer filament. Consequently on the assumption that the stress is uniform across the mid–plane, the force measurement gives the normal stress difference at the mid–plane of the filament where the fluid has experienced a constant extension–rate, even though

the overall extension–rate of the filament is nonuniform. Each material was tested a number of times to ensure reproducibility of the results.

Since the initial sample length is $L_0 = 2.5$mm compared with a plate radius $R_0 = 4.5$mm, the initial sample aspect is small, and consequently at small strains not all of the stress difference is due to the extensional viscosity. Part of the stress difference comes from a radial pressure variation in the cross-section due to the shear flow that is unavoidable at small aspect ratios. To compensate for this effect, we define the corrected transient uniaxial elongation viscosity by

$$\bar{\eta}^{+}_{\text{corr}} = \frac{\langle \sigma_{zz} - \sigma_{rr} \rangle}{\dot{\epsilon}} \left(1 + \frac{\exp\left(-5/3 - \Lambda_0^3\right)}{3\Lambda_0^2} \right)^{-1} \tag{10.3}$$

where $\Lambda_0 = L_0/R_0$ is the initial aspect ratio. The correction is a modification [Rasmussen *et al.* (2010)] of the relation derived from a lubrication analysis at small strains [Spiegelberg *et al.* (1996)]. For large strains, the correction vanishes and the radial variation of the stress in the symmetry plane becomes negligible [Kolte *et al.* (1997)].

10.3.2 Cross–slot extensional rheometry

The cross–slot flow experiments to measure the steady planar extensional rheology were performed using the CSER, in which a cross–slot insert is used in the Cambridge multipass rheometer (MPR) [Mackley *et al.* (1995)]. This instrument allows simultaneous measurement of pressure and optical birefringence as detailed in Coventry and Mackley (2008) and used for a number of different polymer melt flow studies [e.g., Hassell and Mackley (2009); Hassell *et al.* (2009)]. The birefringence was measured using a circularly polarized monochromatic light beam of 514nm using polarizers and quarter waveplates either side of the optical test section which contained stress free quartz windows. The stress–induced birefringence patterns were captured by a digital video camera [Collis and Mackley (2005)]. From the top and bottom reservoirs, the polymer material is driven in opposite directions along two perpendicular channels by pistons at a controlled rate through the cross–slot into two horizontal side channels capped by slave pistons [Figure 10.1(left)]. Thereby, the material is maintained within the MPR and can be forced back by nitrogen pressure through the cross–slot insert into the top and bottom reservoirs for subsequent runs. The cross–slot geometry insert used in this study consists of four perpendicular, intersecting coplanar channels with a depth of 10mm and aspect ratio of approximately 7 [Figure 10.1(right)]. This generates a pure and controllable elongational deformation in the neighborhood of the stagnation line along the middle section of the centreaxis of the cross, but essentially simple shear near the outer walls, e.g., Coventry and Mackley (2008). Full three–dimensional flow

simulations and experiments have been performed for both linear polystyrene [Lord *et al.* (2010)] and LCB–polyethylenes [Hoyle (2011)] in this geometry, where it was demonstrated that this aspect ratio is sufficiently large for the flow to be approximated as a two–dimensional planar flow within the experimental uncertainty of the stress measurements themselves, confirming previous simulation studies of Clemeur *et al.* (2004).

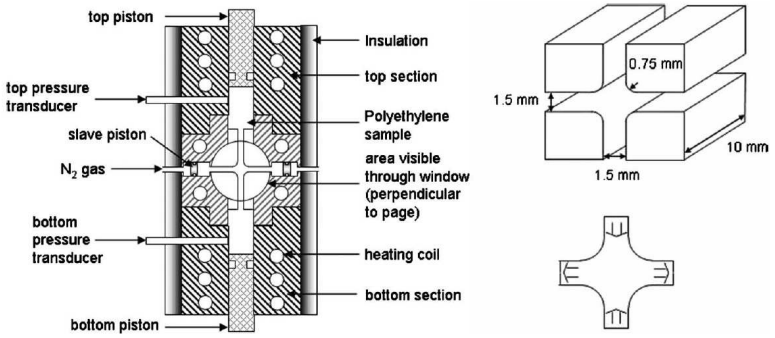

Figure 10.1: (left) Schematic outlining the Cambridge MPR core and (right) the dimensions and flow direction for the crossslot geometry insert as used in the midsection of the MPR. The associated flow directions are indicated by arrows.

At steady state, a molecule at a point along the stagnation line experiences a constant extension–rate $\dot{\varepsilon}_C$ that is approximately proportional to the piston speed, but varies with polymer rheology due to changes in the flow pattern. To determine the extension–rate for each experiment, we performed flow simulations using a multimode Pompom model fitted to the measured rheology of the material. We have shown previously [Hassell *et al.* (2009); Hoyle (2011)] that changes in the velocity field at points around the stagnation line measured using laser Doppler velocimetry are captured by the Pompom model and further are dependent upon the level of LCB present in a material.

The steady–state elongational viscosity η_P^+ is calculated from the tensile stress difference σ_{std} along the stagnation line and the extension–rate $\dot{\varepsilon}_C$ there

$$\eta_P^+ = \frac{\sigma_{\text{std}}}{\dot{\varepsilon}_C}. \tag{10.4}$$

Here, $\sigma_{\text{std}} = \left(\sigma_{xx} - \sigma_{yy}\right)$ is the principal stress difference between the extensional x and the compressional y axes. This was determined from the fringe–counting [using the method detailed in Auhl *et al.* (2011)] as $\sigma_{\text{std}} = \Delta n/C$, where C is the stress–optical coefficient. Stress–optical coefficients taken from Hassell *et al.* (2008) were used, which are in quantitative agreement with the range given in the literature for

polyethylene of $1.2 - 2.4 \times 10^{-9}\text{Pa}^{-1}$ [Macosko (1994)]. According to the theory of rubber elasticity and experiments, the stress–optical coefficient is only weakly dependent on temperature [Koyama and Ishizuka (1989)] and so the same stress–optical coefficient was used for the experiments at 155 and 160 °C. In all cases, the stresses are below the 1MPa limit where the stress–optical rule is expected to be valid [Kotaka *et al.* (1997); Koyama and Ishizuka (1989); McLeish (2002)].

10.4 Results and Discussion

10.4.1 Comparison between the SER and the FSR

For strain rates where data are available, we compare the transient stress growth in Figure 10.2 and 10.3. Figure 10.2 shows the two LCB–HDPEs named HDB4 and HDB6 with data measured from the SER and the FSR, and Figure 10.3 shows the LDPE Dow150R. The comparison of transient data shows good agreement between the two stretching methods up to the point at which the SER samples rupture and break, at Hencky strains of around 4 (the FSR is capable of Hencky strains up to 7). As a general observation for these three materials, the transient build up of stress measured by the FSR is faster than that of the SER. Also, as anticipated the SER never goes far enough in Hencky strain to observe an extensional stress maximum or steady-state value. In contrast, the FSR data show a clear overshoot in stress. The presence of a steady state in Figure 10.2 and 10.3(left) is obscured by the logarithmic axes that compress the large time results. In 10.3(right) the data of Dow150R is plotted as stress–strain curves and the axis of Hencky strain is in linear scale. The steady stress is then clear seen in this figure.

10.4.2 Comparison between the CSER and the FSR

Figure 10.4 shows the steady–state extensional viscosity measurements from the FSR and the CSER for the three polyethylene samples used in this work. The FSR values are obtained from the average stress measurement at large strains and the CSER from the steady–state birefringence patterns. For two of the materials, there are sufficient data to examine the overlap of the two experimental methods (Dow150R and HDB6) where there is good agreement between the two. This is despite the differences in the nature of the flows, with the FSR being uniaxial and the CSER planar extensional flow. Even for HDB4, where there is a gap in the data, the steady–state stress values still show the close agreement to the same trend. Furthermore, as reported by Hassell *et al.* (2009), with increasing the degree of branching, a transition in the birefringence

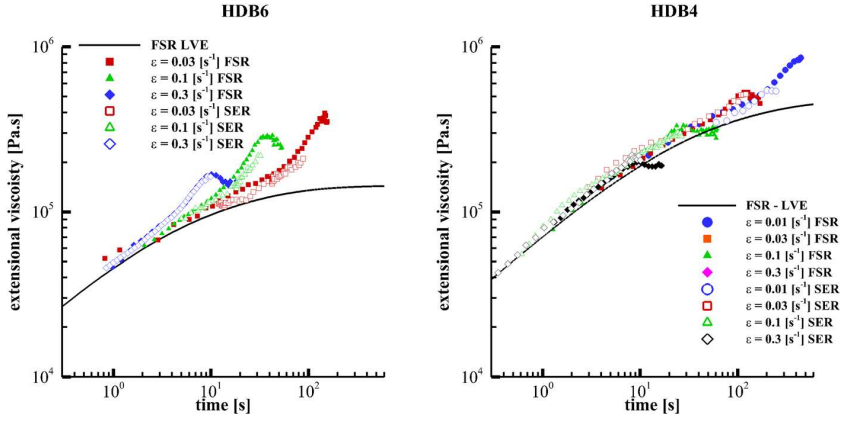

Figure 10.2: A comparison between the transient extensional stress response as measured by the FSR (closed) and the SER (open) for HDB6 (left) and HDB4 (right). The figure shows a good agreement of the initial stress growth, until sample rupture limits the SER to Hencky strains of around 4.

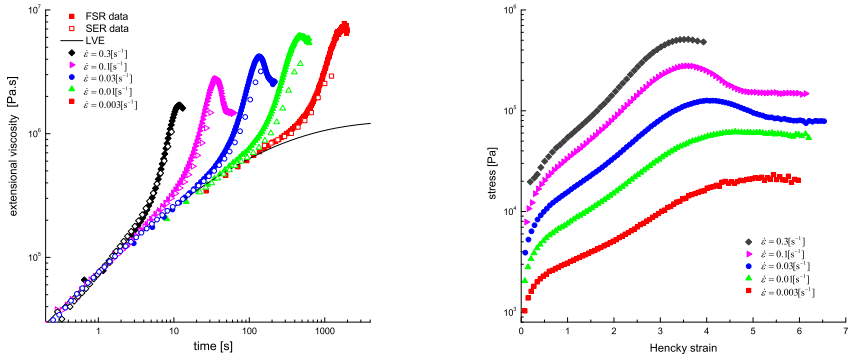

Figure 10.3: (left) A comparison between the transient extensional stress response as measured by the FSR (closed) and the SER (open) for Dow150R. (right) The transient extensional stress as a function of Hencky strain for Dow150R. The steady stress following the stress maximum is clearly seen.

pattern of the CSER from a single cusp along the outflow axis to a W shaped double cusp is observed. This W–cusp pattern indicates that the position of maximum stress difference is no longer at the stagnation line, but away from the outflow axis, which may relate to the stress overshoot observed in the measurements from the FSR. The W–cusps are observed in all the three branched polyethylenes here, where two of them are shown in Figure 10.5.

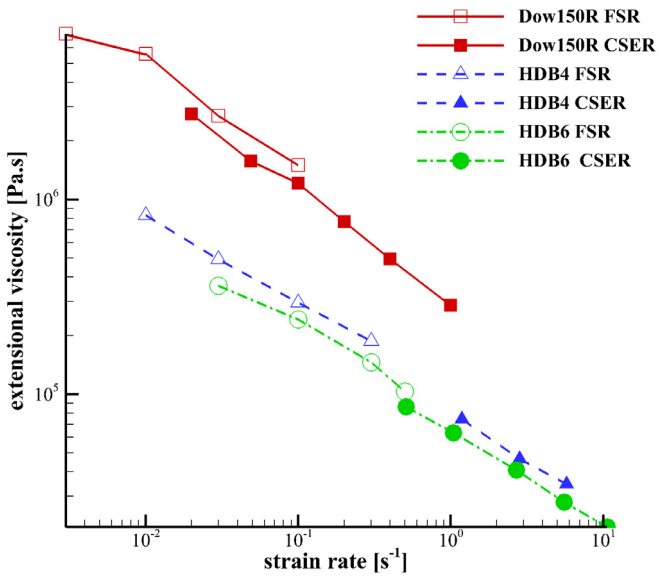

Figure 10.4: (A comparison of the steady-state extensional viscosity measurements from the FSR and the CSER for three polyethylene samples detailed in Table I. The open symbols show the FSR results and the closed symbols show the CSER data.

10.4.3 Stress relaxation following uniaxial extension

In Chapter 8 the stress relaxation following uniaxial extension for the two LDPE melts Lupolen 3020D and Lupolen 1840D was presented. Here we perform the stress relaxation measurements for the LDPE Dow150R. Since the stress relaxation are limited to low Hencky strains by using the SER due to the necking instability [Wang *et al.* (2007)], and the CSER is not available for stress relaxation measurements, here we only present the measurements from the FSR, following the same procedure as described in Chapter 8. Figure 10.6 shows the experimental results. The startup of the flow was a uniaxial extension with three different strain rates. For each rate the flow was stopped at

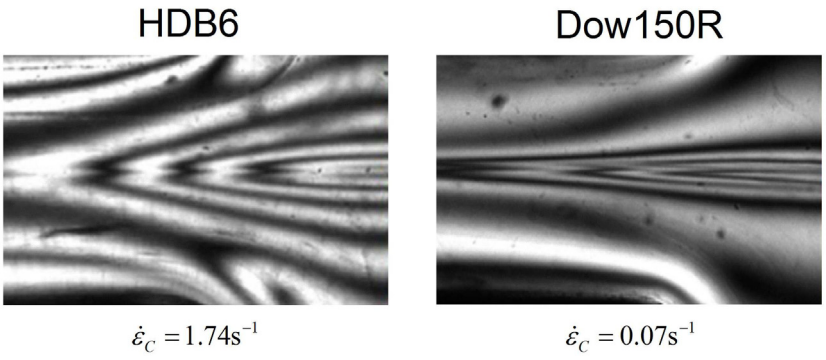

Figure 10.5: W–cusps shown in the birefringence pattern from the CSER for the HDPE HDB6 and the LDPE Dow150R.

a Hencky strain of 3 and 4.5 respectively. With the strain rate $\dot{\epsilon} = 0.1\text{s}^{-1}$, the stress relaxation measurement at $\epsilon_0 = 4.5$ (after the overshoot) show a remarkably faster decrease in the transient viscosity compared with the measurement at $\epsilon_0 = 3$ (before the overshoot), which is in agreement with the observations in Chapter 8. In contrast, with the lowest strain rate $\dot{\epsilon} = 0.01\text{s}^{-1}$ where the stress overshoot is not shown, the transient viscosity in the stress relaxation measurement at $\epsilon_0 = 4.5$ do not go across the one at $\epsilon_0 = 3$, which is obviously different from the ones performed at $\dot{\epsilon} = 0.1\text{s}^{-1}$.

10.5 Conclusions

In this chapter, we have compared three experimental techniques for measuring the extensional viscosity of LCB polymer melts. Both the SER and the FSR measure the startup of uniaxial extensional flow, but with the FSR it is capable of reaching higher Hencky strains due to its feedback control. The CSER measures the steady–state planar extensional viscosity through the stress birefringence at the stagnation line. (The transient viscosity can also be inferred from the stress growth on the incoming stagnation streamline.) All three experimental techniques show good agreement for strain–rates at which they can all operate. However, in general the experimental windows of the FSR and the CSER are complimentary to one another with the FSR operating in a low strain–rate regime and the CSER operating in a high strain–rate regime. Hence, we have a robust technique for probing a materials extensional behavior. For the three materials we investigated here, we could accurately characterize the steady–state extensional viscosity. The experiments revealed consistent and striking phenomena unique to strain-hardening melts (seen for all LCB melts); in the FSR, this is manifest as

overshoots in the transient stress, which produce W–cusps in the CSER. (Further information regarding the numerical comparisons between the filament stretching and the cross–slot flow can be found in the publication by Hoyle *et al.* (2013).)

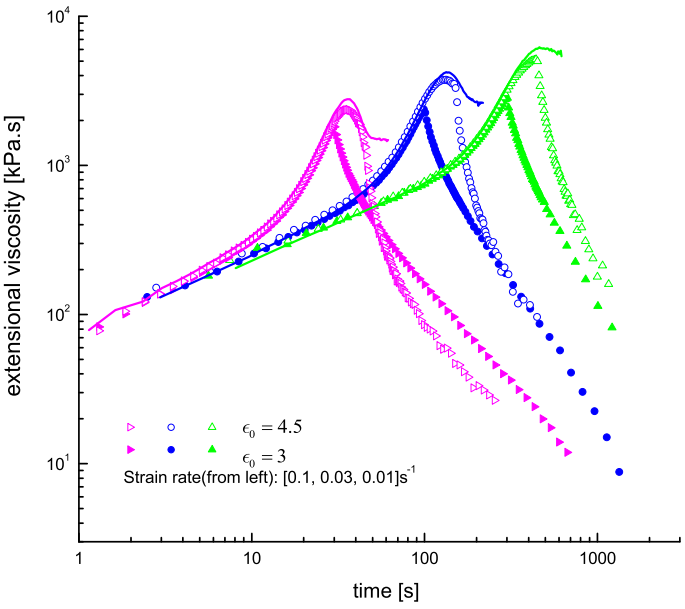

Figure 10.6: The transient extensional viscosity of LDPE Dow150R as a function of time at 160 °C with $\dot{\epsilon} = 0.1, 0.03$ and $0.01 s^{-1}$. For each rate the flow was stopped at a Hencky strain of $\epsilon_0 = 3$ and 4.5 respectively. The lines are the FSR measurements of unixial extension taken from Figure 10.3.

Chapter 11

Summarizing Chapter

In this thesis we have experimentally studied the extensional rheology of linear and branched polymer melts. The experiments were carried out using the unique filament stretching rheometer (FSR) at DTU. An updated control scheme based on the work of Bach (2003) has been implemented in the FSR, so that the polymer melts can be stretched under a well–controlled manner of either constant strain rate or constant stress. We have investigated four categories of polymer melts throughout the thesis from the simplest system to the most complicated system.

In category 1 we have measured the monodisperse linear polystyrene melts and solutions in uniaxial extensional flow. We explored the possible reasons that caused the difference of elongational steady–state viscosity between entangled polymer melts and solutions. It is possible to scale the time constant and the plateau modulus such that polystyrene melts and concentrated polystyrene solutions with the same number of entanglements per chain (Z) have identical LVE properties both in shear and extension. Polystyrene melts and solutions with the same Z differ, however in the non–linear extensional properties. The polymer chains of the solutions are found to be more strain hardening than the melts, especially at lower concentration. It may be due to their higher values of the maximum stretch ratio ($\lambda_{\max}$). At Weissenberg number $Wi_R > 1$, the non–dimensional steady–state viscosity of the solutions shows a plateau region, while the viscosity of the melts still decreases monotonically. Assuming that $\lambda_{\max}$ is the relevant parameter for the non–linear behavior, the polystyrene solutions should behave similarly to some other melts such as polypropylene and polyisoprene which

have the similar values of λ_{max}. Solvents also influence the non–linear behavior. We compared two polystyrene solutions with the same solute and same concentration, but different solvents. The solvents that we used were two styrene oligomers with molar masses of 1 kg/mole and 4 kg/mole, corresponding to less than 2 Kuhn–segments and about 7 Kuhn–segments [Fang *et al.* (2000)] per chain, respectively. Therefore the 1 kg/mole styrene oligomer is close to an isotropic medium, whereas the 4 kg/mole styrene oligomer is a potentially anisotropic medium. It is found that the solution with the nearly isotropic solvent show much more strain hardening than the other solution with the anisotropic medium, when compared under the same Rouse time scale. It may be due to a stretch/orientation–induced reduction of the monomeric (Kuhn–segment's) friction as proposed by Ianniruberto *et al.* (2012).

In category 2 we have measured the bidisperse and polydisperse linear polystyrene melts. The extensional steady–state viscosity of the well–entangled bidisperse blends shows the same trend as the monodisperse melts. The Rouse time and the level of the extensional steady–state viscosity of the blends seem to follow the simple mixing rule. The extensional steady–state viscosity of the polydisperse melt is found to decrease as $\bar{\eta}_{steady} \sim \dot{\epsilon}^{-0.25}$, in which the exponent is in between of well–entangled polystyrene melts ($\bar{\eta}_{steady} \sim \dot{\epsilon}^{-0.5}$) and polystyrene solutions ($\bar{\eta}_{steady} \sim \dot{\epsilon}^{0}$). $\dot{\epsilon}$ is the strain rate. Stress relaxation and reversed biaxial flows both following the uniaxial extension of the polydisperse melt have also been measured. In the stress relaxation phase, the polydisperse melt is observed to relax slower than the monodisperse melt. In the reversed flow measurements, the melt is found to behave like a network at high rates where the strain recovery saturates.

The FSR measurement for category 1 and 2 in this thesis (Chapter 3–6), combined with the previous experiments by Bach *et al.* (2003a), Nielsen *et al.* (2006a), Nielsen *et al.* (2008) and Nielsen and Rasmussen (2008), have established a complete system of the linear polystyrene melts. Further experiments on some other linear polymer melts, such as polypropylene and polyisoprene, will be interesting to test whether the above conclusions can also be applied for general linear polymer melts. Constitutive models which can capture all the above observations are desired.

In category 3 we have measured the monodisperse branched polystyrene melts. Well–defined branched polymers are considered as model polymers for the validation of the developing theoretical models. Here we have measured two well–defined branched polymer melts, including a three–arm asymmetric star polystyrene and an H–shaped polystyrene, in uniaxial extensional flow. The elongational steady stress of the two branched polystyrenes has been compared with a linear polystyrene melt as a function of the Weissenberg number. It is shown that both the star and H–shaped melts behaved like the linear melt in fast extensional flows where the Weissenberg number is bigger than 1, which is in agreement with the observation reported by Ianniruberto and Marrucci (2013).

However, due to the limited amount of materials and the difficulties in handling the experiments, the experimental data for category 3 are still very limited. Well–defined branched polymers with some other molecular architecture, such as comb and dendritic structures, will be interesting to be investigated using the FSR. Rheological characterization combined with other methods such as neutron scattering will be needed for further studies of the polymer dynamics.

In category 4 we have measured the polydisperse branched polymer melts. Many commercially used polymers such as low–density polyethylene (LDPE) belong to this category. A stress maximum during the start–up of uniaxial extensional flow was reported in 1979 for a LDPE melt [Raible *et al.* (1979)]. Subsequently observations of a steady stress following a stress maximum were reported for two LDPE melts [Rasmussen *et al.* (2005)]. However the rheological significance of the stress maximum [Burghelea *et al.* (2011); Rasmussen and Hassager (2012); Burghelea *et al.* (2012)] as well as the existence of steady flow conditions [Wang *et al.* (2007); Lyhne *et al.* (2009)] following the maximum is still a matter of some debate. The extensional measurements reported by Rasmussen *et al.* (2005) were performed under constant strain rate mode. In this thesis we have measured one of the LDPE melts under constant stress mode. The creep measurements confirms the existence of a stress maximum as well as the steady flow after the stress maximum in fast stretching of branched polymer melts. The stress scaling at steady state after the maximum suggests that the maximum marks a transition to a flow state in which branched polymers behave as linear polymers. We have also measured stress relaxation and reversed biaxial flow, both following uniaxial extension, on the two LDPE melts which have been measured by Rasmussen *et al.* (2005). Both the measurements of stress relaxation and reversed flow indicate that the branched LDPE melts behave similarly to linear polymers after the stress overshoot, since the experimental data recovers to the Doi–Edwards predictions. We have also compared the experimental data with the multi mode pom–pom model and the multi mode interchain pressure model. Both models can quantitatively predict the start–up of the uniaxial elongation before the overshoot, but neither one is able to capture even qualitatively the stress relaxation or strain recovery of the material exhibited after the overshoot. Clearly the dynamics involved in the stress overshoot exhibited by branched polymers still needs new theoretical insight.

Finally, we have compared three experimental techniques, including the FSR, the SER and the CSER, for measuring the extensional rheology of branched polymer melts. Both the SER and the FSR measure the start–up of uniaxial extensional flow, but with the FSR it is capable of reaching higher Hencky strains due to its feedback control. The CSER only measures the steady–state extensional viscosity through the stress birefringence at the stagnation line. The results from the unique FSR at DTU have been shown to be consistent with the results from the SER and the CSER.

Appendix A

Accuracy of FSR measurements

A.1 Temperature Influence

The polymer melts used in this thesis are polystyrenes and polyethylenes. Polyethylene melts have very low glass transition temperatures (T_g). For example, the T_g for commercial low–density polyethylene (LDPE) is around $-125\,^{\circ}\mathrm{C}$. Polystyrene melts have much higher T_g. For example, the T_g for commercial polystyrene is around $100\,^{\circ}\mathrm{C}$, and for monodisperse linear polystyrene is around $107\,^{\circ}\mathrm{C}$. Most of our measurements using the filament stretching rheometer (FSR) are performed at $130\,^{\circ}\mathrm{C}$. This temperature is far above the T_g for polyethylenes, but only about $25\,^{\circ}\mathrm{C}$ higher than the T_g for polystyrenes. The measurements for polystyrene melts are much more sensitive to the temperature change than the measurements for polyethylene melts. For example, the time–temperature shift factor a_T from $170\,^{\circ}\mathrm{C}$ to $130\,^{\circ}\mathrm{C}$ for LDPE Lupolen 3020D (in Chapter 8) is 6.4, but for the monodisperse polystyrene PS-290k (in Chapter 3) is about 900. Therefore the accurate temperature plays an important role in the accurate FSR measurements especially for polystyrene melts.

Figure A.1 shows the estimated temperature influence on the level of elongational steady–state viscosity for linear polystyrene melts. The black solid line presents the elongational steady–state viscosity for PS-290k as a function of strain rate at $130\,^{\circ}\mathrm{C}$ (related experimental data can be found in Figure 3.5). The other dashed/dotted lines are the predictions of the steady–state viscosity level at other temperatures using the

time–temperature shift factors a_T calculated by Eq.3.2. It can be seen that 1 °C difference in temperature can cause around 10% deviation of the steady–state viscosity level.

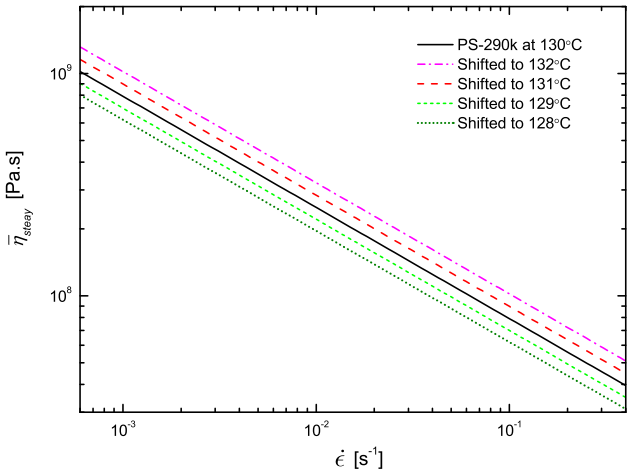

Figure A.1: Estimated temperature influence on the level of elongational steady–state viscosity for linear polystyrene melts.

As described by Bach *et al.* (2003b), the temperature in the FSR oven is regulated by six temperature measurements: one for the nitrogen flow, one for the outer wall of the oven, and the other four for the front, back, side and bottom parts of the inner wall, respectively. Each of the six temperature sensors has been well calibrated. However, there is no temperature measurement in the center of the oven where a filament locates. The filament temperature is investigated by placing an external thermocouple (calibrated before hand) near the filament and measuring the temperature. The temperature accuracy in the FSR is found to be ±0.5 °C.

A.2 Samples Degradation

Prior to FSR measurements, polystyrene samples are usually required pre–stretching to lower the force during stretching. Pre–stretching is normally performed at higher temperatures than the desired experimental temperature, so that the samples relax faster and the pre–stretching process can also be faster. However, too high temperature for pre–stretching results in samples degradation. Degradation can also happen in the molding

process for samples preparation. Samples degradation is checked by comparing the samples after FSR measurements with the fresh samples in size exclusion chromatography (SEC).

A.2.1 Linear melts

Linear polystyrene melts are found to be quite stable up to 160 °C under nitrogen. In all the measurements that the temperatures were not higher than 160 °C in this thesis, samples degradation was not observed for linear polystyrene melts. However, as shown in Figure A.2, degradation was observed for the monodisperse linear polystyrene melt PS-290k, when the sample was kept at 170 °C under nitrogen for about 1.5 hours.

Degradation obviously influence the non–linear rheological behavior as shown in Figure A.3. The black plots in the figure are the uniaxial extensional data for PS-290k taken from Figure 3.3. The blue plots are the stress relaxation measurements in which the degradation was not observed. The start–up of the blue plots shows a good agreement with the black plots. For the stress relaxation measurements the flow for each strain rate was stopped at Hencky strain 3. The red plots are the same stress relaxation measurements as the blue plots, but with the degraded sample as shown in Figure A.2. It can be seen that in the start–up of the flow, the steady–state viscosity level of the degraded sample is around 20% lower. The degraded sample also shows a faster rlaxation process when the flow is stopped.

A.2.2 Branched melts

Compared with linear melts, monodisperse branched melts are more difficult to handle in FSR measurements. On one hand, branched melts usually relax slower than the relative linear melts, and therefore higher pre–stretching temperature is preferred. On the other hand, branched melts seem not as stable as linear melts; arms losing has been observed even below 160 °C.

Figure A.4 compares the stretched sample with the fresh sample in SEC for the H–shaped polystyrene H2A1 which has been measured in Chapter 7. As mentioned in Chapter 7, the samples were pre–stretched at 160 °C. And due to the very limited amount of the material, the stretched samples had to be re–molded and stretched again for several times. In figure A.4, the red curve is for the H2A1 sample that has been reused for three times. The dashed gray line is from a linear polystyrene with a molar mass of 43kg/mole, which is very close to the arm molecular weight (46kg/mole) of H2A1. It can be seen that around 8% of the H2A1 molecules lost arms after the FSR measurements.

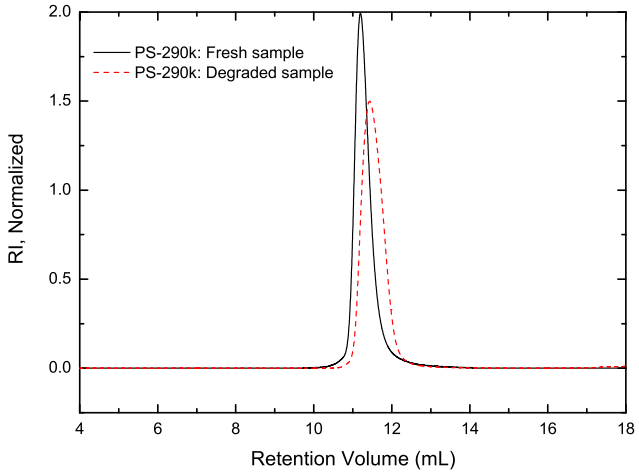

Figure A.2: Comparison between fresh PS-290k and degraded PS-290k in SEC. The degraded sample was kept at 170 °C under nitrogen for about 1.5 hours.

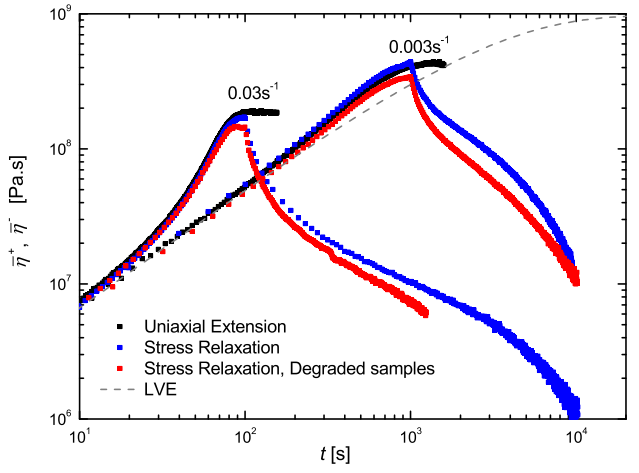

Figure A.3: Comparison of stress relaxation measurements between PS-290k and the degraded samples at 130 °C.

The influence of losing arms for H2A1 is investigated by comparing the measurements of the samples that used for the first time and reused for the third time, as shown in Figure A.5. It can be seen that the measurements repeat quite well, indicating that the degradation during the reusing process has little influence. However, degradation might have already happened when the samples were stretched at the first time. The percentage of deviation between the degraded sample in Figure A.4 and the sample without any degradation is still unknown.

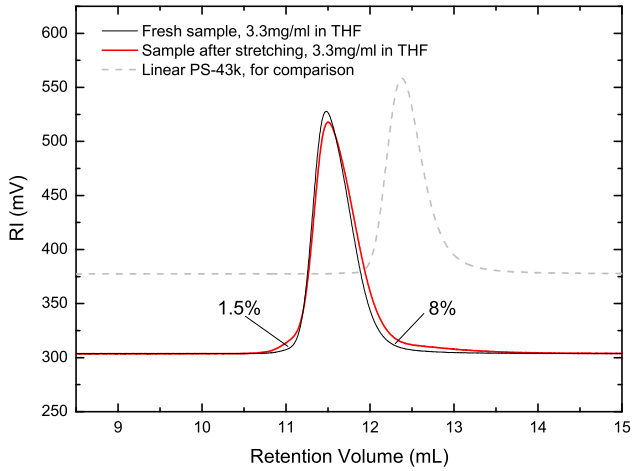

Figure A.4: Comparison between the stretched sample and the fresh sample in SEC for H2A1. The stretched sample was reused for three times.

For the accuracy of future measurements on model branched polystyrene melts, we have performed some preliminary tests to determine the temperature for samples molding and pre–stretching. We heated two well-defined comb polystyrene melts, C622 and C642, to 155 °C and kept them at this temperature under nitrogen for 5 hours. Both C622 and C642 have a backbone of 270kg/mole with 29 arms per backbone. The arm molecular weight for C622 is 11.7kg/mole and for C642 is 47kg/mole. Figure A.6 and A.7 compare the samples before and after heating for C622 and C624, respectively. A slight degradation for C642 after heating was observed. Around 1.3% of the molecules lost arms. For C622 almost no degradation was observed after heating. In the work by Nielsen *et al.* (2006b), the authors also observed arms losing for the pom–pom molecules at 157 °C under nitrogen[1]. Therefore we suggest that the temperature for monodisperse branched polystyrene melts should be kept below 155 °C during the whole procedure.

[1] From the discussion with the authors; not reported in the article.

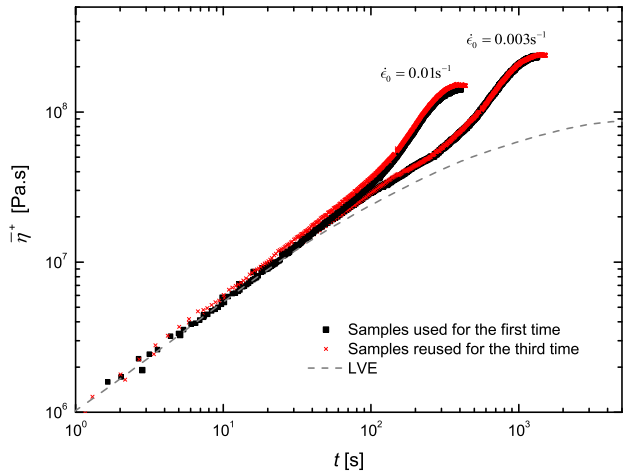

Figure A.5: Comparison of uniaxial extensional measurements between H2A1 samples that used for the first time and reused for the third time.

Figure A.8 compares a star polystyrene melt Star-90k after stretching with the fresh sample in SEC. Star-90k is a three–arm symmetric star polystyrene with arm molecular weight 90k/mole. During the whole procedure of FSR measurements, the highest temperature used for Star-90k was 150 °C (during pre–stretching). Figure A.8 shows a perfect match for the stretched sample and the fresh sample, indicating that degradation did not happen and 150 °C is a safe temperature.

A.3 Bubbles in Samples

Bubbles in samples are usually observed when the samples are not well dried. Both residual solvents and absorbed water (from the humid environment) may cause bubbles in polystyrene samples. Before the measurements, samples should be dried at a temperature close to (but not above) T_g under vacuum overnight. Undried samples may have a lower T_g and give inaccurate results, since polystyrene samples are extremely sensitive to temperature as discussed in Section A.1. Bubbles in the mid–plane of a filament also decrease the cross section area, resulting in an inaccurate calculation of the stress.

Figure A.9 compares the G' G'' data between the well dried and undried samples of

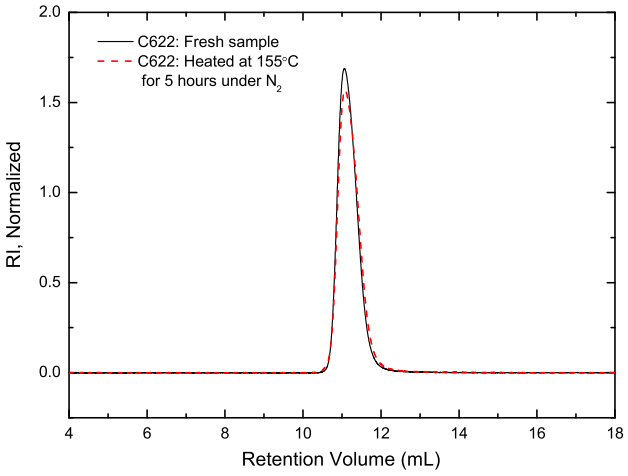

Figure A.6: Comparison between the sample after heating and the fresh sample in SEC for C622.

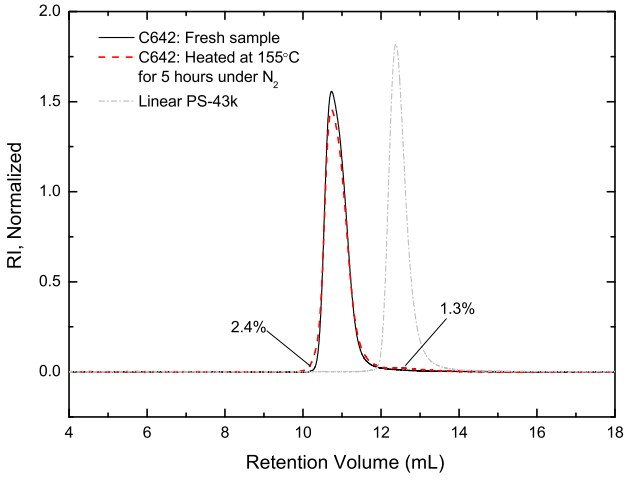

Figure A.7: Comparison between the sample after heating and the fresh sample in SEC for C624.

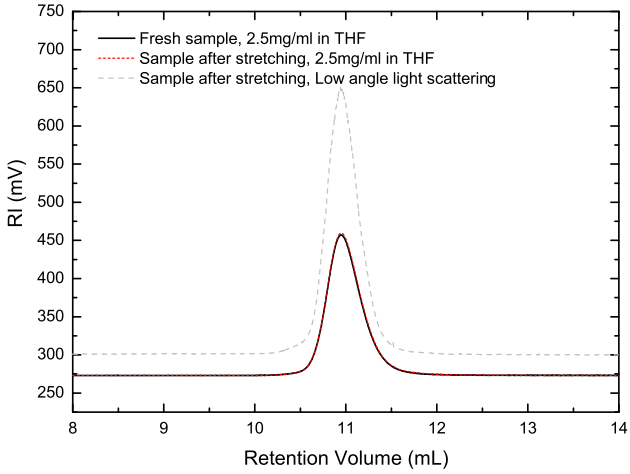

Figure A.8: Comparison between the stretched sample and the fresh sample in SEC for Star-90k.

Star-20k which has been measured in Chapter 7. In the figure, the G' G'' plots for the undried sample has the same shape with the dried sample. But the plots for the undried sample show both a horizontal and a vertical shift compared with the dried sample. The horizontal shift is probably due to the change of T_g. Figure A.10 and Figure A.11 compare the dried and undried samples in FSR measurements for the linear polystyrene melts PS-180k and PS-290k, respectively. The elongational steady–state viscosity for the undried PS-290k sample is around 15% lower than the dried sample, and for the undried PS-180k sample is about 40% lower. It can be seen that the drying process is very important for the accauracy of FSR measurements. If bubbles are seen in the samples, the measurements are not reliable. It should be noted that the measurements for the undried samples can sometimes repeat quite well. Therefore reproducibility can not definitely ensure a reliable measurement.

A.4 Comparison with Previous Published Data at DTU

We first compare the shear rheology of the monodisperse linear polystyrene melts with molar masses of 100, 145, 200, 290, 390 and 550kg/mole. The data of PS-100k is from Nielsen *et al.* (2006a). The data of PS-145k is from Nielsen *et al.* (2008). The data of PS-200k and PS-390k are from Bach *et al.* (2003a). The data of PS-290k and PS-550k

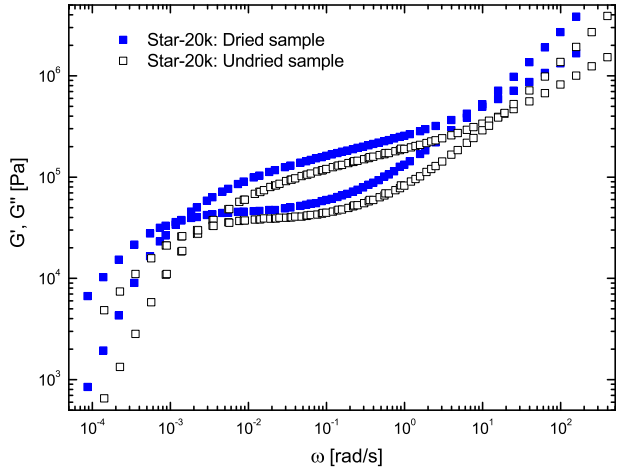

Figure A.9: Comparison of the G' G'' data between the well dried and undried samples of Star-20k at 130 °C.

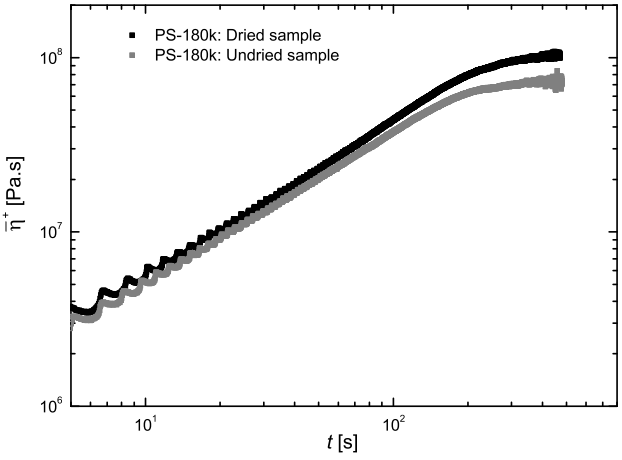

Figure A.10: Comparison of the FSR measurements between the well dried and undried samples of PS-180k at 130 °C. For both samples the strain rate is $0.01 s^{-1}$.

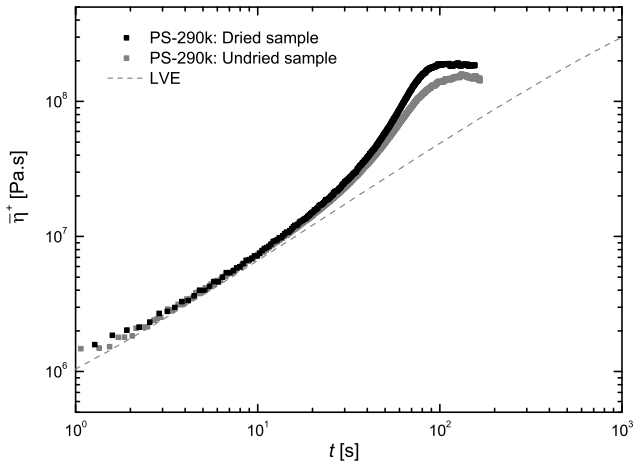

Figure A.11: Comparison of the FSR measurements between the well dried and undried samples of PS-290k at 130 °C. For both samples the strain rate is 0.03s^{-1}.

are from Chapter 3 of this thesis.

Figure A.12 compares the zero shear rate viscosity for the linear polystyrene melts at 130 °C. It can be seen that the data points approximately follow the famous 3.4 power law. Figure A.13 compares the G' G'' for PS-100k, PS-145k, PS-290k, and PS-550k. All the data overlap at the high frequency part. The horizontal shift in Figure A.9 is not observed here.

The G' G'' data at the high frequency part (glassy region) for PS-200k and PS-390k are not available. However, when compare the available data points of PS-200k with the ones of PS-290k, horizontal and vertical shifts are observed as shown in Figure A.14. We performed BSW fitting for PS-200k and PS-390k to predict the G' G'' values in the glassy region. In the BSW fitting, we fixed $n_e = 0.23$ and $n_g = 0.7$ as we did for the monodisperse polystyrene melts and solutions in Chapter 3 and 4. The BSW parameters for PS-200k and PS-390k are listed in Table A.1. The predicted G' G'' curves for PS-200k and PS-390k show an obvious horizontal shift compared with the plots for PS-290k, indicating the T_g of PS-200k and PS-390k is probably lower than the T_g of PS-290k.

Figure A.15 compares the FSR measurements between PS-290k and PS-390k at 130 °C. The data of PS-390k is from Bach *et al.* (2003a), and the data of PS-290k is from Chap-

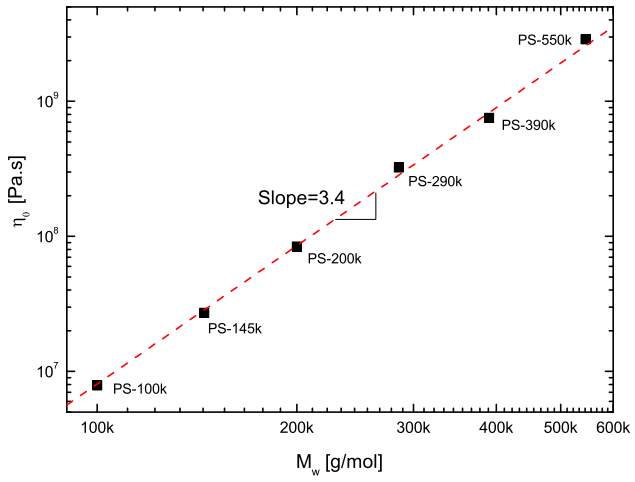

Figure A.12: Comparison of the zero shear rate viscosity for the linear polystyrene melts at 130 °C.

Table A.1: Material properties obtained from the BSW spectrum for PS-200k and PS-390k at 130 °C. The parameters for PS-550k and PS-290k are taken from Table 3.4.

Sample Name	n_e	n_g	G_N^0[Pa]	τ_c[s]	$\tau_{\max}$[s]
PS-550k	0.23	0.7	250000	0.4	61540
PS-290k	0.23	0.7	250000	0.4	6890
PS-390k	0.23	0.7	240000	0.25	1048
PS-200k	0.23	0.7	240000	0.25	15200

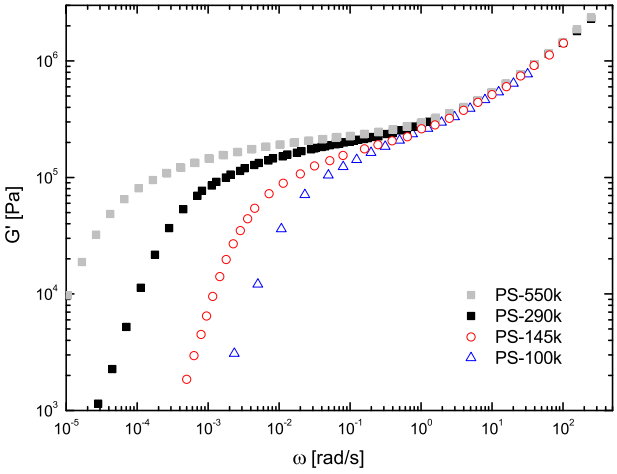

(a) Comparison of G'

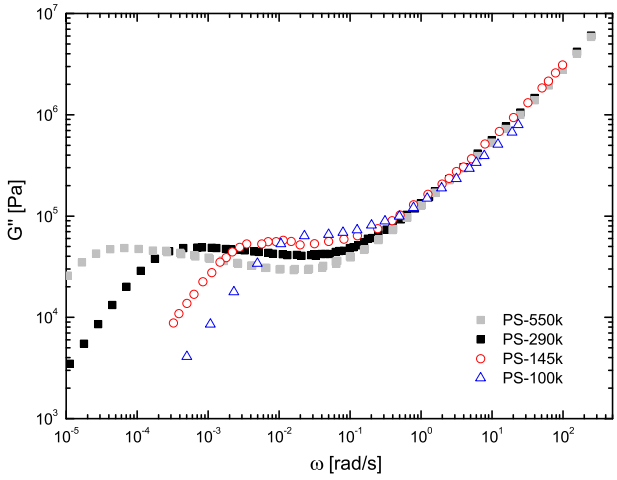

(b) Comparison of G''

Figure A.13: Comparison of the LVE data for the linear polystyrene melts at 130 °C.

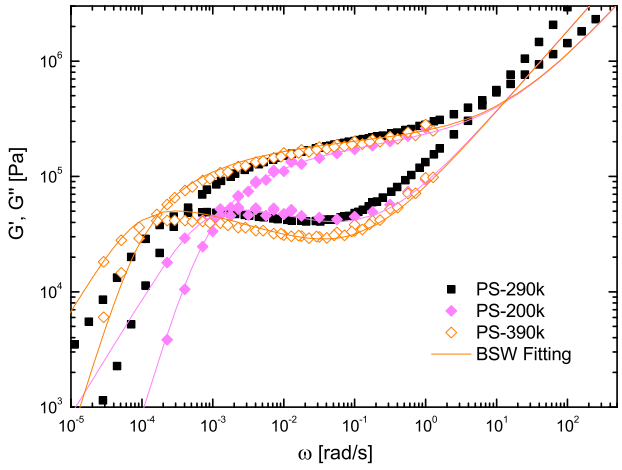

Figure A.14: LVE data fitted with the BSW spectrum for PS-200k and PS-390k at 130 °C.

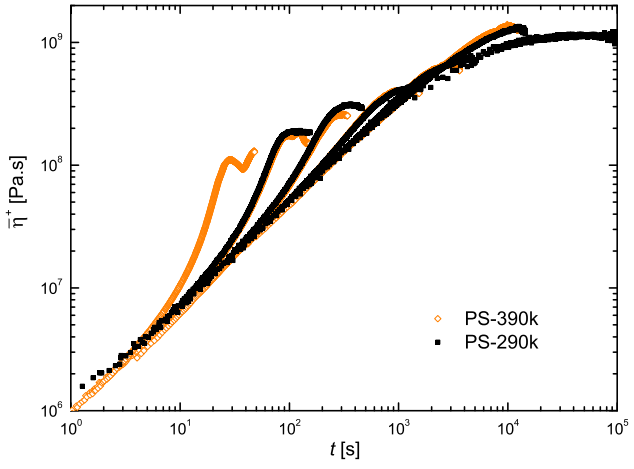

Figure A.15: Comparison of the FSR measurements between PS-290k and PS-390k at 130 °C.

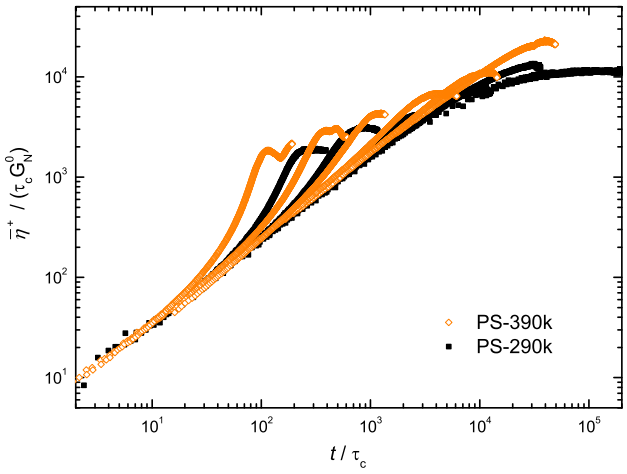

Figure A.16: Comparison of the FSR measurements between PS-290k and PS-390k under non–dimensional parameters.

ter 3. At the same temperature, PS-390k is supposed to be more strain hardening than PS-290k, and should also have a higher level of elongational steady–state viscosity than that of PS-290k. However, the plots for PS-390k are almost the same as the plots for PS-290k in Figure A.15. It may because the T_g of PS-390k is lower than the T_g of PS-290k, as indicated in Figure A.14. This effect may be erased by comparing the data under a same time scale as discussed in Chapter 3. Figure A.16 compares PS-390k with PS-290k under non–dimensional parameters which scale the same way as shown in Figure 3.7 of Chapter 3. The level of the non–dimensional steady–state viscosity of PS-390k is about 30% higher than that of PS-290k, which is reasonable.

Appendix B

Joint Author Statements

Technical University of Denmark *Office for PhD and Continuing Education*

January 2013

Joint author statement

If a thesis contains articles made in collaboration with other researchers, a joint author statement about the PhD-student's part of the article shall be made by each of the co-authors, cf. article 12, section 4 of the Ministerial Order No. 18 February 2008 about the PhD degree

Title of the article:	Stress relaxation and reversed flow of low-density polyethylene melts following uniaxial extension		
Author(s):	Qian Huang, Henrik K. Rasmussen, Anne L. Skov, Ole Hassager		
Journal:	Journal of Rheology 56(6), 1535-1554 (2012)		
PhD-student:	Qian Huang	CPR-no.:	050182-3228
Signature of the PhD-student:	Qian Huang	Date:	27 January 2013
Co-author:	Henrik Koblitz Rasmussen	Signature:	

Description of each author's contribution to the above-mentioned article:

Qian Huang:
Carried out all the experiments and post processing of data. Performed the numerical calculations of the constitutive models. Wrote the first draft of the article manuscript.

Henrik. K. Rasmussen:
Supervised the first author on the experimental work. Checked the numerical calculation results of the Doi-Edwards model and the Interchain Pressure Model. Provided feedback on the manuscript.

Anne. L. Skov:
Engaged in discussions about the results and provided feedback on the manuscript

Ole Hassager:
Supervised the first author on understanding the constitutive models. Engaged in discussions about the results. Provided feedback on the manuscript.

Joint author statements shall be delivered to the **PhD administration** together with the PhD thesis.

Technical University of Denmark *Office for PhD and Continuing Education*

January 2013

Joint author statement

If a thesis contains articles made in collaboration with other researchers, a joint author statement about the PhD-student's part of the article shall be made by each of the co-authors, cf. article 12, section 4 of the Ministerial Order No. 18 February 2008 about the PhD degree

Title of the article:	Stress relaxation and reversed flow of low-density polyethylene melts following uniaxial extension		
Author(s):	Qian Huang, Henrik K. Rasmussen, Anne L. Skov, Ole Hassager		
Journal:	Journal of Rheology 56(6), 1535-1554 (2012)		
PhD-student:	Qian Huang	CPR-no.:	050182-3228
Signature of the PhD-student:	Qian Huang	Date:	27 January 2013
Co-author:	Anne Ladegaard Skov	Signature:	A Skov

Description of each author's contribution to the above-mentioned article:

Qian Huang:
Carried out all the experiments and post processing of data. Performed the numerical calculations of the constitutive models. Wrote the first draft of the article manuscript.

Henrik. K. Rasmussen:
Supervised the first author on the experimental work. Checked the numerical calculation results of the Doi-Edwards model and the Interchain Pressure Model. Provided feedback on the manuscript.

Anne. L. Skov:
Engaged in discussions about the results and provided feedback on the manuscript.

Ole Hassager:
Supervised the first author on understanding the constitutive models. Engaged in discussions about the results. Provided feedback on the manuscript.

Joint author statements shall be delivered to the **PhD administration** together with the PhD thesis.

Technical University of Denmark *Office for PhD and Continuing Education*

January 2013

Joint author statement

If a thesis contains articles made in collaboration with other researchers, a joint author statement about the PhD-student's part of the article shall be made by each of the co-authors, cf. article 12, section 4 of the Ministerial Order No. 18 February 2008 about the PhD degree

Title of the article:	Stress relaxation and reversed flow of low-density polyethylene melts following uniaxial extension		
Author(s):	Qian Huang, Henrik K. Rasmussen, Anne L. Skov, Ole Hassager		
Journal:	Journal of Rheology 56(6), 1535-1554 (2012)		
PhD-student:	Qian Huang	CPR-no.:	050182-3228
Signature of the PhD-student:	Qian Huang	Date:	27 January 2013
Co-author:	Ole Hassager	Signature:	

Description of each author's contribution to the above-mentioned article:

Qian Huang:
Carried out all the experiments and post processing of data. Performed the numerical calculations of the constitutive models. Wrote the first draft of the article manuscript.

Henrik. K. Rasmussen:
Supervised the first author on the experimental work. Checked the numerical calculation results of the Doi-Edwards model and the Interchain Pressure Model. Provided feedback on the manuscript.

Anne. L. Skov:
Engaged in discussions about the results and provided feedback on the manuscript.

Ole Hassager:
Supervised the first author on understanding the constitutive models. Engaged in discussions about the results. Provided feedback on the manuscript.

Joint author statements shall be delivered to the **PhD administration** together with the PhD thesis.

Technical University of Denmark *Office for PhD and Continuing Education*

January 2013

Joint author statement

If a thesis contains articles made in collaboration with other researchers, a joint author statement about the PhD-student's part of the article shall be made by each of the co-authors, cf. article 12, section 4 of the Ministerial Order No. 18 February 2008 about the PhD degree

Title of the article: Transient overshoot extensional rheology of long-chain branched polyethylenes: Experimental and numerical comparisons between filament stretching and cross-slot flow

Author(s): D. M. Hoyle, Q. Huang, D. Auhl, D. Hassell, H. K. Rasmussen, A. L. Skov, O. G. Harlen, O. Hassager, and T. C. B. McLeish

Journal: Journal of Rheology 57(1), 293-313 (2013)

PhD-student: Qian Huang CPR-no.: 050182-3228

Signature of the PhD-student: Qian Huang Date: 7 January 2013

Co-author: David Matthew Hoyle Signature:

Description of each author's contribution to the above-mentioned article:

D. M. Hoyle:
Provided the new modelling and data fitting, plus performed all the simulations. Wrote the first draft of the article manuscript.

Q. Huang:
Carried out the filament stretching experiments and post processing of data. Provided feedback on the manuscript.

D. Auhl:
Carried out the experimental rheology for the oscillatory measurements and SER extensional rheology. Provided feedback on the manuscript.

D. Hassell:
Carried out the experimental work on the cross slot extensional rheometer, using the Cambridge Multi-Pass Rheometer. Provided feedback on the manuscript.

H. K. Rasmussen:
Supervised the second author on the experimental work. Engaged in discussions about the results and the manuscript.

A. L. Skov:
Engaged in discussions about the results and provided feedback on the manuscript.

O. G. Harlen:
Engaged in discussions about the modelling and results, and modified the manuscript.

O. Hassager:
Wrote the part of 'filament stretching rheometry' in the article manuscript. Engaged in discussions about the results and the manuscript.

T. C. B. McLeish:
Engaged in discussions about the modelling and results, and the manuscript.

Joint author statements shall be delivered to the **PhD administration** together with the PhD thesis.

Technical University of Denmark *Office for PhD and Continuing Education*

January 2013

Joint author statement

If a thesis contains articles made in collaboration with other researchers, a joint author statement about the PhD-student's part of the article shall be made by each of the co-authors, cf. article 12, section 4 of the Ministerial Order No. 18 February 2008 about the PhD degree

Title of the article:	Transient overshoot extensional rheology of long-chain branched polyethylenes: Experimental and numerical comparisons between filament stretching and cross-slot flow		
Author(s):	D. M. Hoyle, Q. Huang, D. Auhl, D. Hassell, H. K. Rasmussen, A. L. Skov, O. G. Harlen, O. Hassager, and T. C. B. McLeish		
Journal:	Journal of Rheology 57(1), 293-313 (2013)		
PhD-student:	Qian Huang	CPR-no.:	050182-3228
Signature of the PhD-student:	Qian Huang	Date:	7 January 2013
Co-author:	Dietmar Auhl	Signature:	

Description of each author's contribution to the above-mentioned article:

D. M. Hoyle:
Provided the new modelling and data fitting, plus performed all the simulations. Wrote the first draft of the article manuscript.

Q. Huang:
Carried out the filament stretching experiments and post processing of data. Provided feedback on the manuscript.

D. Auhl:
Carried out the experimental rheology for the oscillatory measurements and SER extensional rheology. Provided feedback on the manuscript.

D. Hassell:
Carried out the experimental work on the cross slot extensional rheometer, using the Cambridge Multi-Pass Rheometer. Provided feedback on the manuscript.

H. K. Rasmussen:
Supervised the second author on the experimental work. Engaged in discussions about the results and the manuscript.

A. L. Skov:
Engaged in discussions about the results and provided feedback on the manuscript.

O. G. Harlen:
Engaged in discussions about the modelling and results, and modified the manuscript

O. Hassager:
Wrote the part of 'filament stretching rheometry' in the article manuscript. Engaged in discussions about the results and the manuscript.

T. C. B. McLeish:
Engaged in discussions about the modelling and results, and the manuscript.

Joint author statements shall be delivered to the **PhD administration** together with the PhD thesis.

Technical University of Denmark *Office for PhD and Continuing Education*

January 2013

Joint author statement

If a thesis contains articles made in collaboration with other researchers, a joint author statement about the PhD-student's part of the article shall be made by each of the co-authors, cf. article 12, section 4 of the Ministerial Order No. 18 February 2008 about the PhD degree

Title of the article: Transient overshoot extensional rheology of long-chain branched polyethylenes: Experimental and numerical comparisons between filament stretching and cross-slot flow

Author(s): D. M. Hoyle, Q. Huang, D. Auhl, D. Hassell, H. K. Rasmussen, A. L. Skov, O. G. Harlen, O. Hassager, and T. C. B. McLeish

Journal: Journal of Rheology 57(1), 293-313 (2013)

PhD-student: Qian Huang CPR-no.: 050182-3228

Signature of the PhD-student: Qian Huang Date: 7 January 2013

Co-author: David Hassell Signature:

Description of each author's contribution to the above-mentioned article:

D. M. Hoyle:
Provided the new modelling and data fitting, plus performed all the simulations. Wrote the first draft of the article manuscript.

Q. Huang:
Carried out the filament stretching experiments and post processing of data. Provided feedback on the manuscript.

D. Auhl:
Carried out the experimental rheology for the oscillatory measurements and SER extensional rheology. Provided feedback on the manuscript.

D. Hassell:
Carried out the experimental work on the cross slot extensional rheometer, using the Cambridge Multi-Pass Rheometer. Provided feedback on the manuscript.

H. K. Rasmussen:
Supervised the second author on the experimental work. Engaged in discussions about the results and the manuscript.

A. L. Skov:
Engaged in discussions about the results and provided feedback on the manuscript.

O. G. Harlen:
Engaged in discussions about the modelling and results, and modified the manuscript.

O. Hassager:
Wrote the part of 'filament stretching rheometry' in the article manuscript. Engaged in discussions about the results and the manuscript.

T. C. B. McLeish:
Engaged in discussions about the modelling and results, and the manuscript.

Joint author statements shall be delivered to the **PhD administration** together with the PhD thesis.

Technical University of Denmark *Office for PhD and Continuing Education*

January 2013

Joint author statement

If a thesis contains articles made in collaboration with other researchers, a joint author statement about the PhD-student's part of the article shall be made by each of the co-authors, cf. article 12, section 4 of the Ministerial Order No. 18 February 2008 about the PhD degree

Title of the article:	Transient overshoot extensional rheology of long-chain branched polyethylenes: Experimental and numerical comparisons between filament stretching and cross-slot flow		
Author(s):	D. M. Hoyle, Q. Huang, D. Auhl, D. Hassell, H. K. Rasmussen, A. L. Skov, O. G. Harlen, O. Hassager, and T. C. B. McLeish		
Journal:	Journal of Rheology 57(1), 293-313 (2013)		
PhD-student:	Qian Huang	CPR-no.:	050182-3228
Signature of the PhD-student:	Qian Huang	Date:	7 January 2013
Co-author:	Henrik Koblitz Rasmussen	Signature:	

Description of each author's contribution to the above-mentioned article:

D. M. Hoyle:
Provided the new modelling and data fitting, plus performed all the simulations. Wrote the first draft of the article manuscript.

Q. Huang:
Carried out the filament stretching experiments and post processing of data. Provided feedback on the manuscript.

D. Auhl:
Carried out the experimental rheology for the oscillatory measurements and SER extensional rheology. Provided feedback on the manuscript.

D. Hassell:
Carried out the experimental work on the cross slot extensional rheometer, using the Cambridge Multi-Pass Rheometer. Provided feedback on the manuscript.

H. K. Rasmussen:
Supervised the second author on the experimental work. Engaged in discussions about the results and the manuscript.

A. L. Skov:
Engaged in discussions about the results and provided feedback on the manuscript.

O. G. Harlen:
Engaged in discussions about the modelling and results, and modified the manuscript.

O. Hassager:
Wrote the part of 'filament stretching rheometry' in the article manuscript. Engaged in discussions about the results and the manuscript.

T. C. B. McLeish:
Engaged in discussions about the modelling and results, and the manuscript.

Joint author statements shall be delivered to the **PhD administration** together with the PhD thesis.

Technical University of Denmark *Office for PhD and Continuing Education*

January 2013

Joint author statement

If a thesis contains articles made in collaboration with other researchers, a joint author statement about the PhD-student's part of the article shall be made by each of the co-authors, cf. article 12, section 4 of the Ministerial Order No. 18 February 2008 about the PhD degree

Title of the article:	Transient overshoot extensional rheology of long-chain branched polyethylenes: Experimental and numerical comparisons between filament stretching and cross-slot flow		
Author(s):	D. M. Hoyle, Q. Huang, D. Auhl, D. Hassell, H. K. Rasmussen, A. L. Skov, O. G. Harlen, O. Hassager, and T. C. B. McLeish		
Journal:	Journal of Rheology 57(1), 293-313 (2013)		
PhD-student:	Qian Huang	CPR-no.:	050182-3228
Signature of the PhD-student:	Qian Huang	Date:	7 January 2013
Co-author:	Anne Ladegaard Skov	Signature:	A Skov

Description of each author's contribution to the above-mentioned article:

D. M. Hoyle:
Provided the new modelling and data fitting, plus performed all the simulations. Wrote the first draft of the article manuscript.

Q. Huang:
Carried out the filament stretching experiments and post processing of data. Provided feedback on the manuscript.

D. Auhl:
Carried out the experimental rheology for the oscillatory measurements and SER extensional rheology. Provided feedback on the manuscript.

D. Hassell:
Carried out the experimental work on the cross slot extensional rheometer, using the Cambridge Multi-Pass Rheometer. Provided feedback on the manuscript.

H. K. Rasmussen:
Supervised the second author on the experimental work. Engaged in discussions about the results and the manuscript.

A. L. Skov:
Engaged in discussions about the results and provided feedback on the manuscript.

O. G. Harlen:
Engaged in discussions about the modelling and results, and modified the manuscript.

O. Hassager:
Wrote the part of 'filament stretching rheometry' in the article manuscript. Engaged in discussions about the results and the manuscript.

T. C. B. McLeish:
Engaged in discussions about the modelling and results, and the manuscript.

Joint author statements shall be delivered to the **PhD administration** together with the PhD thesis.

Technical University of Denmark *Office for PhD and Continuing Education*

January 2013

Joint author statement

If a thesis contains articles made in collaboration with other researchers, a joint author statement about the PhD-student's part of the article shall be made by each of the co-authors, cf. article 12, section 4 of the Ministerial Order No. 18 February 2008 about the PhD degree

Title of the article:	Transient overshoot extensional rheology of long-chain branched polyethylenes: Experimental and numerical comparisons between filament stretching and cross-slot flow		
Author(s):	D. M. Hoyle, Q. Huang, D. Auhl, D. Hassell, H. K. Rasmussen, A. L. Skov, O. G. Harlen, O. Hassager, and T. C. B. McLeish		
Journal:	Journal of Rheology 57(1), 293-313 (2013)		
PhD-student:	Qian Huang	CPR-no.:	050182-3228
Signature of the PhD-student:	Qian Huang	Date:	7 January 2013
Co-author:	Oliver G. Harlen	Signature:	O. Harlen

Description of each author's contribution to the above-mentioned article:

D. M. Hoyle:
Provided the new modelling and data fitting, plus performed all the simulations. Wrote the first draft of the article manuscript.

Q. Huang:
Carried out the filament stretching experiments and post processing of data. Provided feedback on the manuscript.

D. Auhl:
Carried out the experimental rheology for the oscillatory measurements and SER extensional rheology. Provided feedback on the manuscript.

D. Hassell:
Carried out the experimental work on the cross slot extensional rheometer, using the Cambridge Multi-Pass Rheometer. Provided feedback on the manuscript.

H. K. Rasmussen:
Supervised the second author on the experimental work. Engaged in discussions about the results and the manuscript.

A. L. Skov:
Engaged in discussions about the results and provided feedback on the manuscript.

O. G. Harlen:
Engaged in discussions about the modelling and results, and modified the manuscript.

O. Hassager:
Wrote the part of 'filament stretching rheometry' in the article manuscript. Engaged in discussions about the results and the manuscript.

T. C. B. McLeish:
Engaged in discussions about the modelling and results, and the manuscript.

Joint author statements shall be delivered to the **PhD administration** together with the PhD thesis.

Technical University of Denmark *Office for PhD and Continuing Education*

January 2013

Joint author statement

If a thesis contains articles made in collaboration with other researchers, a joint author statement about the PhD-student's part of the article shall be made by each of the co-authors, cf. article 12, section 4 of the Ministerial Order No. 18 February 2008 about the PhD degree

Title of the article:	Transient overshoot extensional rheology of long-chain branched polyethylenes: Experimental and numerical comparisons between filament stretching and cross-slot flow		
Author(s):	D. M. Hoyle, Q. Huang, D. Auhl, D. Hassell, H. K. Rasmussen, A. L. Skov, O. G. Harlen, O. Hassager, and T. C. B. McLeish		
Journal:	Journal of Rheology 57(1), 293-313 (2013)		
PhD-student:	Qian Huang	CPR-no.:	050182-3228
Signature of the PhD-student:	Qian Huang	Date:	7 January 2013
Co-author:	Ole Hassager	Signature:	

Description of each author's contribution to the above-mentioned article:

D. M. Hoyle:
Provided the new modelling and data fitting, plus performed all the simulations. Wrote the first draft of the article manuscript.

Q. Huang:
Carried out the filament stretching experiments and post processing of data. Provided feedback on the manuscript.

D. Auhl:
Carried out the experimental rheology for the oscillatory measurements and SER extensional rheology. Provided feedback on the manuscript.

D. Hassell:
Carried out the experimental work on the cross slot extensional rheometer, using the Cambridge Multi-Pass Rheometer. Provided feedback on the manuscript.

H. K. Rasmussen:
Supervised the second author on the experimental work. Engaged in discussions about the results and the manuscript.

A. L. Skov:
Engaged in discussions about the results and provided feedback on the manuscript.

O. G. Harlen:
Engaged in discussions about the modelling and results, and modified the manuscript.

O. Hassager:
Wrote the part of 'filament stretching rheometry' in the article manuscript. Engaged in discussions about the results and the manuscript.

T. C. B. McLeish:
Engaged in discussions about the modelling and results, and the manuscript.

Joint author statements shall be delivered to the **PhD administration** together with the PhD thesis.

Technical University of Denmark *Office for PhD and Continuing Education*

January 2013

Joint author statement

If a thesis contains articles made in collaboration with other researchers, a joint author statement about the PhD-student's part of the article shall be made by each of the co-authors, cf. article 12, section 4 of the Ministerial Order No. 18 February 2008 about the PhD degree

Title of the article:	Transient overshoot extensional rheology of long-chain branched polyethylenes: Experimental and numerical comparisons between filament stretching and cross-slot flow		
Author(s):	D. M. Hoyle, Q. Huang, D. Auhl, D. Hassell, H. K. Rasmussen, A. L. Skov, O. G. Harlen, O. Hassager, and T. C. B. McLeish		
Journal:	Journal of Rheology 57(1), 293-313 (2013)		
PhD-student:	Qian Huang	CPR-no.:	050182-3228
Signature of the PhD-student:	Qian Huang	Date:	7 January 2013
Co-author:	Tom C. B. McLeish	Signature:	

Description of each author's contribution to the above-mentioned article:

D. M. Hoyle:
Provided the new modelling and data fitting, plus performed all the simulations. Wrote the first draft of the article manuscript.

Q. Huang:
Carried out the filament stretching experiments and post processing of data. Provided feedback on the manuscript.

D. Auhl:
Carried out the experimental rheology for the oscillatory measurements and SER extensional rheology. Provided feedback on the manuscript.

D. Hassell:
Carried out the experimental work on the cross slot extensional rheometer, using the Cambridge Multi-Pass Rheometer. Provided feedback on the manuscript.

H. K. Rasmussen:
Supervised the second author on the experimental work. Engaged in discussions about the results and the manuscript.

A. L. Skov:
Engaged in discussions about the results and provided feedback on the manuscript.

O. G. Harlen:
Engaged in discussions about the modelling and results, and modified the manuscript.

O. Hassager:
Wrote the part of 'filament stretching rheometry' in the article manuscript. Engaged in discussions about the results and the manuscript.

T. C. B. McLeish:
Engaged in discussions about the modelling and results, and the manuscript.

Joint author statements shall be delivered to the **PhD administration** together with the PhD thesis.

Technical University of Denmark *Office for PhD and Continuing Education*

January 2013

Joint author statement

If a thesis contains articles made in collaboration with other researchers, a joint author statement about the PhD-student's part of the article shall be made by each of the co-authors, cf. article 12, section 4 of the Ministerial Order No. 18 February 2008 about the PhD degree

Title of the article:	A control scheme for filament stretching rheometers with application to polymer melts		
Author(s):	José M. Román Marín, Jakob K. Huusom, Nicolas J. Alvarez, Qian Huang, Henrik K. Rasmussen, Anders Bach, Anne L. Skov, Ole Hassager		
Journal:	Accepted in Journal of Non-Newtonian Fluid Mechanics		
PhD-student:	Qian Huang	CPR-no.:	050182-3228
Signature of the PhD-student:	Qian Huang	Date:	27 January 2013
Co-author:	José Manuel Román Marín	Signature:	

Description of each author's contribution to the above-mentioned article:

José M. Román Marín:
Provided the new control scheme and wrote the complete Labview code. Performed experiments to test the control scheme. Wrote the first draft of the article manuscript.

Jakob K. Huusom:
Provided suggestions on the detailed algorithm of the new control scheme.

Nicolas J. Alvarez:
Provided suggestions on the new control scheme. Provided feedback on the manuscript.

Qian Huang:
Performed experiments to test the control scheme. Engaged in discussions about the results. Provided feedback on the manuscript.

Henrik. K. Rasmussen:
Provided suggestions on the new control scheme. Engaged in discussions about the results.

Anders Bach:
Wrote the previous control scheme, which was the inspiration of the article. Engaged in discussions about the new control scheme.

Anne L. Skov:
Engaged in discussions about the results. Provided feedback on the manuscript.

Ole Hassager:
Provided suggestions on the new control scheme. Engaged in discussions about the results. Modified the manuscript.

Joint author statements shall be delivered to the **PhD administration** together with the PhD thesis.

Technical University of Denmark *Office for PhD and Continuing Education*

January 2013

Joint author statement

If a thesis contains articles made in collaboration with other researchers, a joint author statement about the PhD-student's part of the article shall be made by each of the co-authors, cf. article 12, section 4 of the Ministerial Order No. 18 February 2008 about the PhD degree

Title of the article: A control scheme for filament stretching rheometers with application to polymer melts

Author(s): José M. Román Marín, Jakob K. Huusom, Nicolas J. Alvarez, Qian Huang, Henrik K. Rasmussen, Anders Bach, Anne L. Skov, Ole Hassager

Journal: Accepted in Journal of Non-Newtonian Fluid Mechanics

PhD-student: Qian Huang CPR-no.: 050182-3228

Signature of the PhD-student: Qian Huang Date: 27 January 2013

Co-author: Jakob Kjøbsted Huusom Signature:

Description of each author's contribution to the above-mentioned article:

José M. Román Marín:
Provided the new control scheme and wrote the complete Labview code. Performed experiments to test the control scheme. Wrote the first draft of the article manuscript.

Jakob K. Huusom:
Provided suggestions on the detailed algorithm of the new control scheme.

Nicolas J. Alvarez:
Provided suggestions on the new control scheme. Provided feedback on the manuscript.

Qian Huang:
Performed experiments to test the control scheme. Engaged in discussions about the results. Provided feedback on the manuscript.

Henrik. K. Rasmussen:
Provided suggestions on the new control scheme. Engaged in discussions about the results.

Anders Bach:
Wrote the previous control scheme, which was the inspiration of the article. Engaged in discussions about the new control scheme.

Anne L. Skov:
Engaged in discussions about the results. Provided feedback on the manuscript.

Ole Hassager:
Provided suggestions on the new control scheme. Engaged in discussions about the results. Modified the manuscript.

Joint author statements shall be delivered to the **PhD administration** together with the PhD thesis.

Technical University of Denmark *Office for PhD and Continuing Education*

January 2013

Joint author statement

If a thesis contains articles made in collaboration with other researchers, a joint author statement about the PhD-student's part of the article shall be made by each of the co-authors, cf. article 12, section 4 of the Ministerial Order No. 18 February 2008 about the PhD degree

Title of the article: A control scheme for filament stretching rheometers with application to polymer melts

Author(s): José M. Román Marín, Jakob K. Huusom, Nicolas J. Alvarez, Qian Huang, Henrik K. Rasmussen, Anders Bach, Anne L. Skov, Ole Hassager

Journal: Accepted in Journal of Non-Newtonian Fluid Mechanics

PhD-student: Qian Huang CPR-no.: 050182-3228

Signature of the PhD-student: Qian Huang Date: 27 January 2013

Co-author: Nicolas Javier Alvarez Signature:

Description of each author's contribution to the above-mentioned article:

José M. Román Marín:
Provided the new control scheme and wrote the complete Labview code. Performed experiments to test the control scheme. Wrote the first draft of the article manuscript.

Jakob K. Huusom:
Provided suggestions on the detailed algorithm of the new control scheme.

Nicolas J. Alvarez:
Provided suggestions on the new control scheme. Provided feedback on the manuscript.

Qian Huang:
Performed experiments to test the control scheme. Engaged in discussions about the results. Provided feedback on the manuscript.

Henrik K. Rasmussen:
Provided suggestions on the new control scheme. Engaged in discussions about the results.

Anders Bach:
Wrote the previous control scheme, which was the inspiration of the article. Engaged in discussions about the new control scheme.

Anne L. Skov:
Engaged in discussions about the results. Provided feedback on the manuscript.

Ole Hassager:
Provided suggestions on the new control scheme. Engaged in discussions about the results. Modified the manuscript.

Joint author statements shall be delivered to the **PhD administration** together with the PhD thesis.

Technical University of Denmark *Office for PhD and Continuing Education*

January 2013

Joint author statement

If a thesis contains articles made in collaboration with other researchers, a joint author statement about the PhD-student's part of the article shall be made by each of the co-authors, cf. article 12, section 4 of the Ministerial Order No. 18 February 2008 about the PhD degree

Title of the article: A control scheme for filament stretching rheometers with application to polymer melts

Author(s): José M. Román Marín, Jakob K. Huusom, Nicolas J. Alvarez, Qian Huang, Henrik K. Rasmussen, Anders Bach, Anne L. Skov, Ole Hassager

Journal: Accepted in Journal of Non-Newtonian Fluid Mechanics

PhD-student: Qian Huang CPR-no.: 050182-3228

Signature of the PhD-student: Qian Huang Date: 27 January 2013

Co-author: Henrik Koblitz Rasmussen Signature:

Description of each author's contribution to the above-mentioned article:

José M. Román Marín:
Provided the new control scheme and wrote the complete Labview code. Performed experiments to test the control scheme. Wrote the first draft of the article manuscript.

Jakob K. Huusom:
Provided suggestions on the detailed algorithm of the new control scheme.

Nicolas J. Alvarez:
Provided suggestions on the new control scheme. Provided feedback on the manuscript.

Qian Huang:
Performed experiments to test the control scheme. Engaged in discussions about the results. Provided feedback on the manuscript.

Henrik. K. Rasmussen:
Provided suggestions on the new control scheme. Engaged in discussions about the results.

Anders Bach:
Wrote the previous control scheme, which was the inspiration of the article. Engaged in discussions about the new control scheme.

Anne L. Skov:
Engaged in discussions about the results. Provided feedback on the manuscript.

Ole Hassager:
Provided suggestions on the new control scheme. Engaged in discussions about the results. Modified the manuscript.

Joint author statements shall be delivered to the **PhD administration** together with the PhD thesis.

Technical University of Denmark *Office for PhD and Continuing Education*

January 2013

Joint author statement

If a thesis contains articles made in collaboration with other researchers, a joint author statement about the PhD-student's part of the article shall be made by each of the co-authors, cf. article 12, section 4 of the Ministerial Order No. 18 February 2008 about the PhD degree

Title of the article:	A control scheme for filament stretching rheometers with application to polymer melts		
Author(s):	José M. Román Marín, Jakob K. Huusom, Nicolas J. Alvarez, Qian Huang, Henrik K. Rasmussen, Anders Bach, Anne L. Skov, Ole Hassager		
Journal:	Accepted in Journal of Non-Newtonian Fluid Mechanics		
PhD-student:	Qian Huang	CPR-no.:	050182-3228
Signature of the PhD-student:	Qian Huang	Date:	27 January 2013
Co-author:	Anders Bach	Signature:	Anders Bach

Description of each author's contribution to the above-mentioned article:

José M. Román Marín:
Provided the new control scheme and wrote the complete Labview code. Performed experiments to test the control scheme. Wrote the first draft of the article manuscript.

Jakob K. Huusom:
Provided suggestions on the detailed algorithm of the new control scheme.

Nicolas J. Alvarez:
Provided suggestions on the new control scheme. Provided feedback on the manuscript.

Qian Huang:
Performed experiments to test the control scheme. Engaged in discussions about the results. Provided feedback on the manuscript.

Henrik. K. Rasmussen:
Provided suggestions on the new control scheme. Engaged in discussions about the results.

Anders Bach:
Wrote the previous control scheme, which was the inspiration of the article. Engaged in discussions about the new control scheme.

Anne L. Skov:
Engaged in discussions about the results. Provided feedback on the manuscript.

Ole Hassager:
Provided suggestions on the new control scheme. Engaged in discussions about the results. Modified the manuscript.

Joint author statements shall be delivered to the **PhD administration** together with the PhD thesis.

Technical University of Denmark *Office for PhD and Continuing Education*

January 2013

Joint author statement

If a thesis contains articles made in collaboration with other researchers, a joint author statement about the PhD-student's part of the article shall be made by each of the co-authors, cf. article 12, section 4 of the Ministerial Order No. 18 February 2008 about the PhD degree

Title of the article:	A control scheme for filament stretching rheometers with application to polymer melts		
Author(s):	José M. Román Marín, Jakob K. Huusom, Nicolas J. Alvarez, Qian Huang, Henrik K. Rasmussen, Anders Bach, Anne L. Skov, Ole Hassager		
Journal:	Accepted in Journal of Non-Newtonian Fluid Mechanics		
PhD-student:	Qian Huang	CPR-no.:	050182-3228
Signature of the PhD-student:	Qian Huang	Date:	27 January 2013
Co-author:	Anne Ladegaard Skov	Signature:	A Skov

Description of each author's contribution to the above-mentioned article:

José M. Román Marín:
Provided the new control scheme and wrote the complete Labview code. Performed experiments to test the control scheme. Wrote the first draft of the article manuscript.

Jakob K. Huusom:
Provided suggestions on the detailed algorithm of the new control scheme.

Nicolas J. Alvarez:
Provided suggestions on the new control scheme. Provided feedback on the manuscript.

Qian Huang:
Performed experiments to test the control scheme. Engaged in discussions about the results. Provided feedback on the manuscript.

Henrik. K. Rasmussen:
Provided suggestions on the new control scheme. Engaged in discussions about the results.

Anders Bach:
Wrote the previous control scheme, which was the inspiration of the article. Engaged in discussions about the new control scheme.

Anne L. Skov:
Engaged in discussions about the results. Provided feedback on the manuscript.

Ole Hassager:
Provided suggestions on the new control scheme. Engaged in discussions about the results. Modified the manuscript.

Joint author statements shall be delivered to the **PhD administration** together with the PhD thesis.

Technical University of Denmark *Office for PhD and Continuing Education*

January 2013

Joint author statement

If a thesis contains articles made in collaboration with other researchers, a joint author statement about the PhD-student's part of the article shall be made by each of the co-authors, cf. article 12, section 4 of the Ministerial Order No. 18 February 2008 about the PhD degree

Title of the article:	A control scheme for filament stretching rheometers with application to polymer melts		
Author(s):	José M. Román Marín, Jakob K. Huusom, Nicolas J. Alvarez, Qian Huang, Henrik K. Rasmussen, Anders Bach, Anne L. Skov, Ole Hassager		
Journal:	Accepted in Journal of Non-Newtonian Fluid Mechanics		
PhD-student:	Qian Huang	CPR-no.:	050182-3228
Signature of the PhD-student:	Qian Huang	Date:	27 January 2013
Co-author:	Ole Hassager	Signature:	

Description of each author's contribution to the above-mentioned article:

José M. Román Marín:
Provided the new control scheme and wrote the complete Labview code. Performed experiments to test the control scheme. Wrote the first draft of the article manuscript.

Jakob K. Huusom:
Provided suggestions on the detailed algorithm of the new control scheme.

Nicolas J. Alvarez:
Provided suggestions on the new control scheme. Provided feedback on the manuscript.

Qian Huang:
Performed experiments to test the control scheme. Engaged in discussions about the results. Provided feedback on the manuscript.

Henrik. K. Rasmussen:
Provided suggestions on the new control scheme. Engaged in discussions about the results.

Anders Bach:
Wrote the previous control scheme, which was the inspiration of the article. Engaged in discussions about the new control scheme.

Anne L. Skov:
Engaged in discussions about the results. Provided feedback on the manuscript.

Ole Hassager:
Provided suggestions on the new control scheme. Engaged in discussions about the results. Modified the manuscript.

Joint author statements shall be delivered to the **PhD administration** together with the PhD thesis.

Technical University of Denmark *Office for PhD and Continuing Education*

January 2013

Joint author statement

If a thesis contains articles made in collaboration with other researchers, a joint author statement about the PhD-student's part of the article shall be made by each of the co-authors, cf. article 12, section 4 of the Ministerial Order No. 18 February 2008 about the PhD degree

Title of the article:	Creep measurements confirm steady flow after stress maximum in extension of branched polymer melts		
Author(s):	Nicolas J. Alvarez, José M. Román Marín, Qian Huang, Michael L. Michelsen, Ole Hassager		
Journal:	Submitted to Physical Review Letters		
PhD-student:	Qian Huang	CPR-no.:	050182-3228
Signature of the PhD-student:	Qian Huang	Date:	27 January 2013
Co-author:	Nicolas Javier Alvarez	Signature:	

Description of each author's contribution to the above-mentioned article:

Nicolas J. Alvarez:
Derived the expressions of relative coefficients in linear viscoelasticity for creep measurements. Performed the numerical calculations. Carried out the creep measurements in both shear and extension. Wrote the first draft of the article manuscript.

José M. Román Marín:
Implemerted the new control scheme in FSR for creep measurements. Performed experiments to test the control scheme. Carried out creep measurements. Provided feedback on the manuscript.

Qian Huang:
Prepared the samples and carried out part of the experiments. Engaged in discussions about the results. Provided feedback on the manuscript.

Michael L. Michelsen:
Derived the solution to the transformation of shear modulus to creep compliance for constitutive model.

Ole Hassager:
Helped the first author to derive the expressions. Engaged in discussions about the results. Modified the manuscript.

Joint author statements shall be delivered to the **PhD administration** together with the PhD thesis.

Technical University of Denmark *Office for PhD and Continuing Education*

January 2013

Joint author statement

If a thesis contains articles made in collaboration with other researchers, a joint author statement about the PhD-student's part of the article shall be made by each of the co-authors, cf. article 12, section 4 of the Ministerial Order No. 18 February 2008 about the PhD degree

Title of the article:	Creep measurements confirm steady flow after stress maximum in extension of branched polymer melts		
Author(s):	Nicolas J. Alvarez, José M. Román Marín, Qian Huang, Michael L. Michelsen, Ole Hassager		
Journal:	Submitted to Physical Review Letters		
PhD-student:	Qian Huang	CPR-no.:	050182-3228
Signature of the PhD-student:	Qian Huang	Date:	27 January 2013
Co-author:	José Manuel Román Marín	Signature:	

Description of each author's contribution to the above-mentioned article:

Nicolas J. Alvarez:
Derived the expressions of relative coefficients in linear viscoelasticity for creep measurements. Performed the numerical calculations. Carried out the creep measurements in both shear and extension. Wrote the first draft of the article manuscript.

José M. Román Marín:
Implemented the new control scheme in FSR for creep measurements. Performed experiments to test the control scheme. Carried out creep measurements. Provided feedback on the manuscript.

Qian Huang:
Prepared the samples and carried out part of the experiments. Engaged in discussions about the results. Provided feedback on the manuscript.

Michael L. Michelsen:
Derived the solution to the transformation of shear modulus to creep compliance for constitutive model.

Ole Hassager:
Helped the first author to derive the expressions. Engaged in discussions about the results. Modified the manuscript.

Joint author statements shall be delivered to the **PhD administration** together with the PhD thesis.

Technical University of Denmark *Office for PhD and Continuing Education*

January 2013

Joint author statement

If a thesis contains articles made in collaboration with other researchers, a joint author statement about the PhD-student's part of the article shall be made by each of the co-authors, cf. article 12, section 4 of the Ministerial Order No. 18 February 2008 about the PhD degree

Title of the article:	Creep measurements confirm steady flow after stress maximum in extension of branched polymer melts		
Author(s):	Nicolas J. Alvarez, José M. Román Marín, Qian Huang, Michael L. Michelsen, Ole Hassager		
Journal:	Submitted to Physical Review Letters		
PhD-student:	Qian Huang	CPR-no.:	050182-3228
Signature of the PhD-student:	Qian Huang	Date:	27 January 2013
Co-author:	Michael Locht Michelsen	Signature:	

Description of each author's contribution to the above-mentioned article:

Nicolas J. Alvarez:
Derived the expressions of relative coefficients in linear viscoelasticity for creep measurements. Performed the numerical calculations. Carried out the creep measurements in both shear and extension. Wrote the first draft of the article manuscript.

José M. Román Marín:
Implemented the new control scheme in FSR for creep measurements. Performed experiments to test the control scheme. Carried out creep measurements. Provided feedback on the manuscript.

Qian Huang:
Prepared the samples and carried out part of the experiments. Engaged in discussions about the results. Provided feedback on the manuscript.

Michael L. Michelsen:
Derived the solution to the transformation of shear modulus to creep compliance for constitutive model.

Ole Hassager:
Helped the first author to derive the expressions. Engaged in discussions about the results. Modified the manuscript.

Joint author statements shall be delivered to the **PhD administration** together with the PhD thesis.

Technical University of Denmark *Office for PhD and Continuing Education*

January 2013

Joint author statement

If a thesis contains articles made in collaboration with other researchers, a joint author statement about the PhD-student's part of the article shall be made by each of the co-authors, cf. article 12, section 4 of the Ministerial Order No. 18 February 2008 about the PhD degree

Title of the article:	Creep measurements confirm steady flow after stress maximum in extension of branched polymer melts		
Author(s):	Nicolas J. Alvarez, José M. Rorrán Marín, Qian Huang, Michael L. Michelsen, Ole Hassager		
Journal:	Submitted to Physical Review Letters		
PhD-student:	Qian Huang	CPR-no.:	050182-3228
Signature of the PhD-student:	Qian Huang	Date:	27 January 2013
Co-author:	Ole Hassager	Signature:	

Description of each author's contribution to the above-mentioned article:

Nicolas J. Alvarez:
Derived the expressions of relative coefficients in linear viscoelasticity for creep measurements. Performed the numerical calculations. Carried out the creep measurements in both shear and extension. Wrote the first draft of the article manuscript.

José M. Román Marín:
Implemented the new control scheme in FSR for creep measurements. Performed experiments to test the control scheme. Carried out creep measurements. Provided feedback on the manuscript.

Qian Huang:
Prepared the samples and carried out part of the experiments. Engaged in discussions about the results. Provided feedback on the manuscript.

Michael L. Michelsen:
Derived the solution to the transformation of shear modulus to creep compliance for constitutive model.

Ole Hassager:
Helped the first author to derive the expressions. Engaged in discussions about the results. Modified the manuscript.

Joint author statements shall be delivered to the **PhD administration** together with the PhD thesis.

Bibliography

Aho, J., V. H. Rolon–Garrido, S. Syrjala, and M. H. Wagner,"Measurement technique and data analysis of extensional viscosity for polymer melts by Sentmanat extensional rheometer (SER)", Rheol. Acta 49, 359–370 (2010).

Andrade, R. J. and J. M. Maia , "A study on the flow, failure, and rupture mechanisms of low–density polyethylene in controlled–stress uniaxial extensional flow ", J. Rheol. 55(5), 925–937 (2011).

Alvarez, N. J., J. M. Román Marín, Q. Huang, M. L. Michelsen, and O. Hassager, "Creep measurements confirm steady flow after stress maximum in extension of branched polymer melts", submitted to Phys. Rev. Lett. (2012).

Anna, S., C. Rogers, and G. H. McKinley, "Controlling the kinematics of a filament stretching rheometer using a real-time active control mechanism", J. Non-Newtonian Fluid Mech. 87, 307–335 (1999).

Auhl, D., P. Chambon, T. C. B. McLeish, and D. J. Read, "Elongational flow of blends of long and short polymers: effective stretch relaxation time", Phys. Rev. Lett. 103, 136001 (2009).

Auhl, D., D. M. Hoyle, D. Hassell, T. D. Lord, O. G. Harlen, M. R. Mackley, and T. C. B. McLeish, "Cross-slot extensional rheometry and the steady–state extensional response of long chain branched polymer melts", J. Rheol. 55(4), 875–900 (2011).

Bach, A., K. Almdal, H. K. Rasmussen, and O. Hassager, "Elongational viscosity of narrow molar mass distribution polystyrene", Macromolecules 36, 5174–5179 (2003a).

Bach, A., H. K. Rasmussen, and O. Hassager, "Extensional viscosity for polymer melts measured in the filament stretching rheometer", J. Rheol. 47(2), 429–441 (2003b).

Bach, A., "Elongational viscosity for polymer melts measured in the filament stretching rheometer", Ph.D. thesis, Technical University of Denmark (2003).

Bastian, H., "Non-linear viscoelasticity of linear and long-chain-branched polymer melts in shear and extensional flows", Ph.D. thesis, Institut fulr Kunststofftechnologie der Universität Stuttgart (2001).

Baumgaertel, M., A. Schausberger, and H. H. Winter,"The relaxation of polymers with linear flexible chains of uniform length", Rheol. Acta 29, 400–408 (1990).

Bejenariu, A. G., H. K. Rasmussen, A. L. Skov, O. Hassager, and S. M. Frankaer, "Large amplitude oscillatory extension of soft polymeric networks", Rheol. Acta 49, 807–814 (2010).

Bird, R. B., R. C. Armstrong, and O. Hassager, "Dynamics of Polymeric Liquids", Vol. 1 (Wiley, New York, 1987).

Bischoff White, E. E., H. H. Winter, and J. P. Rothstein, "Extensional–flow–induced crystallization of isotactic polypropylene", Rheol. Acta, 51, 303–314 (2012).

Bhattacharjee, P. K., J. P. Oberhauser, G. H. McKinley, L. G. Leal, and T. Sridhar, "Extensional rheometry of entangled solutions", Macromolecules 35, 10131–10148 (2002).

Bhattacharjee, P. K., D. A. Nguyen, G. H. McKinley, and T. Sridhar, "Extensional stress growth and stress relaxation in entangled polymer solutions", J. Rheol. 47(1), 269–290 (2003).

Blackwell, R. J., T. C. B. McLeish, and O. G. Harlen, "Molecular drag–strain coupling in branched polymer melts", J. Rheol. 44(1), 121–136 (2000).

Burghelea, T. I., Z. Starý, and H. Münstedt, "On the 'viscosity overshoot' during the uniaxial extension of a low density polyethylene", J. Non–Newtonian Fluid Mech. 166, 1198–1209 (2011).

Burghelea, T. I., Z. Starý, and H. Münstedt, "Response to the 'Reply to: On the 'viscosity overshoot' during the uniaxial extension of a low density polyethylene' by Rasmussen et al.", J. Non-Newtonian Fluid Mech. 171–172, 107–108 (2012).

Clemeur, N., R. P. G. Rutgers, and B. Debbaut, "Numerical evaluation of three dimensional effects in planar flow birefringence", J. Non–Newtonian Fluid Mech. 123, 105–120 (2004).

Collis, M. W. and M. R. Mackley, "The melt processing of monodisperse and polydisperse polystyrene melts within a slit entry and exit flow", J. Non–Newtonian Fluid Mech. 128(1), 29–41 (2005).

Cogswell, F. N., "Rheology of polymer melts under tension", Plastics & Polymers, 36, 109–111 (1968).

Coventry, K. D. and M. R. Mackley, "Cross–slot extensional flow birefringence observations of polymer melts using a multi-pass rheometer", J. Rheol. 52(2), 401–415 (2008).

Currie, P. K., "Constitutive equations for polymer melts predicted by the Doi–Edwards and Curtiss-Bird kinetic theory models", J. Non-Newtonian Fluid Mech. 11, 53–68 (1982).

Das, C., N. J. Inkson, D. J. Read, and K. Kelmanson, "Computational linear rheology of general branch–on–branch polymers", J. Rheol. 50(2), 207–234 (2006).

Doi, M. and S. F. Edwards, "Dynamics of concentrated polymer systems. VI. Rheological properties", J. Chem. Soc., Faraday Trans. 1 75, 38–54 (1979).

Doi, M., "Stress relaxation of polymeric liquids after double-step strain", J. Polym. Sci.: Polym. Phys. Ed. 18, 1891–1905 (1980).

Doi, M., "Explanation for the 3.4 power law of viscosity of polymeric liquids on the basis of the tube model", J. Polym. Sci.: Polym. Lett. Ed. 19, 265–273 (1981).

Doi, M. and S. F. Edwards, "The theory of polymer dynamics" (Oxford Univ. Press, New York, 1986).

Gennes, P. G de., "Scaling concepts in polymer physics" (Cornell Univ. Press, New York, 1979).

Fang, J., M. Kröger, and H. C. Öttinger, "A thermodynamically admissible reptation model for fast flows of entangled polymers. II. Model predictions for shear and extensional flows", J. Rheol. 44(6), 1293–1317 (2000).

Ferry, J. D. "Viscoelastic properties of polymers" (3rd ed. Wiley, New York, 1980).

Fetters, L. J., D. J. Lohse, and R. H. Colby, "Chain dimensions and entanglement spacings", in Physical Properties of Polymers Handbook, edited by J. E. Mark (AIP, New York, 1996).

Fetters, L. D., J. Lohse, and S. T. Milner, "Packing length influence in linear polymer melts on the entanglement, critical, and reptation molecular weights", Macromolecules 32, 6847–6851 (1999).

Frischknecht, A. L., S. T. Milner, A. Pryke, R. N. Young, R. Hawkins, and T. C. B. McLeish, "Rheology of three–arm asymmetric star polymer melts", Macromolecules 35, 4801–4820 (2002).

Hassell, D. G., D. Auhl, T. C. B. McLeish, O. G. Harlen, and M. R. Mackley, "The effect of viscoelasticity on stress fields within polyethylene melt flow for a cross–slot and contraction–expansion slit geometry", Rheol. Acta 47, 821–834 (2008).

Hassell, D. G., D. Hoyle, D. Auhl, O. Harlen, M. R. Mackley, and T. C. B. McLeish, "Effect of branching in cross-slot flow: the formation of 'W cusps"', Rheol. Acta 48, 551–561 (2009).

Hassell, D. G. and M. R. Mackley, "An experimental evaluation of the behaviour of mono and polydisperse polystyrenes in cross-slot flow", Rheol. Acta 48, 543–550 (2009).

Hassager, O. and R. Hansen, "Constitutive equations for the Doi–Edwards model without independent alignment", Rheol. Acta 49, 555–562 (2010).

Hassager, O., K. Mortensen, A. Bach, K. Almdal, H. K. Rasmussen, and W. Pyckhout-Hintzen, "Stress and neutron scattering measurements on linear polymer melts undergoing steady elongational flow", Rheol. Acta 51, 385–394 (2012).

Hoyle, D. M., "Constitutive modelling of branched polymer melts in non-linear response", Ph.D. thesis, University of Leeds (2011).

Hoyle, D. M., Q. Huang, D. Auhl, D. Hassell, H. K. Rasmussen, A. L. Skov, O. G. Harlen, O. Hassager, and T. C. B. McLeish, "Transient overshoot extensional rheology of long–chain branched polyethylenes: Experimental and numerical comparisons between filament stretching and cross–slot flow", J. Rheol. 57(1), 293–313 (2013).

Huang, Q., H. K. Rasmussen, A. L. Skov, and O. Hassager, "Stress relaxation and reversed flow of low–density polyethylene melts following uniaxial extension", J. Rheol. 56(6), 1535–1554 (2012).

Hutchings, L. R., S. M. Kimani, D. M. Hoyle, D. J. Read, C. Das, T. C. B. McLeish, T. Chang, H. Lee, and D. Auhl,"In silico molecular design, synthesis, characterization, and rheology of dendritically branched polymers: closing the design loop", ACS Macro Lett. 1, 404–408 (2012).

Ianniruberto, G., A. Brasiello, and G. Marrucci, "Simulations of fast shear flows of PS oligomers confirm monomeric friction reduction in fast elongational flows of monodisperse PS melts as indicated by rheooptical data", Macromolecules 45, 8058–8066 (2012).

Ianniruberto, G. and G. Marrucci, "Entangled melts of branched PS behave like linear PS in the steady state of fast elongational flows", Macromolecules 46, 267–275 (2013).

Inkson, N. J., T. C. B. McLeish, O. G. Harlen, and D. J. Groves, "Predicting low density polyethylene melt rheology in elongational and shear flows with 'pom–pom' constitutive equations", J. Rheol. 43, 873–895 (1999).

Jackson, J. K. and H. H. Winter, "Entanglement and Flow Behavior of Bidisperse Blends of Polystyrene and Polybutadiene", Macromolecules 28, 3146–3155 (1995).

Jensen, M. K., O. Hassager, H. K. Rasmussen, A. L. Skov, A. Bach, and H. V. Koldbech, "Planar elongation of soft polymeric networks", Rheol. Acta 49, 1–13 (2010).

Kotaka, T., A. Kojima, and M. Okamoto, "Elongational flow opto-rheometry for polymer melts. 1. Construction of an elongational flow opto–rheometer and some preliminary results", Rheol. Acta 36, 646–656 (1997).

Kolte, M. I., H. K. Rasmussen, and O. Hassager, "Transient filament stretching rheometer II: Numerical simulation", Rheol. Acta 36, 285–302 (1997).

Koyama, K. and O. Ishizuka, "Birefringence of polyethylene melt in transient elongational flow at constant strain rate", J. Polym. Sci., Part B: Polym. Phys. 27, 297–306 (1989)

Larson, R. G., T. Sridhar, L. G. Leal, G. H. McKinley, A. E. Likhtman, and T. C. B. McLeish, "Definitions of entanglement spacing and time constants in the tube model", J. Rheol. 47(3), 809–818 (2003).

Larson, R. G., "Predicting the Flow of Real Polymers", Science 333, 1834–1835 (2011).

Laun, H. M. and H. Münstedt, "Elongational behaviour of a low density polyethylene melt", Rheol. Acta 17, 415–425 (1978).

Lee, K., M. R. Mackley, T. C. B. McLeish, T. M. Nicholson, and O. G. Harlen, "Experimental observation and numerical simulation of transient 'stress fangs' within flowing molten polyethylene", J. Rheol. 45(6), 1261–1277 (2001).

Lee, J. H., L. J. Fetters, and L. A. Archer, "Branch–point motion in asymmetric star polymers", Macromolecules 38, 4484–4494 (2005).

Likhtman, A. E. and T. C. B. McLeish, "Quantitative theory for linear dynamics of linear entangled polymers", Macromolecules 35, 6332–6343 (2002).

Lord, T. D., L. Scelsi, D. G. Hassell, M. R. Mackley, J. Embery, D. Auhl, O. G. arlen, R. Tenchev, P. K. Jimack, and M. A. Walkley, "The matching of 3d rolie–poly viscoelastic numerical simulations with experimental polymer melt flow within a slit and a cross-slot geometry", J. Rheol. 54, 355–373 (2010).

Luap, C., C. Müller, T. Schweizer, and D. C. Venerus, "Simultaneous stress and birefringence measurements during uniaxial elongation of polystyrene melts with narrow molecular weight distribution", Rheol. Acta 45, 83–91 (2005).

Lyhne, A., H. K. Rasmussen, and O. Hassager, "Simulation of Elastic Rupture in Extension of Entangled Monodisperse Polymer Melts", Phys. Rev. Lett. 102, 138301 (2009).

Mackley, M. R., R. T. J. Marshall, and J. B. A. F. Smeulders, "The multipass rheometer", J. Rheol. 39(6), 1293–1309 (1995).

Macosko, C. W., “Rheology, Principles, Measurements and Applications”, (Wiley–VCH, New York, 1994).

Mallat, S. G., “A wavelet tour of signal processing”, (Academic Press, London, 2009), pp.220–303.

Mark, J. E., “Physical properties of polymers handbook” (2nd ed. Springer, New York, 2006), pp.94.

Marrucci, G. and N. Grizzuti, “Fast flows of concentrated polymers: Prediction of the tube model on chain stretching”, Gazz. Chim. Ital. 118, 179–185 (1988).

Marrucci, G. and G. Ianniruberto, “On compatibility of the Cox-Merz rule with the model of Doi and Edwards”, J. Non-Newtonian Fluid Mech. 65, 241–246 (1996).

Marrucci, G. and G. Ianniruberto, “Interchain Pressure Effect in Extensional Flows of Entangled Polymer Melts”, Macromolecules 37, 3934–3942 (2004).

Matta, J. E. and R. P. Tytus, “Liquid stretching using a falling cylinder”, J. Non-Newtonian Fluid Mech. 35, 215–229 (1990).

McLeish, T. C. B. and R. G. Larson, “Molecular constitutive equations for a class of branched polymers: The pom-pom polymer”, J. Rheol. 42(1), 81–110 (1998).

McLeish, T. C. B., J. Allgaier, D. K. Bick, G. Bishko, P. Biswas, R. Blackwell, B. Blottière, N. Clarke, B. Gibbs, D. J. Groves, A. Hakiki, R. K. Heenan, J. M. Johnson, . R. Kant, D. J. Read, and R. N. Young, “Dynamics of entangled H–polymers: theory, rheology, and neutron–scattering”, Macromolecules 32, 6734–6758 (1999).

McLeish, T. C. B., “Tube theory of entangled polymer dynamics”, Advances in Physics 51, 6, 1379–1527 (2002).

McKinley, G. H. and T. Sridhar, “Filament–stretching rheometry of complex fluids”, Annu. Rev. Fluid Mech. 34, 375–415 (2002).

Meissner, J., “Dehnungsverhalten von polyäthylen-schmelzen”, Rheologica Acta 10, 230–242 (1971).

Meissner, J., “Development of a universal extensional rheometer for the uniaxial extension of polymer melts”, Transactions of the society of rheology 16:3, 405–420 (1972).

Meissner, J. and J. Hostettler, “A new elongational rheometer for polymer melts and other highly viscoelastic liquids”, Rheol. Acta 33, 1–21 (1994).

Menezes, E. V. and W. W. Graessley, “Nonlinear rheological behavior of polymer systems for several shear–flow histories”, J. Polym. Sci.: Polym. Phys. Vol. V 20, 1817–1833 (1982).

Milner, S. T. and T. C. B McLeish, "Parameter–free theory for stress relaxation in star polymer melts", Macromolecules 30, 2159–2166 (1997).

Münstedt, H., "New universal extensional rheometer for polymer melts, measurements on a polystyrene sample", J. Rheol. 23, 421–436 (1979).

Münstedt, H., S. Kurzbeck, and L. Egersdörfer, 'Influence of molecular structure on rheological properties of polyethylenes Part II. Elongational behavior", Rheol. Acta 37, 21–29 (1998).

Ndoni, S., Ch. M. Papadakis, F. S. Bates, and K. Almdal, "Laboratory–scale setup for anionic polymerization under inert atmosphere", Rev. Sci. Instrum. 66(2), 1090–1095 (1995).

Nielsen, J. K., H. K. Rasmussen, O. Hassager, and G. H. McKinley, "Elongational viscosity of monodisperse and bidisperse polystyrene melts", J. Rheol. 50, 453–476 (2006a).

Nielsen, J. K., H. K. Rasmussen, M. Denberg, K. Almdal, and O. Hassager, "Nonlinear Branch-Point Dynamics of Multiarm Polystyrene", Macromolecules 39, 8844–8853 (2006b).

Nielsen, J. K., H. K. Rasmussen, and O. Hassager, "Stress relaxation of narrow molar mass distribution polystyrene following uniaxial extension", J. Rheol. 52(4), 885–899 (2008).

Nielsen, J. K. and H. K. Rasmussen, "Reversed extension flow", J. Non-Newtonian Fluid Mech. 155, 15–19 (2008).

Nordmaier, E., U. Lanver, and M. D. Lechner, "The molecular structure of low–density polyethylene 1. Longchain branching and solution properties", Macromolecules 23, 1072–1076 (1990a).

Nordmaier, E., U. Lanver, and M. D. Lechner, "The molecular structure of low–density polyethylene 2. Particle scattering factors", Macromolecules 23, 1077–1084 (1990b).

Oishi, C. M., F. P. Martins, M. F. Tomé, J. A. Cuminato, and S. McKee, "Numerical solution of the eXtended Pom-Pom model for viscoelastic free surface flows", J. Non-Newtonian Fluid Mech. 166, 165–179 (2011).

Orr, N. V. and T. Sridhar, "Probing the dynamics of polymer solutions in extensional flow using step strain rate experiments", J. Non-Newtonian Fluid Mech. 82, 203–232 (1999).

Osaki, K., T. Inoue, and T. Isomura, "Stress overshoot of polymer solutions at high rates of shear", J. Polym. Sci.: Polym. Phys. Vol. 38, 1917–1925 (2000).

Osaki, K., T. Inoue, T. Uematsu, and Y. Yamashita, "Evaluation methods of the longest rouse relaxation time of an entangled polymer in a semidilute solution", J. Polym. Sci.: Polym. Phys. Vol. 39, 1704–1712 (2001).

Raible, T., A. Demarmels, and J. Meissner, "Stress and recovery maxima in LDPE melt elongation", Polym. Bull. 1, 397–402 (1979).

Rasmussen, H. K., J. K. Nielsen, A. Bach, and O. Hassager, "Viscosity overshoot in the start-up of uniaxial elongation of low density polyethylene melts", J. Rheol. 49(2), 369–381 (2005).

Rasmussen, H. K. and T. Eriksson, "Gas displacement of polymer melts in a cylinder: Experiments and viscoelastic simulations", J. Non-Newtonian Fluid Mech. 143, 1–9 (2007).

Rasmussen, H. K., P. Laillé, anf K. Yu, "Large amplitude oscillatory elongation flow", Rheol. Acta, 47, 97–103 (2008).

Rasmussen, H. K., A. L. Skov, J. K. Nielsen, and P. Laillé, "Elongational dynamics of multiarm polystyrene", J. Rheol. 53(2), 401–415 (2009).

Rasmussen, H. K., A. G. Bejenariu, O. Hassager, and D. Auhl, "Experimental evaluation of the pure configurational stress assumption in the flow dynamics of entangled polymer melts", J. Rheol. 54(6), 1325–1336 (2010).

Rasmussen, H. K. and O. Hassager, "Reply to: 'On the 'viscosity overshoot' during the uniaxial extension of a low density polyethylene' ", J. Non-Newtonian Fluid Mech. 171–172, 106 (2012).

Read, D. J., D. Auhl, C. Das, J. D. Doelder, M. Kapnistos, I. Vittorias, and T. C. B. McLeish, "Linking models of polymerization and dynamics to predict branched polymer structure and flow", Science 333, 1871–1874 (2011).

Read, D. J., K. Jagannathan, S. K. Sukumaran, and D. Auhl, "A full–chain constitutive model for bidisperse blends of linear polymers", J. Rheol. 56(4), 827–873 (2012).

Rolón–Garrido, V. H., M. H. Wagner, C. Luap, and T. Schweizer, "Modeling non–Gaussian extensibility effects in elongation of nearly monodisperse polystyrene melts", J. Rheol. 50(3), 327–340 (2006).

Román Marín, J. M., J. K. Huusom, N. J. Alvarez, Q. Huang, H. K. Rasmussen, A. Bach, A. L. Skov, and O. Hassager, "A control scheme for filament stretching rheometers with application to polymer melts", J. Non-Newtonian Fluid Mech. 194, 14–22 (2013).

Roovers, J. and P. M. Toporowski, "Preparation and characterization of H–shaped polystyrenes", Macromolecules 14, 1174–1178 (1981).

Rouse, P. E., "A theory of the linear viscoelastic properties of dilute solutions of coiling polymers", J. Chem. Phys. 21, 1272–1280 (1953).

Ruymbeke, E. van, Y. Masubuchi, and H. Watanabe, "Effective value of the dynamic dilution exponent in bidisperse linear polymers: from 1 to 4/3", Macromolecules 45, 2085–2098 (2012).

Schulze, J. S., T. P. Lodge, C. W. Macosko, J. Hepperle, H. Münstedt, H. Bastian, D. Ferri, D. J. Groves, Y. H. Kim, M. Lyon, T. Schweizer, T. Virkler, E. Wassner, and W. Zoetelief, "A comparison of extensional viscosity measurements from various RME rheometers", Rheol. Acta 40, 457–466 (2001).

Seborg, D. E., T. F. Edgar, and D. A. Mellichamp, "Process Dynamics and Control" (2nd ed., Wiley, USA, 2004).

Sentmanat, M., "Miniature universal testing platform: from extensional melt rheology to solid-state deformation behaviour", Rheol. Acta 43, 657–669 (2004).

Sentmanat, M., B. N. Wang, and G. H. McKinley, "Measuring the transient extensional rheology of polyethylene melts using the SER universal testing platform", J. Rheol. 49, 585–606 (2005).

Shie, S. C, C. T. Wu, and C. C. Hua, "Nonlinear stress relaxation of H–shaped polymer melt revisited using a stochastic pom–pom model", Macromolecules 36, 2141–2148 (2003).

Sips, R, "Mechanical Behavior of Viscoelastic Substances", J. Polymer Sci. 5(1), 69–89 (1950).

Spiegelberg, S. H., D. C. Ables, and G. H. McKinley, "The role of end–effects on measurements of extensional viscosity in filament stretching rheometers", J. Non–Newtonian Fluid Mech. 64, 229–267 (1996).

Sridhar, T. V. Tirtaatmadja, D. A. Nguyen, and R. K. Gupta, "Measurement of extensional viscosity of polymer solutions", J. Non-Newtonian Fluid Mech. 40, 271–280 (1991).

Stadlbauer, M., H. Janeschitz-Kriegl, M. Lipp, G. Eder, and R. Forstner "Extensional rheometer for creep flow at high tensile stress. Part I. Description and validation", J. Rheol. 48(3), 611–629 (2004).

Szabo, P., "Transient filament stretching rheometer part I: Force balance analysis", Rheol. Acta 36, 277–284 (1997).

Tirtaatmadja, V. and T. Sridhar, "A filament stretching device for measurement of extensional viscosity", J. Rheol. 37(6), 1081–1102 (1993).

Urakawa, O., M. Takahashi, T. Masuda, and N. Golshan Ebrahimi, "Damping functions and chain relaxation in uniaxial and biaxial extensions: Comparison with the Doi–Edwards theory", Macromolecules 28, 7196–7201 (1995).

Verbeeten, W. M. H., G. W. M. Peters, and F. P. T. Baaijens, "Differential constitutive equations for polymer melts: The extended Pom–pom model", J. Rheol. 45(4), 823–843 (2001).

Wang, Y., P. Boukany, S. Q. Wang, and X. Wang, "Elastic breakup in uniaxial extension of entangled polymer melts", Phys. Rev. Lett. 99, 237801 (2007)

Wagner, M. H., T. Raible and J. Meissner, "Tensile stress overshoot in uniaxial extension of a LDPE melt", Rheol. Acta 18, 427–428 (1979).

Wagner, M. H. and S. E. Stephenson, "The irreversibility assumption of network disentanglement inflowing polymermelts and its effects onelastic recoil predictions", J. Rheol. 23, 489–504 (1979).

Wagner, M. H. and J. Schaeffer, "Rubbers and polymer melts: Universal aspects of nonlinear stress-strain relations", J. Rheol. 37(4), 643–661 (1993).

Wagner, M. H., H. Bastian, P. Hachmann, J. Meissner, S. Kurzbeck, H. Münstedt, and F. Langouche, "The strain–hardening behaviour of linear and long-chain—branched polyolefin melts in extensional flows", Rheol. Acta 39, 97–109 (2000).

Wagner, M. H., S. Kheirandish, and O. Hassager, "Quantitative prediction of transient and steady-state elongational viscosity of nearly monodisperse polystyrene melts", J. Rheol. 49(6), 1317–1327 (2005).

Wagner, M. H. and V. H. Rolón-Garrido, "Verification of branch point withdrawal in elongational flow of pom–pom polystyrene melt", J. Rheol. 52(5), 1049–1068 (2008).

Wagner, M. H., "The effect of dynamic tube dilation on chain stretch in nonlinear polymer melt rheology", J. Non-Newtonian Fluid Mech. 166, 915–924 (2011).

Wagner, M. H. and V. H. Rolón-Garrido, "Constant force elongational flow of polymer melts: Experiment and modelling", J. Rheol. 56(5), 1279–1297 (2012).

Watanabe, H., S. Ishida, Y. Matsumiya, and T. Inoue, "Test of full and partial tube dilation pictures in entangled blends of linear polyisoprenes", Macromolecules 37, 6619–6631 (2004).

Yaoita, T., T. Isaki, Y. Masubuchi, H. Watanabe, G. Ianniruberto, and G. Marrucci, "Primitive chain network simulation of elongational flows of entangled linear chains: role of finite chain extensibility", Macromolecules 44, 9675–9682 (2011).

Yaoita, T., T. Isaki, Y. Masubuchi, H. Watanabe, G. Ianniruberto, and G. Marrucci, "Primitive chain network simulation of elongational flows of entangled linear chains: stretch/orientation–induced reduction of monomeric friction", Macromolecules 45, 2773–2782 (2012).

Yu, K., J. M. Román Marín, H. K. Rasmussen, and O. Hassager, "3D modeling of dual wind-up extensional rheometers", J. Non-Newtonian Fluid Mech. 165, 14–23 (2010).

Yu, K., H. K. Rasmussen, and A. L. Skov, "Experimental evaluation of the pseudotime principle for nonisothermal polymer flows", J. Rheol. 55(5), 1059–1067 (2011a).

Yu, K., H. K. Rasmussen, J. M. Román Marín, and O. Hassager, "The dynamics of cylindrical samples in dual wind–up extensional rheometers", J. Rheol. 55, 571–580 (2011b).

The Danish Polymer Centre
Department of Chemical and Biochemical Engineering
Technical University of Denmark
Søltofts Plads, Building 227
DK-2800 Kgs. Lyngby
Denmark

Phone: +45 4525 6801
Web: www.dpc.kt.dtu.dk

ISBN : 978-87-92481-99-3